

PHYSICAL FACTORS GOVERNING THE AGGREGATION
OF
HUMAN PLATELETS IN SHEARED SUSPENSIONS

by

© David N. Bell

A thesis submitted to the Faculty of Graduate Studies and Research
in partial fulfillment of the requirements for the degree of
Doctor of Philosophy

© David N. Bell, June, 1988

Department of Medicine
Division of Experimental Medicine
McGill University
Montreal, Quebec

ABSTRACT

The effect of shear rate on the ADP-induced aggregation of human blood platelets in flow through tubes was studied over the full physiologically significant range. The extent of single platelet aggregation at 0.2 μM ADP in citrated platelet-rich plasma, PRP, was greatest at mean tube shear rate, $\bar{G} = 314 \text{ s}^{-1}$; however, aggregate size steadily decreased from $\bar{G} = 39.3$ to 1800 s^{-1} . At 1.0 μM ADP the rate of aggregation increased up to $\bar{G} = 1800 \text{ s}^{-1}$ where virtually no unaggregated platelets remained after 43 s of flow, although, aggregate size was still limited by shear rate. A shear-dependent delay in the onset of aggregation and an increase in collision efficiency with time suggest the existence of a time and shear-dependency in the expression of bonds mediating aggregation. Greater aggregation of platelets from female donors than male donors was due to differences in the ionized calcium concentration, $[\text{Ca}^{2+}]$, in the plasma of donors of different hematocrit when the chelating agent citrate is used as anticoagulant. At physiological $[\text{Ca}^{2+}]$ aggregation was much greater in heparinized and hirudinized plasma than in citrated plasma and no sex difference was present. Aggregation in whole blood was much greater than in PRP due to a shear-dependent increase in the frequency of collision between activated platelets caused by the motion of red cells.

RESUME

L'effet de la vitesse de cisaillement sur l'agrégation des plaquettes humaines induites par l'ADP fut étudié dans un système circulant in vitro, en variant le débit à l'intérieur des limites physiologiques. L'agrégation de plaquettes seules dans le plasma citraté et riche en plaquettes contenant $0.2 \mu\text{M}$ ADP, atteint son maximum quand la vitesse de cisaillement dans le tube était de $\bar{G} = 314 \text{ s}^{-1}$. Il est à noter que la grandeur des agrégats diminue d'une manière consistante entre $\bar{G} = 39.3$ et $1,800 \text{ s}^{-1}$. Avec une concentration d'ADP de $1.0 \mu\text{M}$, le taux d'agrégation augmenta jusqu'à $\bar{G} = 1,800 \text{ s}^{-1}$, quand on ne pouvait presque plus apercevoir des plaquettes non-agrégées après une durée du débit de 43 s, néanmoins, la grandeur des agrégats demeurait toujours limitée par la vitesses de cisaillement. Un délai relié au cisaillement au début de l'agrégation, ainsi qu'une augmentation de l'efficacité de collision avec le temps suggèrent que la formation des liens entre les plaquettes dépend du temps de stimulation et de la vitesse de cisaillement. L'agrégation des plaquettes provenant des femmes était plus marquée que celle provenant des hommes. Ceci est dû à la différence entre les deux concernant la concentration de calcium, $[\text{Ca}^{2+}]$, dans le plasma citraté, car l'hématocrite est différent entre les hommes and les femmes. Avec un taux physiologique de $[\text{Ca}^{2+}]$, l'agrégation était beaucoup plus marquée dans le plasma hépariné ou traité à l'hitudine que dans le plasma citraté, indépendamment du sexe. L'agrégation des plaquettes était plus marquée dans le sang total que dans le plasma enrichi, au cause de l'augmentation de la fréquence de collision entre les plaquettes activées. Cette augmentation dépendait du niveau de contrainte et elle est causée par la mobilité de globules rouges.

To my daughter

Kirsten

ACKNOWLEDGEMENTS

I would like to express my sincere gratitude to my thesis supervisor Dr. H.L. Goldsmith for his guidance, support and encouragement throughout this work.

I am further indebted to both Dr. M.M. Frojmovic of the Department of Physiology and Dr. T.G.M. van de Ven of the Pulp and Paper Research Institute at McGill University for the many helpful discussions concerning this project. The much respected advice from Dr. G.B. Price of the McGill Cancer Centre on issues of biology, and regarding directions for my future career was of great value to me.

I would especially like to thank Mrs. Samira Spain, not only for her excellent technical assistance throughout many of the experiments, but also for her enthusiastic spirit and her valued friendship. The many stimulating conversations on matters scientific and otherwise with Dr. S.P. Tha were also of great value.

I would also like to thank the many good friends whose warmth and generosity is greatly appreciated, especially Marisa, Carolyn and Tina.

Finally, I would like to thank my wife Beverley for providing me with the impetus to undertake this degree and for her patience, understanding and steadfast support in its pursuance. The constant encouragement from my parents, and from my sister Kimberly and my brother Ron was very helpful and greatly appreciated.

PREFACE

The work presented in this thesis falls into four main sections comprising Chapters II to V, respectively. The option provided to the candidate by Section 7 of the Guidelines Concerning Thesis Preparation has been utilized:

"The candidate has the option, subject to approval by the Department, of including as part of the thesis the text of an original paper, or papers suitable for submission to learned journals for publication. In this case, the thesis must still conform to all other requirements explained in Guidelines Concerning Thesis Preparation."

Each of the above cited chapters has been written in a manner suitable for publication in the scientific literature, and thus each is complete in itself with its own Abstract, Introduction, Methods, Results, Discussion and Bibliography. The co-authors on the papers to be submitted are my thesis director, Dr. H.L. Goldsmith and the technician, Ms. S. Spain whose help was required to accomplish the multiple tasks involved in the experiments.

As required by the Guidelines, the chapters follow from each other, creating a coherent dissertation. Additional material, giving background for the experimental method used to count cells, and details of the method of averaging log-volume histograms, are given in Appendices I and II, respectively. Also, as required by the Guidelines, Chapter I is a General Introduction to the subject matter of this thesis, including a literature review and outline of research goals. Chapter VI summarizes

the conclusions, claims to originality, and suggestions for further research.

A Nomenclature is placed at the beginning of Chapter II; it serves to define the symbols used therein, and in subsequent chapters of the thesis.

TABLE OF CONTENTS

Page

CHAPTER I

GENERAL INTRODUCTION

INTRODUCTION	1
1. Role of Platelets in Hemostasis and Thrombosis	2
2. An Historical Perspective	4
SHEAR RATE AND PLATELET AGGREGATION	5
1. Red Cell-Free Platelet Suspensions	6
(a) Shear-Induced Platelet Aggregation	6
(i) Low shear rate	6
(ii) High shear rate	7
(b) Agonist-Induced Platelet Aggregation in Flowing Suspensions	11
2. Whole Blood	15
(a) Platelet Aggregation in Suspension	16
(b) Platelet Aggregation on Natural and Artificial Surfaces	19
(i) Artificial surfaces	20
(ii) Natural surfaces	23
(iii) Intravascular platelet aggregation	26
(c) Factors Controlling Platelet Aggregation on Surfaces	27
(i) Platelet transport	29
(ii) Platelet ADP	32
(iii) Interaction time	34
(d) Pathological Consequences of Free-Flowing Platelet Aggregates	36
(e) Summary	41
COLLISION FREQUENCY AND EFFICIENCY	42
1. Theory	42
2. Model Particles	46
3. Platelet-Rich Plasma	49
4. Summary	56
RATIONALE	57
REFERENCES	58

CHAPTER II

MEASUREMENT OF THE CONCENTRATION AND SIZE OF SINGLE PLATELETS
AND AGGREGATES

ABSTRACT	78
NOMENCLATURE	79
INTRODUCTION	82
MATERIALS AND METHODS	85
1. Platelet-Rich Plasma and Reagents	85
2. Flow System and Mixing Chamber	86
3. Particle Concentration and Size Measurement	89
4. Log-Volume Histograms	91
5. Curve Fitting and Background Subtraction	92
BASIC STATISTICS AND HYPOTHESIS TESTING	95
EXPERIMENTAL ERROR	97
1. Residence Time in Mixing Chamber	97
2. Instrument Calibration	97
3. Count Reproducibility and Suspension Stability	99
COLLISION FREQUENCY AND EFFICIENCY	102
RESULTS	103
1. Single Platelet Distribution	103
(a) Concentration and Size	103
(b) Curve Fitting and Background Subtraction	105
2. Platelet Aggregation	110
(a) Single Platelet Concentration	110
(b) Collision Efficiency	110
(c) Aggregate Growth	113
DISCUSSION	118
1. Single Platelet Volume	118
2. Platelet Aggregation	122
3. Summary	124
REFERENCES	126

CHAPTER III

EFFECT OF SHEAR RATE AND ADP CONCENTRATION

ABSTRACT	131
INTRODUCTION	132
MATERIALS AND METHODS	137
1. Platelet-Rich Plasma and Reagents	137
2. Flow System	137
3. Thromboxane B ₂	138
4. Particle Concentration and Size	138
5. Statistics	140
RESULTS	141
1. Distribution of Single Platelet Volume	141
2. Single Platelet Concentration	144
(a) Effect of Shear Rate and Donor Sex	144
(b) Donor Hematocrit	147
(c) Thromboxane B ₂	149
3. Total Particle Concentration	153
(a) Rate of Aggregation	153
(b) Collision Efficiency	155
4. Aggregate Growth	158
(a) Aggregate Size Distribution	158
(b) Aggregate Growth Rate	158
5. ADP Concentration	167
(a) Single Platelet Concentration	167
(b) Collision Efficiency	169
(c) Rate of Aggregation	169
(d) Aggregate Growth	171
DISCUSSION	178
1. Platelet Size	179
2. Two-Body Collision Theory	180
3. Effect of Shear Rate	183
(a) Low Platelet Stimulation	183
(i) Single platelet aggregation	183
(ii) Mechanisms of ADP-induced platelet aggregation	187
(iii) Aggregate size	191
(b) High Platelet Stimulation	192
4. Sex Difference	194
REFERENCES	196

CHAPTER IV

EXTRACELLULAR FREE Ca²⁺ ACCOUNTS FOR THE SEX DIFFERENCE
IN THE AGGREGATION OF HUMAN PLATELETS
IN CITRATED PLATELET-RICH PLASMA

ABSTRACT 206

INTRODUCTION 207

MATERIALS AND METHODS 209

1. Platelet-Rich Plasma and Reagents 209
 - (a) Citrate 210
 - (b) Heparin 210
 - (c) Hirudin 210
2. Flow Sytem 211
3. Thromboxane B₂ 211
4. Particle Concentration and Size 212
5. Statistics 213
6. Ionized Plasma Calcium 214

RESULTS 214

1. Citrate 214
 - (a) Constant C₁ 214
 - (b) Adjusted C₁ 216
2. Heparin 221
3. Hirudin 225
4. Single Platelet Volume 228

DISCUSSION 231

REFERENCES 238

CHAPTER V

WHOLE BLOOD

ABSTRACT 241

INTRODUCTION 242

MATERIALS AND METHODS 247

1. Whole Blood and Reagents 247
2. Flow System 248
3. ADP Concentration 248
4. Thromboxane B₂ 249
5. Separation of Single Platelets and Aggregates from
Red Cells 249

	Page
6. Particle Concentration and Size	250
7. Statistics	251
EXPERIMENTAL ERROR	252
1. Platelet Extraction Efficiency	252
2. Wall Adhesion	255
RESULTS	256
1. Single Platelet Volume	257
2. Single Platelet Concentration	259
(a) ADP	259
(b) Controls	264
3. Aggregate Size and Growth Rate	266
(a) $\bar{C} = 39.3 \text{ s}^{-1}$	266
(b) $\bar{C} = 314 \text{ s}^{-1}$	271
(c) $\bar{C} = 1800 \text{ s}^{-1}$	279
DISCUSSION	283
1. Wall Adhesion	283
2. Platelet Size	285
3. Shear-Induced and Spontaneous Platelet Aggregation	287
4. ADP-Induced Platelet Aggregation	289
(a) Physical Effects of Red Cells on Platelet Aggregation	289
(b) Low Shear Rate	293
(c) High Shear Rate	294
5. Summary	296
REFERENCES	297

CHAPTER VI

GENERAL CONCLUSIONS	307
CLAIMS TO ORIGINAL RESEARCH	312
SUGGESTIONS FOR FURTHER WORK	315

APPENDIX I

APERTURE-IMPEDANCE PARTICLE COUNTERS

NOMENCLATURE A1

THEORY A3

 1. Principle and General Description A3

 2. Pulse Height vs Particle Volume A5

 (a) Shape Factor and Conductivity A7

 (b) Particle Orientation and Hydrodynamic Field A14

 3. Electrical Field A17

 4. Summary A23

PRACTICE A24

 1. Aperture Length A27

 2. Background Counts A29

 3. Shape Factor A29

REFERENCES A31

APPENDIX II

AVERAGE LOG-VOLUME HISTOGRAMS

1. Standard Normal Deviates A34

2. Standard Log-Volume Histograms A36

 (a) $\Delta x(j) = \Delta x$ A36

 (b) $\Delta x(j) < \Delta x$ A37

 (c) $\Delta x(j) > \Delta x$ A40

3. Average Standard Histograms A40

LIST OF FIGURES

Figure	Page
CHAPTER I	
1. Two-Body Collision in Poiseuille Flow	43
2. Interaction Energy vs Separation Distance	48
CHAPTER II	
1. Flow System and Mixing Chamber	87
2. Particle Concentration and Size	90
3. Residence Time in Mixing Chamber	98
4. Log-Volume Histogram	104
5. Curve Fitting and Background Subtraction	107
6. Single Platelet Concentration	111
7. Collision Efficiency	112
8. Aggregate Growth	114
9. Effect of Shear Rate on Aggregate Growth	116
CHAPTER III	
1. Single Platelet Concentration vs Mean Tube Shear Rate	145
2. Single Platelet Concentration vs Mean Tube Shear Rate	148
3. Correlation of Single Platelet Concentration with Hematocrit..	150
4. Total Particle Concentration	154
5. Collision Efficiency vs $\bar{t}\bar{G}$	157
6. Volume Fraction Histograms at $\bar{G} = 39.3 \text{ s}^{-1}$	159
7. Volume Fraction Histograms at $\bar{G} = 314 \text{ s}^{-1}$	160
8. Volume Fraction Histograms at $\bar{G} = 1800 \text{ s}^{-1}$	161
9. Effect of Shear Rate on Aggregate Growth for Females	163
10. Effect of Shear Rate on Aggregate Growth for Males	165
11. Effect of [ADP] on Single Platelet Concentration	168
12. Aggregate Growth vs [ADP] at $\bar{G} = 39.3 \text{ s}^{-1}$	173
13. Aggregate Growth vs [ADP] at $\bar{G} = 314 \text{ s}^{-1}$	175
14. Aggregate Growth vs [ADP] at $\bar{G} = 1800 \text{ s}^{-1}$	177

CHAPTER IV

1. Aggregation vs $[Ca^{2+}]$	217
2. Effect of $[Ca^{2+}]$ on Aggregate Growth	220
3. Effect of Anticoagulant on Platelet Aggregation	223
4. Aggregate Growth in Heparinized PRP	226
5. Aggregate Growth in Hirudinized PRP	229

CHAPTER V

1. Single Platelet Concentration vs \bar{t} at $\bar{G} = 39.3 \text{ s}^{-1}$	260
2. Single Platelet Concentration vs \bar{t} at $\bar{G} = 314 \text{ s}^{-1}$	262
3. Single Platelet Concentration vs \bar{t} at $\bar{G} = 1800 \text{ s}^{-1}$	263
4. Aggregate Growth at $\bar{G} = 39.3 \text{ s}^{-1}$	268
5. Light micrographs of Platelet Aggregates Containing RBC	273
6. T.E.M. of Section Through Platelet Aggregate Containing RBC ..	274
7. Light Micrographs of Platelet Aggregates Without RBC	276
8. Aggregate Growth at $\bar{G} = 314 \text{ s}^{-1}$	278
9. Aggregate Growth at $\bar{G} = 1800 \text{ s}^{-1}$	281

APPENDIX I

1. Aperture-Impedance Particle Counter	A4
2. Particle Within Aperture	A6
3. Electronically Sensed Particle Volume	A9
4. Particle Shape Factor	A11
5. Fluid Velocity Profile in Aperture	A15
6. Electrical Field within Aperture	A18
7. Voltage Pulse Shape	A20
8. Electronic Filtration of Voltage Pulses	A22
9. Coulter ZM Calibration	A26
10. Deep-Bore Apertures	A28

APPENDIX II

1. Broadening of Single Platelet Log-Volume Histogram by Averaging	A35
2. Mapping of Transformed Histograms onto Standard Histograms ...	A39

LIST OF TABLES

Table	Page
CHAPTER II	
1. Particle Counts of Fixed Platelet Suspensions	101
2. Statistics of the Single Platelet Distribution	109
CHAPTER III	
1. Number of Donors Tested at each Mean Tube Shear Rate	142
2. Average Statistics of the Single Platelet Log-Volume Distributions	143
3. Two-Way Analysis of Variance of Data Shown in Figure 1	146
4. Plasma Thromboxane B ₂ Concentration	151
5. Thromboxane B ₂ Concentration in PRP in Aggregometer after 2.5 min Exposure to Platelet Agonist	152
6. Effect of Shear Rate and Transit Time on Collision Efficiency	156
7. Effect of ADP Concentration on Collision Efficiency and Rate of Aggregation	170
CHAPTER IV	
1. Correlation Coefficients at given Degrees of Freedom	215
2. Normalized Single Platelet Concentration vs. [Ca ²⁺] Citrate PRP	218
3. Normalized Single Platelet Concentration in Heparinized PRP ...	222
4. Collision Efficiency	224
5. Normalized Single Platelet Concentration in Hirudinized PRP ...	227
6. TXB ₂ in Hirudinized PRP	230
7. Average Statistics of the Single Platelet Log-Volume Histograms	232
CHAPTER V	
1. Extraction of Single Platelets and Aggregates from PRP and WB	254
2. Average Statistics of the Single Platelet Log-Volume Histograms	258
3. TXB ₂ and LDH	265

CHAPTER I

GENERAL INTRODUCTION

INTRODUCTION

This thesis constitutes the second phase of an investigation into the ADP-induced aggregation of human platelets in flow through tubes. In the first phase, a microscopic double infusion technique was used to rapidly and uniformly introduce an aggregating agent into the bulk of a platelet suspension undergoing Poiseuille flow (Bell, 1983; Bell et al., 1984; Bell and Goldsmith, 1984). ADP was infused into the flowing suspension through a micropipette tip located concentrically within the entrance of the flow tube, and the aggregation reaction was observed under a microscope at various distances downstream. At 1 μM ADP, both the rate and final extent of aggregation were found to increase over the range of mean tube shear rate from 2 - 54 s^{-1} . Although this technique permitted direct visualization of the aggregation reaction, the microscopic dimensions and constraints on the diffusion of ADP restricted its use to relatively short reaction times and low shear rates. The present technique circumvents the diffusion problem and extends the previous work to longer times, higher shear rates, and whole blood. ADP and platelet suspension are simultaneously infused into a common mixing chamber and, after a brief mixing period, flow through various lengths of polyethylene tubing into 0.5% glutaraldehyde. The effects of shear rate and transit time on platelet aggregation are followed through an analysis of the complete particle volume distribution from 1 - $10^5 \mu\text{m}^3$. Thus, the present technique permits the application of fluid mechanical and colloid theory to the kinetics of platelet activation and aggregation, and as such, provides a convenient marriage of cell biology and suspension rheology.

1. Role of Platelets in Hemostasis and Thrombosis

The development of a circulatory system which adequately preserves the primordial unicellular environment essential for normal cellular metabolism is a sine qua non of multicellularity. A consequence of this vascularization is the potential for tissue necrosis should vessel integrity be disrupted. Several mechanisms have evolved by which organisms repair vessel damage. In arthropods hemocytes are responsible for wound repair (Grégoire, 1970). The equivalent in amphibians is the spindle cell (Loeb, 1927), whereas in mammals the blood platelet is the primary cellular element of hemostasis (Maupin, 1967). Indeed, in man the most firmly established function of platelets is the formation of a hemostatic plug to prevent the rapid extravasation of blood upon vessel trauma.

The alteration of one or more of the steps in hemostatic plug formation can result in bleeding disorders, whereas certain pathological mechanisms of platelet activation and fibrin formation can lead to thrombosis. Although deviation from the normal equilibrium in either direction may be deleterious, most platelet studies are concerned with the etiology and prophylaxis of thromboembolic disorders. Under the appropriate intravascular conditions for thrombogenesis, an initial mural thrombus may grow to occlude the vessel, or it may break away or fragment creating an embolus capable of occluding smaller vessels downstream. Reduced blood flow causing tissue ischemia may be severely debilitating or fatal should the myocardium or the brain be affected.

Thromboembolic disorders manifest themselves in a variety of diseases such as cerebrovascular disease (Gunning et al., 1964), coronary artery disease (Steele et al., 1973; Weiss, 1978), peripheral arteriosclerosis and arterial disease (Meade, 1979; Thomas, 1978), and venous and microvascular thrombosis (Weksler and Nachman, 1981). In addition, hyperresponsive platelets may play an important role in the development of atherosclerosis (Colwell and Halushka, 1980; Fuster et al., 1981; Weksler and Nachman, 1981) which in turn is considered the principal factor determining susceptibility to heart attack or stroke (Mustard et al., 1978).

Thromboembolism has also been shown to be a serious complication of prosthetic cardiac valves and circulatory devices (Salzman, 1971). Both the interaction of platelets with artificial surfaces and the effect of extreme or unusual flow conditions on cells contribute to platelet microaggregate formation (Vroman, 1967; Leonard, 1972). This has been observed in association with hemodialysis (Bischel et al., 1973), clinical perfusion (Rittenhouse et al., 1972), and cardiopulmonary bypass (Allardyce et al., 1966; Solis et al., 1975).

Platelets have been implicated in many other physiological processes including the support of the normal vascular endothelium (Johnson, 1971), stimulation of arterial smooth muscle proliferation (Ross et al., 1974), participation in the inflammatory response and immunological reactions (Caen et al., 1977), as well as in cancer metastasis (Tobelen et al., 1974; de Gaetano and Garattini, 1978).

2. An Historical Perspective

The discovery of platelets awaited the development of a microscope with sufficient resolving power to reveal their undisputed presence. After the introduction to the scientific community of a compound microscope capable of resolution to about 1 μm (Hodgkin and Lister, 1827), Donné (1842) was able to describe little globules in the blood distinct from the previously established red and white globules. At around the same time, Gulliver (Gerber, 1842) and Addison (1842) independently provided the first drawings of these new cells. Several years later, William Osler's description (1874) of single platelets within intact blood vessels, and of their tendency to form granular masses in blood removed from the circulation, was instrumental in establishing the platelet as a normal constituent of blood. Before long, Bizzozero (1882) had confirmed and extended these concepts by observing platelets flowing through the vessels of living animals and demonstrating their role in hemostasis and thrombosis. He also described the change in shape preceding platelet aggregation, and even commented that platelets are capable of releasing substances. Eberth and Schimmelbusch (1886) labelled the platelet shape change as "viscous metamorphosis" and worked out some of the early events of platelet deposition and fibrin formation. The next major development came with the histological studies of Wright (1906) in which he demonstrated the fragmentation of the megakaryocyte cytoplasm yielding single platelets.

The identification of ADP as the specific agent in red cells that stimulates platelet shape change and aggregation (Gaarder, 1961), as well as the development of convenient methods of testing other potential

agonists, antagonists and cofactors (Born, 1962; O'Brien, 1962), set the stage for a new wave of platelet investigation that continues today.

SHEAR RATE AND PLATELET AGGREGATION

Shear rate is the most important physical parameter governing platelet aggregation in flowing suspensions. It determines the platelet collision frequency, the shear and normal stresses which activate single cells and break up aggregates, and the interaction time of cell-cell or cell-surface collisions. Since shear rate is proportional to fluid velocity, these sequelae either promote or inhibit hemostatic or thrombotic mechanisms, depending on flow rate and vessel size.

Time-averaged systemic arterial wall shear rate, G_w , in humans ranges from $100 - 1000 \text{ s}^{-1}$ and may exceed 1000 s^{-1} in the capillaries, based on a parabolic velocity profile for whole blood (Whitmore, 1968; Chien, 1975; Turitto 1982). A higher rate of wall shear would be expected for a blunted velocity profile (Goldsmith, 1972), but it is unlikely that shear rate, G , exceeds 2000 s^{-1} in the normal human vasculature (Turitto and Baumgartner, 1982). The cross-linking of fibrinogen molecules between the membrane glycoprotein complex, GPIIb-IIIa, of activated platelets is the believed mechanism underlying ADP-induced platelet aggregation (Nurden, 1987). However, at a plasma viscosity $\eta = 1.1 \text{ mPa s}$ at 37°C , platelet aggregates must withstand in vivo shear stresses, $\tau = \eta G$, that are an order of magnitude greater than those sufficient to break up both red cell rouleaux formed by nonspecific fibrinogen cross-linking ($\tau \sim 0.2 \text{ N m}^{-2}$, Chien et al., 1967; Schmid-Schönbein et al., 1973) and

the highly specific antigen-antibody bonds between sphered red cells cross-linked by antibody ($\tau \approx 0.2 \text{ N m}^{-2}$, Tha and Goldsmith, 1986).

The predilection of white platelet thrombi to form in regions of high blood flow velocities, i.e., in the arterial as opposed to the venous side of the vasculature, emphasizes the need to focus on the early stages of platelet aggregation in well-defined flow. Studies at $G > 2000 \text{ s}^{-1}$ are most relevant to flow through extracorporeal and prosthetic devices, and through regions of altered blood flow such as stenotic atherosclerotic lesions and rheumatic heart valves. As will be discussed below, high shear stresses and altered flow patterns under these conditions of flow encourage thromboembolic processes through shear-induced platelet activation and platelet-surface interactions, respectively. As a consequence of the overriding influence of shear rate on platelet aggregation, a number of well-defined in vitro, and relatively more qualitative in vivo flow studies have emerged.

1. Red Cell-Free Platelet Suspensions

Studies using red cell-free platelet suspensions are of necessity in vitro. This fact alone is responsible for the major artifact of such studies; however, red cell-free suspensions provide the best medium for an unencumbered analysis of the biochemical and physical aspects of the aggregation reaction. Most of the studies to be discussed were done using citrated PRP, heparinized PRP or washed platelets.

(a) Shear-Induced Platelet Aggregation

(1) Low shear rate: It would appear that shear rates less than 2000 s^{-1}

do not induce aggregation. An initial report of spontaneous aggregation using a cone and plate rotational viscometer (Klose et al., 1975) has not been supported by similar studies using cone and plate viscometers (Belval et al., 1984; Belval and Hellums, 1986), cylindrical (Chang and Robertson, 1976) or parallel plate (Yung and Frojmovic, 1982) Couettes, or steady laminar flow through tubes (Gear 1982; Bell and Goldsmith, 1984).

Spontaneous aggregation was also absent in oscillatory flow in tubes, although the platelets were hypersensitive to post-shear, thrombin induced release (Goldsmith et al., 1976). Platelets have, moreover, been observed to aggregate in a vortex downstream of a sudden tubular expansion (Katano and Goldsmith, 1979a). The reported differences in shear-induced platelet aggregation at low shear rates may depend on the geometry and materials of the device used, the time of exposure to the shear field, and the method of platelet preparation (Breddin et al., 1976). The large surface area to volume ratio of rotational viscometers facilitates the interaction of platelets with the viscometer surface, and the subsequent release of platelet-derived platelet agonists, particularly ADP.

(ii) High shear rate: The shear-induced aggregation of platelets at high shear rates follows progressive changes in the degree of platelet activation, lysis and fragmentation in proportion to the level of fluid shear stress. Such effects, however, are highly dependent on the time of exposure to the shear field and on the proximity of platelets to solid surfaces. Again, work using rotational viscometers has shown that aggregation is induced within 10 s exposure to a threshold shear stress of $\tau = 5 \text{ N m}^{-2}$ ($G = 2800 \text{ s}^{-1}$; Belval et al., 1984). Aggregates were unstable at this level of shear and started to break up within 30 s. However, over

the same time interval, irreversible aggregation was induced at $\tau = 10 \text{ N m}^{-2}$ and coincided with the post-shear impairment of normal platelet serotonin uptake and aggregation in response to exogenous ADP (Hellums and Hardwick, 1981). The release of dense granule serotonin was invoked at $\tau = 15 \text{ N m}^{-2}$ with platelet lysis detectable at $\tau > 60 \text{ N m}^{-2}$ and overt single cell fragmentation at $\tau > 80 \text{ N m}^{-2}$. Thus significant shear-induced platelet aggregation and impairment of normal function can occur in the absence of granule release and/or cell lysis. Platelets also exhibit temporal changes after the initial response of shear-induced activation and aggregation.

Lower shear stresses are sufficient to produce similar results after sustained exposure to the shear field. Aggregates present after 5 min exposure to $\tau = 5 \text{ N m}^{-2}$ coincide with the shear-induced release of platelet dense granule ADP and serotonin (Brown et al., 1975). Some lysis also appears to be present under these conditions. Aggregation is still completely reversible after 5 min exposure to up to $\tau = 7.5 \text{ N m}^{-2}$ (Hellums and Hardwick, 1981), although a larger amount of platelet-derived platelet agonists is released than after 30 s at $\tau = 15 \text{ N m}^{-2}$. Post-shear serotonin uptake and ADP-induced aggregation are impaired at $\tau > 10 \text{ N m}^{-2}$, as they were after 30 s, while single cell fragmentation and aggregate disintegration are observed after 5 min exposure to shear stresses as low as $\tau = 40 \text{ N m}^{-2}$. Thus, sustained exposure to the threshold shear stress can lead to additional platelet aggregation through the shear-induced activation of platelet release. Continued exposure to the shear field also lowers the threshold for both platelet lysis and fragmentation.

High surface area to volume ratios in rotational viscometers enhance platelet lysis at $\tau > 16 \text{ N m}^{-2}$ (Hung et al., 1976), although the use of unsiliconized surfaces and the presence of secondary flow leading to increased platelet wall collisions may have contributed to this effect. Significant ultrastructural platelet damage in the absence of aggregation or serotonin release has been demonstrated after 15 min exposure to $\tau = 4.4 \text{ N m}^{-2}$ in a device designed to enhance platelet-wall collisions (Bernstein et al., 1977). These studies tend to support the premise that platelet damage caused by surface interactions is more important after long exposure times to low shear stresses where platelets damage in suspension is minimal ($\tau < 5 \text{ N m}^{-2}$; Hellums and Hardwick, 1981)

At extremely short exposure times ($< 5 \text{ ms}$) to high shear stresses in narrow bore capillary tubes, aggregation and/or fragmentation was not induced below $\tau = 1500 \text{ N m}^{-2}$, although serotonin release and platelet lysis were initiated at $\tau = 700$ and 1500 N m^{-2} , respectively (Colantuoni et al., 1977). For exposure times as short as 0.1 ms , much higher shear stresses, $\tau > 4000 \text{ N m}^{-2}$, were required to yield measurable release and lysis. Shear stresses as high as $\tau = 10^5 \text{ N m}^{-2}$ have been required to induce release plus a small amount of aggregation after $\sim 0.01 \text{ ms}$ exposure (Bernstein et al., 1977). Despite the release of platelet-derived platelet agonists, short platelet-platelet interaction times and high shear stresses appear to severely inhibit aggregation.

It is interesting that in the absence of lysis, shear stress can induce platelet release at room temperature, yet ADP-induced release is inhibited at this temperature in the aggregometer (Valdorf-Hansen and

Zucker, 1971). The shear-induced release is only partially inhibited by aspirin, and aggregation is unaffected (Stevens et al., 1980; Hardwick et al., 1980). Thus, the induction of release by shear stress involves an additional mechanism, independent of the platelet cyclo-oxygenase mediated arachidonate pathway. Elevation of cytoplasmic ionized calcium appears to be essential to this process since agents that maintain high levels of intracellular platelet cAMP substantially reduce shear-induced platelet aggregation (Hardwick et al., 1981). Other evidence indicates that leakage of cytoplasmic or granule nucleotides due to platelet damage contributes significantly to shear-induced platelet aggregation. After 5 min exposure to low shear stress ($\tau = 4 \text{ N m}^{-2}$), enough ADP ($\sim 1 \mu\text{M}$) has been detected in PRP in the absence of serotonin release to stimulate aggregation, suggesting the leakage of cytoplasmic ATP/ADP from injured platelets (Hardwick et al., 1983). Indeed as mentioned previously, platelet-wall collisions at this level of shear stress can impart striking ultrastructural changes in the platelet membrane, cytoplasm and granules atypical of normal platelet activation but suggestive of platelet damage (Bernstein et al., 1977). The critical shear stress for serotonin release also coincides with that for the release of lactate dehydrogenase (Hardwick et al., 1983) which is an indicator of cell lysis. Colchicine which interferes with normal platelet granule release only partially inhibits shear-induced serotonin release. It seems likely that platelet activation through the action of fluid shear stress on the cell surface can induce release, in addition to platelet aggregation that is, at least initially, independent of the normal release reaction.

(b) Agonist-Induced Platelet Aggregation in Flowing Suspensions

The importance of the release of platelet-derived platelet agonists, particularly ADP, in sustaining and enhancing shear-induced platelet aggregation has led to a number of studies on the effect of flow on agonist-induced platelet aggregation. Since high shear stresses activate platelets and induce release, the aggregation of platelets in response to exogenous agonists is generally confined to shear rates and to agonist concentrations that are below the threshold for release. Room temperature facilitates such studies since platelet release is completely inhibited at ambient temperatures below 27°C (Valdorf-Hansen and Zucker, 1971), although aggregation in response to ADP is enhanced. Studies of agonist-induced platelet aggregation in laminar flow, however, are handicapped by the method of mixing agonist and platelets. Rapid mixing ensures uniform exposure of all cells to the agonist and allows early observation of the aggregation reaction, but usually requires interruption of the conditions of flow that are the subject of study. While most studies address this issue, the development of well-defined laminar flow regimes has tended to supersede considerations of agonist diffusion and exposure time. In addition, most techniques have relied upon gross indices of platelet aggregation, such as changes in suspension turbidity or single platelet concentration, and have not focused on the kinetics of aggregate growth and/or break-up.

An initial effort to follow the early stages of aggregation stemmed from the desire to interpret the optical density changes of a stirred platelet suspension (Born and Hume, 1967). Although the flow regime was not well-defined, rapid mixing was ensured by a rotating stir

bar. Microscopic enumeration of single cells and aggregates after exposure to 1 μM ADP at 37°C, revealed that a 7% increase in the amount of light transmitted through the suspension after 75 s coincided with an 87% decrease in the concentration of single platelets. Within 3 s, the number of aggregates containing 2 - 6 platelets had increased, but by 30 s their numbers had started to decrease. The optical density of the platelet suspension continued to decrease, indicating continued aggregation. However, at the threshold ADP concentration for the platelet release reaction, it was found using an electronic particle counter that 86% of single platelets had aggregated within 20 s (Gear and Lambrecht, 1981). The onset of release, as indicated by the inflection of the optical density tracing at ~ 40 s did not result in the further recruitment of single cells. The continued decrease in the optical density of the suspension may instead reflect the formation of larger aggregates from smaller ones, and/or the consolidation of existing aggregates into tighter, more dense masses. Although the rate of aggregation was not quantitated in terms of suspension shear rate in either study, this work showed that turbidimetric methods of studying platelet aggregation are insensitive to significant changes in single cell and small aggregate concentration.

Despite variability in the ADP concentration and suspension temperature used, a number of studies have shown the aggregation of ADP-stimulated platelets to increase with increasing shear rate over the range $G = 0 - 2200 \text{ s}^{-1}$. Unstable aggregates that formed at 1.5 μM ADP in a parallel plate Couette at 37° were stable at 5 μM ADP (Yung and Frojmovic, 1982); however, the release of endogenous ADP at this level of platelet stimulation would have increased the effective ADP concentration.

A brief period of high shear used to mix the ADP and platelets prevented observation of the early stages of the aggregation reaction. As well, aggregate size and the kinetics of aggregate growth could not be extracted from the changes in suspension turbidity that were used to monitor aggregation.

Chang and Robertson (1976) followed the kinetics of both Brownian motion- and shear-induced aggregation in a cylindrical Couette using an elaborate light scattering theory. Calculation of the concentration of small order multiplets predicted that even after extensive aggregation, single platelets could still account for as much as 35% of the initial particle concentration. It was found that the light scattering phenomena of such suspensions were dominated by single cells. The relatively small maximum attainable concentrations of doublets, triplets and quadruplets (11%, 4% and 2%, respectively) did not permit accurate quantitation of the kinetics of aggregate growth. Consequently, only overall changes in suspension turbidity were used as indices of aggregation. At 10 μM ADP, the rate of aggregation was shown to increase over the range $10 < G < 75 \text{ s}^{-1}$ and level off beyond 75 s^{-1} , although shear rates greater than 100 s^{-1} were not tested. The rate of aggregation increased with increasing ADP concentration, reaching a maximum at 100 μM ADP. Again, the early stages of aggregation were lost due to a 10 s pre-shear mixing period.

The complete aggregation reaction has been observed directly using a microscopic double infusion system which allowed the rapid diffusion of ADP throughout the bulk of a platelet suspension undergoing

Poiseuille flow (Bell et al., 1984; Bell and Goldsmith, 1984). In contrast to conventional fixed-volume rotational viscometers and aggregometer cuvettes, such a flow-through system more closely mimics in vivo conditions. Even though mixing is complete, collisions can occur between platelets at different stages of activation due to the nonlinear velocity profile. At 1 μM ADP the rate and final extent of aggregation reached after a transit time of 40 s increased with increasing mean tube shear rate, \bar{G} , over the range 4 - 54 s^{-1} . The concentration of aggregates of successively increasing size increased and then decreased in accordance with the kinetics of aggregate growth predicted by Smoluchowski for inert colloidal size particles (Smoluchowski, 1917). Aggregates formed most rapidly in the region of the highest shear near the tube wall and as they grew in size and rotated, collisions with the wall culminated in the formation of large (> 100 platelets) centrally-located aggregates. Higher shear rates and longer exposure times were impractical due to the microscopic dimensions of the flow system and constraints on the distance for complete diffusion of ADP.

An independent study also using Poiseuille flow has shown that higher shear rates enhance ADP-induced aggregation (Gear, 1982). Platelets and ADP were pumped through narrow-bore teflon tubing into a Y-junction, and then through a common reaction tube. Aggregation was expressed as a decrease in the concentration of single platelets. At 10 μM ADP and at 37°C, it was found that ~ 50% of the platelets had aggregated within 2 - 4 s of flow through the reaction tube at $\bar{G} = 1300$ or 2200 s^{-1} , with the rate of aggregation higher at the higher shear rate. Again, the release of endogenous ADP at 37°C would considerably augment

the degree of aggregation. This flow system was principally designed to follow the early stages of the aggregation reaction in terms of various agonists, antagonists and cofactors, and not the effects of suspension shear rate. In this regard, the absolute aggregation rate must be interpreted carefully since this was determined by varying the flow rate through fixed lengths of tubing. Short reaction times required high flow rates. Consequently, as reaction time increased, \bar{G} decreased. A cursory look at the effect of shear rate was achieved by changing the tube diameter; however, the relationship between flow rate, transit time and shear rate is not clear. In addition, no details of the flow patterns in the Y-junction were provided although indirect evidence suggested that mixing was virtually instantaneous. In the absence of secondary flow and under conditions of laminar flow at the Reynolds numbers in the junction, mixing would occur only by diffusion and the distance required for the equilibration of ADP across the tube would be flow-dependent. This may be important considering a 1 s lag preceding aggregation at $\bar{G} = 1300 \text{ s}^{-1}$ was eliminated at $\bar{G} = 2200 \text{ s}^{-1}$.

(2) Whole Blood

Studies in whole blood (WB) have the advantage of allowing in vivo experimentation but the results have tended to be more variable due to a general loss of precision in both the induction and measurement of platelet aggregation, and to significant differences between species (Grabowski, 1978). Platelet aggregation in WB is also complicated by the presence of additional humoral factors and cellular components, particularly red cells (rbc), white cells (wbc), and endothelial cells in vivo. Red cells contain large amounts of adenine nucleotides (Gaarder et

al., 1961) that may be liberated during hemolysis. Intact rbc actively take up (Schrader et al., 1972; Gresele et al., 1983; Gresele et al., 1986) the platelet inhibitor (Born and Cross, 1963; Skoza et al., 1967), adenosine, which is formed on the external membrane of rbc by enzymatic dephosphorylation of adenine nucleotides (Parker, 1970; DePierre and Karnosky, 1974; Bartlett, 1977). Endothelial cells produce a potent inhibitor of platelet aggregation, prostaglandin I₂ (prostacyclin; (Moncada et al., 1975; Weiss and Turitto, 1979). White cells also produce prostacyclin (Blackwell et al., 1978; Borgeat and Samuelsson, 1979), dephosphorylate plasma ADP (Bolton and Emmons, 1967; Gilliam et al., 1981), and produce platelet activating factor (Benveniste et al., 1972; Benveniste et al., 1981)

(a) Platelet Aggregation in Suspension

Shear rates below $G = 2000 \text{ s}^{-1}$ do not induce platelet aggregation in citrated WB (Jen and McIntire, 1984). Spontaneous aggregation initially present in heparinized WB prior to shearing was promoted between $G = 100$ and 500 s^{-1} , but the aggregates formed were disrupted at $G > 1000 \text{ s}^{-1}$.

The response of platelets in WB to high shear stress is similar to that of platelets in plasma but, over the same range, the aggregates in WB are larger (Dewitz et al. 1978; Jen and McIntire, 1984). Although the number of aggregates in citrated WB increased with increasing shear stress after 5 min exposure to τ between 7.5 and 45 N m^{-2} in a cylindrical viscometer at 37°C, aggregate size decreased over the same range (Dewitz et al., 1978). Higher stresses up to $\tau = 60 \text{ N m}^{-2}$ produced a sudden drop

in the fraction of platelets within aggregates. After shearing, platelets in WB exhibited impaired aggregation in response to ADP in a manner similar to that found with PRP. A reduction in the total platelet count in WB was observed within 5 min exposure to $\tau < 30 \text{ N m}^{-2}$, however there were no such changes in total platelet count in PRP below $\tau = 40 \text{ N m}^{-2}$ (Hellums and Hardwick, 1981). The count reduction in WB was attributed to platelet destruction at high shear stresses but particles in the size range of platelet fragments were not counted. Platelet adhesion to the viscometer surface may have contributed to the count reduction in WB.

Reversible aggregation could be induced at $\tau = 1 \text{ N m}^{-2}$ subsequent to a 30 s exposure of citrated WB to $\tau = 9 \text{ N m}^{-2}$ in a cone and plate viscometer at room temperature (Jen and McIntire, 1984). At shorter exposure times, higher shear stresses were required to promote the subsequent low shear aggregation. Platelets in heparinized WB showed greater aggregation at high shear stresses than those in cWB, and the aggregates were more stable after short exposure times.

Shear-induced platelet aggregation in PRP has been attributed to ADP released from the shear-activated platelets. The threshold shear stress for serotonin release in both PRP and WB at 23°C is 5 N m^{-2} . The extent of release increases with further increases in shear stress; although, the release in WB is significantly less than in PRP (Hellums and Hardwick, 1981). Since the threshold for aggregation in both PRP and WB occurs at $\tau > 5 \text{ N m}^{-2}$, and both respond similarly to $\tau < 60 \text{ N m}^{-2}$, it is likely that in WB the shear-induced release of platelet ADP also contributes significantly to the induction of aggregation at high shear

stresses. The ADP utilizing enzyme system, creatine phosphate/creatine phosphokinase has been shown to block spontaneous aggregation in heparinized WB and substantially reduce shear-induced platelet aggregation (Jen and McIntire, 1984).

The role of ADP released from lytic or sublytic rbc injury in spontaneous or shear-induced platelet aggregation is not clear. Red cells were observed to enhance platelet adhesion/aggregation in glass bead columns in proportion to the hematocrit (Hellem, 1960). It was then proposed that the transient accumulation of ADP as a result of red cell damage or lysis is responsible for both spontaneous aggregation in vitro and normal hemostasis in vivo. The extension of this mode of platelet activation to thrombosis has given impetus to this hypothesis. Red cells are more sensitive than platelets at very short exposure times (< 5 ms) to very high shear stresses ($\tau > 300 \text{ N m}^{-2}$) but the converse is true for exposure times and shear stresses above and below these values, respectively. Shear stresses greater than 150 N m^{-2} are required to induce measurable hemolysis after 2 min^o exposure in rotational viscometers (Nevaril et al., 1968; Leverett et al., 1972). Shear-induced platelet aggregation after 5 min exposure of WB to $\tau \approx 5 \text{ N m}^{-2}$ at 37°C increased in proportion to the concentration of rbc and to the concentration of radioactively labelled adenine nucleotides liberated from rbc (Reimers et al., 1984). At $\tau = 15 \text{ N m}^{-2}$, a concentration of $0.6 \mu\text{M}$ ADP was measured. However, glutaraldehyde-hardened rbc depleted of ADP could also significantly enhance the shear-induced aggregation of platelets over that in PPP. Hemolysis induced by interaction of rbc with surfaces can occur at much lower shear stresses but only after longer exposure times

(Leverett et al., 1972; Hellums and Hardwick, 1981).

The possibility of sublytic adenine nucleotide leakage from damaged rbc at low shear stresses is still a subject of debate. Spontaneous aggregation in stirred WB (Burgess-Wilson et al., 1984) or rotating plastic vials (Saniabadi et al., 1985) showed a positive correlation with hematocrit in the absence of detectable hemolysis. Several studies have focused on the steady leakage of adenine nucleotides from rbc with time but the overlapping kinetics of ADP formation from ATP and ADP degradation to AMP and adenosine have made determination of the effective ADP concentration during aggregation difficult. A total ATP plus ADP concentration of 0.2 μM has been reported after passage of WB through a glass bead column (McPherson et al., 1974). Since the ratio of ATP:ADP was 1.6:1, and that in rbc is 10:1 (Bishop, 1961), it is possible that the ATP and ADP were released from platelets.

(b) Platelet Aggregation on Natural and Artificial Surfaces

This thesis is concerned specifically with ADP-induced platelet aggregation in flowing suspensions; however, any consideration of platelet aggregation in vivo must also include interactions of platelets with the vessel wall. From a pathological standpoint, the growth of mural thrombi and their subsequent embolization through disruption of platelet-platelet bonds is at least as important as that of platelet-surface bond disruption (Scarborough, 1971). Although the initial adhesive events of thrombus formation are independent of the subsequent platelet-platelet cohesive events mediating thrombus growth, the latter interactions are likely similar to those of platelets aggregating in suspension. Analogous to

platelet aggregation in suspension, the rate and extent of platelet aggregation on surfaces is dependent upon the rate of reaction of platelets with the surface and the conditions of flow. The reaction rate is influenced by the nature of the surface and the localized concentration of platelet agonists released from platelets, rbc, and wbc. Flow rate controls the concentration of reactants at the surface and determines the arrival rate of platelets, a process that is greatly augmented by rbc. At sufficiently high flow rates, the magnitude of the shear stress controls the removal rate of platelets interacting with the surface. Finally, thrombus height is also limited by the flow rate since small increases in height produce large increases in shear stress at the thrombus surface. In the following discussion, the central role of blood flow rate in determining thrombus growth through the arrival rate of new platelets and the time available for surface interaction, as well as the force removing platelets interacting with the thrombus and the convection of ADP downstream, is considered. Through this discussion it will be revealed that the process of thrombus formation is a dynamic continuum from initial platelet adhesion through to aggregation and embolization involving spatial and temporal interactions between surfaces, cells and humoral factors.

(1) Artificial surfaces: The properties of artificial surfaces that control thrombus formation and blood coagulation have received much attention (Mason, 1971). In vitro, the reactivity of a surface to platelets is primarily controlled by its ability to induce platelet aggregation rather than just adhesion (Salzman, 1963). Efforts to describe a universal quality that predicts the degree of thrombogenicity

have focused on surface free energy and critical surface tension by extension of Lampert's (1931) rule that wettability by water is inversely proportional to the clotting time. Nyilas et al. (1975) found that thrombogenicity increased in proportion to the contribution of polar forces to the composite surface free energy. However, no single parameter seems to dictate the compatibility of a given material with blood. In general, surfaces that are more hydrophilic or have equal numbers of positive and negative charges are more compatible.

Exposure of native (nonanticoagulated) blood to artificial surfaces results in platelet adhesion that is mediated by the prior adsorption and subsequent alteration of plasma proteins, particularly fibrinogen (Petschek et al., 1968; Dutton et al., 1968; Baier and Dutton, 1969; Zucker and Vroman, 1969). In the absence of prior activation, platelets initially form a monolayer on surfaces such as glass, polyurethane, and nylon with the rate of adhesion proportional to shear rate for $G_w < 100 \text{ s}^{-1}$ (Petschek et al., 1968; Nyilas et al., 1975). The parallel adhesion of wbc during the initial platelet adhesion ceases at a critical shear rate ($G_w < 20 \text{ s}^{-1}$), depending on the nature of the surface involved. In these studies blood flowing from the severed carotid artery of a dog impinged upon the test material and was deflected radially across the surface. The surface shear rate increased with increasing radial distance from a stagnation point located at the center of the impinging fluid. Thus, as the flow rate increased the limiting shear rate for adhesion moved closer to the stagnation point causing the outer radius of the adherent wbc ring to decrease.

Although the initial events of platelet adhesion appear to be independent of the surface material (Friedman et al., 1970), the degree of subsequent thrombus growth is not. When large thrombi form, they appear to originate from sites of surface inhomogeneities (AVCO Everett Research Lab., 1972). Platelet thrombi develop a characteristic wedge-shaped profile with the upstream edge higher than the downstream edge. Platelets contacting the upstream edge are often pushed downstream, but remain attached causing the thrombus to grow primarily downstream. The surface which was formerly covered with a monolayer of platelets becomes covered with numerous localized thrombi separated by large areas devoid of platelets. Despite frequent total or partial embolization of the thrombus, a fibrin mesh eventually develops on the downstream surface in which rbc and wbc are trapped.

In an effort to separate aggregation from adhesion in a growing thrombus, Grabowski et al., (1978) induced aggregation by infusing ADP into flowing citrated, canine blood through a synthetic membrane onto which a standardized layer of adherent platelets had been preformed. The repeated growth and embolization of surface aggregates was proportional to the ADP concentration. At millimolar ADP concentrations, the growth rate prior to embolization increased monotonically over the range $99 < G_w < 986 \text{ s}^{-1}$. In the micromolar range of ADP, aggregate growth decreased beyond $G_w = 394 \text{ s}^{-1}$. Aggregation was enhanced by the formation of a region of disturbed flow downstream of the leading edge of the aggregate when aggregate size exceeded $50 \mu\text{m}$. As will be discussed in more detail in another section, low shear rates and long residence times in zones of recirculation allow longer times for platelet activation and

promote platelet adhesion and aggregation. The repeated embolization of aggregates at a critical size and/or lifespan indicates that platelet-platelet interactions are stronger than platelet-surface interactions under the above conditions. In the above range of shear, wbc were not observed to adhere.

(ii) Natural surfaces: The intact endothelium is nonthrombogenic but removal of the endothelial cells exposes a highly thrombogenic surface. The nonthrombogenic activity of endothelium has been ascribed to heparan sulfate in the endothelial cell glycocalyx (Wechezak et al., 1975) and to prostacyclin produced by these cells (Moncada et al., 1975; Weiss and Turitto, 1979). There is evidence to suggest that collagen is the principal component of the vessel wall that stimulates platelet adhesion and aggregation (Baumgartner, 1977). Washed platelets exhibit greater aggregation and release on collagen-coated glass than on fibrinogen- or fibronectin-coated glass, while adhesion on albumin-coated glass is inhibited (Adams and Feuerstein, 1980). Platelets have been observed to adhere to fibrillar structures of the subendothelial matrix of cultured endothelial cells that remain after the cells have been removed by treatment with 0.5% Triton X-100 detergent (Sakariassen et al., 1983). In heparinized blood, platelets initially adhere randomly to glass tubes coated with type I collagen in a manner similar to that on artificial surfaces (Adams et al., 1983) but in the former case have been reported to adhere preferentially along the collagen fibrils (Sakariassen et al., 1983). Although platelet adhesion to collagen is virtually instantaneous, a 15 - 30 s lag precedes aggregation, even under optimal conditions (Wilner et al., 1969). After several minutes, scattered aggregates are

separated by areas devoid of platelets. In the collagen-coated tubes of Adams et al. (1983), most aggregates had an elliptical base that grew predominantly downstream parallel to the direction of flow but also with some growth occurring transverse to the direction of flow. No embolization was observed at $G_w = 160 \text{ s}^{-1}$ while both the width and length of aggregates increased linearly with time with the arrival rate of platelets the rate limiting step. The release of ADP induced by collagen was probably sufficient to induce downstream aggregation after the failure of the initial contact upstream to establish stable bond formation. This also produced a migration of the center of the mass downstream.

Type I collagen should actually be considered a pseudo-artificial surface. Although collagen is a major component of the subendothelium, the basement membrane is composed mostly of type IV collagen (Miller, 1984) which is structurally and biochemically distinct from type I (Timpl et al., 1981; Schuppan et al., 1980). The subendothelium also contains several other glycoproteins such as elastin, laminin (Terranova et al., 1980), and fibronectin (Jaffe, 1978; Yamada, 1978), and glycosaminoglycans such as heparan sulfate and hyaluronic acid that are not present on a collagen coated tube.

Baumgartner and coworkers have systematically investigated the effect of shear rate on platelet adhesion and aggregation on exposed subendothelium. Everted rabbit abdominal aortae completely denuded of endothelium in situ by balloon catheter formed the inner core of an annular perfusion chamber through which blood flowed at controlled rates

(Baumgartner, 1973). This group considered platelets in contact with, and/or spread upon, the subendothelium as platelet adhesion, and thrombus growth as platelet aggregation. For citrated human blood (cWB) at $G_w < 650 \text{ s}^{-1}$, increasing the shear rate increased the rate of adhesion but for $G_w > 800 \text{ s}^{-1}$, the rate of adhesion was independent of shear rate (Turitto et al., 1980). Thrombus growth was negligible below $G_w = 200 \text{ s}^{-1}$ but beyond this shear rate, the rate and extent of thrombus growth increased with increasing shear rate up to $G_w = 10,000 \text{ s}^{-1}$. Thrombus growth reached a maximum within 5 - 10 min but was transient and only a monolayer of platelets covering the entire surface remained after 40 min.

In native blood (nWB) at physiological $[\text{Ca}^{2+}]$, thrombus size was much larger than in cWB and increased over the range $650 < G_w < 3300 \text{ s}^{-1}$ (Baumgartner et al., 1980; Turitto et al., 1980). After 2 - 3 min perfusion, the thrombi in nWB also extended well into the annular space above the subendothelium and were irregularly shaped with large overhanging projections in contrast to the smaller more streamlined thrombi in cWB. Numerous wbc were observed to adhere in nWB but never in cWB. Fibrin covered 30% of the subendothelium at $G_w = 650 \text{ s}^{-1}$ but coverage decreased to 0% at $G_w = 3300 \text{ s}^{-1}$ emphasizing that fibrin formation is not important for platelet aggregation at high shear rates. As expected the adhesion and aggregation of platelets from patients afflicted with classical hemophilia were the same as that of platelets from normal subjects in both cWB and nWB at all shear rates (Weiss, et al. 1978). These patients had normal levels of fibrinogen, factor VIII von Willebrand's factor (FVIII:vWF), and factor VIII antigen but no factor VIII procoagulant activity, i.e., the inability to form fibrin.

(iii) Intravascular platelet aggregation: Thrombus growth is characterized by a first order rate constant (Begent and Born, 1970). Iontophoretic application of ADP to small venules (40 - 70 μm) in the hamster cheek pouch yielded a maximum growth rate prior to embolization at mean blood velocities of 0.30 - 0.40 mm s^{-1} , independent of vessel size. Higher velocities (0.60 - 2.50 mm s^{-1}) produced a decrease in aggregate growth rate which eventually levelled off, while no aggregates formed above 3.0 mm s^{-1} . The combination of short platelet-surface interaction times and high shear stress may have restricted aggregate growth, although the dilution of ADP at high flow rates may have limited the extent of platelet activation. The crucial role of ADP in in vivo aggregation is illustrated by the lack of thrombi in the absence of ADP.

The growth rate of thrombi produced within 10 min at the site of laser injury to rabbit ear chamber arterioles of 14 to 32 μm diameter was also first order and independent of blood velocity over the range 1 - 6 mm s^{-1} (Arfors et al., 1976). The maximum thrombus size prior to embolization was also independent of flow rate over the same range. Since shear rate increases linearly with flow rate for vessels of a given diameter, the constancy of thrombus size prior to embolization suggests additional factors control thrombus growth. For example, thrombus lifespan may be limiting since the age of each thrombus at the moment of embolization would be the same for a constant rate of growth.

Of the various in vivo techniques developed, all rely on some form of cell or tissue trauma to initiate thrombus formation. ADP initiated thrombus formation only in concert with mild endothelial cell

damage introduced by the method of iontophoresis. Although the source was not identified, ADP was also required for thrombus initiation after laser injury to rat mesenteric blood vessels (Seiffge and Kremer, 1986). The number of laser lesions required to induce thrombus formation was proportional to blood velocity in arterioles ($2 - 10 \text{ mm s}^{-1}$) but not in venules ($1 - 4.5 \text{ mm s}^{-1}$). Since more lesions were always required in the arterioles, the discrepancy between arterioles and venules is presumably due to the higher range of shear rate in the former, although it may be that the ADP is simply diluted more at the higher flow rates. The dilution of ADP may also account for the constant rate of thrombus growth and maximum size above blood flow velocities of $\sim 1 \text{ mm s}^{-1}$, despite a steady rise in shear rate. In the above studies, however, the shear rate and final ADP concentration could not be precisely determined. Where measurements of shear rate have been made, the time to initiate platelet aggregation in injured mouse cerebral microvessels increased with increasing wall shear rate over the range $200 < G_w < 1400 \text{ s}^{-1}$ (Rosenblum and El-Sabban, 1982). It still remains, however, that the release of chemical mediators invoked by the non-specific tissue damage used in this study may be increasingly diluted as a function of flow rate. It should be noted that such in vivo studies do play a vital role in the visualization of thrombus formation qualitatively in terms of the response to various stimuli, inhibitors and cofactors.

(c) Factors Controlling Platelet Aggregation on Surfaces

Classical mass transport theory has been used to explain platelet adhesion and aggregation on surfaces in terms of the arrival rate of platelets and the reaction rates for adhesion and aggregation. (Turitto

et al., 1980). Platelets in the bulk of flowing suspensions are brought into the vicinity of a reaction site by fluid convection. In the absence of rbc, secondary flow or turbulence, cells travel on streamlines parallel to the surface and thus cannot reach a fluid-solid interface by convection alone. The interaction of platelets with a surface is controlled by Brownian diffusion. The sum of the two processes, known as convective-diffusive transport, controls the rate of platelet transport to a unit area of surface, or platelet flux. At low shear rates, the rates of adhesion and aggregation are primarily dependent on platelet flux and this is called the diffusion-limited case. Mass transport theory predicts a flux of platelets to the surface that increases with increasing shear rate to the power 0.33. At high shear rates the rate of reaction of platelets with the surface limits the rate of adhesion and this is called the reaction-limited case. The adhesion and aggregation reaction of platelets at the surface is modeled by a first order reaction. Different reaction rate coefficients would be expected for adhesion and aggregation.

However, as pointed out by Turitto (1982) care must be taken in not overextending the mass transport theory when considering platelet adhesion and aggregation, particularly at high shear rates. Here the theory does not take into account the short platelet-surface interaction times, the shear-induced activation of platelets, high shear stresses preventing stable bond formation, and platelet detachment kinetics. Short platelet-surface interaction times at high shear rates may limit the rate of adhesion for a finite reaction rate. The high platelet flux to the surface would counteract this effect producing an adhesion rate apparently

independent of shear rate. The effects of short interaction times and the shear-dependent stability of platelet bonds can generally be accounted for by a decrease in the reaction rate coefficient with increasing shear rate, as indeed found by Turitto et al. (1980). The shear-induced activation of platelets and the release of ADP from aggregated platelets may serve to increase the reaction rate coefficient for aggregation compared to adhesion. It may also be that, once formed, the platelet-platelet bond is stronger than the platelet-surface bond and able to withstand high shear stresses. This is evident by the tendency of aggregates to form at inhomogeneities on artificial surfaces (AVCO Everett Research Lab, 1972), to roll up on or peel off of surfaces (Grabowski et al., 1974), and to embolize completely in vivo rather than fragment at high flow rates (Begent and Born, 1970; Arfors et al., 1976). The relative strength of the adhesion and aggregation forces would depend on the nature of the surface and its ability to activate adherent platelets (Adams and Feuerstein, 1980). Finally, the platelet flux to an aggregate protruding into the vessel lumen would be expected to be proportional to the flow rate and to the cross-sectional area of the aggregate. Therefore, aggregate growth rate would not be as limited by diffusional mechanisms as would be adhesion onto a flat surface by platelets travelling along streamlines parallel to the surface.

(i) Platelet transport: In cWB at $G_w < 650 \text{ s}^{-1}$, the rate of adhesion on subendothelium was found to increase with increasing shear rate due to the increase in platelet flux to the surface. Platelet flux was proportional to the 0.74 power of the shear rate as opposed to the 0.33 power predicted by theory (Turitto et al., 1980). The enhanced arrival rate of platelets

was most likely due to the increased diffusivity of platelets in WB ($\propto G^{0.61}$) caused by the rbc. Red cells considerably increase the lateral dispersion of platelets (Turitto et al., 1972) leading to increased numbers of platelet collisions with (Goldsmith, 1972), and higher platelet concentrations near (Tangelder et al., 1982; Tangelder et al., 1985; Corattiyi and Eckstein, 1986), the vessel wall. Adams and Feuerstein (1981) also found that the rate of platelet accumulation at physiological $[Ca^{2+}]$ at the entrance of a collagen-coated glass tube was proportional to the shear rate raised to the exponent 0.77 for $G_w < 320 \text{ s}^{-1}$. At $G_w > 800 \text{ s}^{-1}$, the rate of adhesion on subendothelium was found to be independent of shear rate and was presumed to be limited by a finite rate of reaction of platelets with the surface (Turitto et al., 1980). Between $G_w = 650$ and 800 s^{-1} , there was a transition from predominantly diffusion-controlled to predominantly reaction-controlled adhesion.

In contrast, the aggregation of platelets on the above-mentioned surfaces was limited only by platelet flux. In cWB the rate of thrombus growth on subendothelium increased with increasing shear rate up to $G_w = 10,000 \text{ s}^{-1}$ (Turitto et al., 1980). The rate and extent of aggregation was even greater in nWB at physiological $[Ca^{2+}]$ (Baumgartner et al., 1980). Thus, surface aggregates can withstand shear stresses that induce platelet activation and release, and impede aggregate growth in suspension (Dewitz et al., 1978). The increase in aggregation at high shear rates in the absence of increased adhesion suggests that the reaction-rate coefficient of the former is greater. Adhesion in cWB appeared to be greater than in nWB but this was likely due to the scavenging of free platelets by the rapidly growing thrombi in nWB. The

formation of large aggregates separated by areas devoid of platelets is a common feature of aggregation on artificial surfaces (AVCO Everett Research Lab., 1972), collagen (Adams and Feuerstein, 1980; Adams et al., 1983), and subendothelium (Baumgartner et al., 1980). Rapid aggregate growth at these foci may deplete the surface platelet concentration sufficiently to inhibit thrombus growth at other sites in the immediate vicinity. On less reactive surfaces, such as fibrinogen and fibronectin, platelet aggregation is diminished and adhesion is more diffuse over the entire surface (Adams and Feuerstein, 1980). The exponential growth of aggregate volume at a constant flow rate in vivo (Begent and Born, 1970; Arfors et al., 1976) reflects the increase in platelet flux to the aggregate surface that is in proportion to the cross-sectional area of the aggregate. However, above blood flow velocities of $\sim 1 \text{ mm s}^{-1}$ in arterioles, thrombus growth was independent of flow rate and likely limited by the rate of reaction of platelets (Begent and Born, 1970; Arfors et al., 1976; Seiffge and Kremer, 1986). Since the platelet flux is proportional to the flow rate, the fraction of platelets participating in thrombus growth must have decreased with increasing flow rate. This may be interpreted as a decrease in collision efficiency (as defined below) with increasing flow rate mediated in part, perhaps, by the increased dilution of ADP and a decreased reaction rate coefficient.

The reaction rate coefficient has been found to depend upon $[\text{Ca}^{2+}]$ which is an essential cofactor for both adhesion and aggregation. The coefficients in cWB where the $[\text{Ca}^{2+}]$ is depressed are lower than those in nWB (Baumgartner et al., 1980; Turitto, et al., 1980). This hypothesis was substantiated by increasing the citrate concentration further and

lowering $[Ca^{2+}]$ even more. Adhesion was inhibited at $G_w > 650 \text{ s}^{-1}$ and thrombus formation was abolished at all shear rates. In normal cWB where $[Ca^{2+}] \sim 50 \mu\text{M}$, the $[Ca^{2+}]$ is sufficient to maintain normal adhesion but diminished aggregation. Thus, the aggregation rate coefficient is more sensitive to low $[Ca^{2+}]$ than the adhesion rate coefficient which appears to be independent of $[Ca^{2+}]$ at low shear rates.

(ii) Platelet ADP: Since platelet shape change is generally considered a prerequisite for platelet aggregation in suspension in vitro (Frojmovic and Milton, 1982; Milton and Frojmovic, 1984), it is assumed that shape change must precede platelet aggregation on a mural thrombus. A concentration of ADP at the thrombus surface is required that would induce platelet shape change within the short time available for a passing platelet to become activated and adhere. The induction of aggregation by ADP infusion and its absence without the infusion of ADP both in vivo (Begent and Born, 1970) and in vitro (Grabowski et al., 1978), as well as the inhibition of spontaneous aggregation on both glass (McPherson et al., 1974) and collagen (Tschopp and Baumgartner, 1976) by enzymes that degrade ADP, strongly suggest that ADP is the critical agent mediating aggregation. Furthermore, preincubation of platelets with aspirin which prevents the prostaglandin-mediated release of platelet ADP almost completely inhibits platelet aggregation on subendothelium (Weiss et al., 1975) and collagen (Muggli et al., 1980) but not adhesion. These results also show that platelet activation is a prerequisite for platelet aggregation on surfaces, and that in flowing suspensions ADP concentrations at surfaces are sufficient to activate newly arriving platelets in time for them to form stable bonds.

In the absence of significant shear-induced platelet activation or leakage of adenine nucleotides from rbc through lytic or sublytic injury, the ability of a surface to induce the release of endogenous platelet ADP would determine the rate and extent of thrombus growth and hence the degree of thrombogenicity. At low shear rates, the formation of thrombin in native (nonanticoagulated) blood through the activation of factor XII and the intrinsic coagulation cascade would greatly augment the extent of platelet release and, independently, the degree of thrombogenicity through fibrin formation. However, high localized ADP concentrations are necessary to support aggregate growth at high shear rates due to the rapid convection of platelets away from the thrombus surface.

Adams and Feuerstein (1981) have shown that the surface concentration of ADP produced by porcine platelets aggregating on collagen-coated glass tubes is at least sufficient to induce shape change. Calculations show that the concentration of ADP ranged from $0.6 \mu\text{M}$ at $G_w = 80 \text{ s}^{-1}$ to $1.8 \mu\text{M}$ at $G_w = 320 \text{ s}^{-1}$ at the surface, but decreased dramatically with increasing distance from the surface. The higher ADP concentration at higher shear rates was caused by a higher rate of accumulation of platelets. At all shear rates platelet accumulation was observed to decrease exponentially from tube entrance to exit (Adams and Feuerstein, 1980). It was also found that the percent release of ADP by platelets increased with increasing distance downstream so that the surface ADP concentration remained relatively constant along the length of the tube. The depletion of platelets near the wall due to initial aggregation at the tube entrance may have accounted for the reduced aggregation downstream while the synergistic action of released ADP

convected downstream and the release induced by collagen could have been responsible for increased platelet release downstream.

The maximum surface shear rate in this work was below the level at which Grabowski et al. (1978) observed a decrease in the rate of aggregation at the same [ADP]. Grabowski et al. attributed the decrease in aggregation at micromolar ADP to an increase in the dilution of ADP at high flow rates. Even though at millimolar ADP the surface [ADP] also decreased with increasing shear rate, it remained sufficiently suprathreshold so as not to limit the aggregation reaction. Thus, at the threshold range of [ADP] for shape change, aggregation and release in suspension, the rate of reaction is limited by the degree of platelet activation. This is reflected in a rate of aggregation that is reaction-limited at lower shear rates. Grabowski and coworkers calculated a reaction time of only 0.2 s, in keeping with estimates of the reaction time for ADP-induced aggregation in vivo from Begent and Born's data (Grabowski and Leonard, 1973; Richardson, 1973). The reaction times seem reasonable for ADP-induced aggregation since Gear (1984) has detected shape change within 0.5 s exposure to ADP or thrombin. Thus, as the shear rate increases and the interaction time decreases, the rate of aggregation is severely limited by a finite reaction rate at low [ADP]. At high [ADP], the reaction rate coefficient is so high that the rate of aggregation is still diffusion-limited at $G_w = 1000 \text{ s}^{-1}$.

(iii) Interaction time: Born (1980) has argued that the interaction time of platelets with the wall of a severed arteriole could be as short as 10 ms. This is not likely to inhibit adhesion since Adams and Feuerstein

(1980) have demonstrated stable adhesion on collagen after interaction times of less than 33 ms, but these reaction times are more than an order of magnitude shorter than those measured for platelet shape change. Since platelets aggregate without delay, one must postulate a faster shape change than can be measured presently, longer interaction times, or a mechanism of aggregation that is independent of prior platelet activation. Gear (1984) has shown that the rate of shape change is greatly accelerated by the synergistic action of adrenalin. The synergistic action of other platelet agonists such as serotonin and thromboxane A₂ that are released from platelets in concert with ADP should also support a much faster rate of platelet activation and a shorter reaction time. In the same severed arteriole mentioned above, a sudden increase in blood flow velocity through the open end can result in wall shear stresses up to $\tau_w = 10^4 \text{ N m}^{-2}$, particularly if the vessel lumen is reduced by the encroaching platelet plug. As discussed previously, such shear stresses are capable of inducing platelet activation and release in PRP in less than one millisecond. Thus, the synergism of chemical and mechanical stimulation could be sufficient to activate platelets rapidly enough to promote aggregation. In such cases the reaction rate coefficient would be very high. An increase in the radial velocity component of platelets caused by the motion of rbc may also increase the interaction time.

Fibrinogen is required for ADP- or collagen-induced platelet aggregation in suspension, yet washed platelets aggregate on collagen-coated surfaces without added fibrinogen (Adams and Feuerstein, 1980). In one patient with congenital afibrinogenemia with normal levels of factor VIII and vWF, adhesion onto subendothelium was normal in nWB and

slightly greater in cWB (Weiss et al., 1978). Surprisingly, thrombus formation in nWB was normal up to $G_w = 3300 \text{ s}^{-1}$ but strongly inhibited in cWB at $G_w = 1300 \text{ s}^{-1}$. It is likely that fibrinogen is released from the α -granules of adherent platelets but fibrinogen-independent mechanisms of aggregation have been proposed. If these mechanisms do not require the mutual exposure of otherwise latent adhesive membrane receptors, such as GP IIb-IIIa for fibrinogen binding, on single platelets and aggregates, then aggregation could be induced through changes in only the membrane of the adherent or aggregated platelets that permit binding of unactivated platelets.

(d) Pathological Consequences of Free-Flowing Platelet
Aggregates

At high shear stresses direct platelet activation and/or damage in the bulk of sheared suspensions dominates the process of shear-induced aggregation. This may be true of devices in which a uniform shear field is generated but one would expect the shear-induced activation of platelets in suspension in cylindrical vessels to be greatest near the wall where the shear stress is maximal. Average wall shear stresses in the intact microcirculation ($\tau < 4 \text{ N m}^{-2}$; Lipowsky and Zweifach, 1977) are below the threshold for platelet activation, regardless of exposure time. This is in agreement with the relative absence of thrombotic processes originating in the microvasculature (Turitto, 1982). Platelets are exposed to shear stresses that may be as high as 100 N m^{-2} at the surface of normal cardiac valves but for only 1 - 10 ms (Roschke and Harrison, 1977), which is below the threshold for activation. Peak shear stresses in the aorta and the coronary artery during systole have been estimated to

range from 15 to 35 N m^{-2} (Ling et al., 1968; Atabek et al., 1975; Benson et al., 1980) but the duration of this level of shear would not be sufficient to activate platelets. In diseased arteries, however, where the vessel lumen is reduced, such as caused by the intimal thickening of atherosclerosis, the fluid shear stress through this region increases in proportion to the cube of the reduction in vessel diameter, for a constant rate of flow (May et al., 1963; Young et al., 1975). In a multiply stenosed coronary artery that is ~50% occluded, the maximum shear stress at the apex of the stenotic plaque has been estimated to exceed $\tau = 40 \text{ N m}^{-2}$ (Back et al., 1977). Even though this shear stress is sufficient to remove endothelial cells from the vessel wall (Fry, 1968), it is considered insufficient to induce platelet activation due to the short particle transit times past this surface (Born, 1980; Hellums and Hardwick, 1981). However, if only a few platelets are activated and these cells are subsequently trapped within a zone of recirculation immediately downstream of the stenosis (Karino and Goldsmith, 1979a) then localized aggregation may be promoted. In general, in areas of flow separation such as occur at mural stenoses, bifurcations, or in the carotid sinus, there is a region of high shear stress and short exposure time in close proximity to one or more zones of recirculation where relatively low shear stresses but long particle residence times exist (Turitto, 1982; Goldsmith and Karino, 1979). In many cases these regions are connected by fluid streamlines (Yu and Goldsmith, 1973; Karino and Motomiya, 1984; Karino, 1986) so that cells activated by high shear stress can be subsequently delayed for one or more orbits in a zone of low shear stress but with sufficiently high collision frequency to promote aggregation. Since all vortices studied to date in the human circulation at physiological flow

rates are open (Karino, 1986), any aggregates formed would be eventually shed downstream. Free-flowing aggregates have been experimentally produced and shed from a zone of recirculation in an ex vivo flow device (Morton et al., 1975). Thus, diseases that increase the shear-induced activation of platelets such as through vessel narrowing may enhance the formation of free-flowing platelet aggregates.

An increase in the fraction of completely degranulated platelets in the peripheral blood of patients following coronary bypass surgery indicates that activated platelets do circulate (van Oost et al., 1983). The reported circulation of platelet aggregates in patients predisposed to chronic thromboembolic disease (Wu and Hoak, 1974), however, has been attributed to an artifact of the isolation of the cells (Kohanna et al., 1984). The absence of circulating aggregates is not surprising since they would have been expected to be filtered out by the first microcirculatory bed encountered. In the case of the sudden onset of an acute vascular crisis, the origin of occlusive aggregates should be immediately upstream of the microcirculatory bed concerned. Indeed the visual disturbances experienced by patients suffering transient ischemic attacks has been attributed to platelet emboli travelling through the retinal vessels (Gunning et al., 1964; Pickering, 1968). Platelet aggregates intermittently shed from upstream carotid artery vortices may well be the source of these emboli.

It should be mentioned that platelet emboli shed from mural thrombi located preferentially in, or immediately downstream of, zones of recirculation (Karino and Goldsmith, 1979b; Mitchell and Schwartz, 1963;

Packham et al., 1967) could also contribute to free-flowing aggregates. However, the cause of the platelet adhesion, whether mediated by shear-activation or vessel wall alteration remains to be established. Certainly, in the majority of cases of acute myocardial infarction, the rupture of a pre-existing stenotic atherosclerotic plaque precedes subsequent coronary artery occlusive thrombosis, involving predominately platelets (Falk, 1983). The extent of occlusion is highly dependent on the degree of pre-existing vessel narrowing. Below 70% narrowing, plaque rupture rarely precipitates complete occlusion. The avid adhesion of platelets to the ruptured plaque is enhanced by a high rate of delivery of cells, while high shear stresses across the surface of the plaque may be sufficient to activate passing platelets. The size of recirculation zones immediately downstream of the rupture may determine the extent of ensuing thrombosis through a combination of relative stasis allowing fibrin formation and trapping of platelets promoting aggregation.

The obvious importance of free flowing platelet aggregates, independent of pre-existing mural thrombi, is demonstrated by their effects on the cerebral and myocardial circulation, and on the circulation through various microcirculatory beds. In the absence of significant cerebrovascular disease, transient ischemic attacks may be induced by hyperresponsive platelets (Al-Mefty et al., 1979). It is known that platelet emboli resulting from cardio-pulmonary bypass are responsible for significant neuropathological damage (Hill et. al., 1969). In the case of fatal myocardial infarction in the absence of detectable upstream atherosclerotic lesions or mural thrombi, the fraction of subjects displaying intravascular platelet aggregation in the coronary circulation

at autopsy (Jorgensen, 1967) is similar to that of pigs in which myocardial infarction was induced up to 2 hours after intra-coronary ADP injection (Jorgensen et al., 1967). The absence of such aggregates in all subjects examined may reflect the transient nature of these aggregates which are not stabilized by fibrin and are easily disrupted, but which may survive long enough to cause ischemia and ultimately infarction.

The high shear stresses ($\tau > 10^3 \text{ N m}^{-2}$) over the surface of prosthetic cardiac valves at exposure times between 1 - 10 ms (Roschke et al., 1975) are capable of damaging platelets, and perhaps even more so, red cells. A major complication of extracorporeal circulation is end organ dysfunction caused by platelet emboli. In a simulation of extracorporeal circulation using native canine blood exposed to polyurethane, a zone of recirculation was placed downstream of the initial blood-surface contact (Morton et al., 1975). The combination of platelet surface interaction causing ADP release and the activation of coagulation factors producing thrombin was sufficient to activate platelets and induce aggregation in, and repeated embolization from, the zone of recirculation. Conditions which lead to red cell trauma and the release of intracellular ADP from red cells (Harrison and Mitchell, 1966; Chambliss et al., 1950) have been purported to induce platelet aggregation, and these aggregates may in turn be responsible for both primary vessel wall damage (Mustard et al., 1977) and ischemia. The longer exposure times (0.1 - 1 s) to the lower shear stresses in extracorporeal circulatory devices can lead to greater platelet aggregation and destruction (Addonizio et al., 1979) in addition to platelet adhesion (Richardson et al., 1976), the degree of which is highly dependent on vessel geometry as just discussed.

(e) Summary

Shear stresses below $\tau \sim 5 \text{ N m}^{-2}$ do not activate platelets in suspension. Higher shear stresses can induce platelet activation and release culminating aggregation, the extent and stability of which depends on the magnitude of the shear field and the time of exposure to it. A graded response from aggregation through to lysis occurs within 10 s exposure to shear stresses between 5 and 60 N m^{-2} . Lower shear stresses are sufficient to produce similar effects after longer exposure times. At equivalent shear rates, rbc increase aggregate size, presumably through the ability to increase platelet diffusivity. The release of ADP from injured rbc also appears to greatly enhance aggregation but the relative contributions of mechanical forces and chemical stimulation are not clear.

The shear-induced activation of platelets in suspension can lead to free-flowing platelet aggregates in certain pathological conditions. Flow disturbances in vascular prostheses and extracorporeal circulatory devices in concert with surface activation may also promote the formation of free-flowing aggregates.

Aggregation on surfaces is controlled by the diffusional processes which determine the transport of platelets to a growing nidus of aggregation primarily through the shear-dependent mixing motion of red cells. The ability of a surface to induce platelet activation and release controls the rate of reaction between incoming platelets and the site of aggregation. The combination of very high shear stresses and potent chemical activation produce large reaction rate coefficients which do not appear to limit aggregation. Subendothelium is highly thrombogenic and, even in the absence of fibrin stabilization, surface aggregates can

withstand very high shear stress, at least transiently.

Platelet aggregation in suspension at physiological shear rates below those sufficient to induce activation ($G < 2000 \text{ s}^{-1}$), would be controlled by similar mechanisms through the frequency and efficiency of collisions between activated platelets. As will be discussed below, collision frequency is primarily determined by shear rate, and collision efficiency by fluid mechanical forces and platelet-platelet interaction times in relation to the degree of agonist-induced platelet activation.

COLLISION FREQUENCY AND EFFICIENCY

1. Theory

A two-body collision theory has been developed for neutral rigid spheres in shear flow (Smoluchowski, 1917; Goldsmith and Mason, 1967) and extended to interactions between charged colloidal size particles by van de Ven and Mason (1977) using an analysis of the particle trajectory (van de Ven and Mason, 1976a,b; Arp and Mason, 1977), and the DLVO theory of colloid stability (Derjaguin and Landau, 1941; Verwey and Overbeek, 1948). In dilute suspensions, particle velocity is equal to the undisturbed fluid velocity provided the particle is small in relation to the dimensions of the flow channel (Trevelyan and Mason, 1951; Goldsmith and Mason, 1962). Collisions between particles travelling on adjacent fluid streamlines at different velocities (Fig. 1) result in the formation of doublets, some of which are transient and separate after collision, while others are permanent (Takamura et al., 1979, 1981a,b; van de Ven, 1982). The binary collision frequency between unequal-sized rigid spheres in simple shear

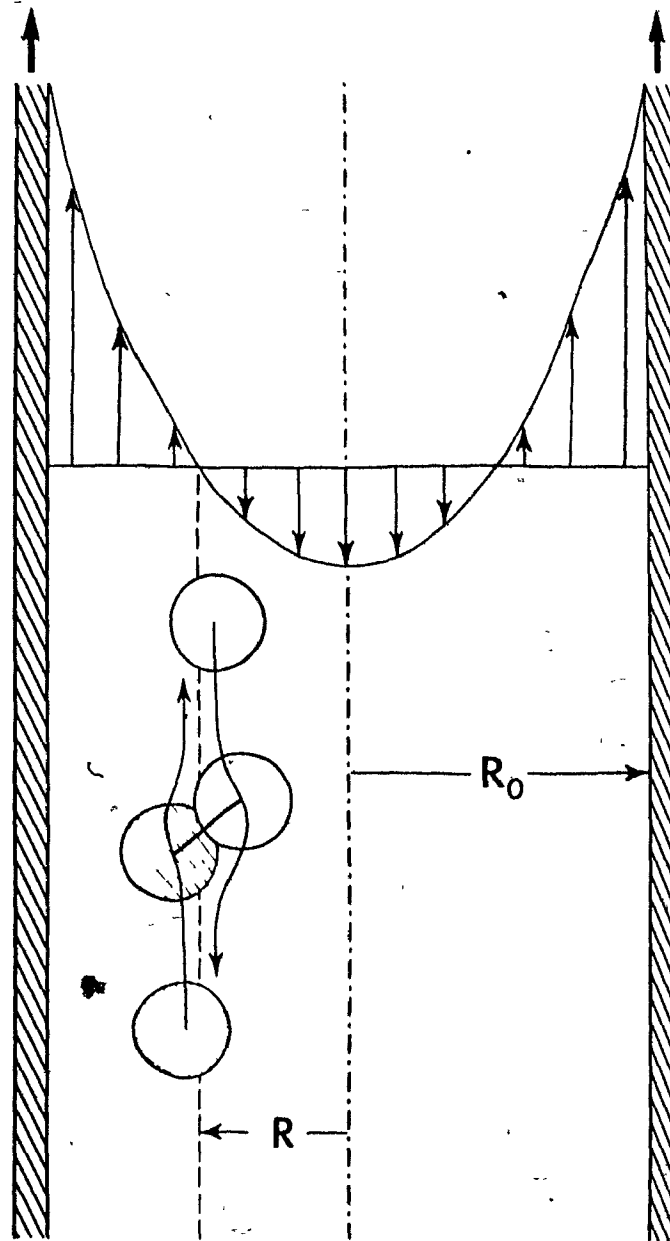


Figure 1: Two-Body Collision in Poiseuille Flow

Schematic in the median plane showing a collision between two rigid spheres travelling at different velocities through a tube of radius R_0 and separated by a radial distance $<$ one sphere diameter between sphere centers. The faster moving sphere nearer the tube center (unshaded) approaches and collides with a slower moving sphere near the tube wall (shaded). The slower sphere is shown travelling in the direction opposite to the faster sphere because the collision has been drawn with the axial velocity of the center of the collision doublet at radial position R fixed relative to the observer. This is equivalent to moving the tube upward with a velocity equal to but in a direction opposite to the fluid velocity at R , generating the parabolic velocity profile as shown.

flow is given by (Manley and Mason, 1955):

$$j_{12} = \frac{4}{3} G(b_1 + b_2)^3 N_2, \quad [1]$$

where j_{12} is the number of collisions experienced by a single sphere of radius b_1 with spheres of radius b_2 and number concentration N_2 . For monodisperse suspensions Eq. [1] reduces to (Smoluchowski, 1917; Manley and Mason, 1952):

$$j = \frac{32}{3} Gb^3 N, \quad [2]$$

where j is the two-body collision frequency for spheres of radius b and concentration N . Here, collisions are defined as the rectilinear approach of sphere centers to within a distance of $\leq 2b$.

Eq. [2] has been shown to apply in Poiseuille flow at any given radial position, R , in a tube of radius, R_0 , where the shear rate is given by:

$$G(R) = \frac{4Q}{\pi R_0^4} R, \quad [3]$$

and Q is the volume flow rate. The effect of unequal particle flux due to an unsymmetrical collision cross section caused by the curvature of the tube, as well as the nonlinear velocity profile, can be neglected providing $b/R_0 \ll 1$ (Goldsmith and Mason, 1964). The total number of two-body collisions per unit volume of suspension for equal-sized spheres can then be expressed as:

$$J = \frac{1}{2} Nj = \frac{4\phi GN}{\pi}, \quad [4]$$

where ϕ is the volume fraction of suspended particles. Because of the nonuniform shear field, the mean tube shear rate, $\bar{G} = 2Q/\pi R_0^3$, is used. The factor of $\frac{1}{2}$ is included because every collision involves two particles.

Equation [2] was originally derived by Smoluchowski in order to describe the kinetics of aggregating dispersions; however, it applies only to two-body collisions between equal-sized spheres and relies on purely geometrical arguments which neglect the influence of both interparticle and fluid mechanical forces. It also assumes that all collisions result in permanent doublet formation without subsequent break-up. Inclusion of the orthokinetic collision or capture efficiency, $\alpha_0 = j_c/j$, in Eq. [2], where j_c is the capture frequency, accounts for the influence of both interaction and hydrodynamic forces on particle capture (van de Ven and Mason, 1977). If $\alpha_0 = 1$, then $j_c = j$ and every collision results in capture; however, in the absence of attractive forces permanent capture is impossible (Brenner, 1961), although orbital pairs can exist (van de Ven, 1982). The addition of α_0 also relaxes the requirement of rectilinear approach since, theoretically, spheres can be captured from distances between sphere centers $> 2b$ ($\alpha_0 \rightarrow \infty$).

Assuming no aggregate break-up and neglecting the formation of higher order aggregates, the kinetics of aggregation are first order with respect to the total particle concentration, N_∞ (Swift and Friedlander, 1964):

$$\frac{dN_\infty}{dt} = -\frac{4\phi\alpha_0\bar{G}N_\infty}{\pi} \quad [5]$$

Integration of Eq. [4] yields:

$$\ln \frac{N_{\infty}(t)}{N_{\infty}(0)} = - \frac{4\phi\alpha_0 \bar{G}t}{\pi}, \quad [6]$$

where $N_{\infty}(0)$ and $N_{\infty}(t)$ are the total particle concentrations at time 0 and t , respectively. The total particle concentration decays exponentially and a plot of $\ln N_{\infty}(t)$ vs t should give a straight line, the slope of which yields α_0 . Thus, measurement of the total particle concentration over the early stages of aggregation provides a value for α_0 .

2. Model Particles

The collision efficiency of various colloidal dispersions has been measured over a range of suspension shear rate. Swift and Friedlander (1964) sheared 0.9 μm diameter polystyrene latex particles suspended in concentrated electrolyte over the range $1 - 80 \text{ s}^{-1}$ using a cylindrical Couette. They verified that the kinetics of shear-controlled aggregation are first order with respect to the total particle concentration. Based on the incorrect assumption of additivity of the independent collision rates due to Brownian motion and shear (van de Ven, 1982), Swift and Friedlander measured a combined collision efficiency (0.364) similar to that of Brownian motion alone (0.375), and independent of shear rate. However, as demonstrated by van de Ven and Mason (1977), calculation of α_0 from Swift and Friedlander's data over the range of shear rate where the influence of Brownian motion can be neglected ($20 < G < 80 \text{ s}^{-1}$), shows that the collision efficiency in fact decreases with increasing shear rate. Similarly, Curtis and Hocking (1970) found α_0 to decrease from 0.552 to 0.318 as shear rate increased from 1 to 112 s^{-1} , respectively,

for 2 μm diameter polystyrene latex spheres suspended in 0.15 M NaCl and sheared in a Couette viscometer. Zeichner and Schowalter (1977) also found a decrease in α_0 with increasing shear rate in Couette flow.

The measured values of α_0 in the above studies are likely maximal for a given shear rate since the high ionic strength of the suspensions used would minimize double layer repulsive forces acting between particles. According to the DLVO theory of colloid stability, doublet formation is the product of competition between relatively long range van der Waals attractive forces and double layer repulsive forces emanating from charged particles (Fig. 2). In the presence of sufficient repulsive forces, an energy barrier prevents close contact. Doublets formed at relatively large separations between surfaces are captured in a weak secondary energy minimum in which the particles can exhibit independent rotation and small changes in the separation distance during rotation. External forces causing collisions of energy sufficient to overcome the energy barrier form doublets firmly held in a primary energy minimum. Subsequent disruption of such doublets requires a much higher force than was required to form them due to the depth of this minimum. In the absence of double layer repulsion, no energy barrier exists and with only van der Waals attractive forces present, the particles would be mutually captured in a primary energy minimum.

In a study of orthokinetic aggregation in which both attractive and repulsive forces operate, van de Ven and Mason (1977) used a theoretical analysis of particle trajectories during collision to evaluate the boundary of the capture cross section. This is the limiting distance

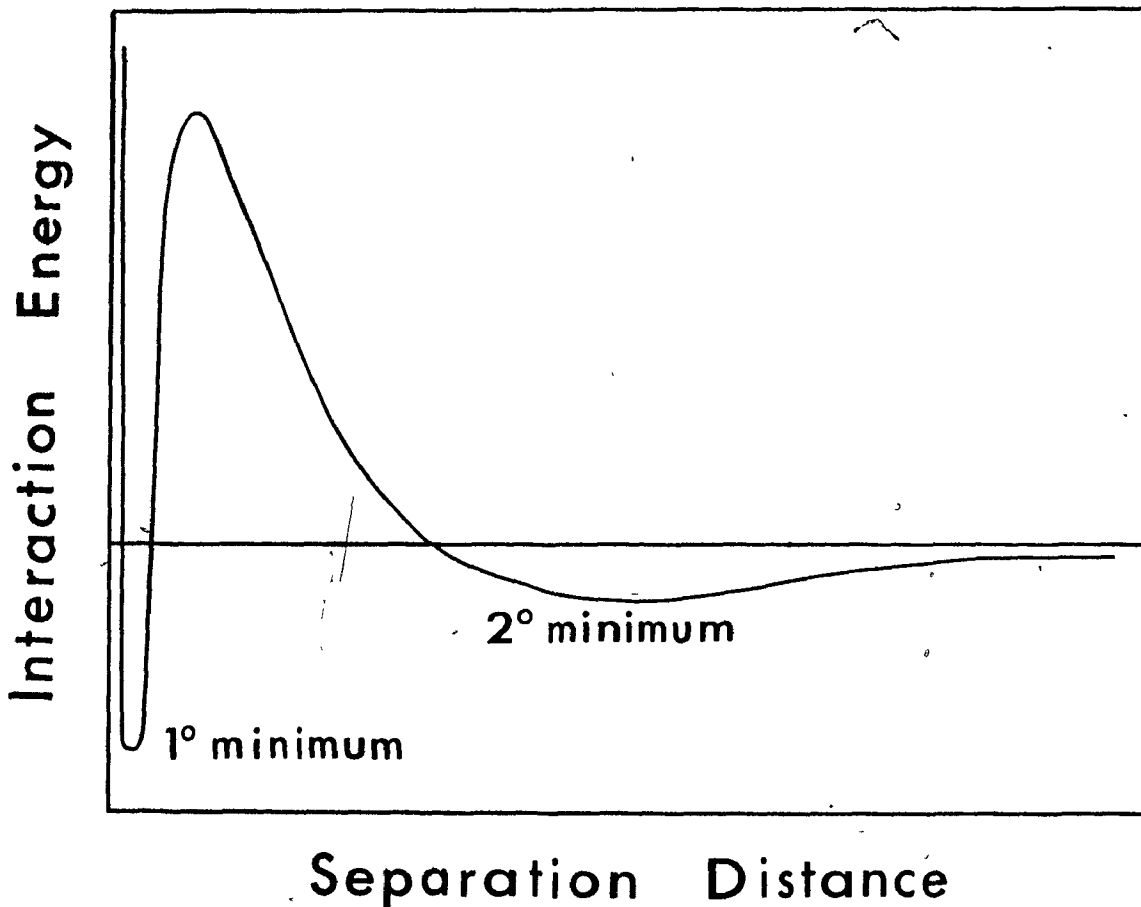


Figure 2: Interaction Energy vs. Separation Distance

Schematic representation of the interaction energy between two charged rigid spheres as a function of the distance of separation of their surfaces as described by the DLVO theory. Competition between repulsive forces due to overlapping of the electrical double layers of the spheres and relatively long range attractive van der Waals forces produces energy curves as shown. The depth of the primary energy minimum is governed by Born repulsive forces due to an adsorbed layer of water or counter ions (Stern layer) and by van der Waals forces. An energy barrier resists the approach of surfaces to a distance at which they could be captured in the primary energy minimum. At larger separation distances there is a smaller secondary minimum.

between sphere centers beyond which particle capture does not occur and which provides an estimate of α_0 . Van de Ven and Mason's calculations showed α_0 to depend principally upon shear rate, surface potential, Hamaker constant, ionic strength and particle size. When only attractive interaction forces operate between colliding particles, α_0 decreases with increasing shear rate. For 2 μm diameter polystyrene latex spheres in aqueous suspensions of high ionic strength, α_0 decreases from 0.56 to 0.10 over the range of shear rate from 1 to 9000 s^{-1} , respectively. It was also shown that, under these conditions, the capture frequency is actually proportional to $G^{0.82}$ and not G .

In the presence of double layer repulsive forces, the calculated α_0 follows a complex relationship with increasing shear rate due to a transition from particles captured in a secondary energy minimum to those captured in a primary energy minimum. Depending on the height of the energy barrier resisting primary doublet formation, α_0 suddenly decreases at a given critical shear rate which prevents secondary doublet formation. Much higher shear rates are required for the formation of primary doublets, at which point α_0 increases but subsequently decreases as the shear rate is further increased. Van de Ven and Mason (1977) also verified these predictions experimentally using the above mentioned spheres in 10^{-3} M KCl. At the critical shear rate of 16 s^{-1} , α_0 dropped from 0.45 to 0 and increased transiently at $G = 24 \text{ s}^{-1}$, but decreased thereafter.

3. Platelet-rich Plasma

Polystyrene latex spheres the size of human platelets suspended in

a medium of the ionic strength of plasma serve as a model for two-body interactions between platelets. Platelet-rich plasma at a volume fraction of $\sim 0.3\%$ is sufficiently dilute so as not to limit applicability of the two-body collision theory; however, the treatment of either unactivated or activated platelets as rigid spheres is at best a rough approximation. Although rigid, unactivated platelets are better characterized as oblate spheroids of axis ratio 0.36 (Frojmovic et al., 1976). Upon activation, the platelets undergo a morphological transformation to become roughly spherical and extend numerous pseudopods, depending on the degree of activation and the time of exposure to a given agonist (Frojmovic and Milton, 1982). Thus, no single shape adequately describes the wide spectrum of shape available to the platelet; however, the selection of a sphere has an obvious theoretical advantage and is more appropriate for the activated cells which are of most interest here. It should be noted that the presence of pseudopods would likely increase the effective collision cross section of a sphere of size equivalent to that of a platelet excluding pseudopods. Indeed, Brownian motion-controlled collision efficiencies greater than 1.0 have been found for human platelets exposed to $1 \mu\text{M}$ ADP (Frojmovic and Longmire, 1986). Such high collision efficiencies can be explained by considering the diffusional interactions between cells with 2 or 3 pseudopods of length from $2 - 3 \mu\text{m}$ (van de Ven, personal communication).

The DLVO theory of colloid stability has been successful in describing interactions between charged latex spheres; however, it is unable to predict the observed interactions between blood cells in plasma and physiological salt solutions. The measured electrophoretic mobility

of human platelets in isotonic saline at pH 7.4 was found to be $\sim 0.9 \mu\text{m s}^{-1} \text{V}^{-1} \text{cm}^{-1}$, corresponding to a net negative charge density of not less than 2900esu cm^{-2} (Seaman, 1967, Seaman and Brooks, 1970). At the high ionic strength of plasma or saline, the DLVO theory predicts that electrical double layer repulsion would extend only $\sim 1 \text{nm}$ from the surface of a platelet. This double layer thickness would allow the cells to approach close enough for the longer range van der Waals forces to capture them in the secondary energy minimum. A calculation using a model of a lipid bilayer coated with charged mucoprotein, when applied to platelets or red cells, shows that there is a secondary minimum with an interaction potential $\approx 100 \text{kT} \mu\text{m}^{-2}$ at a distance $5 - 8 \text{nm}$ from the surface, more than enough to hold cells together (Parsegian and Gingell, 1972). Yet, in the absence of fibrinogen cross-linking, neither platelets nor red cells aggregate in physiological salt solutions at normal pH. The failure of colloid stability theory to describe interactions between blood cells appears to be due mainly to the existence of the glycocalyx which extends up to 5nm into the medium and prevents the cells from forming aggregates (Parsegian and Gingell, 1972; Lerche, 1982). Only under nonphysiological conditions, such as low pH or low ionic strength, has aggregation between blood cells in saline been observed (Parsegian and Gingell, 1973; Lerche, 1982).

The aggregation of platelets is unlike that of inert spheres in that it involves an active, time-dependent exposure of specific receptor sites for binding fibrinogen monomers, which in turn cross-link the platelets in a manner analogous to polymer bridging (Takamura et al., 1981b). Thus, the interplay between van der Waals attraction and double

layer repulsion is likely secondary to high affinity receptor-ligand interactions and is only of significance during the earliest and latest stages of platelet activation when the magnitude of the receptor-mediated process is limiting. In light of this last consideration, values of α_0 are likely to be time-dependent and vary in proportion to agonist strength. Since the two-body collision theory is strictly applicable only to the early stages of the aggregation of dilute, monodisperse suspensions, any such measurements of α_0 in PRP should coincide with the period of maximum platelet activation.

Chang and Robertson (1976) used changes in the turbidity of suspensions of rabbit platelets after exposure to 10 μM ADP at 25°C to calculate a Brownian motion collision efficiency, 0.301, which remained constant over a period of 10 min and was similar to that determined by direct microscopic enumeration, 0.368. They also calculated the collision efficiency due to Brownian motion and shear together and obtained a value that was constant at 0.25. It is interesting that they assumed additivity of collision rates due to Brownian motion and shear, as did Swift and Friedlander (1964), and found the collision efficiency to be independent of shear rate over a similar range, $10 < G < 75 \text{ s}^{-1}$. It should be noted that all measurements of collision efficiency were preceded by both a 10 s premixing period and subsequently, at least 30 s of increased suspension turbidity attributed to shape change. Thereafter the collision efficiency remained constant for up to 10 min, the maximum time tested. This is surprising considering that not only is platelet deactivation usually evident within this time but significant multiplet formation would be expected at the ADP concentration used and this would interfere with

measurements of α_0 .

Bell et al. (1984) measured α_0 for human platelets undergoing Poiseuille flow after exposure to 1 μM ADP at 22°C by microscopic enumeration of the doublet concentration. Although α_0 decreased from 0.140 to 0.011 between mean ADP exposure times of 74 and 175 s at $\bar{G} = 5.6 \text{ s}^{-1}$, the fraction of multiplets containing > 3 platelets increased from 6 to 11% over the same period. Since the incorporation of doublets into higher order multiplets would reduce the doublet concentration, and hence artificially lower α_0 , it was important to measure α_0 over short, but equivalent, reaction times. With the flow-through system employed, this was difficult at high shear rates; however, for reaction times < 30 s, α_0 decreased from 0.27 to 0.04 as the shear rate was increased from 7.9 to 54 s^{-1} (Bell and Goldsmith, 1984).

Aggregate growth was also found to follow the kinetics predicted by Smulochowski (1917) wherein there is a continuous rise and fall in the concentration of aggregates of successively increasing size, and a tandem decrease in the single and total particle concentration. As much as 60% of the platelets had aggregated within one minute and it is likely that the extent of aggregation would increase further with longer exposure times.

The problem of the time-dependency of α_0 was specifically addressed by Belval and Hellums (1986) who used a sophisticated iterative procedure to continuously model the shape of the evolving particle volume distribution of an aggregating platelet suspension. Values of α_0 were

systematically adjusted to generate the best fit curve to the experimentally determined distribution. An additional variable was also included to account for the aggregate void volume. Smoluchowski's theory treats all newly formed particles as spheres that are the product of the coalescence of two smaller colliding spheres, thus neglecting the influence of unoccupied spaces between rigid spheres on the resultant particle collision cross section. For activated platelets, which are not smooth spheres, this effect would be exacerbated (Born and Hume, 1967). The large average void volume fraction of 0.75 that gave the best fit indicates that most of an aggregate is empty space and/or of irregular shape (Belval and Hellums, 1986).

In the absence of exogenous agonist, the collision efficiency averaged over the first 60 s for heparinized PRP sheared in a cone and plate viscometer was 0 for $G < 2000 \text{ s}^{-1}$, in keeping with the lack of shear-induced platelet aggregation at this level of shear. Higher shear rates produced a rise in α_0 up to a maximum of 1.3×10^{-3} at $G = 5000 \text{ s}^{-1}$, which subsequently decreased to 0.7×10^{-3} at $G = 10,000 \text{ s}^{-1}$. Within 10 s at $G = 5000 \text{ s}^{-1}$, α_0 reached a maximum of 2.3×10^{-3} but decreased to 10^{-3} over the next 50 s.

The rise in α_0 over the range $2000 < G < 5000 \text{ s}^{-1}$ can be accounted for by an increasing level of platelet activation mediated through the shear-dependent release of platelet-derived agonists discussed earlier. However, beyond a maximum state of platelet activation, further increases in shear rate ($G = 10,000 \text{ s}^{-1}$) would only result in a higher fraction of inefficient collisions. Despite the lower collision efficiency, the

extent of aggregation observed at $G = 10,000 \text{ s}^{-1}$ was greatest. At this shear rate, the high collision rate can support an appreciable rate of aggregation, as found by Bell and Goldsmith (1984) at much lower shear rates for ADP-induced aggregation. It is unlikely that aggregate dispersal or platelet fragmentation would be significant at the short exposure times to this level of shear.

The decrease in α_0 beyond 10 s exposure to the shear field may represent platelet deactivation, the effects of which would be enhanced at high shear stresses. It is also possible that the collision efficiency is not independent of particle size as assumed in the analysis of Belval and Hellums (1986). Unequal-sized particles do not readily approach one another to within distances over which colloidal forces are appreciable (van de Ven, 1982). Consequently α_0 is smaller for interactions between unequal-sized particles and this would be of importance at high levels of aggregation. However, in the presence of absorbed polymers, aggregation rates for equal- and unequal-sized particles are comparable since polymer bridging can act over the minimum distance of approach between unequal-sized particles. In such cases, aggregates of equal-sized particles are more readily dispersed than those of unequal-sized particles by shear stresses that are capable of disrupting polymer bonds. Since fibrinogen cross-linking between activated platelets is analogous to polymer bridging, it is possible that α_0 is indeed independent of particle size at shear rates below those capable of breaking the fibrinogen-platelet bond.

4. Summary

None of the limiting assumptions of the two-body collision theory outlined above is inordinately strained by application of this theory to platelet aggregation. The aggregation of platelets is sufficiently different from that of model particles, however, to require additional explanation for the deviation from the inverse relationship between collision efficiency and shear rate that is predicted when attractive forces dominate. The induction of aggregation is completely different at low ($G < 54 \text{ s}^{-1}$) and high ($G > 2000 \text{ s}^{-1}$) shear rates studied thus far. At low concentrations of ADP, α_0 decreases rapidly with small increases in shear rate, yet its value remains above zero. This is important at high shear stresses, since extremely small collision efficiencies are sufficient to support a high rate of aggregation due to the high collision frequency. It also suggests the presence of a high shear-resistant, platelet-platelet bond that persists through shear rates that inhibit the formation of weaker bonds. The following experiments were, therefore, designed to examine platelet collision efficiency in the transition range, $55 < G < 2000 \text{ s}^{-1}$, as a means of verifying such a mechanism. At these shear rates, α_0 can be satisfactorily determined in Poiseuille flow using Eq. [6] provided an exogenous agonist is present and measurements are confined to the early stages of aggregation. Changes in α_0 with ADP exposure time require techniques which do not rely strictly on collisions between equal-sized particles, such as the population balance method of Belval and Hellums (1986).

RATIONALE

It has long been known that ADP is one of the principal mediators of platelet aggregation in stirred suspensions. Studies in vitro, ex vivo, and in vivo have also shown that ADP is crucial to aggregation in flowing blood. Much is known of the effects of high shear stress on platelets, particularly its ability to activate platelets and induce aggregation and release. However, much of the work at lower shear rates has not dealt specifically with the physiological range of shear, and have been concentrated in rotational viscometers where surface area-to-volume ratios are high. The in vivo work has remained comparatively qualitative in that ADP concentrations and/or shear rates were not precisely known. Thus, the present work is an investigation of the effect of shear rate on ADP-induced platelet aggregation over the full physiological range. An in vitro system was designed that allowed precise control over the [ADP] and the shear rate. A cylindrical vessel was also chosen to more closely mimic in vivo conditions. Within this range of shear rate, the effects of shear rate, [ADP], [Ca²⁺], and rbc are fully investigated and interpreted in terms of existing collision theory.

REFERENCES

- ADAMS, G.A., AND FEUERSTEIN, I.A. (1980). Visual fluorescent and radio-isotope evaluation of platelet accumulation and embolization. Trans. Am. Soc. Artif. Intern. Organs 26, 17-22.
- ADAMS, G.A., AND FEUERSTEIN, I.A. (1981). Platelet adhesion and release: Interfacial concentration of released materials. Am. J. Physiol. 240, H99-H108.
- ADAMS, G.A., BROWN, S.J., MCINTYRE, L.V., ESKIN, S.G., AND MARTIN, R.R. (1983). Kinetics of platelet adhesion and thrombus growth. Blood 62, 69-74.
- ADDISON, W. (1842). On the colourless corpuscles and on the molecules and cytoplasts in the blood. Lond. Med. Gaz. N.S. 1841/1842, 30, 144.
- ADDONIZIO, V.P., SMITH, J.B., GUIOD, L.F., STRAUSS, J.F., COLMAN, R.W., AND EDMUNDS, L.H. (1979). Thromboxane synthesis and platelet protein release during simulated extracorporeal circulation. Blood 54, 371-376.
- ALLARDYCE, D.B., YOSHIDA, S.H., AND ASHMORE, P.G. (1966). The importance of microembolism in the pathogenesis and of organ dysfunction caused by prolonged use of the pump oxygenator. J. Thorac. Cardiovasc. Surg. 52, 706-715.
- AL-MEFTY, O., MARANO, G., RAJARAMAN, S., NUGENT, G.R., AND RODMAN, N. (1979). Transient ischemic attacks due to increased platelet aggregation and adhesiveness. J. Neurosurg. 50, 449-453.
- ARFORS, K.-E., COCKBURN, J.S., AND GROSS, J.F. (1976). Measurement of growth rate of laser-induced intravascular platelet aggregation and the influence of blood flow velocity. Microvasc. Res. 11, 79-87.
- ARP, P.A., AND MASON, S.G. (1977). The kinetics of flowing dispersions. VIII. Doublets of rigid spheres (theoretical). J. Colloid Interface Sci. 61, 21-43.

- ATABEK, H.B., LING, S.C., AND PATEL, D.J. (1975). Analysis of coronary flow in thoracotomized dogs. Circ. Res. **37**, 752-761.
- AVCO EVERETT RESEARCH LABORATORY (1972). The fluid mechanics of thrombus formation. NASA Contractor Report. National Aeronautics and Space Administration, Washington, D.C.
- BACK, L.H., RADBILL, J.R., AND CRAWFORD, D.W. (1977). Analysis of pulsatile, viscous blood flow through diseased coronary arteries of man. J. Biomech. **10**, 339-353.
- BAIER, R.E., AND DUTTON, R.C. (1969). Initial events in interactions of blood with a foreign surface. J. Biomed. Mat. Res. **3**, 191-206.
- BARTLETT, G.R. (1977). Metabolism by man of intravenously administered adenine. Transfusion **17**, 367-373.
- BAUMGARTNER, H.R. (1973). The role of blood flow in platelet adhesion, fibrin, deposition and formation of mural thrombi. Microvasc. Res. **5**, 167-179.
- BAUMGARTNER, H.R. (1977). Platelet interaction with collagen fibrils in flowing blood. I. Reaction of human platelets with α chymotrypsin-digested subendothelium. Thromb. Haemost. **37**, 1-16.
- BAUMGARTNER, H.R., TURRITO, V., AND WEISS, H.J. (1980). Effect of shear rate on platelet interaction with subendothelium in citrated and native blood. II. Relationships among platelet adhesion, thrombus dimensions, and fibrin formation. J. Lab. Clin. Med. **95**, 208-221.
- BEGENT, N., AND BORN, G.V.R. (1970). Growth rate in vivo of platelet thrombi, produced by iontophoresis of ADP, as a function of mean blood flow velocity. Nature **227**, 926-930.
- BELL, D.N. (1983). Platelet Aggregation in Poiseuille Flow: A Double Infusion Technique. M.Sc. Thesis, McGill University.
- BELL, D.N., AND GOLDSMITH, H.L. (1984). Platelet aggregation in Poiseuille flow: II. Effect of shear rate. Microvasc. Res. **27**, 316-330.

- BELL, D.N., TEIRLINCK, H.C., AND GOLDSMITH, H.L. (1984). Platelet aggregation in Poiseuille flow: I. A double infusion technique. Microvasc. Res. 27, 297-315.
- BELVAL, T., AND HELLUMS, J.D. (1986). The analysis of shear-induced platelet aggregation with population balance mathematics. Biophys. J. 50, 479-487.
- BELVAL, T., HELLUMS, J.D., AND SOLIS, T. (1984). The kinetics of platelet aggregation induced by shear. Microvasc. Res. 28, 279-288.
- BENSON, T.J., NEREM, R.M., AND PEDLEY, T.J. (1980). The assessment of wall shear stress in arteries, applied to the coronary circulation. Cardiovasc. Res. 14, 568-576.
- BENVENISTE, J., COCHROME, C.G., AND HENSON, P.M. (1972). Leukocyte-dependent histamine release from rabbit platelets: the role of IgE basophils, and a platelet-activating factor. J. Exp. Med. 136, 1356-1377.
- BENEVISTE, J., JOUVIN, E., AND PIROTZKY, E. et al. (1981). Platelet activating factor (PAF-acether): Molecular aspects of its release and pharmacological actions. Int. Arch. Allergy Appl. Immunol. (Suppl.) 66, 121-126.
- BERNSTEIN, E.F., MARZEC, U., AND JOHNSTON, G.G. (1977). Structural correlates of antiplatelet agents on platelets exposed to shear stress. Trans. Am. Soc. Artif. Int. Org. 23, 617-625.
- BISCHEL, M.D., ORRELL, F.L., SCOLES, B.C., MOHLER, J.G., AND BARBOUR, B.H. (1973). Effects of microemboli on blood filtration during hemodialysis. Trans. Amer. Soc. Artif. Int. Org. 19, 492-497.
- BISHOP, C. (1961). Changes in nucleotides of stored or incubated human blood. Transfusion 1, 349-354.
- BIZZOZERO, J. (1882). Ueber einer neuen Formbestandheil der Blutes und desser Rolle bei Thrombose und der Blutgerinnung. Virchows Arch. Path. Anat. 90, 261-332.

- BLACKWELL, G.J., FLOWER, R.J., RUSSEL-SMITH, N., SALMON, J.A., THOROGOOD, P.B., AND VANE, J.R. (1978). Prostacyclin is produced in whole blood. Brit. J. Pharmacol. **64**, 436.
- BOLTON, C.H., AND EMMONS, P.R. (1967). Adenosine diphosphate breakdown by the plasma of different species and by the human whole blood and white cells. Thromb. Diathes. Haemorrh. **18**, 779-787.
- BORGEAT, P., AND SAMUELSON, B. (1979). Arachidonic acid metabolism in polymorphonuclear leukocytes. Effects of ionophore A23187. Proc. Nat. Acad. Sci. USA **76**, 2148-2152.
- BORN, G.V.R. (1962). Aggregation of blood platelets by adenosine diphosphate and its reversal. Nature **194**, 927-929.
- BORN, G.V.R. (1980). Hemodynamic and biochemical interactions in intravascular platelet aggregation. Ciba Foundation Symposium **71** pp. 61-77.
- BORN, G.V.R., AND CROSS, M. (1963). The aggregation of blood platelets. J. Physiol. (London) **168**, 178-195.
- BORN, G.V.R., AND HUME, M. (1967). Effects of the numbers and sizes of platelet aggregates on the optical density of plasma. Nature **215**, 1027-1029.
- BREDDIN, K., GRUN, H., KRZYWANEK, H.J., AND SCHREMMER, W.P. (1976). On the measurement of spontaneous platelet aggregation. The platelet aggregation test III. Methods and first clinical results. Thromb. Haemost. **35**, 667-691.
- BRENNER, H. (1961). The slow motion of a sphere through a viscous fluid towards a plane surface. Chem. Eng. Sci. **16**, 242-251.
- BROWN, C.H., LEVERETT, L.B., LEWIS, C.W., ALFREY, C.P., AND HELLUMS, J.D. (1975). Morphological, biochemical, and functional changes in human blood platelets subjected to shear stress. J. Lab. Clin. Med. **86**, 462-471.
- BURGESS-WILSON, M.E., GREEN, S., HEPTINSTALL, S., AND MITCHELL, J.R.A. (1984). Spontaneous platelet aggregation in whole blood: dependence on age and haematocrit. Lancet **2**, 1213.

- CAEN, J.P., CRONBERG, S., AND KUBISZ, P. (1977). "Platelets: Physiology and Pathology", p. 68, Grune & Stratton, New York.
- CHAMBLISS, J.R., DEMMING, J., WELLS, K., CLINE, W.W., AND ECKSTEIN, R.W. (1950). Effects of hemolysed blood on coronary blood flow. Am. J. Physiol. **163**, 545-553.
- CHANG, H.N., AND ROBERTSON, R. (1976). Platelet aggregation by laminar shear and Brownian motion. Ann. Biomed. Eng. **4**, 151-183.
- CHIEN, S. (1975). Biophysical behavior of red cells in suspensions. In "The Red Cell" (D. MacN. Surgenor, ed.), pp. 1031-1133, Academic Press, New York.
- CHIEN, S., USAMI, S., DELLENBACK, R.J., GREGERSEN, M.I., NANNINGA, L.B., AND GUEST, M.M. (1967). Blood viscosity influence of erythrocyte aggregation. Science **157**, 829-831.
- COLANTUONI, G., HELLUMS, J.D., MOAKE, J.L., AND ALFREY, C.P. (1977). The response of human platelets to shear stress at short exposure times. Trans. Am. Soc. Artif. Intern. Organs **23**, 626-631.
- COLWELL, J.A., AND HALUSHKA, P.V. (1980). Platelet function in diabetes mellitus. Br. J. Haematol. **44**, 521-526.
- CORATTIYL, V., AND ECKSTEIN, E.C. (1986). Regional platelet concentration in blood flow through capillary tubes. Microvasc. Res. **32**, 261-270.
- CURTIS, A.S.G., AND HOCKING, L.M. (1970). Collision efficiency of equal spherical particles in shear flow. Trans. Faraday Soc. **66**, 1381-1390.
- DE GAETANO, G., AND GARATTINI, S. (1978). "Platelets: A Multidisciplinary Approach," Raven Press, New York.
- DE PIERRE, J.W., AND KARNOSKY, M. (1974). Evidence for an ecto-adenosine monophosphate, adenosine triphosphate and p-nitrophenyl phosphatase. J. Biol. Chem. **249**, 7111-7120.
- DERJAGUIN, B.V., AND LANDAU, L.D. (1941). Theory of the stability of strongly charged lyophobic sols and of adhesion of strongly charged particles in solution of electrolytes. Acta Physicochim. URSS **14**, 633-662.

- DEWITZ, T.S., MARTIN, R.R., SOLIS, R.T., HELSUMS, J.D., AND MCINTYRE, L.V. (1978). Microaggregate formation in whole blood exposed to shear stress. Microvasc. Res. 16, 263-271.
- DONNÉ, A. (1842). De l'origine des globules du sang, de leur mode de formation et de leur fin. C. R. Acad. Sci. (Paris) 14, 336-368.
- DUTTON, R.C., BAIER, R.E., DEDRICK, R.L., AND BOWMAN, R.L. (1968). Initial thrombus formation on foreign surfaces. Trans. Am. Soc. Artif. Int. Org. 14, 57-62.
- EBERTH, J.C., AND SCHIMMELBUSCH, C. (1886). Experimentelle Untersuchungen über Thrombose. Virchows Arch. Path. Anat. 103, 39-87.
- FALK, E., (1983). Plaque rupture with severe pre-existing stenosis precipitating coronary thrombosis. Characteristics of coronary atherosclerotic plaques underlying fatal occlusive thrombi. Br. Heart J. 50, 127-134.
- FRIEDMAN, L.I., LIEM, H., GRABOWSKI, E.F., LEONARD, E.F., AND MCCORD, C.W. (1970). Inconsequentiality of surface properties for initial platelet adhesion. Trans. Am. Soc. Artif. Intern. Organs 16, 63-76.
- FROJMOVIC, M.M. (1978). Rheoptical studies of platelet structure and function. Progr. Hemost. Thromb. 4, 279-319.
- FROJMOVIC, M.M., AND LONGMIRE, K.A. (1986). Platelet aggregation in Brownian diffusion: Evidence for long range interactions for human but not rabbit platelets. Biorheology 23, 228 (Abstract).
- FROJMOVIC, M.M., NEWTON, M., AND GOLDSMITH, H.L. (1976). The microrheology of mammalian platelets: Studies of rheo-optical transients and flow in tubes. Microvasc. Res. 11, 203-215.
- FROJMOVIC, M.M., AND MILTON, J.G. (1982). Human platelet size, shape, and related functions in health and disease. Physiol. Rev. 62, 185-261.
- FRY, D.L. (1968). Acute vascular endothelial changes associated with increased blood velocity gradients. Circ. Res. 22, 165-197.

- FUSTER, V., CHESEBRO, J.H., FRYE, R.L., AND ELVEBACK, L.R. (1981). Platelet survival and the development of coronary artery disease in the young adult: effects of cigarette smoking, strong family history and medical therapy. Circulation **63**, 546-551.
- GAARDER, A., JONSEN, J., LALAND, S., HELLEM, A., AND OWREN, P.A. (1961). Adenosine diphosphate in red cells as a factor in the adhesiveness of human blood platelets. Nature **192**, 531-532.
- GEAR, A.R.L., AND LAMBRECHT, J.K. (1981). Reduction in single platelets during primary and secondary aggregation. Thromb. Haemost. **45**, 298.
- GEAR, A.R.L. (1982). Rapid reactions of platelets studied by a quenched flow approach: Aggregation kinetics. J. Lab. Clin. Med. **100**, 866-886.
- GEAR, A.R.L. (1984). Rapid platelet morphological changes visualized by scanning electron microscopy: kinetics derived from a quenched flow approach. Brit. J. Haematol. **56**, 387-398.
- GERBER, F. (1842). "Elements of General and Minute Anatomy of Man and the Mammalia", added note and appendix comprising researches on anatomy of the blood, chyle, etc., by G. Gulliver, London.
- GILLIAM, P.S., AND TIMOTHY, J.P. (1981) Subcellular localization and properties of adenosine diphosphatase activity in human polymorphonuclear leukocytes. Biochem. Biophys. Acta **673**, 234-242.
- GOLDSMITH, H.L. (1972). The flow of model particles and blood cells and their relation to thrombogenesis. In "Advances in Hemostasis and Thrombosis" (T.H. Spaet, ed.), pp. 97-139, Grune and Stratton, New York.
- GOLDSMITH, H.L., AND KARINO, T. (1979). Mechanically induced thromboemboli. In "Quantitative Cardiovascular Studies. Clinical and Research Applications of Engineering Principles" (N.H.C. Hwang, D.R. Gross, and D.J. Patel, eds.), pp. 289-351, University Park Press, Baltimore.

- GOLDSMITH, H.L., MARLOW, J.C., AND YU, S.K. (1976). The effect of oscillatory flow on the release reaction and aggregation of human platelets. Microvasc. Res. 11, 335-359.
- GOLDSMITH, H.L., AND MASON, S.G. (1962). Particle motions in sheared suspensions XIII. The spin and rotation of discs. J. Fluid Mech. 12, 88-96.
- GOLDSMITH, H.L., AND MASON, S.G. (1964). The flow of suspensions through tubes. III. Collisions of small uniform spheres. Proc. Roy. Soc. A 282, 569-591.
- GOLDSMITH, H.L., AND MASON, S.G. (1967). The microrheology of dispersions. In "Rheology: Theory and Applications" (F.R. Eirich, ed.), Vol. 4, pp. 85-250. Academic Press, New York.
- GOLDSMITH, H.L., AND TURITTO, V.T. (1986). Rheological aspects of thrombosis and haemostasis: basic principles and applications. Thromb. Haemost. 55, 415-435.
- GRABOWSKI, E.F. (1978). Roles of blood flow in platelet adhesion and aggregation. In "Thrombosis - Animal and Clinical Models" (H.J. Day, B.A. Molony, E. Nishizawa, and R.H. Rynbrandt, eds.), pp. 73-103, Plenum Press, New York.
- GRABOWSKI, E.F., FRANTA, J.T., AND DIDISHEIM, P. (1978). Platelet aggregation in flowing blood in vitro. II. Dependence of aggregate growth rate on ADP concentration and shear rate. Microvasc. Res. 16, 183-195.
- GRABOWSKI, E.F., HERTHER, K.K., AND DIDISHEIM, P. (1974). Platelet aggregation quantified in an ex vivo chamber by means of video densitometry. Thromb. Diath. Haemorrh. Suppl. 60, 127-134.
- GRABOWSKI, E.F., AND LEONARD, E.F. (1973). The roles of convection and diffusion in platelet aggregation. Microvasc. Res. 6, 122.
- GRÉGOIRE, C. (1970). Haemolymph coagulation in arthropods. In "The Haemostatic Mechanism in Man and Other Animals" (R.G. MacFarlane, ed.), pp. 45-74, Academic Press, New York.

- GRESELE, P., ZOJA, C., DECKMYN, H., ARNOU, J., VERMYLEN, J., AND VERSTRAETE, M. (1983). Dipyridamole inhibits platelet aggregation in whole blood. Thromb. Haemost. **50**, 852-856.
- GRESELE, P., ARNOU, J., DECKMYN, H., AND VERMYLEN, J. (1986). Mechanism of the antiplatelet action of dipyridamole in whole blood: modulation of adenosine concentration and activity. Thromb. Haemost. **55**, 12-18.
- GUNNING, A.J., PICKERING, G.W., ROBB-SMITH, A.H.T., AND RUSSELL, R.R. (1964). Mural thrombosis of the internal carotid artery and subsequent embolism. Quart. J. Med. **33**, 155-195.
- HARDWICK, R.A., GRITSMAN, H.N., STROMBERG, R.R., AND FRIEDMAN, L.I. (1983). The biochemical mechanisms of shear-induced platelet aggregation. Trans. Am. Soc. Artif. Intern. Organs **29**, 448-453.
- HARDWICK, R.A., HELLUMS, J.D., MOAKE, J.L., PETERSON, D.M., AND ALFREY, C.P. (1980). Effects of antiplatelet agents on platelets exposed to shear stress. Trans. Am. Soc. Artif. Intern. Organs **26**, 179-183.
- HARDWICK, R.A., HELLUMS, J.D., PETERSON, D.M., MOAKE, J.L., AND OLSON, J.D. (1981). The effect of PGI₂ and theophylline on the response of platelets subjected to shear stress. Blood **58**, 678-681.
- HARRISON, M.J., AND MITCHELL, J.R. (1966). The influence of red-blood cells on platelet adhesiveness. Lancet **2**, 1163-1164.
- HELLEM, A.J. (1960). The adhesiveness of human blood platelets in vitro. Scand. J. Clin. Lab. Invest. **12**, (Suppl. 51), 1-117.
- HELLUMS, J.D., AND HARDWICK, R.A. (1981). Response of platelets to shear stress - a review. In "The Rheology of Blood, Blood Vessels and Associated Tissues" (D.R. Gross and N.H.C. Hwang, eds.), pp. 160-183, Sijthoff and Noordhoff, Rockville, Maryland.
- HILL, J.D., AGUILAR, M.J., BARANCO, A., OSBORN, J.J., AND GERBODE, F. (1969). Neuropathological manifestations of cardiac surgery. Ann. Thorac. Surg. **7**, 409-419.
- HODGKIN, T., AND LISTER, J.J. (1827). Microscopic observation of the blood and other animal tissues. Phil. Mag. **2**, 130.

- HUNG, T.C., HOCHMUTH, R.M., JOIST, J.H., AND SUTERA, S.P. (1976). Shear-induced aggregation and lysis of platelets. Trans. Am. Soc. Artif. Intern. Org. 22, 285-296.
- JAFFE, E., AND MOSHER, D. (1978). Synthesis of fibronectin by cultured human endothelial cells. J. Exp. Med. 147, 1779-1791.
- JEN, C.J., AND MCINTIRE, L.V. (1984). Characteristics of shear-induced aggregation in whole blood. J. Lab. Clin. Med. 103, 115-124.
- JOHNSON, S.A. (1971). Endothelial supporting function of platelets. In "The Circulating Platelet" (S.A. Johnson, ed.), pp. 283-299, Academic Press, New York.
- JØRGENSEN, L. (1967). The role of platelet embolism from crumbling thrombi and of platelet aggregates arising in flowing blood. In "Thrombosis" (S. Sherry, K.M. Brinkhous, E. Genton, and J.M. Stengle, eds.), pp. 506-533, National Academy of Sciences., Washington.
- JØRGENSEN, L., ROWSELL, H.C., HOVIG, T., GLYNN, M.F., AND MUSTARD, J.F. (1967). Adenosine diphosphate-induced platelet aggregation and myocardial infarction in swine. Lab. Invest. 17, 616-644.
- KARINO, T. (1986). Microscopic structure of disturbed flows in the human arterial and venous systems and its implication in the localization of vascular diseases. Int. J. Angiol. 5, 297-313.
- KARINO, T., AND GOLDSMITH, H.L. (1979a). Aggregation of human platelets in an annular vortex distal to a tubular expansion. Microvasc. Res. 17, 217-237.
- KARINO, T., AND GOLDSMITH, H.L. (1979b). Adhesion of human platelets to collagen on the walls distal to a tubular expansion. Microvasc. Res. 17, 238-262.
- KARINO, T., AND MOTOMIYA, M. (1984). Flow patterns in the human carotid artery bifurcation. Stroke 15, 50-56.
- KLOSE, J.J., RIEGER, H., AND SCHMID-SCHÖNBEIN, H. (1975). A rheological method for the quantitation of platelet aggregation in vitro and its kinetics under defined flow conditions. Thromb. Res. 7, 261-272.

- KOHANNA, F.H., SMITH, M.H., AND SALZMAN, E.W. (1984). Do patients with thromboembolic disease have circulating platelet aggregates? Blood **64**, 205-209.
- LAMPERT, H. (1931). Die physikalische Seite des Blutgerinnungs Problems. George Thieme Verlag, Leipzig.
- LEONARD, E.F. (1972). The role of flow in thrombogenesis. Bull. N.Y. Acad. Med. **48**, 273-280.
- LERCHE, D. (1982). Spontaneous aggregation of washed human erythrocytes in isotonic media of reduced ionic strength. Conclusions about the spatial arrangement of the N-terminal part of the glycoporphins. Biorheology **19**, 587-598.
- LING, S.C., ATABEK, N.B., FRY, D.L., PATEL, D.J., AND JANICKI, J.S. (1968). Application of heated-film velocity and shear probes to hemodynamic studies. Circ. Res. **23**, 789-801.
- LIPOWSKY, H.H., AND ZWEIFACH, B.J. (1977). Methods for the simultaneous measurement of pressure differentials and flow in single unbranched vessels of the microcirculation for rheological studies. Microvasc. Res. **14**, 345-361.
- LOEB, I. (1927). Amoeboid movement and agglutination in amoebocytes of Limulus and the relation of these processes to tissue formation and thrombosis. Protoplasma **2**, 512.
- MANLEY, R. ST.J., AND MASON, S.G. (1952). Particle motions in sheared suspensions. II. Collisions of uniform spheres. J. Coll. Sci. **7**, 354-369.
- MANLEY, R. ST.J., AND MASON, S.G. (1955). Particle motions in sheared suspensions. III. Further observations on collisions of spheres. Can. J. Chem. **33**, 763-773.
- MASON, R.G. (1971). The interaction of blood hemostatic elements with artificial surfaces. Progr. Hemost. Thromb. **1**, 141-164.
- MAUPIN, B. (1967). Les plaquettes sanguines des mammifères. Biol. Med. **56**, 143-192.

- MAY, A.G., DEWEESE, J.A., AND ROB, C.G. (1963). Hemodynamic effects of arterial stenosis. Surgery 53, 513-524.
- MCPHERSON, V.J., ZUCKER, M.B., FRIEDBERG, N.B., AND RIFKIN, P.L. (1974). Platelet retention in glass bead columns: further evidence for the importance of ADP. Blood 44, 411-425.
- MEADE, T.W. (1979). The epidemiology of arterial thrombosis. Thromb. Haemost. 42, 260.
- MERRILL, E.W., BENIS, A.M., GILLILAND, E.R., SHERWOOD, T.K., AND SALZMAN, E.W. (1965). Pressure-flow relations of human blood in hollow fibers at low flow rates. J. Appl. Physiol. 20, 954-967.
- MILLER, E. (1984). Chemistry of collagens and their distribution. In "Extravascular Matrix Biochemistry" (K. Piez and A. Reddi, eds.) pp. 41-81, Elsevier, New York.
- MILTON, J.G., AND FROJMOVIC, M.M. (1984). Adrenaline and adenosine diphosphate-induced platelet aggregation require shape change: Importance of pseudopods. J. Lab. Clin. Med. 104, 805-815.
- MILTON, J.G., GLUSHAK, C., WONG, T., AND FROJMOVIC, M.M. (1981). Comparison of the time course for ADP-induced shape change, aggregation and onset of refractoriness. Thromb. Haemost. 46, 408.
- MITCHELL, J.R.A., AND SCHWARTZ, C.J. (1963). The relationship between myocardial lesions and coronary artery disease. II. A select group of patients with massive cardiac necrosis or scarring. Br. Heart J. 25, 1-24.
- MONCADA, S., GRYGLEWSKI, S., BUNTING, S., AND VANE, J.R. (1975). An enzyme isolated from arteries transforms prostaglandin endoperoxides to an unstable substance that inhibits platelet aggregation. Nature 263, 663-665.
- MORTON, W.A., PARMENTIER, E.M., AND PETSCHER, H.E. (1975). Study of aggregate formation in regions of separated blood flow. Thromb. Diath. Haemorrh. 34, 840-854.

- MUGGLI, R. BAUMGARTNER, H.R., TSCHOPP, T.B., AND KELLER, H. (1980). Automated densitometry and protein assays as a measure for platelet adhesion and aggregation on collagen-coated slides under controlled flow conditions. J. Lab. Clin. Med. **95**, 195-207.
- MUSTARD, J.F., MOORE, S., PACKHAM, M.A., AND KINLOUGH-RATHBONE, R.L. (1977). Platelets, thrombosis and atherosclerosis. Proc. Biochem. Pharmacol. **13**, 312-325.
- MUSTARD, J.F., PACKHAM, M.A., AND KINLOUGH-RATHBONE, R.L. (1978). Platelets and thrombosis in the development of atherosclerosis and its complications. In "Thrombosis - Animal and Clinical Models" (H.J. Day, B.A. Molony, E.B. Nishizawa, and R.H. Rynbrandt, eds.), pp. 7-30, Plenum Press, New York.
- NURDEN, A.T. (1987). Platelet membrane glycoproteins and their clinical aspects. In "Thrombosis and Haemostasis" (M. Verstraete, J. Vermeylen, R. Lijnen, and J. Arnout, eds.), pp. 93-125, Leuven Univ. Press, Leuven, Belgium.
- NYILAS, E., MORTON, W.A., LEDERMAN, D.M., CHIU, T.-H., AND CUMMING, R.D. (1975). Interdependence of hemodynamic and surface parameters in thrombosis. Trans. Am. Soc. Artif. Intern. Org. **21**, 55-69.
- O'BRIEN, J.R. (1962). Platelet aggregation. Part II. Some results from a new method of study. J. Clin. Path. **15**, 452-455.
- OSLER, W. (1874). An account of certain organisms occurring in the liquor sanguinis. Proc. Roy. Soc. **22**, 391.
- PACKHAM, M.A., ROWSELL, H.C., JORGENSEN, L., AND MUSTARD, J.F. (1967). Localized protein accumulation in the wall of the aorta. Exp. Mol. Pathol. **7**, 214-232.
- PARKER, J.C. (1970). Metabolism of external adenine nucleotides by human red blood cells. Am. J. Physiol. **218**, 1568-1574.
- PARSEGIAN, V.A., AND GINGELL, D. (1972). Some features of physical forces between biological cell membranes. J. Adhesion **4**, 283-306.

- PARSEGIAN, V.A., AND GINGELL, D. (1973). A physical force model of biological membrane interaction. In "Recent Advances in Adhesion" (L.H. Lee, ed.), pp. 153-192, Gordon and Breach, New York.
- PETSCHKE, H.E., ADAMIS, D., AND KANTROWITZ, A.R. (1968). Stagnation flow thrombus formation. Trans. Am. Soc. Artif. Intern. Org. 14, 256-259.
- PICKERING, G.W. (1968). High Blood Pressure. Churchill, London. ???pp.
- RICHARDSON, P.D. (1973). Effect of blood flow velocity on growth rate of platelet thrombi. Nature (London) 245, 103-104.
- RICHARDSON, P.D., GALETTI, P., AND BORN, G.V.R. (1976). Regional administration of drugs to control thrombosis in artificial organs. Trans. Am. Soc. Artif. Intern. Org. 22, 22-29.
- RITTENHOUSE, E.A., HESSEL, E.A., II, ITO, C.S., AND MERENDINO, K.A. (1972). Effect of dipyridomole on microaggregate formation in the pump oxygenator. Ann. Surg. 175, 1-12.
- ROSENBLUM, M.I., AND EL-SABBAN, F. (1982). Influence of shear rate on platelet aggregation in cerebral microvessels. Microvasc. Res. 23, 311-328.
- ROSCHKE, E.J., AND HARRISON, E.C. (1977). Fluid shear stress in prosthetic heart valves. J. Biomech. 10, 299-311.
- ROSCHKE, E.J., HARRISON, E.C., AND BLANKENHORN, D.H. (1975). Fluid shear stresses during the opening sequence of prosthetic heart valves. Proc. 28th Annual Conf. Eng. Med. Biol. D5.4.
- ROSS, R., GLOMSET, J., KARIYA, B., AND HARKER, L. (1974). A platelet-dependent serum factor that stimulates the proliferation of arterial smooth muscle cells in vitro. Proc. Natl. Acad. Sci. 71, 1207-1210.
- SAKARIASSEN, K.S., AARTS, P.A.M.M., DEGROOT, P.G., HOUDIJK, W.P., AND SIXMA, J.J. (1983). A perfusion chamber developed to investigate platelete interaction in flowing blood with human vessel wall cells, their extracellular matrix, and purified components. J. Lab. Clin. Med. 102, 522-535.

- SANIABADI, A.R., LOWE, G.D.O., BARBENEL, J.C., AND FORBES, C.D. (1985). Further studies on the role of red blood cells in spontaneous platelet aggregation. Thromb. Res. **38**, 225-232.
- SALZMAN, E.W. (1963). Measurement of platelet adhesiveness. J. Lab. Clin. Med. **62** 724-735.
- SALZMAN, E.W. (1971). Nonthrombogenic surfaces: critical review. Blood **38**, 509-523.
- SCARBOROUGH, D.E. (1971). The pathogenesis of thrombosis in artificial organs and vessels. Curr. Topics Path. **54**, 95-124.
- SCHMID-SCHÖNBEIN, H., GOSEN, J.V., HEINICH, L., KLOSE, H.J., AND VOLGER, E. (1973). A counter rotating "rheoscope chamber" for the study of the microrheology of blood cell aggregation by microscopic observation and microphotometry. Microvasc. Res. **6**, 366-376.
- SCHRADER, J., BERNE, R.M., AND RUBIO, R. (1972). Uptake and metabolism of adenosine by human erythrocyte ghosts. Am. J. Physiol. **223**, 159-166.
- SCHUPPAN, D., TIMPL, R., AND GLANVILLE, R. (1980). Discontinuities in the triple helical sequence Gly-x-y of basement membrane (type IV) collagen. FEBS Letters **115**, 297-300.
- SEAMAN, G.V.F. (1967). Surface potential and platelet aggregation. Thromb. Diathes. Haemorrh. Suppl. **XXVI**, 53-68.
- SEAMAN, G.V.F., AND BROOKS, D.E. (1970). Electrochemical aspects of platelet adhesion and aggregation. Thromb. Diathes. Haemorrh. Suppl. **XLII**, 93-107.
- SEIFFGE, D., AND KREMEK, E. (1986). Influence of ADP, blood flow velocity, and vessel diameter on the laser-induced thrombus formation. Thromb. Res. **42**, 331-341.
- SKOZA, L., ZUCKER, M.B., JERUSHALMY, Z., AND GRANT, R. (1967). Kinetic studies of aggregation induced by adenosine diphosphate and its inhibition by chelating agents, guanido compounds, and adenosine. Thromb. Diath. Haemorrh. **18**, 713-725.

- SMOLUCHOWSKI, M. VON (1917). Versuch einer mathematischen Theorie der Koagulationskinetik kolloider Lösungen. Z. Physik. Chem. **92**, 129-168.
- SOLIS, R.T., KENNEDY, P.S., BEALL, A.C., NOON, G.P., AND DEBAKEY, M.E. (1975). Cardiopulmonary bypass: microembolization and platelet aggregation. Circulation **52**, 103-108.
- STEELE, P., WELLY, H.S., DAVIES, H., AND GENTON, E. (1973). Platelet function studies in coronary disease. Circ. **48**, 1194-1200.
- STEVENS, D.E., JOIST, J.H., AND SUTERA, S.P. (1980). Role of platelet-prostaglandin synthesis in shear-induced platelet alterations. Blood **56**, 753-758.
- SWIFT, D.L., AND FRIEDLANDER, S.K. (1964). The coagulation of hydrosols by Brownian motion and laminar shear flow. J. Coll. Sci. **19**, 621-647.
- TANGELDER, G.J., TEIRLINCK, H.C., SLAAF, D.W., AND RENEMAN, R.S. (1985). Distribution of blood platelets in flowing arterioles. Am. J. Physiol. **248**, H318-H323.
- TANGELDER, G.F., SLAAF, D.W., TEIRLINCK, H.C., ALEWIJNGE, R., AND RENEMAN, R.S. (1982). Localisation with a thin optical section of fluorescent blood platelets flowing in a microvessel. Microvasc. Res. **23**, 214-230.
- TAKAMURA, K., GOLDSMITH, H.L., AND MASON, S.G. (1979). The microrheology of colloidal dispersions. IX. Effects of simple and polyelectrolytes on rotation of doublets of spheres. J. Colloid Interface Sci. **72**, 385-400.
- TAKAMURA, K., GOLDSMITH, H.L., AND MASON, S.G. (1981a). The microrheology of colloidal dispersions. XII. Trajectories of orthokinetic pair collisions of doublets of spheres in a simple electrolyte. J. Colloid Interface Sci. **82**, 175-189.
- TAKAMURA, K., GOLDSMITH, H.L., AND MASON, S.G. (1981b). The microrheology of colloidal dispersions. XIII. Trajectories of orthokinetic pair collisions of doublets of spheres in a polyelectrolyte. J. Colloid Interface Sci. **82**, 190-202.

- TERRANOVA, V., ROHRBACH, D., AND MARTIN, G. (1980). Role of laminin in the attachment of Pam 212 (epithelial) cells to basement membrane collagen. Cell 22, 719-726.
- THA, S.P., AND GOLDSMITH, H.L. (1986). Interaction forces between human red cells agglutinated by antibody. II. Measurement of hydrodynamic force of break-up. Biophys. J. 50, 1117-1126.
- THOMAS, D. (1978). (ed.) Thrombosis. Brit. Med. Bull. 34, 101-212.
- TIMPL, R., WIEDEMANN, H., VAN DELDEN, V., FURTHMAYR, H., AND KUHN, K. (1981). A network model for the organization of type IV collagen molecules in basement membrane. Eur. J. Biochem. 120, 203-211.
- TOBELEN, G.M., ISRAEL, L., AND CAEN, J.P. (1974). Hémostase et cancer. Path. Biol. 22, 803.
- TREVELYAN, B.J., AND MASON, S.G. (1951). Particle motions in sheared suspensions. I. Rotations. J. Colloid Sci. 6, 354-367.
- TSCHOPP, T.B., AND BAUMGARTNER, H.R. (1976). Enzymatic removal of ADP from plasma: unaltered platelet adhesion but reduced aggregation on subendothelium and collagen fibrils. Thromb. Hemost. 35, 334-341.
- TURITTO, V.T. (1982). Blood viscosity, mass transport and thrombogenesis. In "Progress in Thrombosis and Hemostasis", Vol. 6 (T.H. Spaet, ed.), pp. 139-177, Grune and Stratton, New York.
- TURITTO, V.T., AND BAUMGARTNER, H.R. (1982). Platelet surface interactions. In "Hemostasis and Thrombosis, Basic Principles and Clinical Practice" (R.W. Colman, J. Hirsh, V.J. Marder and E.W. Salzman, eds.), pp. 354-379, J.B. Lippincott, Philadelphia.
- TURITTO, V.T., BENIS, A.M., AND LEONARD, E.F. (1972). Platelet diffusion in flowing blood. Ind. Eng. Chem. Fundam. 11, 216-223.
- TURITTO, V.T., WEISS, H.J., BAUMGARTNER, H.R. (1980). The effect of shear rate on platelet interaction with subendothelium exposed to citrated human blood. Microvasc. Res. 19, 352-365.

- VALDORF-HANSEN, J.F., AND ZUCKER, M.B. (1971). Effect of temperature and inhibitors on serotonin-¹⁴C release from human platelets. Am. J. Physiol. **220**, 105-111.
- VAN DE VEN, T.G.M. (1982). Interactions between colloidal particles in simple shear flow. Adv. Colloid Interface Sci. **17**, 105.
- VAN DE VEN, T.G.M., AND MASON, S.G. (1976a). The microrheology of colloidal dispersions. IV. Pairs of interacting spheres in shear flow. J. Colloid Interface Sci. **57**, 505-516.
- VAN DE VEN, T.G.M., AND MASON, S.G. (1976b). The microrheology of colloidal dispersions. V. Primary and secondary doublets in shear flow. J. Colloid Interface Sci. **57**, 517-534.
- VAN DE VEN, T.G.M., AND MASON, S.G. (1977). The microrheology of colloidal dispersions. VII. Orthokinetic doublet formation of spheres. Coll. Polymer Sci. **255**, 468-479.
- VAN OOST, B., VON HIEN-HAGG, I.H., TIMMERMANS, A.P.M., AND SIXMA, J.J. (1983). The effect of thrombin on the density distribution of blood platelets: detection of activated platelets in the circulation. Blood **62**, 433-438.
- VERWEY, E.G., AND OVERBEEK, J. Th.G. (1948). "Theory of the Stability of Lyophobic Colloids", Elsevier Scientific Publishing Company, Amsterdam, 205 pp.
- VROMAN, L. (1967). Surface activity in blood coagulation. In "Blood Clotting Enzymology" (W.H. Seegers, ed.) pp. 279-322, Academic Press, New York.
- WECHEZAK, A.R., MANSFIELD, P.B., AND WAY, S.A. (1975). Platelet interaction with cultured endothelial cells following in vitro injury. Artery **1**, 507.
- WEISS, H. J. (1978). Antiplatelet therapy (second of two parts). New Eng. J. Med. **298**, 1403-1406.

- WEISS, H.J., TSCHOPP, T.B., AND BAUMGARTNER, H.R. (1975). Impaired interaction (adhesion-aggregation) of platelets with the subendothelium in storage-pool disease and after aspirin ingestion. A comparison with von Willebrand's disease. N. Eng. J. Med. **293**, 619-623.
- WEISS, H.J., AND TURITTO, V.T. (1979). Prostacyclin (Prostaglandin I₂, PGI₂) inhibits platelet adhesion and thrombus formation on subendothelium. Blood. **53**, 244-250.
- WEISS, H.J., TURITTO, V.T., BAUMGARTNER, H.R. (1978). Effect of shear rate on platelet interaction with subendothelium in citrated and native blood. I. Shear rate-dependent decrease of adhesion in von Willebrand's disease and the Bernard-Soulier syndrome. J. Lab. Clin. Med. **92**, 750-764.
- WEKSLER, B.B., AND NACHMAN, R.L. (1981). Platelets and atherosclerosis. Am. J. Med. **71**, 331-333.
- WHITMORE, R.L. (1968). "Rheology of the Circulation" Pergamon Press, Oxford.
- WILNER, G.D., WOSSEL, H.L., AND LEROY, E.C. (1969). Aggregation of platelets by collagen. J. Clin. Invest. **47**, 2616-2621.
- WRIGHT, J.H. (1906). The origin and nature of the blood platelets. Boston Med. Surg. J. **154**, 643-645.
- WU, K.K., AND HOAK, J.C. (1974). A new method for the quantitative detection of platelet aggregates in patients with arterial insufficiency. Lancet **2**, 924-926.
- YAMADA, K., AND OLDE, K. (1978). Fibronectin - adhesive glycoproteins of cell surface and blood. Nature **275**, 179-184.
- YOUNG, D.F., CHOLUIN, N.R., ROTH, A.C. (1975). Pressure drop across artificially induced stenoses in the femoral arteries of dogs. Circ. Res. **36**, 735-743.
- YU, S.K., AND GOLDSMITH, H.L. (1973). Behavior of model particles and blood cells at spherical obstructions in tube flow. Microvasc. Res. **6**, 5-31.

YUNG, W., AND FROJMOVIC, M.M. (1982). Platelet aggregation in laminar flow. Part I. Adenosine diphosphate concentration, time and shear rate dependence. Thromb. Res. **28**, 367-378.

ZEICHNER, G.R., AND SCHOWALTER, W.R. (1977). Use of trajectory analysis to study stability of colloidal dispersions in flow fields. AI. Chem. Eng. J. **23**, 243-254.

ZUCKER, M.B., AND VROMAN, L. (1969). Platelet adhesion induced by fibrinogen adsorbed onto glass. Proc. Soc. Exp. Biol. **131**, 318-320.

CHAPTER II

MEASUREMENT OF THE CONCENTRATION AND SIZE
OF SINGLE PLATELETS AND AGGREGATES

ABSTRACT

A double infusion flow system and particle sizing technique were developed to study the effect of time and shear rate on ADP-induced platelet aggregation in Poiseuille flow. Citrated platelet-rich plasma, PRP, and 2 μM ADP were simultaneously infused into a 40 μl cylindrical mixing chamber at a fixed flow ratio PRP:ADP = 9:1. After rapid mixing by a rotating magnetic stirbar, the platelet suspension flowed through 1.19 or 0.76 mm i.d. polyethylene tubing for mean transit times, \bar{t} , from 0.1 to 86 s, over a range of mean tube shear rate, \bar{G} , from 39.3 to 940 s^{-1} . Known volumes of suspension were collected into 0.5% buffered glutaraldehyde, and all particles in the volume range 1 to $10^5 \mu\text{m}^3$ were counted and sized using a Coulter ZM particle counter and logarithmic amplifier in conjunction with a multichannel pulse-height analyzer. The decrease in the single platelet concentration served as an overall index of aggregation and the decrease in the total particle concentration was used to calculate the collision capture efficiency during the early stages of aggregation. Aggregate growth was followed by changes in the volume fraction of particles of successively increasing size. Preliminary results demonstrate that both collision efficiency and particle volume fraction reveal important aspects of the aggregation process not indicated by changes in the single platelet concentration alone.

NOMENCLATURE

b	Sphere radius
D	Maximum absolute difference between $F^-(x_k)$ and $G(x_k)$ over all classes, $k = 1$
D_{crit}	Maximum value of D beyond which $f^-(x_1)$ is not normally distributed, $p < 0.05$
D_t	Translational diffusion coefficient
E	Sum of squared error
$f(x_1); f^-(x_1)$	Measured platelet and aggregate log-volume histogram; minus background
f_m	Maximum class content of $f(x_1)$
$F(x_1); F^-(x_1)$	Normalized cumulative measured platelet and aggregate log-volume histogram; minus background
g	Acceleration due to gravity
$g(x_1); G(x_1)$	Histogram of fitted Gaussian distribution to $f(x_1)$; normalized cumulative Gaussian histogram
$g_1; g_2$	Skewing; kurtosis of Gaussian distribution
$G; \bar{G}$	Shear rate; mean value in Poiseuille flow
h, h'	Channel numbers of pulse-height analyser
i, k	Histogram class number
j; J_c	Two-body collision; capture frequency

J	Total two-body collision frequency per unit volume of suspension
l, u	Lower, upper histogram classes
L, U	Lower, upper volume of classes l and u
$n(x_i), n_{L,U}$	Content of class i of any histogram, number of particles between L and U .
$N; N_{L,U}, N_{L,U}(\bar{t})$	Number concentration of equal-sized spheres; between L and U , at time \bar{t} .
$N_{\infty}(t)$	Total particle concentration at time t
Pe	Péclet number
Q	Volume flow rate
r	Radius of curvature of coiled tube
R_0	Tube radius
Re	Tube Reynolds number
s, s^2	Standard deviation, variance of x_i
S	Suspension dilution factor
$t; \bar{t}$	Time; mean transit time
\bar{U}	Mean linear velocity in Poiseuille flow
u_s	Sedimentation velocity
$v(x_i)$	Volume of class i

$V_h, V_{h'}$ Volume of sphere in channel numbers h and h'

x Limits of integration of normalized Gaussian density function corresponding to histogram classes

$x_i; \bar{x}$ Mark of class i of the log-volume histogram; mean value

X_3 Distance down flow tube from exit of chamber

Δx Class width

$y(x_i), y'(x_i)$ Measured, fitted background log-volume histogram

GREEK AND SCRIPT SYMBOLS

α, β, γ Constants

α_0 Orthokinetic collision capture efficiency

η Suspending fluid viscosity

$\bar{\mu}, \mu_{med}, \mu_{mod}$ Mean, median, mode of linear platelet volume distribution

$\rho; \rho_1$ Suspending fluid; particle density

σ Standard deviation of linear platelet volume distribution

$\Phi, \Phi(x_i), \Phi_{L,U}$ Particle volume fraction: total, of histogram class i , between L and U

INTRODUCTION

This work constitutes the second phase of an investigation into the effect of shear rate on the ADP-induced aggregation of human platelets in Poiseuille flow. In the first phase, ADP was infused into a flowing suspension of platelets through a micropipette tip located concentrically within the entrance of a 100 μm diameter flow tube. The aggregation reaction was followed under a microscope at various distances downstream and recorded on cine film (Bell, 1983; Bell *et al.*, 1984; Bell and Goldsmith, 1984). At 1 μM ADP, both the rate and final extent of aggregation in citrated platelet-rich plasma, PRP, were found to increase over the range of mean tube shear rate from 2 - 54 s^{-1} . This technique permitted direct visualization of the aggregation reaction; however, the microscopic dimensions and constraints on the diffusion of ADP restricted its use to relatively short reaction times and low shear rates. The present technique circumvents the diffusion problem and extends the previous work to longer reaction times and higher shear rates. ADP and PRP are simultaneously infused into a common mixing chamber and, after a brief mixing period, flow through various lengths of polyethylene tubing into 0.5% glutaraldehyde. The effects of shear rate and transit time on platelet aggregation are followed through an analysis of the volume distribution of single platelets and aggregates from 1 - $10^5 \mu\text{m}^3$. The present flow system also permits the use of higher molecular weight platelet agonists such as thrombin and collagen, and can be readily adapted for use with whole blood.

A resistive particle counter and logarithmic amplifier are used in conjunction with a multichannel pulse height-analyzer to generate

continuous distributions of single platelet and aggregate log-volume. A logarithmic expansion increases the dynamic working range of the particle counter and provides the large range of volume over which aggregate size is measured. A logarithmic scale is also convenient for platelet sizing since numerous studies have demonstrated that platelet size is log-normally distributed (Bahr and Zeitler, 1965; von Behrens, 1972; Paulus, 1975).

Platelet aggregation has been traditionally measured through the decrease in the optical density of stirred suspensions of platelets aggregating in response to an exogenous agonist (Born, 1962). Efforts to relate the concentration and size of aggregates to the optical density of the suspensions have shown that relatively small changes in suspension turbidity at early exposure times are accompanied by large decreases in the concentration of single platelets (Born and Hume, 1967), but that large decreases in turbidity later in time at high ADP concentrations are not necessarily associated with the further aggregation of single platelets (Gear and Lambrecht, 1981). Nichols and Bosmann (1979) measured the distribution of aggregate size and found that the relationship between particle concentration and optical density was nonlinear, and that in the presence of disaggregation the point of minimum optical density did not correlate with the point of maximum aggregate size. Chang and Robertson (1976) used an elaborate light scattering theory to follow the kinetics of aggregate growth in response to ADP at shear rates less than 75 s^{-1} in a cylindrical Couette, but found the light scattering phenomena to be dominated by single platelets, even after extensive aggregation. Gear (1982) used a resistive particle counter to measure the ADP-induced decrease in the concentration of single platelets in flow through tubes at

mean shear rates less than 2200 s^{-1} , but did not deal with the effect of shear rate on the kinetics of aggregate growth. Aggregate size distributions have been generated for shear-induced platelet aggregation in cone and plate viscometers ($> 3000 \text{ s}^{-1}$), (Belval et al. 1984; Belval and Hellums, 1986) where it was observed that single platelets are still the most numerous particles at advanced stages of aggregation. In the lower physiological range of shear rate ($< 2000 \text{ s}^{-1}$; Whitmore, 1968; Chien, 1975; Turitto and Baumgartner, 1982) of the present experiments, it is shown that aggregate growth is highly dependent on shear rate, and that changes in the concentration of single platelets do not adequately reflect changes in aggregate growth. Suspensions such as PRP readily lend themselves to the application of two-body collision theory that can further characterize the effect of shear rate on agonist-induced platelet aggregation in Poiseuille flow.

In this chapter, the flow system and particle counting and sizing procedure are introduced. A representative donor is used to illustrate the time course of ADP-induced aggregation over a range of mean tube shear rate from $39.3 - 940 \text{ s}^{-1}$ through changes in the number concentration and volume of single platelets and aggregates. The fraction of collisions that result in the formation of stable aggregates, or the collision efficiency, is determined from changes in the total particle concentration, according to classical two-body collision theory (Smoluchowski, 1917; Manley and Mason, 1952). Subsequent chapters use the technique described herein to study the effects of shear rate, donor sex and red blood cells on the time course of ADP-induced platelet aggregation in suspensions flowing through tubes.

MATERIALS AND METHODS

1. Platelet-Rich Plasma and Reagents

Venous blood was slowly drawn from healthy volunteers via a 19 gauge needle and winged infusion set into 30 ml plastic syringes containing 1/10 volume, 3.8% sodium citrate. All donors had refrained from aspirin ingestion for at least 10 days prior to blood withdrawal and no female donors were taking oral contraceptives. After mixing by gently inverting the syringe, the blood was transferred to polycarbonate tubes and kept under a mixture of 95% air and 5% CO₂ to preserve pH 7.4. All subsequent platelet suspensions were maintained under this gas mixture.

The blood was incubated at 37°C for 30 min, centrifuged at room temperature at 100g for 20 min, and the supernatant PRP containing from 3 to 5 × 10⁵ cells μl⁻¹ transferred to a 60 ml plastic luerlok syringe. The suspension was diluted to 3.30 × 10⁵ cells μl⁻¹ with platelet-poor plasma, PPP, which was obtained by centrifuging the remaining blood at 2000g for 20 min.

Frozen aliquots of 2.0 mM adenosine-5'-diphosphate, ADP, (Sigma, St. Louis, MO) were thawed immediately prior to use and diluted in modified Tyrodes solution (137 mM NaCl, 2.7 mM KCl, 11.9 mM NaHCO₃, 0.36 mM NaH₂PO₄·H₂O) at pH 7.4. Electron microscope grade glutaraldehyde (J.B. EM Services, Pointe Claire-Dorval, QC) was diluted to 0.5% (v/v) in Isoton II (Coulter Electronics, Hialeah, FL). One per cent (v/v) silicone (Siliclad, Clay Adams, Parsippany, NJ) was used to siliconize the mixing chamber prior to experiments.

Monodisperse polystyrene latex spheres of 2.02, 5.00, 9.82 and 20.54 μm diameter (Coulter Electronics) were used to calibrate the particle sizing equipment.

2. Flow System and Mixing Chamber

All experiments were done at $23 \pm 1^\circ\text{C}$. Platelet-rich plasma and ADP were simultaneously infused into a common mixing chamber (Fig. 1a) by independent syringe pumps (Models 957 and 903, respectively, Harvard Apparatus, Millis, MA) at a fixed flow ratio, PRP:ADP = 9:1 (Fig. 1b). The infusion pumps responded linearly over the range of flow rates used to within $\pm 1.1\%$ and $\pm 0.4\%$ for the ADP and PRP flow rates, respectively. For flow rates $> 81 \mu\text{l s}^{-1}$ it was necessary to use custom-made syringe pumps with motors of higher torque, reproducible to $\pm 1.1\%$ and $\pm 2.6\%$ for the ADP and PRP pumps, respectively.

The mixing chamber was constructed by placing a polyethylene-coated magnetic stirbar (4 mm long, 1 mm diameter) within a cylindrical section of polyethylene tubing (6 mm i.d., 9.5 mm o.d., 1.5 mm height), and sealing both between two glass slides. Platelet-rich plasma and ADP entered the chamber through five of six alternately located (3 PRP, 2 ADP) 18 gauge stainless steel tubes (20 mm long) spaced equidistant around the circumference of the mixing chamber. The rapidly mixed platelet suspension exited via the remaining stainless steel tube and flowed through 1.19 or 0.76 mm (i.d.) polyethylene tubing (Clay Adams, Parsippany, NJ) up to 15.25 m long. Known volumes of the eluted platelet suspension were collected into 0.5% isotonic glutaraldehyde to give an $\sim 20\times$ dilution of the plasma. The exact volume of the effluent was then

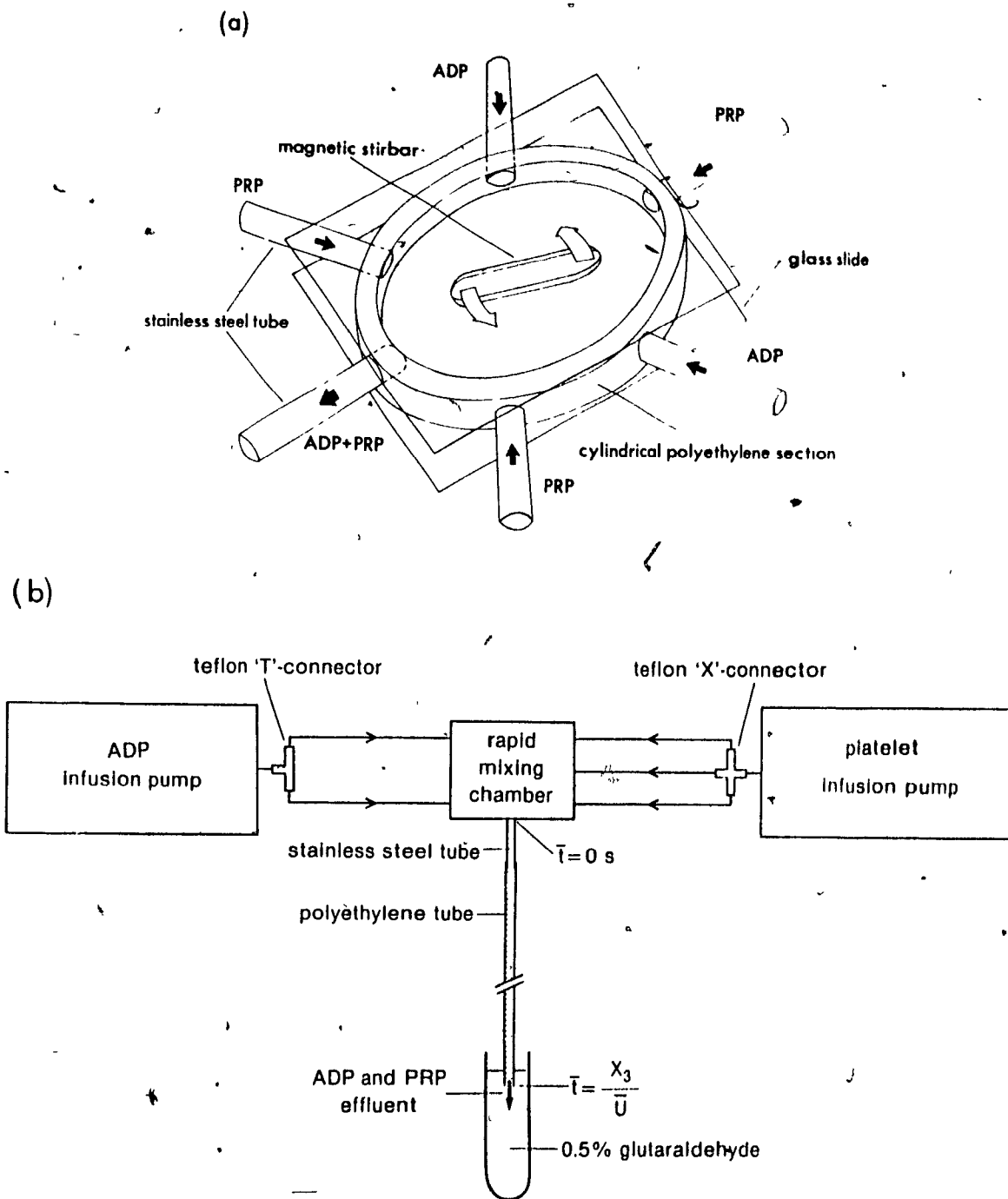


Figure 1: Flow System and Mixing Chamber

Platelet-rich plasma and ADP were simultaneously infused into a common mixing chamber (Fig. 1a) by independent syringe pumps (Fig. 1b). After rapid mixing, the platelet suspension containing $0.2 \mu\text{M}$ ADP and $3.0 \times 10^5 \text{ cells } \mu\text{l}^{-1}$ flowed through polyethylene tubes up to 15.25 m long. Known volumes of effluent were collected into 0.5% glutaraldehyde.

determined by weight. Suspensions of fixed cells were maintained at room temperature with constant end-over-end rotation to prevent particle sedimentation until the concentrations were measured (< 2 days).

Mean transit times of the platelet suspension through the flow tube, $\bar{t} = X_3/\bar{U}$, where X_3 is the distance down the flow tube and \bar{U} is the mean linear fluid velocity, ranged from < 0.1 to 86 s, depending on the volume flow rate, Q , and tube radius, R_0 .

Volume flow rates of the platelet suspension through the flow tube were preset from 13 to 104 $\mu\text{l s}^{-1}$ (1.19 mm i.d.) and from 54 to 81 $\mu\text{l s}^{-1}$ (0.76 mm i.d.), and assuming Poiseuille flow, resulted in mean tube shear rates, $\bar{G} = 2Q/\pi R_0^3$, from 39.3 to 940 s^{-1} , inclusive.

Tube Reynolds numbers, $Re = 2R_0\bar{U}\rho/\eta$, where ρ and η are the suspending phase density and viscosity, 1.02 g ml^{-1} and 1.8 mPa s , respectively for human plasma at 22°C, were < 80, thus ensuring laminar flow over the range of flow rates tested.

Tubes > 1 m long were coiled vertically to prevent particle sedimentation within the flow tube. For all flow rates tested, the value of $Re \sqrt{(R_0/r)}$, where r is the radius of curvature of the coiled tube (400 mm), was below the critical value of 10^4 at which secondary flow becomes significant (Schlichting, 1968).

3. Particle Concentration and Size Measurement

The number and size of single platelets and aggregates were determined using an electronic particle counter (Fig. 2; Coulter ZM). Voltage pulses corresponding to particle volume derived from the Coulter ZM pre-amplifier were amplified logarithmically (Coulter Logarithmic Range Expander) and then collated into a histogram of the logarithm of particle volume using a 100 channel, pulse-height analyzer (Coulter Channelyzer C1000).

Particles of volume 1 to $10^2 \mu\text{m}^3$, corresponding to equivalent sphere diameter from 1.24 to 5.76 μm , were measured using a 50 μm diameter \times 60 μm length aperture (1.5 mA, attenuation 16, base channel threshold 10, window width 100, negative polarity, edit off). Particles of volume 10^2 to $10^5 \mu\text{m}^3$, corresponding to equivalent sphere diameter from 5.76 to 57.6 μm , were measured using a 100 μm diameter \times 120 μm length aperture (0.15 mA, attenuation 8, base channel threshold 20, window width 100, negative polarity, edit off).

The suspensions of fixed cells were diluted in Isoton II electrolyte and counted for 100 s with the stopcock of the mercury manometer open and the sample continuously withdrawn to give total particle counts between 15,000 and 20,000, and between 5,000 and 40,000 on the 50 \times 60 and 100 \times 120 μm apertures, respectively. At a constant pressure differential of ~ 200 mm Hg, the mean volume flow rate through the 50 \times 60 μm aperture was $11.3 \pm 0.6 \mu\text{l s}^{-1}$, while on the 100 \times 120 μm aperture it was $44.8 \pm 0.7 \mu\text{l s}^{-1}$.

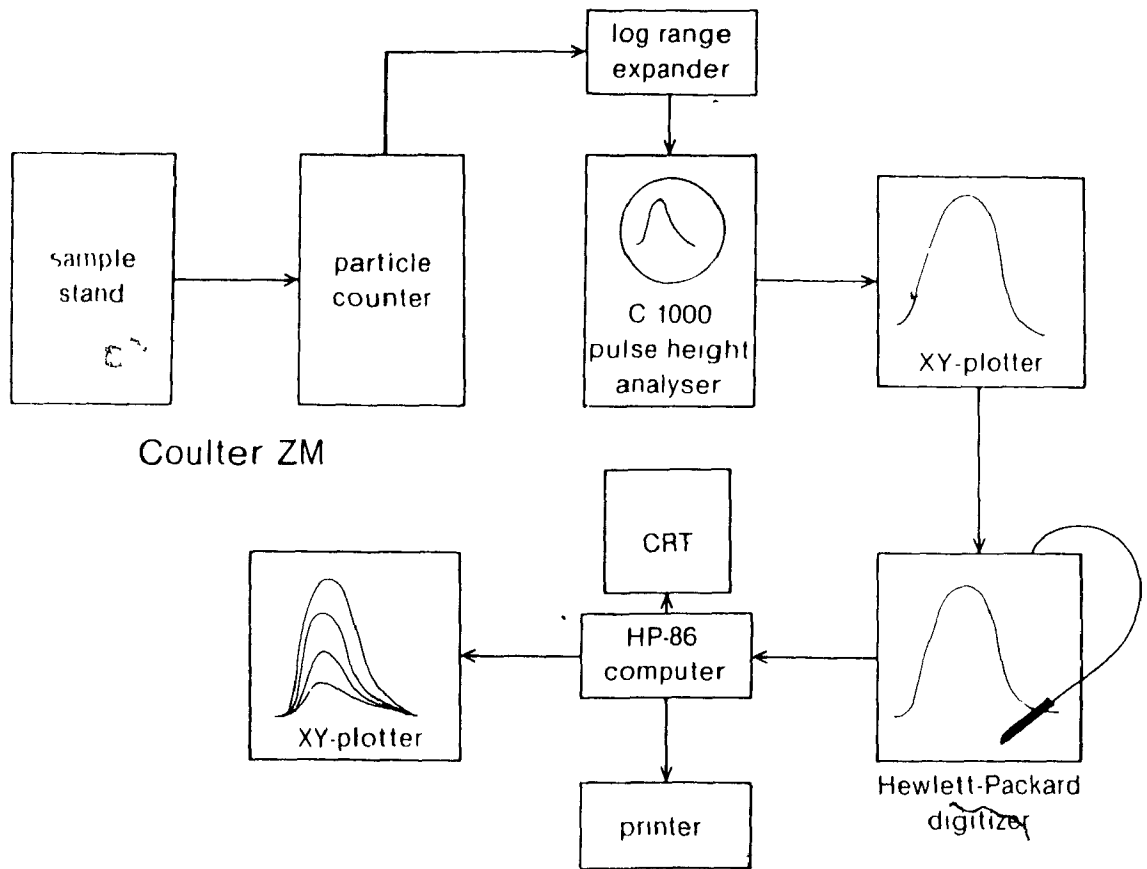


Figure 2: Particle Concentration and Size

Voltage pulses corresponding to particle volume derived from the Coulter ZM were amplified logarithmically, and then collated into a log-volume histogram using a 100 channel pulse-height analyser. Separate histograms from 50×60 and $100 \times 120 \mu\text{m}$ (diameter \times length) apertures were manually transposed into a microcomputer using a digitizer and joined to form a single, continuous histogram from $1-10^5 \mu\text{m}^3$. Integration of the composite histogram yielded the relative fraction of particles of a given volume.

The sedimentation velocity, u_s , of particles during counting was estimated using Stokes equation,

$$u_s = \frac{2 (\rho_1 - \rho) b^2 g}{9 \eta}, \quad [1]$$

where ρ_1 is the particle density, b , the radius of the equivalent sphere and g , the acceleration due to gravity. The density of fixed platelets ($\sim 1.097 \text{ g ml}^{-1}$) was determined by isopycnic centrifugation in Percoll (Pharmacia, Dorval, QC). For the largest particle counted on the $50 \times 60 \mu\text{m}$ aperture ($b = 2.88 \mu\text{m}$) suspended in Isoton II ($\rho = 1.007 \text{ g ml}^{-1}$; $\eta = 0.95 \text{ mPa s}$), sedimentation during the 100 s counting time is negligible (0.17 mm). The largest particle counted on the $100 \times 120 \mu\text{m}$ aperture ($b = 28.8 \mu\text{m}$), however, would sediment 17.1 mm in 100 s. Therefore, particles measured on this aperture were kept in suspension during counting by constant mixing.

4. Log-Volume Histograms

Permanent tracings (Coulter XY4 Recorder) of the log-volume histograms were manually transposed into a microcomputer (Hewlett Packard 86, Kirkland, QC) using a digitizer (HP 9111A). The upper limit of the last class of the histogram obtained using the $50 \times 60 \mu\text{m}$ aperture was joined to the lower limit of the first class of the histogram obtained using the $100 \times 120 \mu\text{m}$ aperture, to generate a single, continuous 250 class histogram over the range of log-volume from 0 to 5. The mark and the volume of the i^{th} class are given by $x_i = (i-0.5)\Delta x$ and $v(x_i) = 10^{x_i}$, respectively, where $\Delta x = 5/250$ is the class width. The generalized class content, $n(x_i)$, corresponds in turn to either the number of particles in

the i^{th} class of the measured distribution of platelet and aggregate log-volumes, $f(x_i)$, or that of the measured background distribution in glutaraldehyde-fixed PPP, $y(x_i)$. The number concentration per histogram class is given by $N(x_i) = S n(x_i)$, where S is the suspension dilution factor.

The number of particles counted between the lower, $L = v(x_\ell)$, and upper, $U = v(x_u)$, volumes corresponding to the lower, ℓ , and upper, u , histogram classes is given by:

$$n_{L,U} = \sum_{i=\ell}^u n(x_i), \quad [2]$$

and the number concentration by $N_{L,U} = S n_{L,U}$.

The volume fraction of particles between L and U is given by:

$$\bar{\Phi}_{L,U} = \sum_{i=\ell}^u \Phi(x_i), \quad [3]$$

where $\Phi(x_i) = N(x_i)v(x_i)$ is the volume fraction per histogram class.

5. Curve Fitting and Background Subtraction

All platelet distributions showed a pronounced negative skew in the small volume range due to contaminating background in the glutaraldehyde-fixed plasma suspensions. Background was proportional to the concentration of fixed plasma in the electrolyte/cell suspension, and subtraction from $f(x_i)$ at each mean transit time was facilitated by fitting an exponential curve to $y(x_i)$ and a normal curve to $f(x_i)$ at $\bar{t} = 0$ s.

A normal curve of the form:

$$g(x_1) = f_m e^{-(x_1 - \bar{x})^2/2s^2} \quad [4]$$

was fitted to $f(x_1)$, with f_m the maximum class content of $f(x_1)$, and \bar{x} and s^2 the respective mean and variance of x_1 :

$$\bar{x} = \frac{\sum_{i=l}^u x_1 f(x_1)}{\sum_{i=l}^u f(x_1)}, \quad [5a]$$

$$s^2 = \frac{\sum_{i=l}^u f(x_1)(x_1 - \bar{x})^2}{\sum_{i=l}^u f(x_1) - 1}. \quad [5b]$$

The classes l and u were selected by inspecting $f(x_1)$ and truncating the lower and upper bounds of the single platelet distribution to reduce the effect of background and microaggregate contamination, respectively, on both the initial estimate of \bar{x} and s , and the fitting of $g(x_1)$ to $f(x_1)$.

A trial and error iterative procedure minimized the sum of squared errors,

$$E = \sum_{i=l}^u [f(x_1) - g(x_1)]^2. \quad [6]$$

Equation [6] was computed using the initial estimates of f_m , \bar{x} and s which were then successively varied by increments proportional to their magnitude, and E computed again. If E decreased, the newly adjusted parameter replaced the previous parameter. In either case, the increment

was decreased by a fractional amount and the procedure repeated until the increment was < 1% of the initial increment of each parameter. This was usually the case after 70-80 iterations.

The exponential:

$$y'(x_1) = \alpha e^{\beta x_1}; \tag{7}$$

where α and β are constants, was fitted to the measured background histogram, $y(x_1)$, over the first fifty classes. Expressing Eq. [7] as:

$$\ln y'(x_1) = \ln \alpha + \beta x_1, \tag{8}$$

allowed a straight line regression of $\ln y(x_1)$ on x_1 . The class contents were weighted in proportion to $y(x_1)$ in order to counteract the approximate $1/y(x_1)$ weighting which results from using $\ln y(x_1)$ instead of $y(x_1)$ in the regression. The weighted least squares condition:

$$\sum_{i=1}^{50} y(x_1) [\ln y(x_1) - \ln \alpha - \beta x_1]^2 = \text{minimum}, \tag{9}$$

gives rise to the normal equations (Kenney and Keeping, 1951):

$$\ln \alpha \sum_{i=1}^{50} y(x_1) + \beta \sum_{i=1}^{50} x_1 y(x_1) = \sum_{i=1}^{50} y(x_1) \ln y(x_1), \tag{10a}$$

$$\ln \alpha \sum_{i=1}^{50} x_1 y(x_1) + \beta \sum_{i=1}^{50} x_1^2 y(x_1) = \sum_{i=1}^{50} x_1 y(x_1) \ln y(x_1), \tag{10b}$$

and hence α and β . Since the background count in PPP was always less than that in the autologous PRP, the magnitude of background was adjusted by the factor $\gamma = [f(x_1) - g(x_1)]/y'(x_1)$, to give the same content in class 1

of the resultant histogram:

$$f^-(x_1) = f(x_1) - \gamma y'(x_1), \quad [11]$$

as that predicted by $g(x_1)$. A proportionate amount of background was subtracted from the content of each class of $f(x_1)$ at $\bar{t} = 0$ s, and at all subsequent transit times, over the range $x_1 = 0$ to 5 using Eq. [11]. The use of Eq. [7] prevented the transfer of random fluctuations in the class contents of $y(x_1)$ due to low particle counts to $f^-(x_1)$ after background subtraction.

BASIC STATISTICS AND HYPOTHESIS TESTING

Assuming a normal distribution of x_1 , the mean, $\bar{\mu}$, standard deviation, σ , median, μ_{med} , and mode, μ_{mod} , of the linear distribution were calculated using (Kenney and Keeping, 1951; Documenta Geigy, 1962):

$$\log \bar{\mu} = \bar{x} + \frac{1}{2}s^2 \ln 10, \quad [12a]$$

$$\sigma^2 = \bar{\mu}^2 (10^{s^2 \ln 10} - 1), \quad [12b]$$

$$\log \mu_{\text{med}} = \bar{x}, \quad [12c]$$

$$\log \mu_{\text{mod}} = \bar{x} - s^2 \ln 10. \quad [12d]$$

The assumption of log-normality of single platelet volume was tested using the Kolmogorov-Smirnov, K-S, one sample test (Young, 1977). The maximum absolute difference determined over all classes, $k = 1$:

$$D = \max |F^-(x_k) - G(x_k)|, \quad 1 < k < u \quad [13]$$

between the normalized cumulative log-volume histogram,

$$F^-(x_k) = \frac{\sum_{i=1}^k f^-(x_i)}{\sum_{i=1}^u f^-(x_i)} \quad [14]$$

and the equivalent normalized Gaussian density function,

$$G(x_k) = \int_{x=0}^{x=x_k + \frac{1}{2}\Delta x} \frac{1}{s\sqrt{2\pi}} e^{-(x - \bar{x})^2/2s^2} dx, \quad [15]$$

based on the sample statistics \bar{x} and s , was compared to a critical maximum difference D_{crit} . The histogram class u , corresponding to the largest single platelet log-volume was determined by inspection of $f^-(x_1)$. The null hypothesis,

$$H_0: F^-(x_k) = G(x_k) \quad [16]$$

was rejected at the 5% significance level, and $f^-(x_1)$ was not considered to be normally distributed, if $D > D_{crit} = 0.886/\sqrt{[\sum_{i=1}^u f^-(x_i)]}$ (Lilliefors, 1967). Skewing, g_1 , and kurtosis, g_2 , of $f^-(x_1)$ and their standard errors were determined using standard equations for frequency distributions (Sokal and Rohlf, 1969). The significance of deviation of these sample statistics from the parametric value of zero was tested using two-tailed Student's t-tests. The above statistics were also applied to the single platelet region of $f(x_1)$ in which case $F(x_1)$ replaced $F^-(x_1)$ in the K-S test.

EXPERIMENTAL ERROR

1. Residence Time in Mixing Chamber

The length of time platelets spend in the mixing chamber was measured by injecting a 5 μl pulse of concentrated, glutaraldehyde-hardened platelets into the chamber through one entry port while diluent was pumped through the remaining entry ports at total volumetric flow rates corresponding to those used in the experiments. Figure 3 shows the fraction of particles recovered from the chamber vs time after injection. Only at the lowest two flow rates, 13 and 26 $\mu\text{l s}^{-1}$, was the residence time substantial. Above 52 $\mu\text{l s}^{-1}$, 50% of the particles had exited by 0.7 s, and 90% by 1.3 s. At the highest flow rate tested, essentially all particles had exited the chamber within 1 s after injection, which was the shortest sampling time feasible with the current technique.

2. Instrument Calibration

Over a four decade expansion the volume of the equivalent sphere, V_h , in channel number, h , of the pulse-height analyzer is given by:

$$V_h = V_{h'} \times 10^{(h - h')/25}, \quad [17]$$

where $V_{h'}$ is the modal volume of a spherical calibration standard in channel number h' . The measured modal volume of standard calibration spheres was assumed equal to the mean volume calculated from the mean diameter stated by the manufacturer. Since the coefficient of variation of the sphere volumes is less than 8% any error in this assumption is slight. The lower and upper channel limits for the 50 \times 60 and the 100 \times

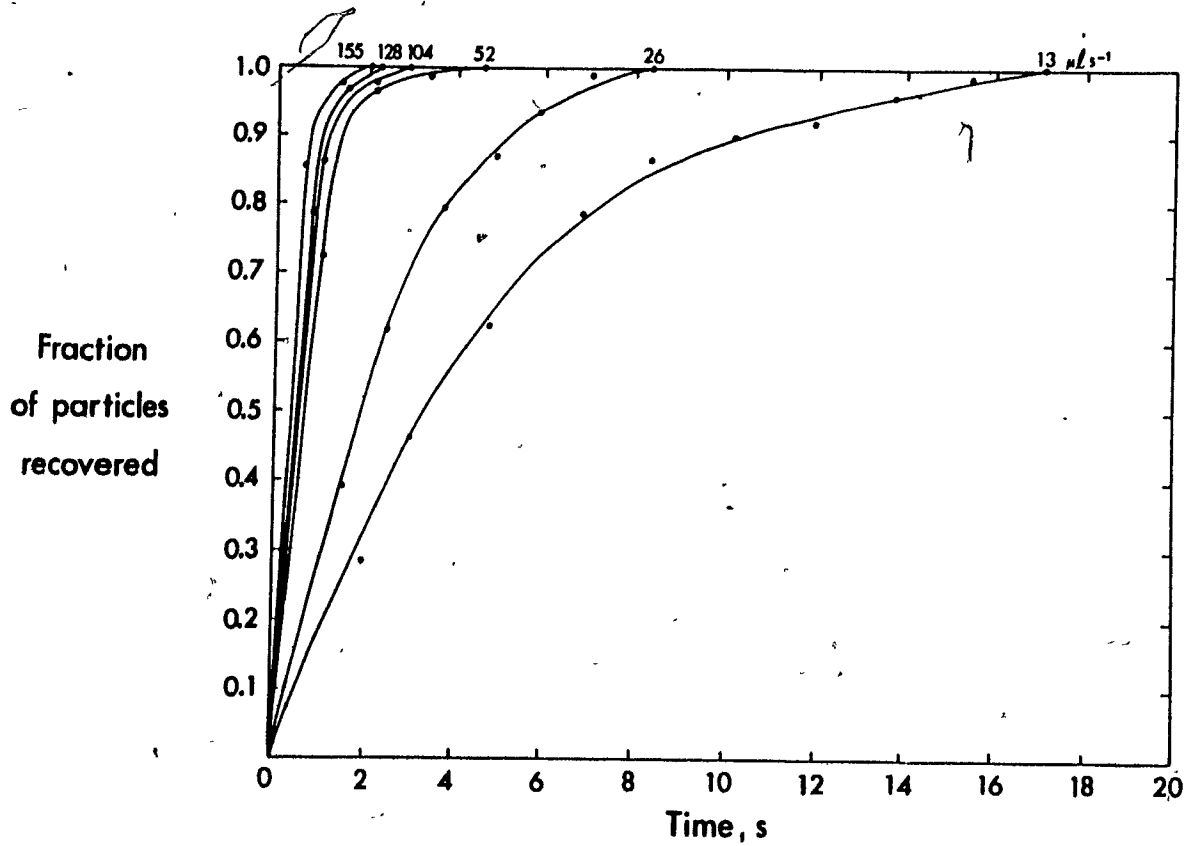


Figure 3: Residence Time in Mixing Chamber

The fraction of platelets recovered from the mixing chamber after injection of a $5 \mu\text{l}$ pulse of concentrated, glutaraldehyde-hardened platelets at time 0 s for flow rates from 13 to $155 \mu\text{l s}^{-1}$.

120 μm aperture were 9 and 59, and 7 and 82, respectively.

The response of the instrument at the setting for the 50 \times 60 μm aperture was tested over the range $1-10^2 \mu\text{m}^3$ using 2.02 μm and 5.00 μm diameter spheres and found to be perfectly logarithmic within a 6% error inherent in the assignment of a particle volume to a given channel of the pulse-height analyzer. The lower limit of the 100 \times 120 μm aperture was matched to the upper limit of the 50 \times 60 μm aperture using the 5.00 μm calibration standard. The 100 \times 120 μm aperture was calibrated up to 4540 μm^3 using 9.82 and 20.5 μm spheres. The expansion using this aperture was not perfectly logarithmic, however. Over and above the 6% assignment error, the measured modal volumes of the 9.82 and 20.5 μm diameter spheres were 6.5% and 8% greater than the respective calculated mean volumes. The over-estimation of the true particle volume appeared to increase with increasing particle size; however, since the instrument calibration was tested every three months and found to remain constant throughout the duration of the experiments, all particles were measured under the same conditions.

3. Count Reproducibility and Suspension Stability

Dilute particle suspensions were required to ensure accurate volume and concentration measurement. Due to the slow response time of the d.c. restorer of the log range expander, complete volume distributions of particle suspensions were noticeably shifted to smaller volumes in a concentration-dependent manner. Particle concentrations $< 14 \mu\text{l}^{-1}$ and $< 4 \mu\text{l}^{-1}$ were required to prevent any volume shifts on the 50 \times 60 and 100 \times 120 μm apertures, respectively.

Due to the larger volume of the deep-bore apertures (length/diameter = 1.2), particle coincidence is greater than in the equivalent standard apertures. Measurements made on serial dilutions of stock calibration suspensions were compared to hemacytometer counts. Coincidence was < 10% below 20 and 6 particles per μl in the 50×60 and $100 \times 120 \mu\text{m}$ apertures, respectively. This measure of coincidence also includes a 2 to 3% count reduction due to the selectivity of the particle sizing circuitry of the pulse-height analyzer (Coulter Channelyzer Manual, 1978). The combined count loss was uncorrected due to the difficulty in determining the contribution of particles of different sizes to the level of coincidence in polydisperse suspensions. This error, as well as the concentration-dependent shifting of the volume distributions, was minimized by using dilute samples and counting for long periods of time.

Table 1 shows particle counts, $n_{L,U}$, of platelet suspensions collected into 0.5% glutaraldehyde after $\bar{t} = 0.2$ and $.43$ s exposure to $0.2 \mu\text{M}$ ADP at $Q = 104 \mu\text{l s}^{-1}$. Particles measured on the $50 \times 60 \mu\text{m}$ aperture corresponded primarily to single platelets ($L = 1, U = 10^2 \mu\text{m}^3$) while those on the $100 \times 120 \mu\text{m}$ aperture were strictly aggregates ($L = 10^2, U = 10^5 \mu\text{m}^3$). Multiple particle counts taken on the same sample dilution using each aperture were reproducible to $\pm 2\%$. A 3% pipetting error in concert with this random counting error produced a maximum 5% variation in measured particle counts. After four days storage of the fixed platelet suspensions with constant mixing, there was no significant change in mean particle counts using either aperture. Thus, there was no particle aggregation or break-up induced by the fixation and storage procedure, as also shown by Nichols and Bosmann (1979).

TABLE 1

Particle Counts of Fixed Platelet Suspensions

TIME AFTER EFFLUENT COLLECTION, hr	0.2 s		43 s	
	1-10 ² , μm ³ *	10 ² -10 ⁵ , μm ³ †	1-10 ² , μm ³ *	10 ² -10 ⁵ , μm ³ **
3	16823 ± 1.39%	6526 †	13158 ± 0.64% †	42435 ± 0.29%
24	16954 ± 2.28%	6528 ± 1.17% **	12665 ± 1.65%	40797 ± 2.12%
98	16505 ± 1.15%	6712 †	12534 ± 0.79%	43270 ± 1.89%

Particle counts (± C.V.) in fixed platelet suspensions using the 50 × 60 μm (1 - 10² μm³) and 100 × 120 μm (10² - 10⁵ μm³) apertures after \bar{t} = 0.2 and 43 s exposure to 0.2 μM ADP. Separate but constant suspension dilutions were used for each aperture. Multiple counts were taken on the same suspension up to 98 hr post-fixation.

* n = 5 ** n = 3 † n = 2

COLLISION FREQUENCY AND EFFICIENCY

The two-body collision frequency for monodisperse suspensions of rigid spheres in simple shear flow is given by (Smoluchowski, 1917; Manley and Mason, 1952):

$$j = \frac{32}{3} Gb^3N, \quad [18]$$

where b is the sphere radius and N the number concentration. Collisions are defined as the rectilinear approach of sphere centers to within a distance of $< 2b$ and provided $b/R_0 \ll 1$, Eq. [18] has been shown to apply in Poiseuille flow (Goldsmith and Mason, 1964). Using the mean tube shear rate, \bar{G} , the total number of two-body collisions per unit volume of suspension is then:

$$J = \frac{1}{2}Nj = \frac{4\Phi\bar{G}N}{\pi}, \quad [19]$$

where Φ is the volume fraction of suspended particles.

Inclusion of the orthokinetic collision capture efficiency, $\alpha_0 = j_c/j$ in Eq. [18] where j_c is the collision capture frequency, accounts for the influence of both interaction and hydrodynamic forces on particle capture (van de Ven and Mason, 1977). If $\alpha_0 = 1$, then $j_c = j$ and every collision results in capture; however, in the absence of attractive forces permanent capture is impossible (Br nner, 1961). The addition of α_0 also relaxes the requirement of rectilinear approach since, theoretically, spheres can be captured from distances between sphere centers $> 2b$ ($\alpha_0 \rightarrow \infty$).

Assuming no aggregate break-up and neglecting the formation of

higher order aggregates, the kinetics of aggregation are first order with respect to the total particle concentration, N_{∞} (Swift and Friedlander, 1964):

$$\frac{dN_{\infty}}{dt} = - \frac{4\Phi\alpha_0 \bar{G}N_{\infty}}{\pi} \quad [20]$$

Integration of Eq. [20] yields:

$$\ln \frac{N_{\infty}(t)}{N_{\infty}(0)} = - \frac{4\Phi\alpha_0 \bar{G}t}{\pi}, \quad [21]$$

where $N_{\infty}(0) = N$ and $N_{\infty}(t)$ are the total particle concentrations at time 0 and t , respectively. Thus, the total particle concentration decays exponentially and a plot of $\ln N_{\infty}(t)$ vs t should give a straight line, the slope of which yields α_0 .

In the present work the influence of Brownian motion on aggregation can be neglected due to the large value of the Peclet number, $Pe = \bar{G}b^2/D_t > 1200$ where D_t is the translational diffusion coefficient for a single sphere calculated from the Stokes-Einstein equation. Thus, the measurement of the total particle concentration over the early stages of aggregation provides a value for α_0 .

RESULTS

1. Single Platelet Distribution

(a) Concentration and Size

Prior to background subtraction, the single platelet volumes of unsheared suspensions appeared log-normally distributed (Fig. 4, $\bar{t} = 0$ s). Of a total 278,000 particles per $\mu\ell$, > 99% were in the range 1 - 30 μm^3 ,

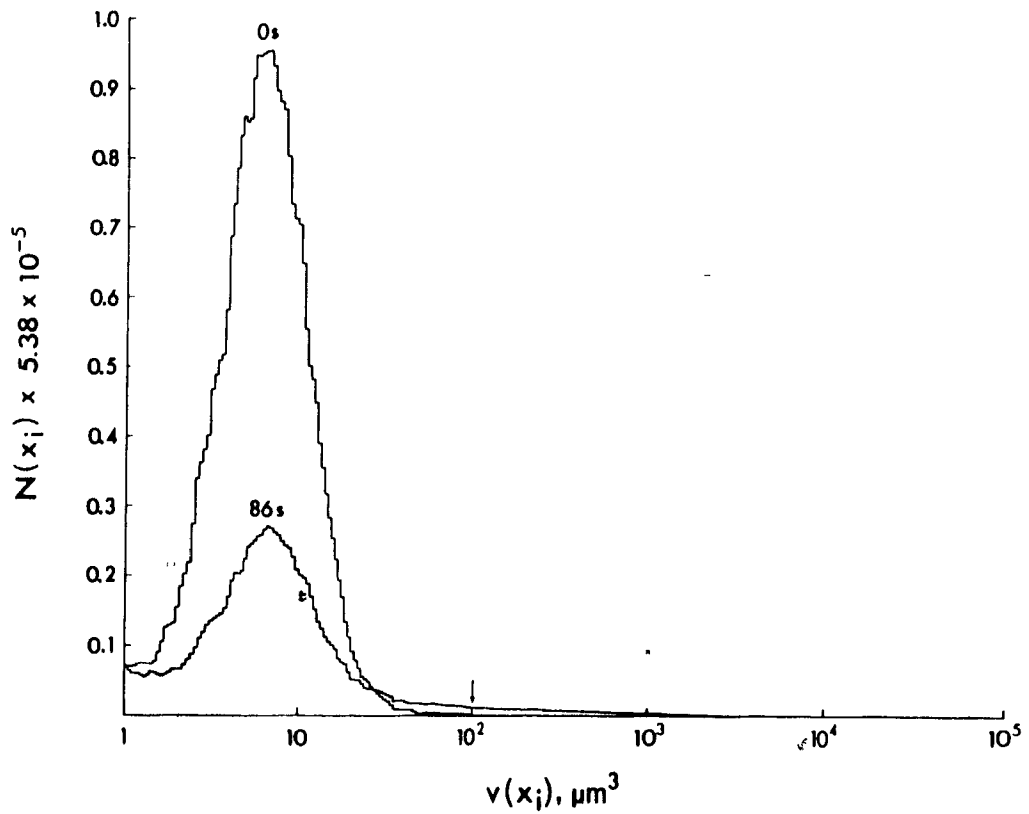


Figure 4: Log-Volume Histogram

The number concentration per histogram class $N(x_i)$ plotted against the equivalent sphere volume $v(x_i)$ over the range $x_1 = 0 - 5$ for an unsheared control, $\bar{t} = 0$ s, and after $\bar{t} = 86$ s exposure to $0.2 \mu\text{M}$ ADP at $\bar{G} = 314 \text{ s}^{-1}$. Arrow at $100 \mu\text{m}^3$ denotes point at which separate histograms from the 50×60 and $100 \times 120 \mu\text{m}$ apertures were joined.

consisting principally of single platelets. Aside from the presence of some contaminating white blood cells of modal volume ~ 170 and $370 \mu\text{m}^3$, measurements using the $100 \times 120 \mu\text{m}$ aperture showed only $\sim 0.06\%$ of particles as aggregates greater than $100 \mu\text{m}^3$.

Shearing the suspension at $\bar{G} = 314 \text{ s}^{-1}$ in the presence of $0.2 \mu\text{M}$ ADP produced a time-dependent loss of single platelets accompanied by the formation of aggregates of successively increasing size (Fig. 4; $\bar{t} = 86 \text{ s}$). Of the 98,000 particles per μl remaining $\sim 4\%$ had volumes greater than $100 \mu\text{m}^3$, while more than 90% were in the volume range of single platelets. Thus, extensive aggregation involving as much as 2/3 of the original single cells reduced the fraction of singlets of the total number of particles by only 10%, and demonstrates the need for employing two apertures to count sufficient numbers of both single cells and aggregates in the same suspension. The accuracy of the sampling technique is evident by the continuity of the log-volume histogram in the region where the separate histograms from each aperture were joined (Fig. 4, arrow).

(b) Curve fitting and background subtraction

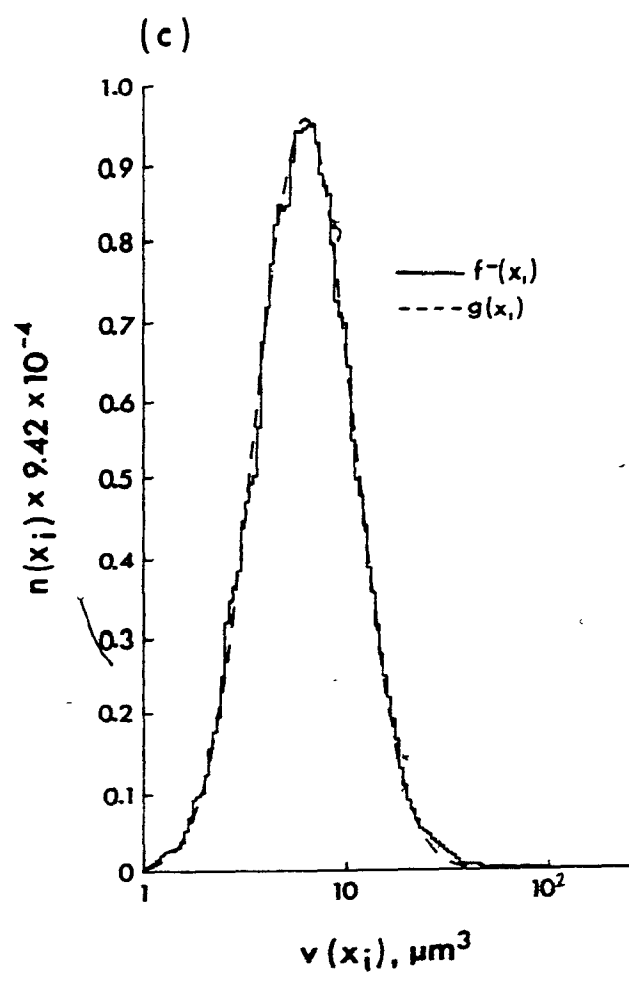
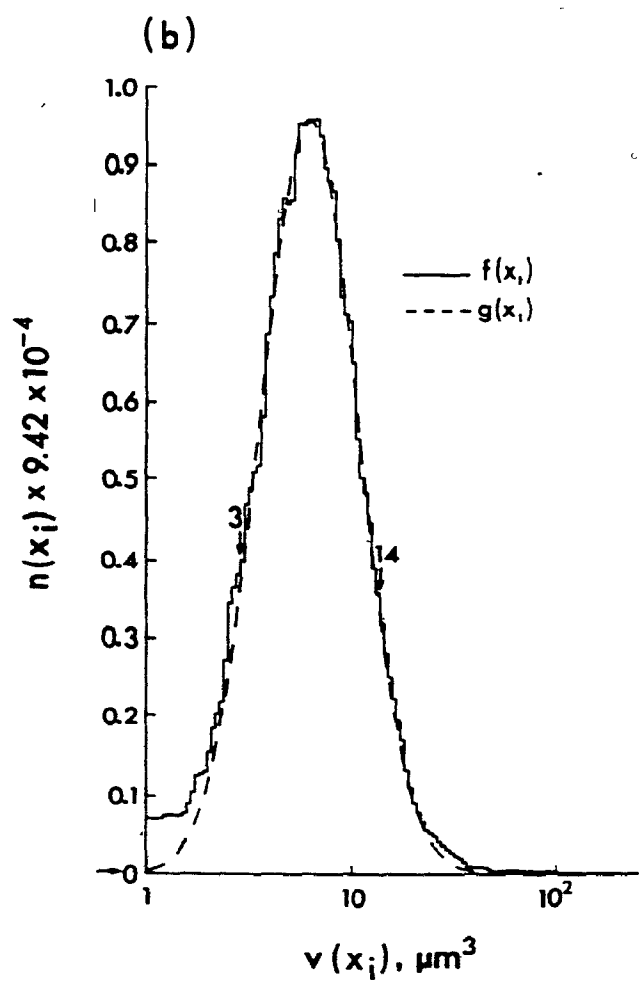
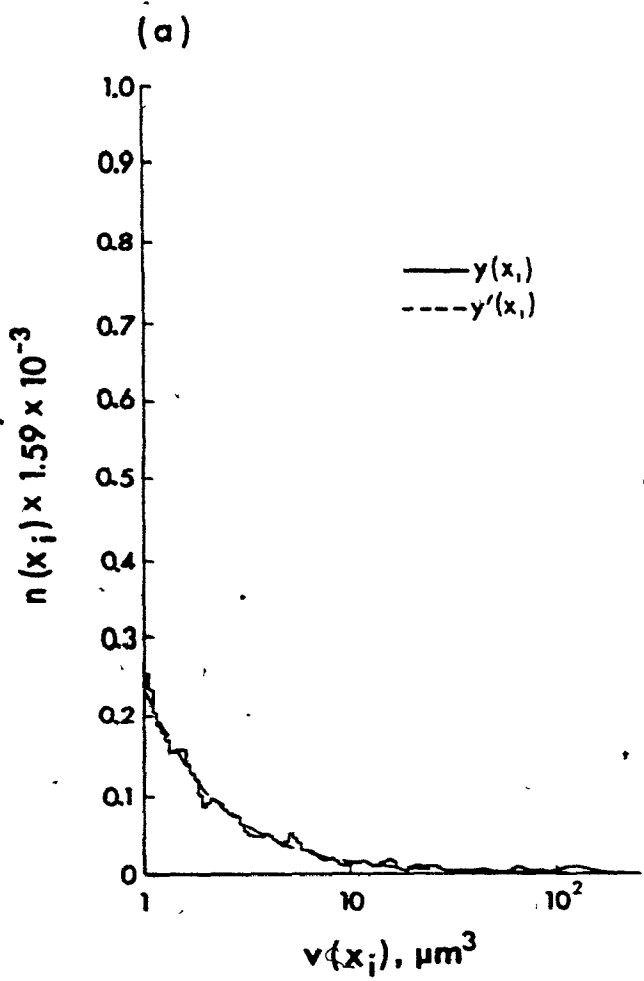
The presence of contaminating background in the small volume region of fixed-plasma suspensions interfered with the evaluation of the true shape of the distribution of single platelet log-volume (Fig. 4). The relative influence of background also increased as particle concentration decreased. Approximately 3% of particles counted as single platelets fell in the range $1 - 1.7 \mu\text{m}^3$ at $\bar{t} = 0 \text{ s}$, while at $\bar{t} = 86 \text{ s}$ this region accounted for 7.5% of the single platelets. Figure 5a shows the distribution of background in the autologous PPP of the platelet

Figure 5: Curve Fitting and Background Subtraction

(a) Exponential curve, $y'(x_1)$, (broken line) fitted to the measured distribution of background, $y(x_1)$, (solid line) in the autologous PPP of the platelet suspension in Figure 4.

(b) Normal curve, $g(x_1)$, (broken line) fitted to the single platelet log-volume histogram, $f(x_1)$, (solid line) over the range $3 - 14 \mu\text{m}^3$ (vertical arrows). The fitted curve was then extrapolated in both directions to encompass the range $1 - 100 \mu\text{m}^3$. The horizontal arrow denotes the frequency in class 1 of $g(x_1)$.

(c) Background was subtracted from each class of $f(x_1)$ over the ~~range~~ $1 - 10^5 \mu\text{m}^3$ using $y'(x_1)$ to give the same content in class 1 of the newly formed distribution, $f^-(x_1)$, (solid line) as that predicted by $g(x_1)$. The broken line shows $g(x_1)$ fitted to $f(x_1)$ prior to background subtraction.



suspension shown in Figure 4. Clearly this distribution is well-matched to a decreasing exponential curve.

Figure 5b shows the normal curve initially fitted to the measured log-volume histogram at $\bar{t} = 0$ s over the region of the single platelet distribution where the influence of background and microaggregate contamination could be safely neglected (vertical arrows), and then afterwards extrapolated to include these regions of overlap. As shown by the ordinate, the background in PPP was less than that in PRP. Using the exponential curve, background was subtracted to give the same content in class 1 of the resultant histogram as that predicted by the normal curve (horizontal arrow). It is evident that after background subtraction a normal curve closely fits the distribution of the logarithm of single platelet volume (Fig 5c). A proportionate amount of background was subtracted from the log-volume histograms at all subsequent mean transit times.

The Kolmogorov-Smirnov test strongly supported ($p < 0.05$) the assumption of log-normality of the distribution of single platelet volume and justified use of the fitted normal curve during background subtraction (Table 2, left). The presence of background produced a significant negative skewing ($g_1 < 0$) of the single platelet distribution which became significantly positive after $\sim 4\%$ of the total particles were subtracted as background. Positive skewing was more pronounced in the case of extensive aggregation (Table 2, right) where, as expected, the distribution of log-volumes was no longer normal. The deviation from log-normality was accompanied by an increase in mean and median volumes of this distribution. The mode remained constant, however, indicating that

TABLE 2

Statistics of the Single Platelet Distribution

Statistic	Control, $\bar{t} = 0$ s		Aggregation, $\bar{t} = 86$ s	
	$f(x_1)$	$f^-(x_1)$	$f(x_1)$	$f^-(x_1)$
\bar{x}	0.78	0.79	0.79	0.85
s	0.27	0.25	0.34	0.29
s/\bar{x} , %	34	31	43	34
g_1	-0.137 ***	0.068 ***	-0.062 ***	0.223 ***
g_2	0.225 ***	0.076	-0.072 *	0.118 **
D	0.01550	0.00624 *	0.03096	0.02622
D_{crit}	0.00703	0.00718	0.00616	0.00656
$n_{1,50}$	15863	15213	20699	18214
$\bar{\mu}$	7.2	7.3	8.3	8.9
σ	4.8	4.5	7.6	6.7
$\sigma/\bar{\mu}$, %	67	62	91	76
μ_{med}	6.0	6.2	6.2	7.1
μ_{mod}	4.1	4.5	3.4	4.5

Statistics of the single platelet log-volume and volume distributions over the range 1-50 μm^3 for the data in Figure 4 prior to, $f(x_1)$, and after, $f^-(x_1)$, background subtraction. Logarithmic data are shown in the upper part and after the appropriate linear transformation in the lower part for the unshered control, $\bar{t} = 0$ s, (left), and after 86 s exposure to 0.2 μM ADP at $\bar{G} = 314 \text{ s}^{-1}$ (right). Symbols are as described in the text and volumes of the linear statistics are in μm^3 . Significantly different from zero: *** $p < 0.001$, ** $p < 0.002$, * $p < 0.05$

the removal of ~ 12% of the particles as background was valid.

2. Platelet Aggregation

(a) Single Platelet Concentration

One index of the degree of platelet aggregation is the time-dependent decrease in the concentration of single cells, $N_{1,30}(\bar{t})$, relative to the concentration at $\bar{t} = 0$ s. Figure 6 shows the effect of mean tube shear rate on the normalized single platelet concentration. A noticeable 4 s lag preceded aggregation at all \bar{G} tested. Aggregation then proceeded at rates dependent upon \bar{G} . At $\bar{G} = 940 \text{ s}^{-1}$ the lag phase was so protracted that the initial rate of aggregation was much reduced, as was the final extent of aggregation reached at $\bar{t} = 86$ s. The maximum rate and final extent of aggregation occurred at $\bar{G} = 157 \text{ s}^{-1}$. Above and below this shear rate, the degree of aggregation was always lower when measured by the decrease in the single platelet concentration.

(b) Collision Efficiency

Equation [21] shows that the collision efficiency, α_0 , is proportional to the slope of a plot of $-\ln[N_{1,10^5}(\bar{t})/N_{1,10^5}(0)]$ vs \bar{t} , where $N_{1,10^5}(\bar{t})$ is the total measured particle concentration at time \bar{t} . Such plots are shown in Figure 7 for the data in Figure 6, and reveal a time- and shear rate-dependency for α_0 in the aggregating suspensions. Actual measurements of collision efficiency can only be made over the region of constant slope after the onset of aggregation. After the initial lag, α_0 remained relatively constant between $\bar{t} = 4$ and 43 s, but decreased with increasing \bar{G} from $\alpha_0 = 0.105$ at $\bar{G} = 39.3 \text{ s}^{-1}$ to $\alpha_0 = 0.001$ at $\bar{G} = 940 \text{ s}^{-1}$.

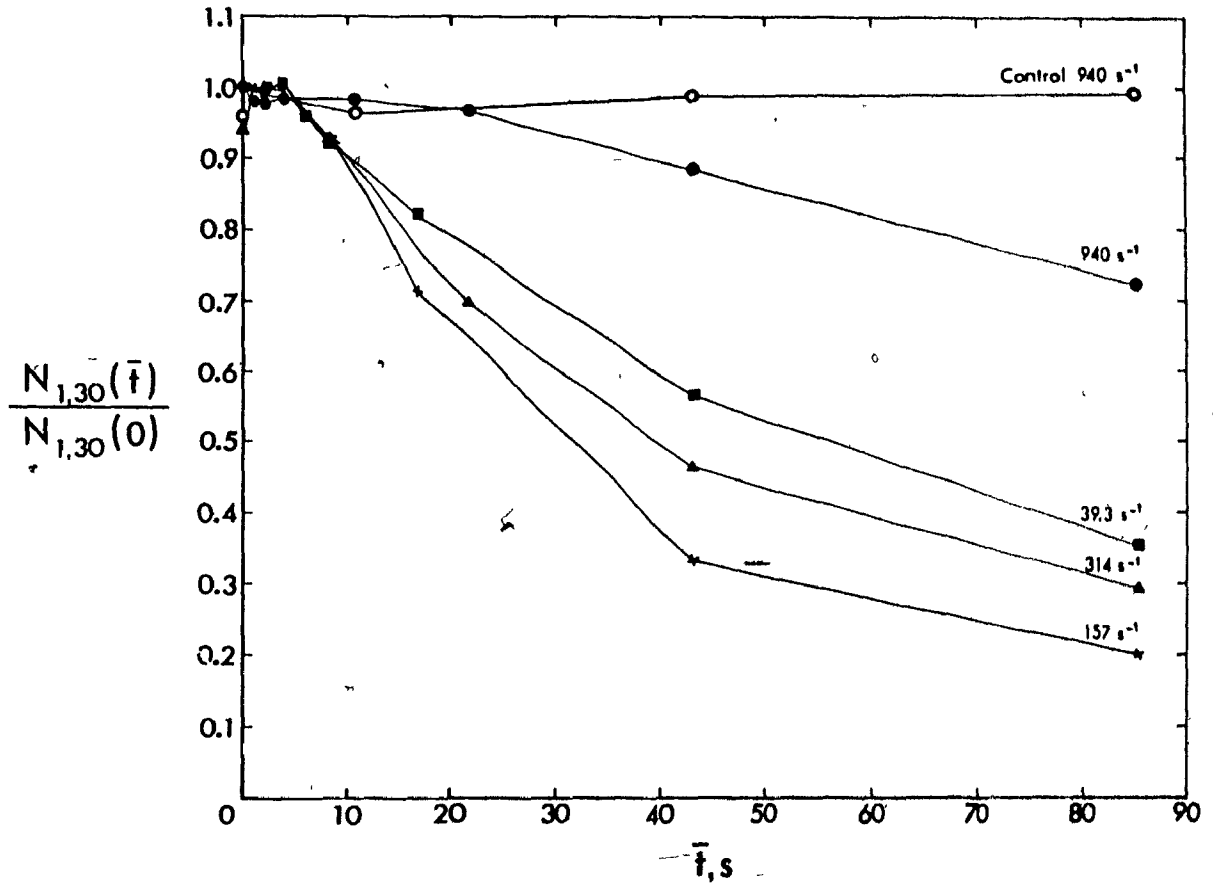


Figure 6: Single Platelet Concentration

The normalized single platelet concentration, $N_{1,30}(\bar{t})/N_{1,30}(0)$, plotted against \bar{t} for $\bar{G} = 39.3, 157, 314, \text{ and } 940 \text{ s}^{-1}$.

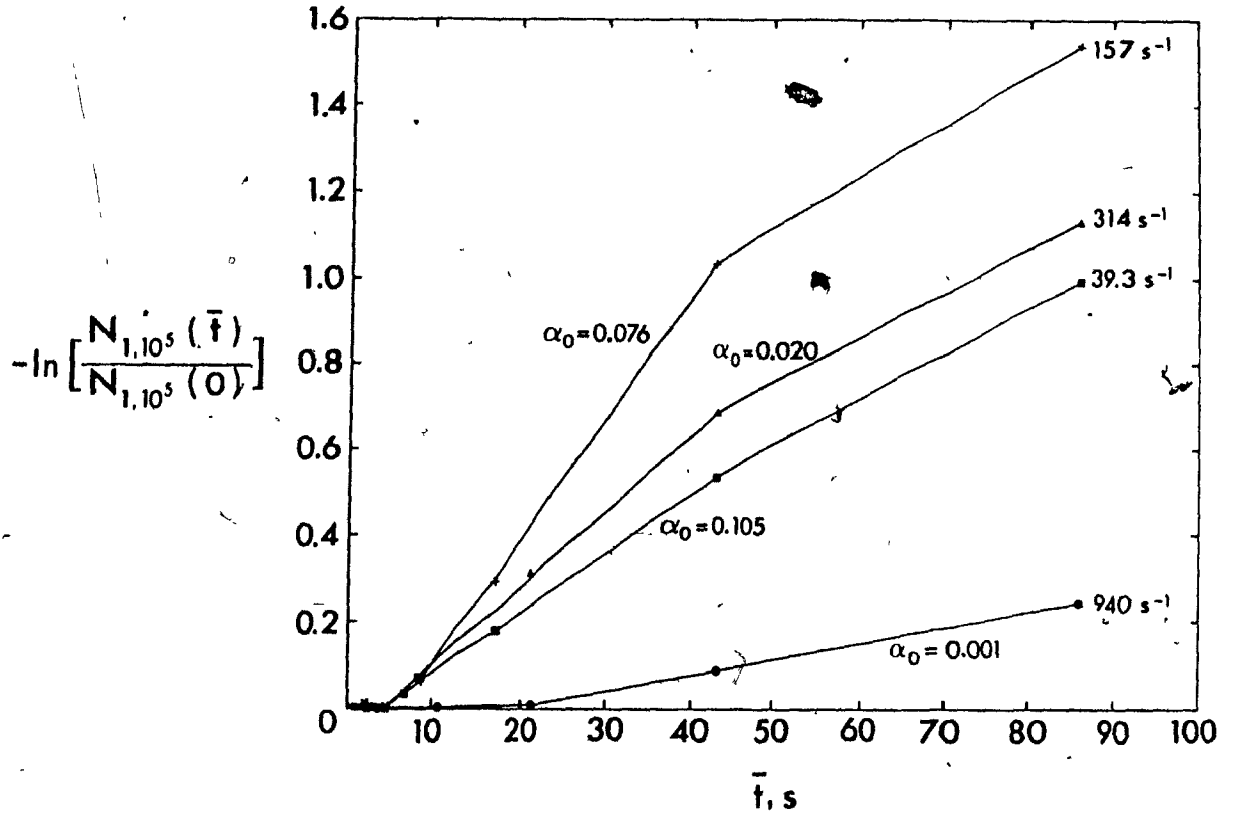


Figure 7: Collision Efficiency

The negative logarithm of the normalized, total particle concentration, $-\ln[N_{1,10^5}(\bar{t})/N_{1,10^5}(0)]$, plotted against \bar{t} for each of the four shear rates in Figure 6. The values of α_0 were calculated over the range $\bar{t} = 4.3$ to 43 s at $\bar{G} < 314 \text{ s}^{-1}$ and the range $\bar{t} = 21$ to 43 s at $\bar{G} = 940 \text{ s}^{-1}$ using Eq. [21].

Beyond $\bar{t} = 43$ s, α_0 appeared to decrease at all \bar{G} below 940 s⁻¹.

(c) Aggregate Growth

As shown in Figure 4, the number concentration of aggregates of volume > 100 μm^3 was so low that frequency histograms do not adequately reflect the contribution of such particles to the total platelet concentration. As a result, the particle volume fraction per histogram class, $\Phi(x_1)$, was plotted against particle volume, $v(x_1)$, in Figure 8 for the same data as in Figure 4 after background was subtracted. The relative contribution of large aggregates to the total volume fraction of cells is readily apparent. Figure 8 shows the formation of distinct peaks of aggregates of successively increasing size with increasing \bar{t} . A maximum aggregate size is also indicated by the sharp drop in particle volume fraction at 10^4 μm^3 at $\bar{t} = 86$ s.

The volume fraction of particles between lower, L, and upper, U, volume limits, $\Phi_{L,U}(\bar{t})$, normalized to the total volume fraction of particles at $\bar{t} = 0$ s, $\Phi_{1,10^5}(0)$, was plotted against \bar{t} in Figure 9 for each of the four shear rates shown in Figure 6. The decrease in the volume fraction of single cells, $1-30$ μm^3 , paralleled the decrease in the number concentration of the same particles in Figure 6. At any given mean transit time the combined volume fraction of aggregates and single cells equals the total volume fraction, $1-10^5$ μm^3 .

At $\bar{G} = 39.3$ s⁻¹ (Fig. 9a), there was a significant fraction of particles between 30 and 10^3 μm^3 at the earliest sampling time, $\bar{t} = 2$ s, and the fraction of single cells was concomitantly reduced. With

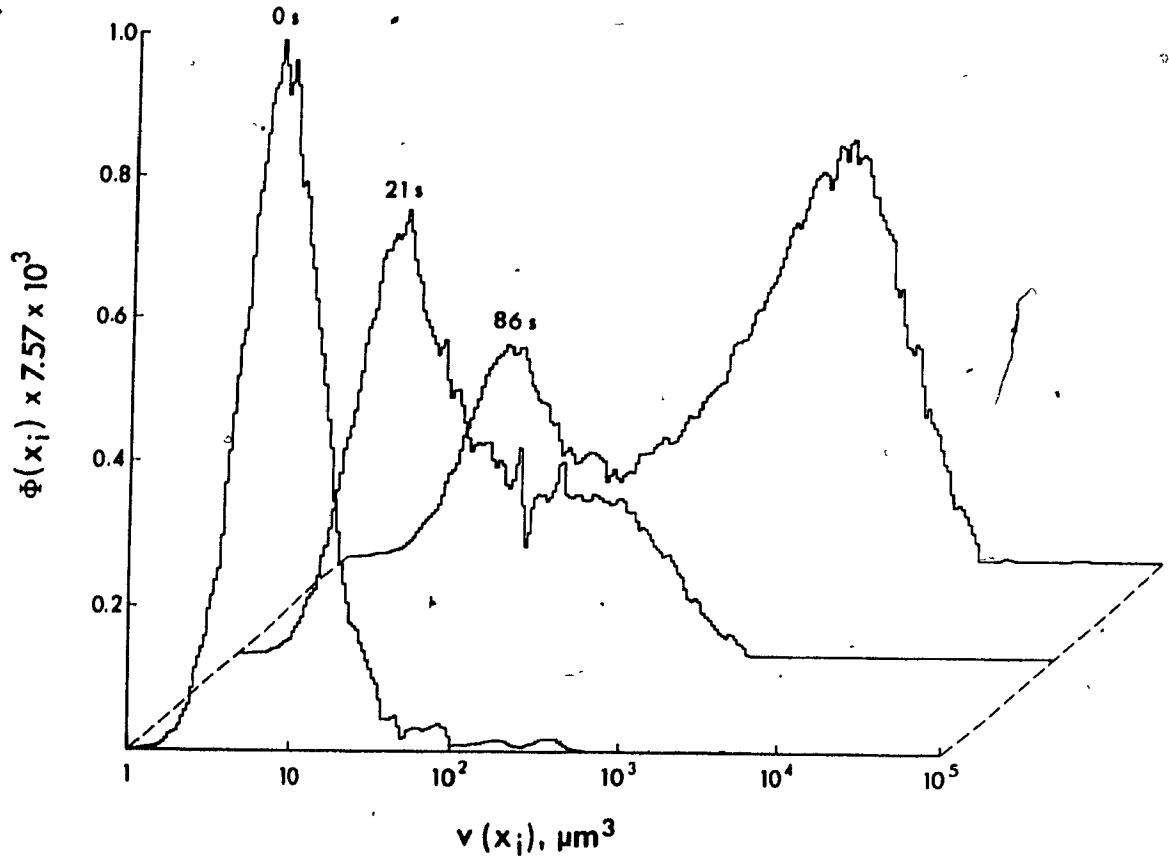
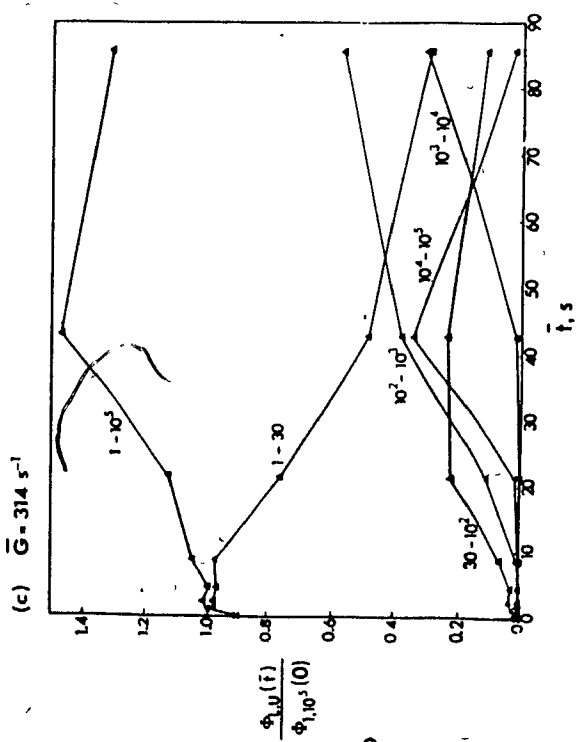
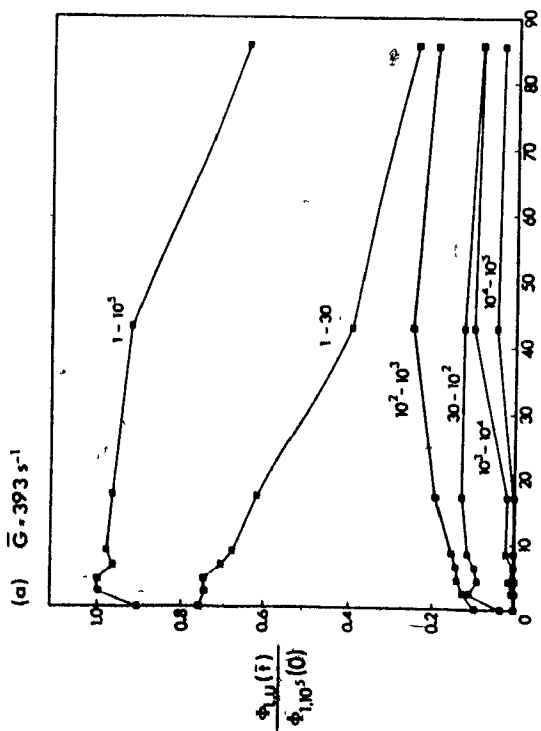
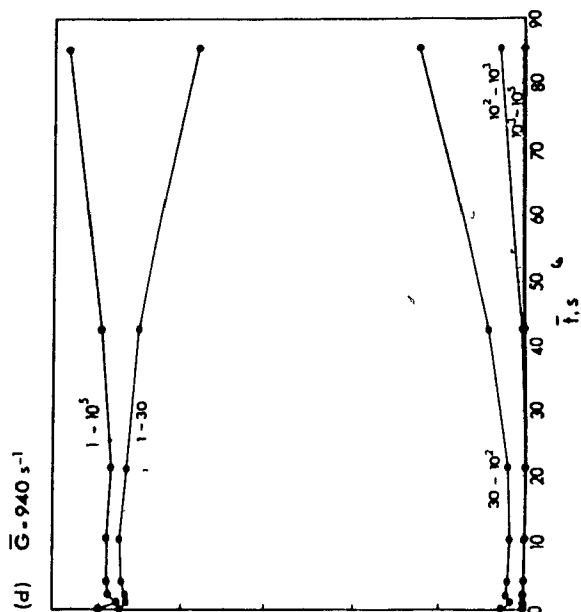
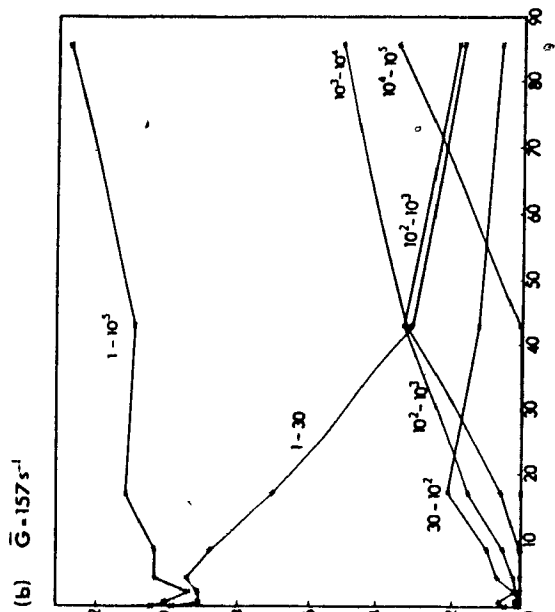


Figure 8: Aggregate Growth

Three-dimensional plot of the volume fraction per histogram class, $\Phi(x_i)$, vs particle volume, $v(x_i)$, for the data of Figure 4 at $t = 0, 21$ and 86 s after background was subtracted.

Figure 9: Effect of Shear Rate on Aggregate Growth

The normalized volume fraction of particles between lower, L, and upper, U, volume limits, $\Phi_{L,U}(\bar{t})/\Phi_{1,10^5}(0)$, plotted against \bar{t} for the data of Figure 6. The volume limits, L-U, from 1-30, 30-10², 10²-10³, 10³-10⁴, 10⁴-10⁵, and 1-10⁵ μm^3 are shown beside their respective plots.



increasing \bar{t} , there was a slight increase in the volume fraction of particles of volume from $30-10^3 \mu\text{m}^3$, followed by an increase in the fraction of particles from $10^3-10^5 \mu\text{m}^3$. During this same time period, the volume fraction of single cells dropped from 75% to 25% of the initial total particle volume fraction.

At $\bar{G} = 157 \text{ s}^{-1}$ (Fig. 9b), the formation of aggregates of successively increasing size with increasing \bar{t} was evident. The sharp drop in the fraction of particles from $1-30 \mu\text{m}^3$ was accompanied by a successive rise and fall in the volume fraction occupied by small aggregates, followed by the steady accumulation of aggregates from $10^3-10^4 \mu\text{m}^3$, and finally of aggregates from $10^4-10^5 \mu\text{m}^3$ beginning at $\bar{t} = 43 \text{ s}$. There was a noticeable increase in the total volume fraction with the appearance of aggregates $> 10^3 \mu\text{m}^3$.

The pattern of aggregation at $\bar{G} = 314 \text{ s}^{-1}$ (Fig. 9c) was similar to that at $\bar{G} = 157 \text{ s}^{-1}$; however, prior to the formation of aggregates from $10^3-10^4 \mu\text{m}^3$, there was an early ($\bar{t} = 43 \text{ s}$) rise in the fraction of particles of volume $10^4-10^5 \mu\text{m}^3$ to $\sim 30\%$ of the total which then decreased to only $\sim 3\%$ by $\bar{t} = 86 \text{ s}$. This decrease was accompanied by both the appearance of smaller aggregates from $10^3-10^4 \mu\text{m}^3$ and a further rise in the volume fraction of aggregates from $10^2-10^3 \mu\text{m}^3$, although the volume fraction of single cells decreased only slightly. This pattern of aggregation is suggestive of aggregate break-up at long \bar{t} . Thus, analyses of aggregation limited to changes in the single platelet concentration or volume fraction do not reveal the changing pattern of aggregate growth.

The modest decrease in the single platelet volume fraction at $\bar{G} = 940 \text{ s}^{-1}$ (Fig. 9d) was accompanied by the formation of only small aggregates $< 10^3 \mu\text{m}^3$.

DISCUSSION

The present work follows directly from previous investigations by this laboratory into the ADP-induced aggregation of human platelets in Poiseuille flow (Bell et al., 1984; Bell and Goldsmith, 1984). The problem of introducing an aggregating agent rapidly and uniformly into a suspension of platelets flowing through a tube was solved by placing a small mixing chamber at the tube entrance. Such a flow system permitted the analysis of platelet aggregation over a wide range of shear rates at both the early and late stages of the reaction. Particle counting and sizing instrumentation were then configured to minimize errors inherent in their operation, and to allow the rapid measurement of the continuous volume distribution of single platelets and aggregates over the range $1-10^5 \mu\text{m}^3$. This chapter introduces the technique and, using a representative donor, demonstrates the pattern of changes in particle volume and concentration during platelet aggregation through the analysis of the complete log-volume histogram.

1. Single Platelet Volume

A dual aperture counting and sizing procedure was necessary to minimize sizing artifacts due to high particle-to-aperture diameter ratios. The dynamic working range of each aperture was increased by using a logarithmic amplifier which allowed the continuous measurement of all

single platelets and aggregates in the range of volume from $1-10^5 \mu\text{m}^3$. A logarithmic expansion was also chosen because numerous studies have established a log-normal distribution of platelet size, whether determined by diameter, mass or volume (von Behrens, 1972; Bahr and Zeitler, 1965; Paulus, 1975). Single platelets and all other particles from $1-10^2 \mu\text{m}^3$ were measured using a $50 \mu\text{m}$ diameter \times $60 \mu\text{m}$ length aperture, and particles from $10^2-10^5 \mu\text{m}^3$ were measured using a $100 \mu\text{m}$ diameter \times $120 \mu\text{m}$ length aperture. The statistical analysis of the shape of the platelet log-volume distributions provided a sensitive measure of departures from normality, and of the presence of microaggregates. The large variance in single platelet volume and the low number concentration of aggregates precluded the resolution of distinct peaks of microaggregates. From inspection of control platelet suspensions where the concentration of microaggregates was low, the range $1-30 \mu\text{m}^3$ was selected to be principally single platelets, despite considerable overlap of single platelet and microaggregate volume. A more conservative estimate of the single platelet volume range, $1-50 \mu\text{m}^3$, was selected for the statistical analysis of the single platelet volume distribution in order to reduce subjective bias in the selection of platelet volume.

Good agreement was found with the log-normal model for the distribution of single platelet volume. In shear flow, both native and fixed unactivated, single platelets behave as rigid oblate ellipsoids of revolution with a mean axis ratio of 0.36 (Frojmovic et al., 1976). Aperture-impedance particle counters such as the Coulter ZM measure the volume of liquid displaced by a particle in the sensing zone of the aperture through an incremental increase in the resistance of the

suspending electrolyte. It is well-known, however, that these instruments overestimate the volume of suspended particles by factors dependent on particle shape (Grover et al., 1969a; Hurley, 1970), orientation in and trajectory through the aperture (Shank et al., 1969; Akeson and Mel, 1986), and the ratio of particle diameter to aperture diameter (Smythe, 1961; 1964). Most single platelets are measured in the central core of the aperture where the electrical field and fluid velocity are uniform, and experience little rotation on transit through the aperture (Grover et al., 1969a; Kachel, 1979; Waterman et al., 1975). Thus, the shape factor, which is the ratio of the voltage pulse height generated by a given particle to the minimum pulse height generated by a particle of the same volume, can be considered constant at 1.2 when the major axis of the platelet is aligned with the aperture axis (Velik and Gorin, 1940; Grover et al., 1969a). Since the Coulter ZM was calibrated with spheres of shape factor 1.5 (Gregg and Steidley, 1965; Grover et al., 1969a, 1969b; Hurley, 1970), the measured volume of single cells and aggregates were those of the equivalent spherical particle. The measured single platelet volume must then be multiplied by 1.5/1.2 to give the absolute single platelet volume. The correction factor of 1.25 has been experimentally verified for the ratio of the volume of the approximately spherical platelets suspended in EDTA to the approximately discoid platelets in citrated plasma, and found to remain relatively constant after fixation of the cells in glutaraldehyde (Mundschenk et al., 1976). In addition, after exposure to 10 μ M ADP, the volume of the more spherical shape-changed platelets was ~ 25% greater than the uncorrected volume of their unactivated more discoid counterparts when measured on a Coulter Counter (Holme and Murphy, 1980). Thus, in the absence of shape change, the

absolute mean single platelet volume given in Table 2 after background subtraction is $9.1 \mu\text{m}^3$. A statistical analysis of the mean platelet volume of several donors is given in Chapter III of this thesis. Since activated platelets and aggregates can assume a wide array of complex shapes having separate shape factors, both were treated as the equivalent spherical particle for the analysis of aggregation. No shape factor was necessary to determine the absolute equivalent sphere volume of these particles.

The shape factor also increases with increasing particle diameter to aperture diameter ratios above 0.2 (Smythe, 1961; 1964). Since the diameter of the largest spherical particle measured on the $50 \times 60 \mu\text{m}$ aperture was only 12% of the aperture diameter, all equivalent sphere volumes measured on this aperture were absolute within the limitations given above and below. On the $100 \times 120 \mu\text{m}$ aperture, however, particle size can reach 58% of the aperture diameter over the volume range of the present experiments. Consequently, the volume of particles $> 4000 \mu\text{m}^3$ was overestimated. Since all platelet suspensions were measured under identical conditions, aggregation was satisfactorily followed through the relative changes in the concentration of particles of an approximate absolute equivalent sphere volume.

The electrical field only reaches a radially uniform value at distances greater than one aperture diameter into the aperture (Grover et al., 1969a). The volume of particles traveling on trajectories near the aperture wall where both the electrical field and fluid velocity are nonuniform is overestimated (Shank et al., 1969; Thom et al., 1969; Kachel, 1979). There is no single correction factor for such

measurements; however, the use of deep-bore apertures with length to diameter ratios of 1.2 considerably reduced the positive skewing of the single platelet log-volume distribution caused by the overestimated particle volumes. Indeed, as shown in Table 2, the slight positive skewing of the single platelet log-volume histogram after background subtraction was insufficient to influence the positive fit of a normal distribution as verified by the Kolmogorov-Smirnov test. This test is easy to perform for continuous frequency distributions and is more powerful than the parametric chi-square test since no assumption is made about the distribution of sampling error. The artifactual positive skewing could be further reduced by using a hydrodynamic focusing device to direct the particle stream through the center of the aperture (Spielman and Goren, 1968; Kachel et al., 1970). The deep-bore apertures provided satisfactory results, however, and were more convenient for processing the large number of samples to be counted and sized in the present experiments.

2. Platelet Aggregation

A ready index of the degree of aggregation is the decrease in the concentration of single cells. Analysis of the aggregation of platelets from a representative donor revealed a substantial delay before the onset of aggregation at all mean tube shear rates tested and suggested the existence of a limiting shear rate above which aggregation is prevented. Although the rate of aggregation was greatest at $\bar{G} = 157 \text{ s}^{-1}$, the collision efficiency, α_0 , decreased steadily with increasing mean tube shear rate from $\bar{G} = 39.3$ to 940 s^{-1} . Intuitively, this can be understood by realizing that the two-body collision frequency predicted by Eq. [18]

for $\bar{G} = 157 \text{ s}^{-1}$ was 4x that at $\bar{G} = 39.3 \text{ s}^{-1}$. Thus, the slope of the curve at $\bar{G} = 157 \text{ s}^{-1}$ in Figure 6 should be 4x that at $\bar{G} = 39.3 \text{ s}^{-1}$, simply to maintain the same collision efficiency. The inverse relationship between α_0 and \bar{G} is in agreement with theory and experiment for suspensions of charged colloidal particles (van de Ven and Mason, 1977). Since the theory is strictly applicable to collisions between single equal-sized spherical particles, and assumes no doublet break-up, it is valid only at the early stages of platelet aggregation. As a result, the decrease in α_0 at long mean transit times may simply be due to a lowered collision rate from the lower particle concentration, despite the greater collision cross-section of the larger particles. Indeed, in the case where aggregation was less extensive, $\bar{G} = 940 \text{ s}^{-1}$, the collision efficiency still appeared to be constant at $\bar{t} = 86 \text{ s}$.

Neither changes in the single platelet concentration nor the collision efficiency yielded information on the pattern of aggregate growth. Since the number concentration of aggregates was so low, the volume fraction of particles was used as an index of aggregate size. Volume fraction histograms revealed that aggregate size increased in discrete increments, even for very large-sized aggregates where the potential variation in size and shape is great, and that, at any given \bar{t} and \bar{G} , there is a maximum upper limit to particle size. More surprisingly, analyses of changes in the concentration of particles of discrete sizes showed that at $\bar{G} = 314 \text{ s}^{-1}$ there was an initial rapid growth of large aggregates that appeared to break up at longer mean transit times. This clearly illustrates the antagonistic effects of collision rate and fluid shear stress, both of which are dependent on

shear rate. The rapid formation of large aggregates is indicative of a "snowball" effect at high collision rates (Bell and Goldsmith, 1984), and the subsequent break-up is indicative of platelet deactivation at long mean transit times. Although break-up is not evident at $\bar{G} = 157 \text{ s}^{-1}$, the collision rate was not sufficient to support the "snowball" effect and the rapid formation of large aggregates. The large increase in the total volume fraction of particles accompanying the formation of large aggregates of volume between 10^3 and $10^5 \mu\text{m}^3$ is likely the result of an increase in the aggregate void volume (Born and Hume, 1967; Belval and Hellums, 1986), and of the artifactual overestimation of the volume of large particles discussed previously. The total volume fraction subsequently decreased with the formation of aggregates of volume greater than the maximum volume measured in the present experiments, $10^5 \mu\text{m}^3$.

A much higher shear rate, $\bar{G} = 940 \text{ s}^{-1}$, appeared to inhibit aggregate formation initially. The continued formation of aggregates at $\bar{t} = 86 \text{ s}$, at this shear rate, however, suggests the presence of more than one type of platelet-platelet bond: an early bond of weak strength and a stronger bond that forms later in time. Thus, the critical shear rate for either the inhibition of aggregation or the initiation of aggregate break-up is likely time-dependent.

3. Summary

The present work demonstrates an effective technique for following platelet aggregation in Poiseuille flow after rapid and uniform exposure of the cells to known concentrations of ADP. The entire volume distribution of particles between 1 and $10^5 \mu\text{m}^3$ can be analyzed over a

wide range of shear rate and transit time. Changes in the single platelet concentration provide a ready measure of the overall rate and extent of aggregation while changes in the total particle concentration yield values of the collision efficiency. A sensitive index of aggregate growth is provided by changes in the volume fraction of particles in suspension. Together, all three approaches provide a complete account of the aggregation process.

The following chapters of this thesis constitute a comprehensive study on the ADP-induced aggregation of human platelets in Poiseuille flow covering many donors. The effects of shear rate, transit time, donor sex, ADP concentration, and red blood cells are followed through the measurement of the single platelet concentration, the collision efficiency and the volume fraction of particles.

REFERENCES

- AKESON, S.P., AND MEL, H.C. (1986). Deformability and other rheological interactions of red blood cells in electronic sizing. Biorheology 23, 1-5.
- BAHR, G.F., AND ZEITLER, E. (1965). The determination of the dry mass in populations of isolated particles. Lab. Invest. 14, 955.
- BELL, D.N. (1983). Platelet Aggregation in Poiseuille Flow: A Double Infusion Technique. M.Sc. Thesis, McGill University.
- BELL, D.N., AND GOLDSMITH, H.L. (1984). Platelet aggregation in Poiseuille flow: II. Effect of shear rate. Microvasc. Res. 27, 216-330.
- BELL, D.N., TEIRLINCK, H.C., AND GOLDSMITH, H.L. (1984). Platelet aggregation in Poiseuille flow: I. A double infusion technique. Microvasc. Res. 27, 297-315.
- BELVAL, T., AND HELLUMS, J.D. (1986). The analysis of shear-induced platelet aggregation with population balance mathematics. Biophys. J. 50, 479-487.
- BELVAL, T., HELLUMS, J.D., AND SOLIS, T. (1984). The kinetics of platelet aggregation induced by shear. Microvasc. Res. 28, 279-288.
- BORN, G.V.R. (1962). Aggregation of blood platelets by adenosine diphosphate and its reversal. Nature 194, 927-929.
- BORN, G.V.R., AND HUME, M. (1967). Effects of the numbers and sizes of platelet aggregates on the optical density of plasma. Nature 215, 1027-1029.
- BRENNER, H. (1961). The slow motion of a sphere through a viscous fluid towards a plane surface. Chem. Eng. Sci. 16, 242-251.
- CHANG, H.N., AND ROBERTSON, R. (1976). Platelet aggregation by laminar shear and Brownian motion. Ann. Biomed. Eng. 4, 151-183.

- CHIEN, S. (1975). Biophysical behavior of red cells in suspensions. In "The Red Cell" (D. MacSurgenor, ed.), pp. 1031-1133. Academic Press, New York, NY.
- COULTER CHANNELYZER MANUAL. Manual for the Coulter Channelyzer C1000. Coulter Electronics, Hialeah, Florida. 1978.
- DOCUMENTA GEIGY (1962). "Scientific Tables" (K. Diem, ed.), p.164. Geigy Pharmaceuticals, Montreal, QC.
- FROJMOVIC, M.M., NEWTON, M., AND GOLDSMITH, H.L. (1976). The microrheology of mammalian platelets: Studies of rheo-optical transients and flow in tubes. Microvasc. Res. 11, 203-215.
- GEAR, A.R.L. (1982). Rapid reactions of platelets studied by a quenched flow approach: Aggregation kinetics. J. Lab. Clin. Med. 100, 866-886.
- GEAR, A.R.L., AND LAMBRECHT, J.K. (1981). Reduction in single platelets during primary and secondary aggregation. Thromb. Haemost. 45, 298.
- GOLDSMITH, H.L., AND MASON, S.G. (1964). The flow of suspensions through tubes. III. Collisions of small uniform spheres. Proc. Roy. Soc. A 282, 569-591.
- GREGG, E.C., AND STEIDLEY, K.D. (1965). Electrical counting and sizing of mammalian cells in suspension. Biophys. J. 5, 393-405.
- GROVER, N.B., NAAMAN, J., BEN-SASSON, S., AND DOLJANSKI, F. (1969a). Electrical sizing of particles in suspensions. I. Theory. Biophys. J. 9, 1398-1425.
- GROVER, N.B., NAAMAN, J., BEN-SASSON, S., DOLJANSKI, F., AND NADAV, E. (1969b). Electrical sizing of particles in suspensions. II. Experiments with rigid spheres. Biophys. J. 9, 1415-1425.
- HOLME, S. AND MURPHY, S. (1980). Coulter Counter and light transmission studies of platelets exposed to low temperature, ADP, EDTA, and storage at 22°. J. Lab. Clin. Med. 96, 480-493.
- HURLEY, J. (1970). Sizing particles with a Coulter counter. Biophys. J. 10, 74-79.

- KACHEL, V., METZGER, H., AND RUHENSTROTH-BAUER, G. (1970): The influence of the particle path on the volume distribution curves according to the Coulter method. Z. Ges. Exp. Med. 153, 331-347.
- KACHEL, V. (1979). Electrical resistance pulse sizing (Coulter sizing). In "Flow Cytometry and Sorting" (M.R. Melamed, P.F. Mullaney, and M.L. Mendelsohn, eds.), pp. 61-104. Wiley, New York, NY.
- KENNEY, J.K., AND KEEPING, E.S. (1951). "Mathematics of Statistics" (Part Two). D. Van Nostrand, Toronto, ON.
- LILLIEFORS, H.W. (1967). On the Kolmogorov-Smirnov test for normality with mean and variance unknown. Am. Statist. Assoc. J. 62, 399.
- MANLEY, R. ST.J., AND MASON, S.G. (1952). Particle motions in sheared suspensions. II. Collisions of uniform spheres. J. Coll. Sci. 7, 354-369.
- MUNDSCHENK, D.D., CONNELLY, D.P., WHITE, J.G., AND BRUNNING, R.D. (1976). An improved technique for the electronic measurement of platelet size and shape. J. Lab. Clin. Med. 88, 310-315.
- NICHOLS, A.R., AND BOSMANN, H.B. (1979). Platelet aggregation: newly quantified using nonempirical parameters. Thromb. Haemost. 42, 679-693.
- PAULUS, J. (1975). Platelet size in man. Blood 46, 321-336.
- SCHLICHTING, H. (1968). "Boundary Layer Theory", 6th edition, p. 589. McGraw Hill, New York, NY.
- SHANK, B.B., ADAMS, R.B., STEIDLEY, K.D., AND MURPHY, J.R. (1969). A physical explanation of the bimodal distribution obtained by electronic sizing of erythrocytes. J. Lab. Clin. Med. 74, 630-641.
- SMOLUCHOWSKI, M. VON (1917). Versuch einer mathematischen Theorie der Koagulationskinetik kolloider Lösungen. Z. Physik. Chem. 92, 129-168.
- SMYTHE, W.R. (1961). Flow around a sphere in a circular tube. Phys. Fluids 7, 756-759.

- SMYTHE, W.R. (1964). Flow around spheroids in a circular tube. Phys. Fluids 7, 633-638.
- SOKAL, R.R., AND ROHLF, F.J. (1969). "Biometry". Freeman, San Francisco, CA.
- SPIELMAN, L., AND GOREN, S.L. (1968). Improving resolution in Coulter counting by hydrodynamic focusing. J. Coll. Int. Sci. 26, 175-182.
- SWIFT, D.L., AND FRIEDLANDER, S.K. (1964). The coagulation of hydrosols by Brownian motion and laminar shear flow. J. Coll. Sci. 19, 621-647.
- THOM, R., HAMPE, A., AND SAUERBREY, G. (1969). Die elektronische Volumenbestimmung von Blutkörperchen und ihre Fehlerquellen. Z. Ges. Exp. Med. 151, 331-349.
- TURITTO, V.T., AND BAUMGARTNER, H.R. (1982). Platelet surface interactions. In "Hemostasis and Thrombosis, Basic Principles and Clinical Practice" (R.W. Colman, J. Hirsh, V.J. Marder and E.W. Salzman, eds.), pp. 354-379. J.B. Lippincott, Philadelphia, PA.
- VAN DE VEN, T.G.M., AND MASON, S.G. (1977). The microrheology of colloidal dispersions. VII. Orthokinetic doublet formation of spheres. Coll. Polymer. Sci. 255, 468-479.
- VELICK, S., AND GOREN, M. (1940). The electrical conductivity of suspensions of ellipsoids and its relation to the study of avian erythrocytes. J. Gen. Physiol. 23, 753-771.
- VON BEHRENS, W.E. (1972). Platelet size. Thesis submitted for the degree of Doctor of Medicine, University of Adelaide, Adelaide, South Australia.
- WATERMAN, C.S., ATKINSON, E.E., WILKINS, B., FISCHER, C.L., AND KIMZEY, S.L. (1975). Improved measurement of erythrocyte volume distribution by aperture-counter signal analysis. Clin. Chem. 21, 1201-1211.

WHITMORE, R.L. (1968). "Rheology of the Circulation". Pergamon Press, Oxford, UK.

YOUNG, I.T. (1977). Proof without prejudice: Use of the Kolmogorov-Smirnov test for the analysis of histograms from flow systems and other sources. J. Histochem. Cytochem. 25, 935-941.

CHAPTER III

EFFECT OF SHEAR RATE AND ADP CONCENTRATION

ABSTRACT

The effect of shear rate on the ADP-induced aggregation of human platelets in Poiseuille flow was studied using a previously described technique for measuring the concentration and volume of single platelets and aggregates in platelet-rich plasma, PRP (Chapter II, this thesis). The rate and extent of aggregation were explained in terms of the effect of shear rate on the number of collisions between activated platelets and the level of fluid shear stress. At a low level of platelet stimulation in citrated plasma, changes in the single platelet concentration with time and shear rate suggest that more than one type of platelet-platelet bond mediates platelet aggregation at physiological shear rates. Changes in the single platelet concentration, however, do not adequately reflect changes in the rate of aggregate growth which was generally observed to decrease with increasing mean tube shear rate from 39.3 to 1800 s^{-1} . Both the rate of single platelet aggregation and aggregate growth were always greater for female donors than for male donors. This sex difference is related to differences in the hematocrit between the two groups. At high levels of platelet stimulation, the rate of single platelet aggregation was much higher but aggregate size was still limited at high shear rates.

INTRODUCTION

Shear rate is the most important physical parameter governing platelet aggregation in flowing suspensions. It determines the platelet collision frequency, the shear and normal stresses which activate single cells and break up aggregates, and the interaction time of cell-cell or cell-surface collisions. Since shear rate is proportional to fluid velocity, these factors either promote or inhibit hemostatic or thrombotic mechanisms, depending on flow rate and vessel size. The predilection of white platelet thrombi to form in regions of high blood flow velocities, i.e., in the arterial as opposed to the venous side of the vasculature, emphasizes the need to focus on the effect of shear rate on platelet aggregation in well-defined flow. Time-averaged systemic arterial wall shear rate in humans ranges from 100 - 1000 s^{-1} and may exceed 1000 s^{-1} in the capillaries, based on a parabolic velocity profile for whole blood (Whitmore, 1968; Chien, 1975; Turitto 1982). A higher rate of wall shear would be expected for a blunted velocity profile (Goldsmith, 1972), but it is unlikely that shear rate exceeds 2000 s^{-1} in the normal human vasculature (Turitto and Baumgartner, 1982). It has been shown in vitro that shear rates less than 2000 s^{-1} are insufficient to activate platelets directly and induce aggregation (Chang and Robertson, 1976; Gear, 1982; Yung and Frojmovic, 1982; Bell and Goldsmith, 1984; Belval et al., 1984; Belval and Hellums, 1986). However, the higher shear rates commonly found in extracorporeal flow devices and vascular prostheses can induce platelet aggregation, release and lysis depending on the magnitude of the fluid shear stress and the time of exposure to the shear field (Brown et al., 1975; Colantuoni et al., 1977; Dewitz et al., 1978; Belval et al., 1984;

Jen and McIntire, 1984).

The importance of the release of platelet-derived platelet agonists, particularly ADP, in sustaining and enhancing shear-induced platelet aggregation has led to a number of studies on the effect of flow on agonist-induced platelet aggregation. Since high shear stresses activate platelets and induce release, the aggregation of platelets in response to exogenous agonists is generally confined to shear rates and to agonist concentrations that are below the threshold for release. Room temperature facilitates such studies since platelet release is inhibited at ambient temperatures below 27°C (Valdorf-Hansen and Zucker, 1971), although aggregation in response to ADP is enhanced. Studies of agonist-induced platelet aggregation in laminar flow, however, are handicapped by the method of mixing agonist and platelets. Rapid mixing ensures uniform exposure of all cells to the agonist and allows early observation of the aggregation reaction, but usually requires interruption of the conditions of flow that are the subject of study. While most studies address this issue, the development of well-defined laminar flow regimes has tended to supersede considerations of agonist diffusion and exposure time. In addition, most techniques have relied upon gross indices of platelet aggregation, such as changes in suspension turbidity or single platelet concentration, and have not focused on the kinetics of aggregate growth and/or break-up.

Despite variability in the ADP concentration and suspension temperature used, several studies have shown the aggregation of ADP-stimulated platelets to increase with increasing shear rate over the

range from 0 - 2200 s^{-1} . Chang and Robertson (1976) followed the kinetics of both Brownian motion- and shear-induced aggregation at 25°C in a cylindrical Couette using measurements of suspension turbidity. At 10 μM ADP, the rate of aggregation was shown to increase over the range of shear rate from 10 to 75 s^{-1} and level off beyond 75 s^{-1} , although shear rates greater than 100 s^{-1} were not tested. The rate of aggregation increased with increasing ADP concentration, reaching a maximum at 100 μM ADP; however, the early stages of aggregation were lost due to a 10 s pre-shear mixing period. As well, aggregate size and the kinetics of aggregate growth could not be extracted from the changes in suspension turbidity that were used to monitor aggregation. Unstable aggregates that formed at 1.5 μM ADP in a parallel plate Couette at shear rates less than 150 s^{-1} at 37°C were stable at 5 μM ADP (Yung and Frojmovic, 1982); however, the release of endogenous ADP at the higher level of platelet stimulation would have increased the effective ADP concentration. Again, a brief period of high shear used to mix the ADP and platelets prevented observation of the early stages of the aggregation reaction.

The complete aggregation reaction has been observed directly using a microscopic double infusion system which allowed the rapid diffusion of ADP throughout the bulk of a platelet suspension undergoing Poiseuille flow (Bell et al., 1984; Bell and Goldsmith, 1984). In contrast to conventional fixed-volume rotational viscometers and aggregometer cuvettes, such a flow-through system more closely mimics in vivo conditions. Even though mixing is complete, collisions can occur between platelets at different stages of activation due to the nonlinear velocity profile. At 1 μM ADP, at room temperature the rate and final

extent of aggregation after a transit time of 40 s increased with increasing mean tube shear rate, \bar{G} , over the range 4 - 54 s^{-1} . The concentration of aggregates of successively increasing size increased and then decreased in accordance with the kinetics of aggregate growth predicted by Smoluchowski for inert colloidal size particles (Smoluchowski, 1917). Aggregates formed most rapidly in the region of the highest shear near the tube wall and as they grew in size and rotated, collisions with the wall resulted in the formation of large (> 100 platelets) centrally-located aggregates. Higher shear rates and longer exposure times were impractical due to the microscopic dimensions of the flow system and constraints on the distance for complete diffusion of ADP. Independent measurements of the decrease in the concentration of single platelets in Poiseuille flow have shown that higher shear rates enhance ADP-induced aggregation (Gear, 1982). At 10 μM ADP and at 37°C, it was found that ~ 50% of the platelets had aggregated within 2 - 4 s of flow through the reaction tube at $\bar{G} = 1300$ or 2200 s^{-1} , with the rate of aggregation higher at the higher shear rate. Again, the release of endogenous ADP at 37°C would considerably augment the degree of aggregation.

Surface-mediated aggregation has also been induced by exogenous ADP in vitro and in vivo. Grabowski et al. (1978) induced the repeated growth and embolization of aggregates adherent to a synthetic membrane through which ADP was infused. At millimolar ADP concentrations, the growth rate prior to embolization increased monotonically over the range of surface shear rate from 99 - 986 s^{-1} but in the micromolar range of ADP, aggregate growth decreased beyond surface shear rates of 394 s^{-1} .

Iontophoretic application of ADP to small venules (40 - 70 μm) in the hamster cheek pouch yielded a maximum growth rate prior to embolization at mean blood velocities of 0.30 - 0.40 mm s^{-1} , independent of vessel size (Begent and Born, 1970). Higher velocities (0.60 - 2.50 mm s^{-1}) produced a decrease in aggregate growth rate which eventually levelled off, while no aggregates formed above 3.0 mm s^{-1} . The combination of short platelet-surface interaction times and high shear stress may have restricted aggregate growth, although the dilution of ADP at high flow rates may have limited the extent of platelet activation.

This work examines the effect of shear rate on the ADP-induced aggregation of human platelets in Poiseuille flow. In the preceding chapter a method was introduced for rapidly mixing ADP and platelet suspension prior to flowing through fixed lengths of polyethylene tubing at controlled rates. The number concentration and volume of single platelets and aggregates were measured in the glutaraldehyde-fixed effluent using an electronic particle counter. Aggregation was expressed in terms of the decrease in the concentration of single platelets and through changes in the volume fraction of single cells and aggregates over the volume range from 1 - $10^5 \mu\text{m}^3$. The two-body collision efficiency was calculated from changes in the total particle concentration according to existing theory. This chapter uses the method of Chapter II to follow the aggregation of platelets in the citrated plasma of a large group of donors over a range of mean tube shear rate from 39.3 to 1800 s^{-1} at 0.2 and 1.0 μM ADP at room temperature.

MATERIALS AND METHODS

1. Platelet-Rich Plasma and Reagents

Experiments were performed as described in Chapter II. Venous blood was slowly drawn from equal numbers of healthy, age-matched male and female volunteers into 1/10 volume, 3.8% sodium citrate. All donors had refrained from aspirin ingestion for at least 10 days prior to blood withdrawal and no female donors were taking oral contraceptives. Hematocrit, HCT, was determined on undiluted venous blood at the time of blood withdrawal. After incubating the blood at 37°C for 30 min, platelet-rich plasma, PRP, was prepared at room temperature by centrifuging the whole blood at 100g for 20 min, and platelet-poor plasma, PPP, by centrifuging the remaining blood at 2000g for a further 20 min. All platelet suspensions were maintained under a mixture of 95% air and 5% CO₂ to preserve pH 7.4. Frozen aliquots of 2.0 mM adenosine-5'-diphosphate, ADP, and 100 NIH U ml⁻¹ human thrombin (Sigma, St. Louis, MO) were thawed immediately prior to use and diluted in modified Tyrodes (137 mM NaCl, 2.7 mM KCl, 11.9 mM NaHCO₃, 0.36 mM NaH₂PO₄·H₂O) at pH 7.4. Fifty millimolar acetyl salicylic acid, ASA, was solubilized by treatment with 5 N NaOH and then titrated to pH 7.4 with 1 N HCl. When required, PRP was incubated for 10 min at 37°C with 1% (v/v) stock ASA. For work done at room temperature, the PRP was incubated for a further 10 min in a 22°C water bath.

2. Flow System

All flow experiments were performed at 23 ± 1°C. Platelet-rich plasma was adjusted with PPP to 3.30 × 10⁵ cells μl⁻¹ and infused into a small cylindrical mixing chamber (6 mm i.d., 9.5 mm o.d., 1.5 mm height)

using a syringe pump. ADP was simultaneously infused into the mixing chamber via an independent syringe pump at a fixed flow ratio, PRP:ADP = 9:1. After rapid mixing, the PRP-ADP suspension exited the chamber and flowed through lengths of 0.595 or 0.380 mm radius, R_0 , polyethylene tubing (Clay Adams, Parsippany, NJ), for preset mean cell transit times, $\bar{t} = X_3/\bar{U}$, from < 0.1 to 86 s, where X_3 is the distance down the flow tube and \bar{U} is the mean linear fluid velocity. The aggregation reaction was instantaneously and permanently arrested by collecting known volumes of the effluent into 20x the suspension volume of 0.5% (v/v) isotonic glutaraldehyde (J.B. EM Services, Pointe Claire-Dorval, QC). Total volume flow rates, Q , were preset from 13 to 155 $\mu\text{l s}^{-1}$ to generate mean tube shear rates, $\bar{G} = 2Q/\pi R_0^3$, between 39.3 and 1800 s^{-1} .

3. Thromboxane B₂

Thromboxane B₂, TXB₂, was measured to a lower limit of 50 pg ml⁻¹ in the plasma of selected experiments by radioimmunoassay, RIA, using ³H-TXB₂ (New England Nuclear, NEK700A, Lachine QC). Approximately 800 μl of unfixed effluent platelet suspension were collected into 1 ml plastic syringes and immediately filtered free of cells using 0.2 μm pore syringe filter units (Millex-GS, Millipore, Mississauga, ON). The filtered plasma was incubated for 20 min at 37°C and stored at -20°C until the RIA was performed.

4. Particle Concentration and Size

The number concentration and size of single platelets and aggregates were measured using an electronic particle counter (Coulter ZM, Coulter Electronics, Hialeah, FL) in conjunction with a logarithmic

amplifier (Coulter Log Range Expander) and a 100 channel pulse height analyzer (Coulter Channelyzer C1000) to generate a 250 class log-volume histogram over the volume range $1 - 10^5 \mu\text{m}^3$. As described in detail in Chapter II, permanent tracings (Coulter XY4 Recorder) of each histogram were manually transposed into a microcomputer (HP 86, Hewlett Packard, Kirkland, QC) using a digitizer (HP 9111A). The distribution of background in the small volume range of the log-volume histograms was measured separately in PPP and then fitted by a decreasing exponential function using a weighted least squares regression. Using a trial and error iterative procedure, a normal curve was fitted to the distribution of single platelet log-volume over the range where the influence of background and microaggregate contamination is minimal. Background was subtracted from the measured log-volume histograms to give the same content in class 1 of the resultant histogram as that predicted by a normal distribution of single platelet log-volume. The number concentration per histogram class is $N(x_i)$, particle volume $v(x_i)$, and volume fraction $\Phi(x_i) = N(x_i)v(x_i)$, where x_i is the mark of the i^{th} class. Computer-integration of the log-volume histograms yielded the number of particles counted, $n_{L,U}(\bar{t})$, the number concentration, $N_{L,U}(\bar{t})$, and the volume fraction, $\Phi_{L,U}(\bar{t})$, of particles between lower, L, and upper, U, volume limits at time \bar{t} .

Average log-volume histograms were generated from multiple donors at each mean transit time after the individual histograms were transformed into equivalent histograms using the average of the mean single platelet volume and standard deviation of all donors concerned. The mean, normalized volume fraction of the i^{th} class is given by

$\bar{\Phi}(x_1) = [\bar{N}(x_1)v(x_1)]/[\bar{N}(x_m)v(x_m)]$, where $\bar{N}(x_1)$ is the mean normalized particle concentration per histogram class, and $\bar{N}(x_m)$ and $v(x_m)$ are the respective mean normalized number concentration and volume of the class of maximum concentration, m , at $\bar{t} = 0$ s. Details of the transformation and averaging are described in Appendix II. The ultimate effect of these procedures is to provide an estimate of the changes in particle volume in relation to the mean single platelet volume and standard deviation, as opposed to simply averaging changes in absolute volume.

5. Statistics

The mean, $\bar{\mu}$, mode, μ_{mod} , median, μ_{med} , and standard deviation, σ , of the linear volume distribution were calculated from the mean, \bar{x} , and standard deviation, s , of the log-volume distribution, assuming a normal distribution of the latter (Kenney and Keeping, 1951; Documenta Geigy, 1962). The assumption of log-normality of single platelet volume was tested using the Kolmogorov-Smirnov, K-S, one sample test (Young, 1977; Lilliefors, 1967). Skewing, g_1 , and kurtosis, g_2 , of the log-volume histograms and their standard errors were determined using standard equations for frequency distributions (Sokal and Rohlf, 1969). The significance of deviation of these sample statistics from the parametric value of zero was tested using two-tailed Student's t-tests. Two-tailed t-tests were also used to test the significance of correlation coefficients. Two-way analyses of variance for unequal sample sizes were used to test the significance of the effects of shear rate and donor sex on platelet aggregation.

RESULTS

1. Distribution of Single Platelet Volume

Forty male and forty female donors of age 31 ± 11 (\pm S.D., $n = 57$) and 30 ± 6 ($n = 56$) years, respectively, were used in a total of 113 experiments involving 9 shear rates as shown in Table 1. The data are grouped according to sex because of large differences in the degree of aggregation between male and female donors.

Table 2 shows average statistics of the individual single platelet log-volume histograms after background was subtracted as described in Chapter II. The distribution of single platelet volume in citrated PRP was log-normal according to the Kolmogorov-Smirnov one sample test for 74% of 47 male donors and 60% of 42 female donors. All volumes are those of the equivalent sphere due to the variation in single platelet and aggregate shape discussed in Chapter II. Platelet volume distributions from both male and female donors that were log-normal shared the same average mean volume, $\bar{\mu} = 7.3 \mu\text{m}^3$. The average standard deviation, mode and median of the two sexes were also virtually identical, and neither group exhibited significant skewing or kurtosis. For both groups of donors, the average measures of platelet volume of distributions that were rejected by the K-S test were always greater than those of their log-normal counterparts, although none of the differences was statistically significant. The apparent increase in cell volume of the rejected distributions coincided with significant positive skewing ($g_1 > 0$, $p < 0.02$) and an increased tendency toward leptokurtosis ($g_2 > 0$, $p < 0.01$).

TABLE 1

Number of Donors Tested at each Mean Tube Shear Rate

R_o mm	\bar{G} s^{-1}	Number of donors	
		Male	Female
0.595	39.3	13	13
	78.6	14	11
	157	6	7
	314	6	6
0.380	627	6	6
	940	5	5
	1250	12	10
	1490	6	6
	1800	6	6

TABLE 2

Average Statistics of the Single Platelet Log-Volume Distributions

Statistic	Male		Female	
	Log-Normal	Not Log-Normal	Log-Normal	Not Log-Normal
No. Donors	35	12	25	17
HCT, %	46.1 ± 2.2	44.9 ± 2.5	40.4 ± 2.5	40.1 ± 3.0
$\bar{\mu}$	7.3 ± 0.9	7.4 ± 1.1	7.3 ± 1.0	7.5 ± 1.1
σ	4.6 ± 0.8	4.7 ± 0.7	4.5 ± 0.9	4.7 ± 0.9
μ_{mod}	4.5 ± 0.5	4.5 ± 0.7	4.5 ± 0.4	4.5 ± 0.5
μ_{med}	6.2 ± 0.7	6.3 ± 0.9	6.3 ± 0.7	6.3 ± 0.9
g_1	0.014 ± 0.037	*0.050 ± 0.112	0.022 ± 0.046	***0.086 ± 0.066
g_2	-0.035 ± 0.069	**0.104 ± 0.154	0.002 ± 0.081	**0.108 ± 0.098
$n_{L,U}(0)$	15385 ± 1313	15380 ± 1244	14904 ± 1269	15080 ± 1173

Statistics of individual platelet log-volume distributions calculated at $\bar{t} = 0$ s over the range 1 - 50 μm^3 after background was subtracted were averaged for the stated number of donors of each sex. The distributions were further partitioned into those that were accepted as normal by the K-S one sample test and those that were rejected. Symbols are as described in the text and volumes are in μm^3 . Significantly different from zero: * $p < 0.02$, ** $p < 0.01$, *** $p < 0.001$.

2. Single Platelet Concentration

(a) Effect of Shear Rate and Donor Sex

The mean single platelet concentration prior to shearing was $279,000 \pm 23,000$ cells μl^{-1} (\pm S.D.) for the male donors and $278,000 \pm 34,000$ cells μl^{-1} for the female donors. Figure 1 shows the single platelet concentration after $\bar{t} = 43$ s exposure to $0.2 \mu\text{M}$ ADP, $N_{1,30}(\bar{t})$, normalized to a control at 0 s, $N_{1,30}(0)$, as a function of the mean tube shear rate. A two-way analysis of variance verified that the extent of aggregation of platelets from female donors was significantly greater than that of platelets from male donors ($p < 0.001$) over the range of shear rate $39.3 < \bar{G} < 1800 \text{ s}^{-1}$ (Table 3). The sex difference was greatest at $\bar{G} = 314 \text{ s}^{-1}$ where $76\% \pm 3.4$ (S.E.M., $n = 6$) of single platelets from the female donors but only $49\% \pm 3.9$ ($n = 6$) of those from male donors had aggregated. Significant changes ($p < 0.001$) in the single platelet concentration as a function of mean tube shear rate produced a similar pattern of aggregation for both groups of donors. Aggregation increased as the shear rate increased up to a maximum at $\bar{G}_{\text{max}} = 157$ and 314 s^{-1} for male and female donors, respectively. Thereafter, aggregation decreased linearly with increasing shear rate down to a minimum at $\bar{G} = 940$ and 1250 s^{-1} for male and female donors, respectively. Further increases in shear rate, however, produced an increase in aggregation for both sexes. The two aggregation curves intersect at $\bar{G} = 1250 \text{ s}^{-1}$ where aggregation had begun to increase for the male donors while it was still decreasing for the female donors.

Although no significant aggregation was observed in the controls in which modified Tyrodes was infused (Table 3), and no sex difference was

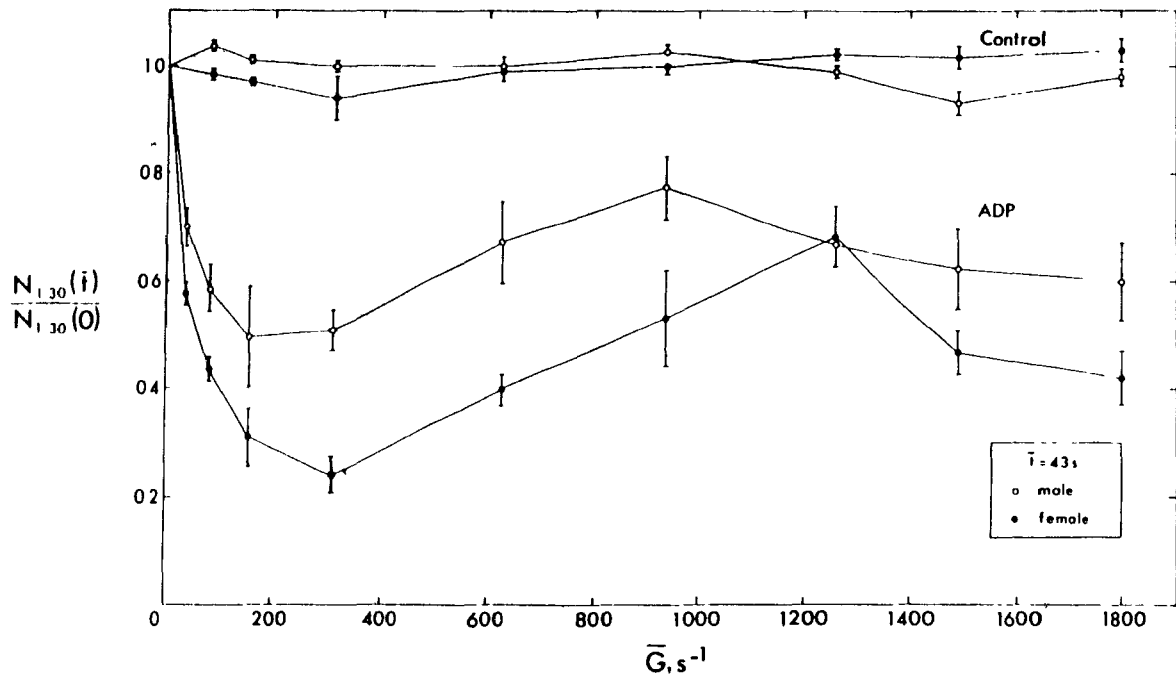


Figure 1: Single Platelet Concentration vs. Mean Tube Shear Rate

The normalized single platelet concentration, $N_{1,30}(\bar{t})/N_{1,30}(0)$, (\pm S.E.M.) after $\bar{t} = 43$ s exposure to $0.2 \mu\text{M}$ ADP as a function of mean tube shear rate for male and female donors. In the control runs modified Tyrodes was infused instead of ADP.

TABLE 3

Two-Way Analysis of Variance of Data Shown in Figure 1

ADP

Test	Sum of Squares	df	Mean Square	F-Ratio	p
Sex	906988	1	906988	45.4	< 0.001
Shear	1275183	8	159398	7.97	< 0.001
Sex × Shear	268612	8	33577	1.68	n.s.
Error	2199741	110	19997		

CONTROL

Test	Sum of Squares	df	Mean Square	F-Ratio	p
Sex	53	1	53	0.026	n.s.
Shear	21072	7	3010	1.447	n.s.
Sex × Shear	46384	7	6626	3.186	< 0.006
Error	137273	66	2080		

present, a significant interaction ($p < 0.006$) between donor sex and mean tube shear rate was reflected in reciprocal single platelet concentrations. This pattern was produced by the break-up of preformed aggregates, ($N_{1,30}(\bar{t})/N_{1,30}(0) > 1$) for the males at $\bar{G} < 940 \text{ s}^{-1}$ and for the females at $\bar{G} > 940 \text{ s}^{-1}$ in conjunction with a slight degree of aggregation ($N_{1,30}(\bar{t})/N_{1,30}(0) > 0.93$) of the platelets from the respective donors of the opposite sex. It is interesting that in the controls the single platelet concentrations for the male and female donors reversed at the same shear rate at which the ADP aggregation curves intersect.

The sex difference persisted through all mean transit times between $\bar{t} = 2.1$ and 86 s as shown in Figure 2. At $\bar{G}_{\text{max}} = 314 \text{ s}^{-1}$ for the female donors, only $13\% \pm 2.4$ ($n = 5$) of single platelets remained unaggregated after $\bar{t} = 86$ s, while for male donors after the same mean transit time, $37\% \pm 9.2$ ($n = 6$) were unaggregated at $\bar{G}_{\text{max}} = 157 \text{ s}^{-1}$. For both groups of donors, the aggregation curves for $\bar{t} < 11$ s show the length of an initial time delay in the onset of significant aggregation (lag phase) to increase with increasing mean tube shear rate. The effect of the lag phase was more pronounced for the female donors where changes in the single platelet concentration were greatest. Here, the length of the lag phase decreased at $\bar{G}_{\text{max}} = 314 \text{ s}^{-1}$, but by $\bar{G} = 1250 \text{ s}^{-1}$ it approached $\bar{t} = 21$ s, similar to that for the male donors.

(b) Donor Hematocrit

A strong correlation of the normalized single platelet concentration with donor hematocrit ($r = 0.91$, $p < 0.001$) was obtained

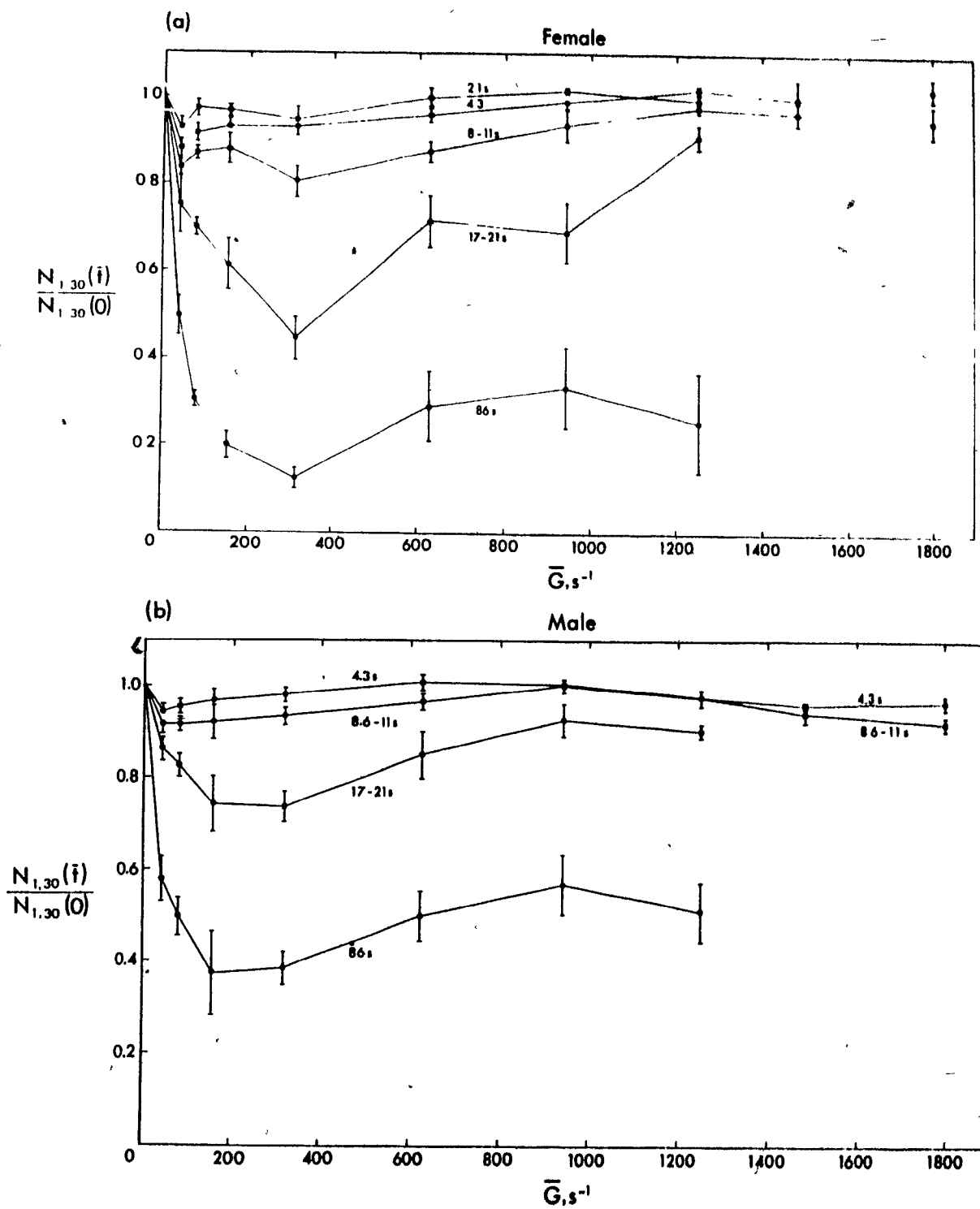


Figure 2: Single Platelet Concentration vs. Mean Tube Shear Rate

Normalized single platelet concentration, $N_{1,30}(\bar{t})/N_{1,30}(0)$, (\pm S.E.M.) vs mean tube shear rate for female (a) and male (b) donors after $2.1 < \bar{t} < 86/s$ -exposure to $0.2 \mu M$ ADP.

when male and female donors at $\bar{t} = 43$ s and $\bar{G} = 314$ s⁻¹ were grouped together (Fig. 3). Similar, but generally less significant, correlations were found at all mean tube shear rates from 39.3 to 1800 s⁻¹, except at $\bar{G} = 1250$ s⁻¹ ($r = -0.07$) where no sex difference existed.

(c) Thromboxane B₂

The concentration of TXB₂ was measured in PRP at $940 < \bar{G} < 1800$ s⁻¹ for several male and female donors (Table 4). Although TXB₂ concentrations as high as 6 ng ml⁻¹ in PRP and 10 ng ml⁻¹ in PPP were obtained during platelet preparation, neither sex showed significant changes in TXB₂ concentration from that at $\bar{t} = 0$ s in either control or ADP infusion runs. Concentrations of TXB₂ at $\bar{t} = 0$ s slightly greater than those in PRP during platelet preparation resulted from the dilution of PRP with PPP to obtain the required platelet concentration for the flow experiments. Thromboxane B₂ concentration did not correlate with donor hematocrit in either PPP ($r = -0.43$, $n = 10$) or in the PRP of the ADP infusion runs at $\bar{t} = 43$ or 86 s ($r = 0.05$, $n = 28$), nor did it correlate with the normalized single platelet concentration at $\bar{G} = 1250$ ($r = 0.27$, $n = 11$), 1490 ($r = 0.30$, $n = 7$) or 1800 s⁻¹ ($r = 0.46$, $n = 10$).

For comparison, PRP from three donors was stirred in standard aggregometer cuvettes and TXB₂ was measured after exposure of the platelets to ADP or thrombin for 2.5 min in the presence and absence of 500 μM ASA (Table 5). At 22°C, 100 μM ADP was incapable of inducing TXB₂ generation, and 5 U ml⁻¹ thrombin was capable of inducing only a modest amount of ASA-insensitive TXB₂ production. At 37°C, 100 μM ADP produced TXB₂ concentrations less than those produced by 5 U ml⁻¹ thrombin at 22°C.

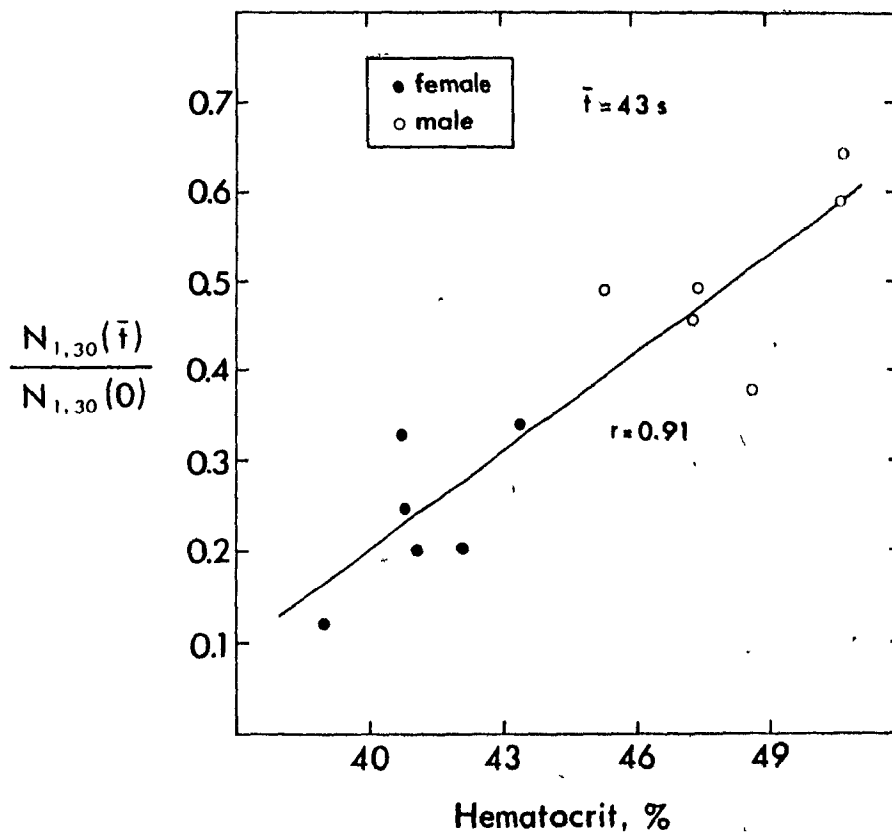


Figure 3: Correlation of Single Platelet Concentration with Hematocrit

Normalized single platelet concentration, $N_{1,30}(\bar{t})/N_{1,30}(0)$, vs donor hematocrit for the male and female donors combined at $\bar{t} = 43 \text{ s}$ and $\bar{G} = 314 \text{ s}^{-1}$.

TABLE 4

Plasma Thromboxane B₂ Concentration
ng ml⁻¹ (\pm S.D.)

\bar{G} , s ⁻¹	Sex	n*	Platelet Preparation		Control			ADP		
			PRP	PPP	\bar{t} = 0 s	< 1 s	86 s	\bar{t} < 1 s	43 s	86 s
940	M	1	1.09	6.00	1.09	1.10	1.65	0.68	-	1.23
1250	M	6	0.87 (2)	3.30 (4) ± 1.23	2.15 ± 1.59	2.13 ± 1.55	2.09 ± 1.58	2.27 (5) ± 1.46	-	1.97 ± 1.50
	F	5	4.40 (1)	9.98 (3) ± 5.68	4.05 ± 3.04	4.08 ± 2.89	4.15 ± 3.32	5.40 (3) ± 4.42	-	4.43 ± 3.15
1490	M	4	0.34 (2)	2.05 (1)	1.48 ± 2.08	1.65 (3) ± 2.02	1.77 ± 1.84	1.16 (3) ± 0.79	1.44 ± 1.93	-
	F	3	1.24 (2)	9.60 (1)	1.93 ± 2.14	1.29 (1)	2.59 (2)	2.58 (2)	1.60 ± 2.18	-
1800	M	5	-	-	6.19 ± 4.00	-	6.05 ± 4.05	5.81 ± 3.64	6.15 ± 4.16	-
	F	5	-	-	2.00 ± 2.37	-	2.11 ± 2.54	2.60 ± 2.02	2.32 ± 2.04	-

* Number of donors, except where indicated in parentheses

TABLE 5

Thromboxane B₂ Concentration (ng ml⁻¹) in PRP in Aggregometer
after 2.5 min Exposure to Platelet Agonist

Temperature	Agonist	Donor 1 female		Donor 2 male		Donor 3 female	
		-	+ *	-	+	-	+
22 °C	<u>ADP</u>						
	0.2 μM	2.96	-	0.00	-	4.06	-
	1.0 μM	2.78	-	0.14	-	4.25	-
	10 μM	2.75	-	0.31	-	3.95	4.55
	100 μM	2.82	-	0.90	0.78	4.10	-
	<u>Thrombin</u>						
	0.1 U ml ⁻¹	2.28	-	1.40	-	5.55	-
1 U ml ⁻¹	2.63	-	16.2	-	6.19	5.45	
5 U ml ⁻¹	43.8	-	25.5	29.5	40.1	-	
37 °C	<u>ADP</u>						
	1 μM	-	-	1.04	-	4.55	-
	10 μM	-	-	-	3.12	-	-
	100 μM	21.4	-	16.0	3.78	12.2	7.00
	<u>Thrombin</u>						
	0.1 U ml ⁻¹	-	-	1.75	-	-	-
	1 U ml ⁻¹	3.25	-	-	-	-	-
5 U ml ⁻¹	260	-	266	-	390	47.5	

* Incubated with (+) or without (-) 500 μM ASA for 10 min.

Thromboxane B₂ generation in the former was, however, inhibited by ASA. Aspirin also inhibited most of the large quantity of TXB₂ produced by 5 U ml⁻¹ thrombin at 37°C, although significant amounts of TXB₂, comparable to those produced at 22°C, persisted.

3. Total Particle Concentration

(a) Rate of Aggregation

Mean values of the negative logarithm of the total particle concentration at time \bar{t} , $N_{1,10^5}(\bar{t})$, normalized to that at $\bar{t} = 0$ s, $N_{1,10^5}(0)$, were plotted against \bar{t} for the female donors in Figure 4. Although the extent of aggregation was greatest at $\bar{G} = 314$ s⁻¹, the highest rate of aggregation occurred within the first $\bar{t} = 2$ s at $\bar{G} = 39.3$ s⁻¹ where the single platelet concentration decreased at a rate of $4.2\% \text{ s}^{-1} \pm 0.9$ (\pm S.E.M., $n = 10$). At this shear rate, the rate of aggregation steadily decreased with increasing mean transit time.

The combined effects of an initial lag phase followed by progressively increasing then decreasing rates of aggregation produced sigmoid aggregation curves for all $\bar{G} > 39.3$ s⁻¹. The length of the lag phase increased with increasing mean tube shear rate reaching $\bar{t} \sim 11$ s at $\bar{G} = 1250$ s⁻¹. In addition, as the mean tube shear rate was raised, not only did the maximum rate of aggregation decrease, but it occurred at progressively increasing mean transit time. At $\bar{G} = 314$ s⁻¹ the maximum rate of aggregation of $2.8\% \text{ s}^{-1} \pm 0.2$ ($n = 5$) occurred between $\bar{t} = 8.6$ and 21 s, while at $\bar{G} = 1250$ s⁻¹ the rate was maximal at $1.0\% \text{ s}^{-1} \pm 0.2$ ($n = 5$) between $\bar{t} = 21$ and 43 s. Male donors exhibited a pattern of aggregation similar to that of the female donors at the same shear rate

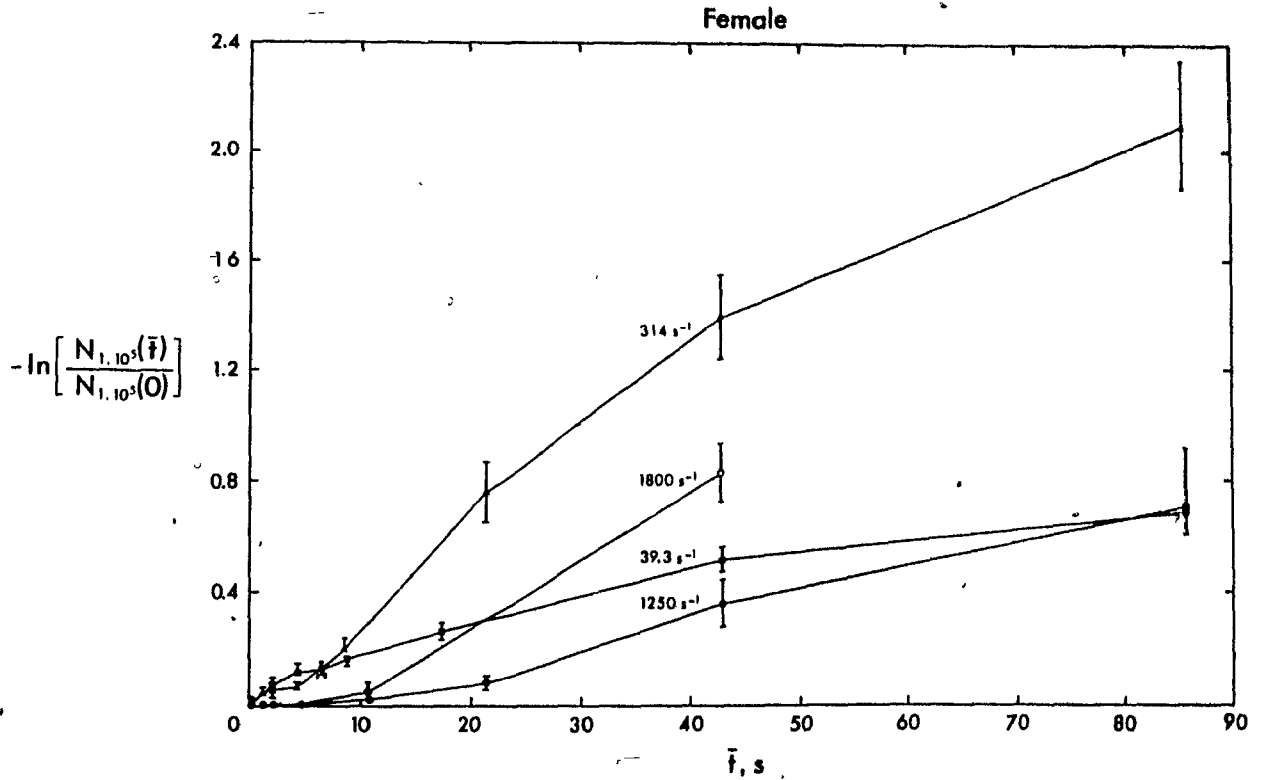


Figure 4: Total Particle Concentration

The negative logarithm of the normalized, total particle concentration, $-\ln\left[\frac{N_{1,10^5}(\bar{t})}{N_{1,10^5}(0)}\right]$, (\pm S.E.M) plotted against \bar{t} at $\bar{G} = 39.3, 314, 1250$ and 1800 s^{-1} for the female donors.

but always with much longer lag phases and reduced rates of aggregation.

(b) Collision Efficiency

In addition to providing an index of the rate of aggregation, the slope of the curves in Figure 4 can be used to calculate the collision efficiency according to Eq. [21] of Chapter II. The individual collision efficiencies of all donors at each mean tube shear rate were averaged over three time intervals for both sexes as shown in Table 6. A maximum collision efficiency, $\alpha_0 = 0.282$, was obtained at $\bar{G} = 39.3 \text{ s}^{-1}$ between $\bar{t} = 0$ and 4.3 s. Throughout all three time intervals, α_0 either decreased or remained constant as the mean tube shear rate was increased up to $\bar{G} = 1250 \text{ s}^{-1}$ where $\alpha_0 < 0.002$. Considering the high collision rate at $\bar{G} = 1800 \text{ s}^{-1}$, a small but significant increase in collision efficiency was sufficient to support a high rate of aggregation (Fig. 4).

The dependence of collision efficiency on time and shear rate together is revealed in Figure 5 where α_0 is plotted against the logarithm of the product $\bar{t}\bar{G}$. For any given time interval, increasing $\bar{t}\bar{G}$ has the effect of increasing the shear rate. The individual curves were more clearly delineated by plotting α_0 vs. $\bar{t}\bar{G}$, rather than α_0 vs. \bar{G} . Between $\bar{t} = 0$ and 4.3 s, the collision efficiency followed an apparent exponential decrease with increasing mean tube shear rate. A similar decline in collision efficiency with increasing shear rate over the time interval from $\bar{t} = 4.3$ to 8.6 s was interrupted between $\bar{G} = 157$ and 314 s^{-1} , but resumed at a higher rate of decrease beyond $\bar{G} = 314 \text{ s}^{-1}$. The collision efficiency remained relatively constant in the interval from $\bar{t} = 8.6$ to 21 s for $\bar{G} < 157 \text{ s}^{-1}$. Higher shear rates, however, produced a sharp drop

TABLE 6

Effect of Shear Rate and Transit Time on Collision Efficiency

SEX	\bar{G}, s^{-1}	$\alpha \times 10^3 (\pm S.E.M.)$		
		$\bar{t} = 0 - 4.3 s$	4.3 - 8.6 s	8.6 - 21 s
Male	39.3	126 ± 32.0	72.6 ± 22.9	62.9 ± 15.6
	157	21.2 ± 11.0	27.2 ± 8.7	52.4 ± 12.3
	314	8.01 ± 2.62	14.8 ± 4.7	23.8 ± 3.3
	1250	2.42 ± 0.84	0.99 ± 0.41	2.05 ± 0.46
	1800	2.11 ± 0.72	1.76 ± 0.50	-
Female	39.3	282 ± 69.1	94.1 ± 30.5	115 ± 21.9
	157	40.8 ± 7.61	37.6 ± 10.5	101 ± 20.1
	314	18.6 ± 5.23	37.7 ± 8.79	53.2 ± 8.05
	1250	0.01 ± 0.01	1.92 ± 0.58	2.14 ± 0.71
	1800	0.66 ± 0.36	2.45 ± 0.95	-

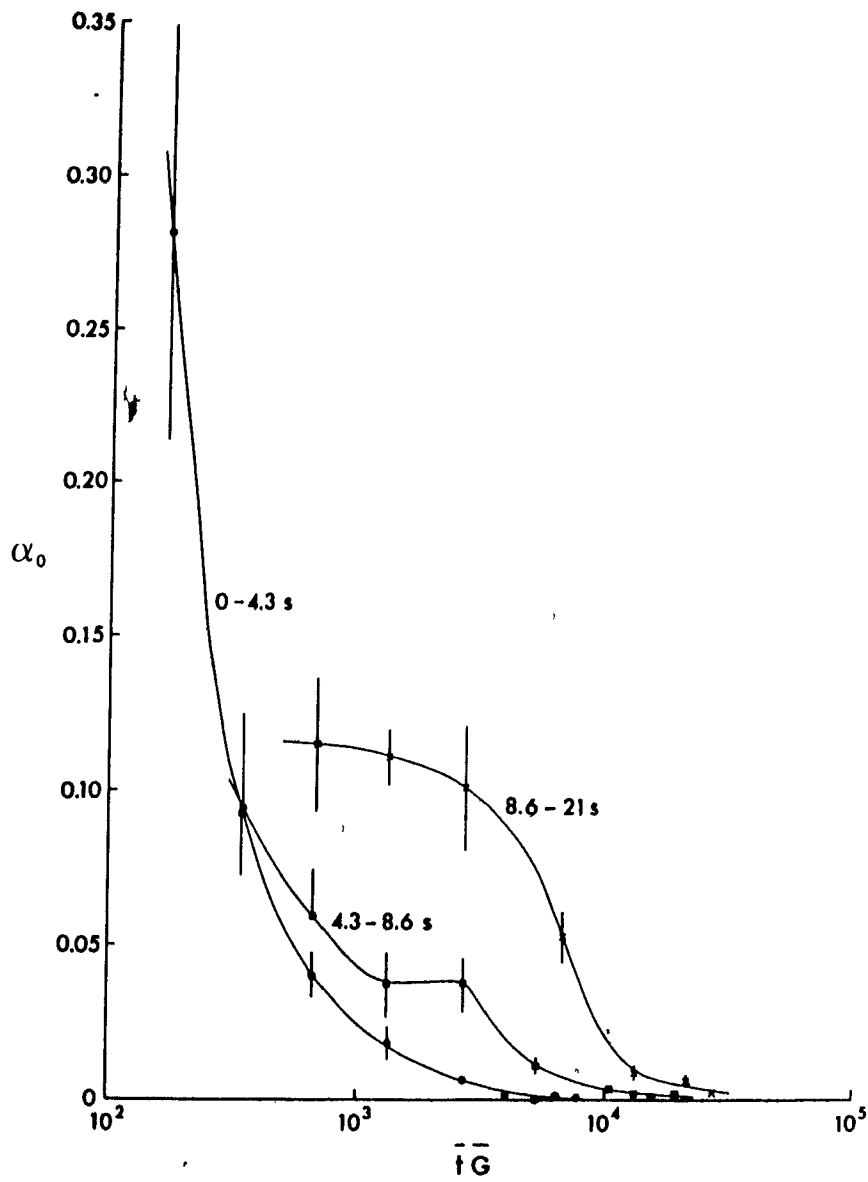


Figure 5: Collision Efficiency vs. \bar{tG}

Collision efficiency, α_0 , (\pm S.E.M) over three time intervals, $\bar{t} = 0 - 4.3, 4.3 - 8.6$ and $8.6 - 21$ s plotted against \bar{tG} .

in collision efficiency in this time interval.

4. Aggregate Growth

(a) Aggregate Size Distribution

The evolving pattern of aggregate growth for the female donors is illustrated in Figures 6 - 8 through plots of the normalized average class volume fraction, $\bar{\Phi}(x_i)$, versus particle volume. The decrease in single platelet concentration ($1 - 30 \mu\text{m}^3$) was accompanied by a sequential rise and fall of aggregates of successively increasing volume. Joining the steadily decreasing rate of aggregation with time shown earlier at $\bar{G} = 39.3 \text{ s}^{-1}$ was the formation of aggregates having a broad spectrum of size at $\bar{t} = 86 \text{ s}$. At $\bar{G} = 314 \text{ s}^{-1}$, no distinct aggregate peaks were present prior to $\bar{t} = 8.6 \text{ s}$ but by $\bar{t} = 21 \text{ s}$ aggregates of relatively discrete size were present. As aggregation continued, the upper limit of aggregate size increased. By $\bar{t} = 86 \text{ s}$, most aggregates were present in one large group, a significant proportion of which exceeded $10^5 \mu\text{m}^3$, the largest volume measured. Although there was considerable aggregation at $\bar{G} = 1800 \text{ s}^{-1}$, the aggregates occupied a size range considerably narrower than at the same mean transit time at $\bar{G} = 314 \text{ s}^{-1}$. A similar pattern of aggregate growth was exhibited by the male donors; however, aggregate size was always much reduced compared to that for the female donors at the same mean transit time and mean tube shear rate.

(b) Aggregate Growth Rate

Figures 6 - 8 illustrate the continuity in the evolving distribution of aggregate size, but they do not convey a sense of the rate of aggregate growth. This is provided in Figures 9 and 10 for female and

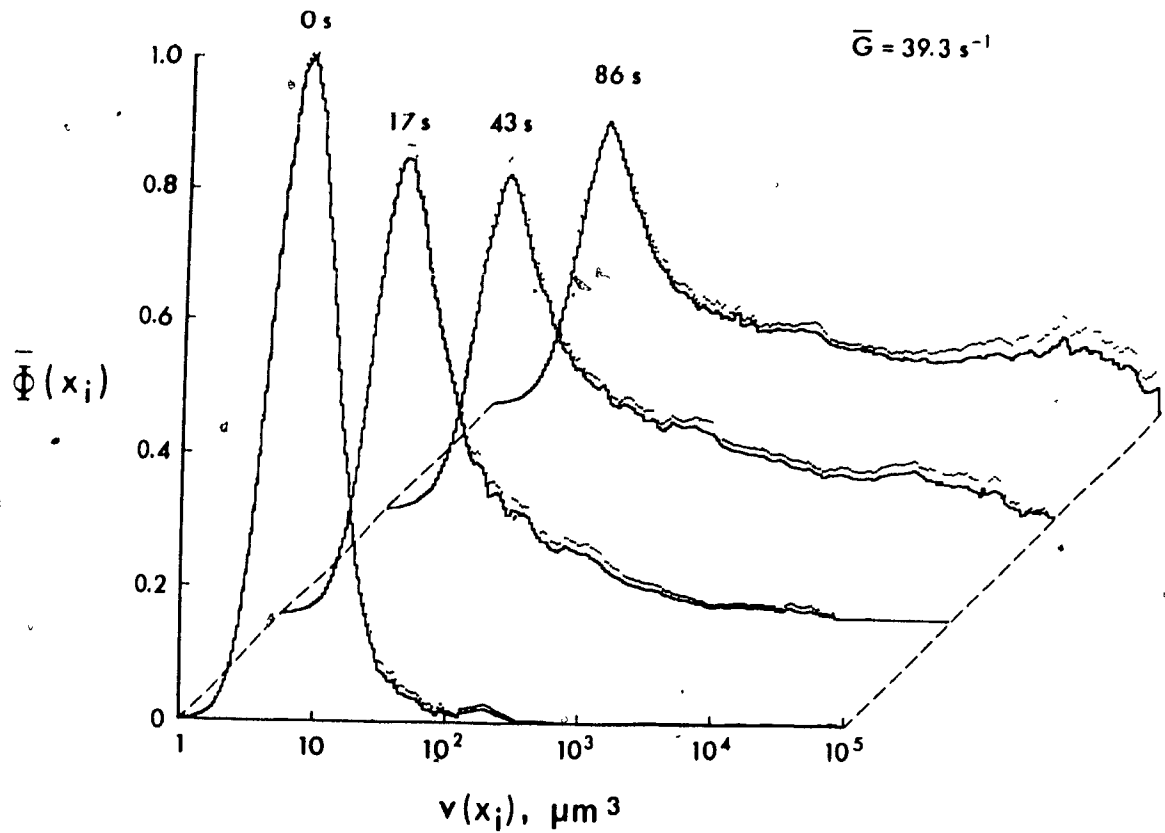


Figure 6: Volume Fraction Histograms at $\bar{G} = 39.3 \text{ s}^{-1}$

Three-dimensional plot of the mean, normalized class volume fraction $\bar{\Phi}(x_i)$, (\pm S.E.M, dotted line) vs particle volume at mean transit times from $\bar{t} = 0 - 86 \text{ s}$ for the female donors at $\bar{G} = 39.3 \text{ s}^{-1}$.

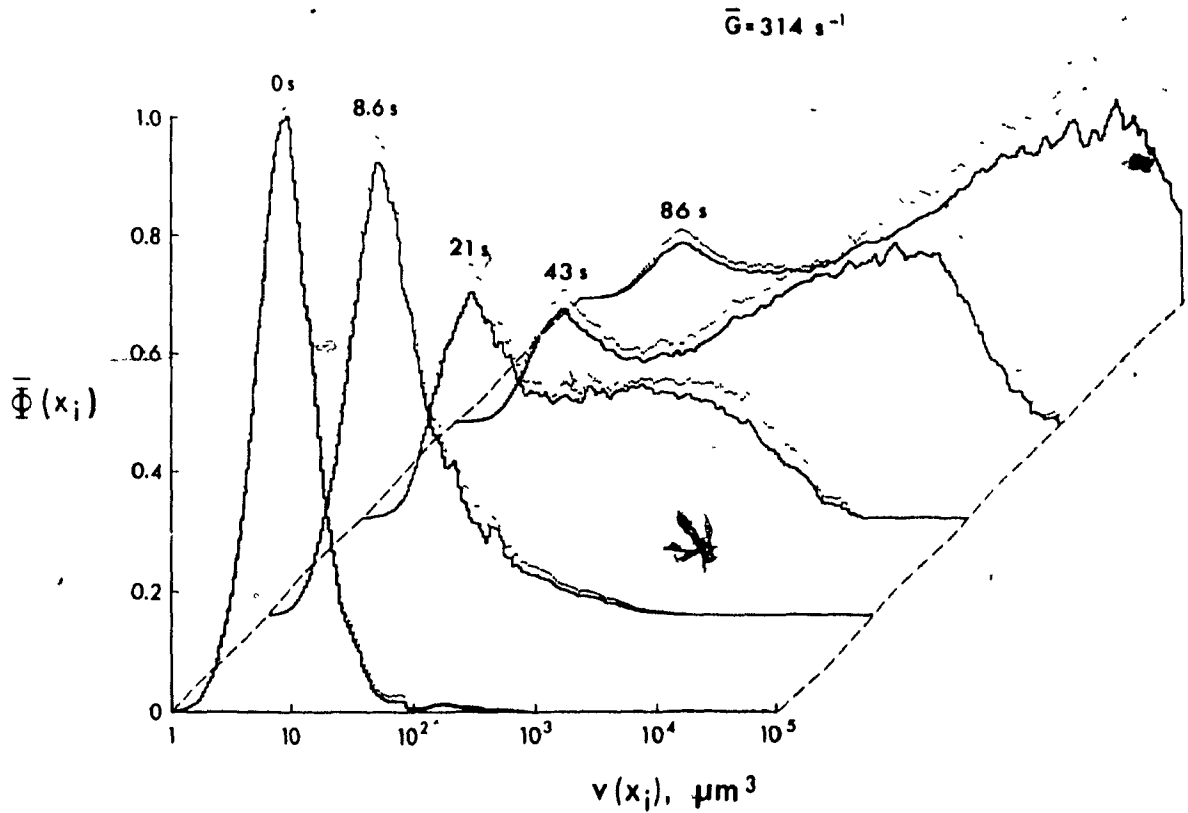


Figure 7: Volume Fraction Histograms at $\bar{G} = 314 \text{ s}^{-1}$

Three-dimensional plot of the mean, normalized class volume fraction $\bar{\Phi}(x_i)$, (\pm S.E.M, dotted line) vs particle volume at mean transit times from $\bar{t} = 0 - 86 \text{ s}$ for the female donors at $\bar{G} = 314 \text{ s}^{-1}$.

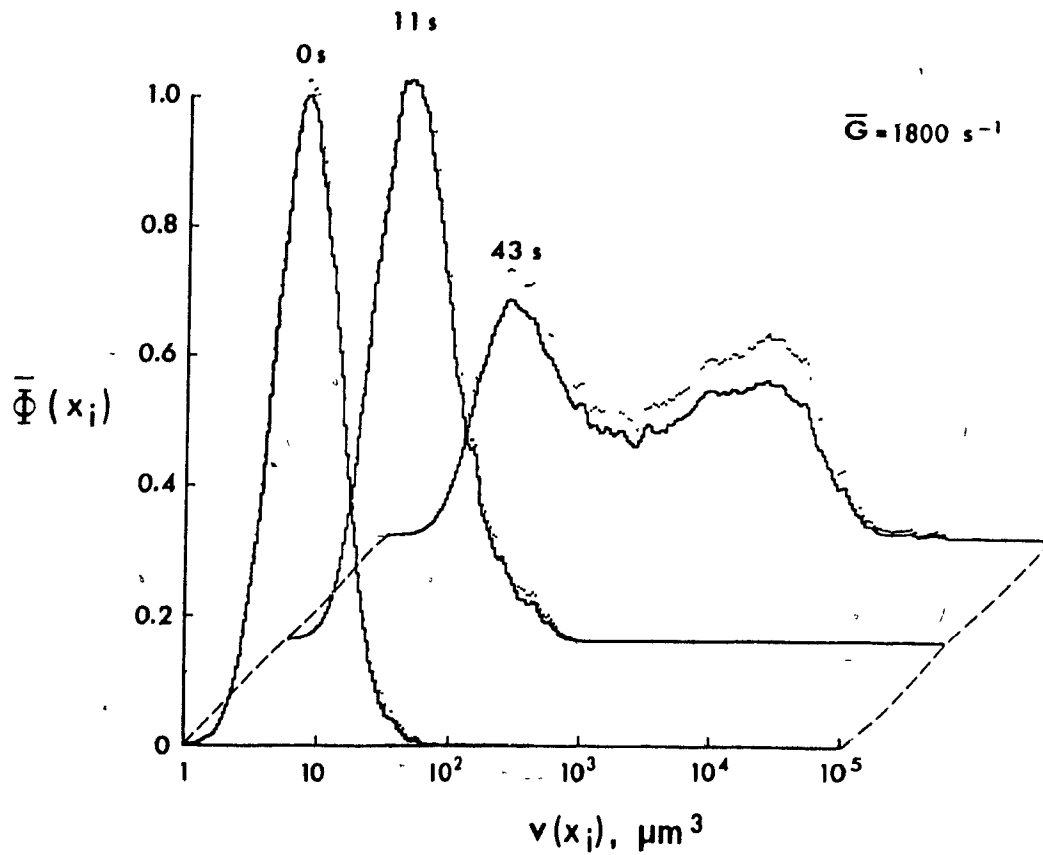
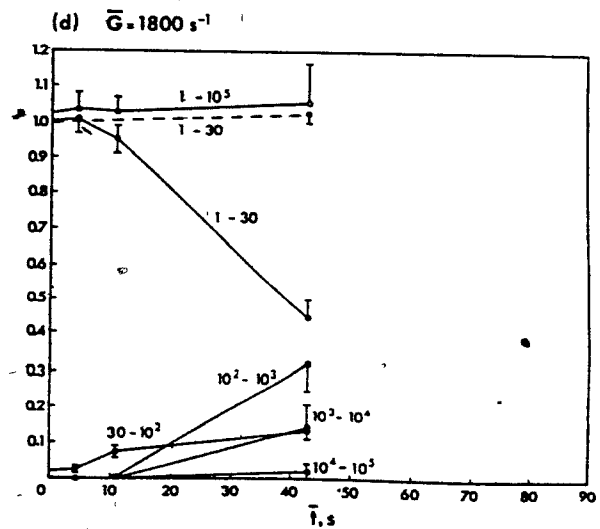
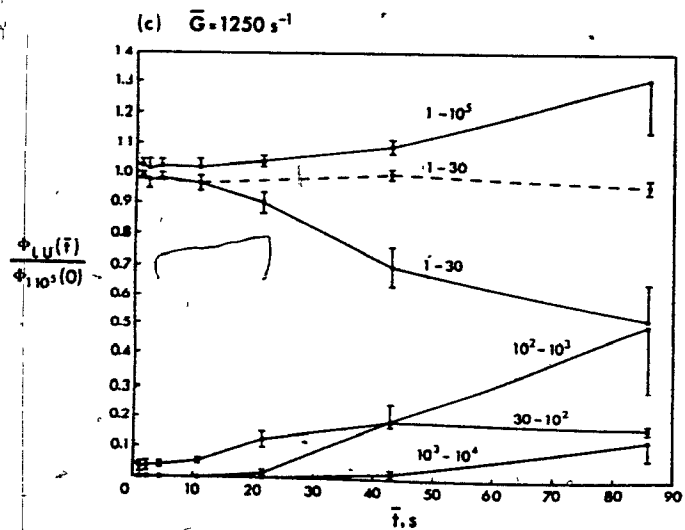
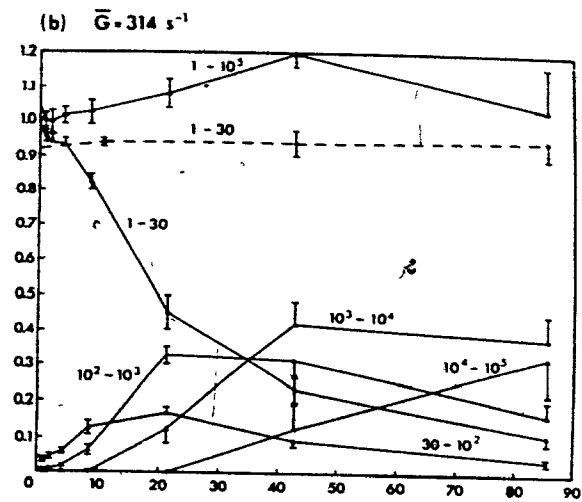
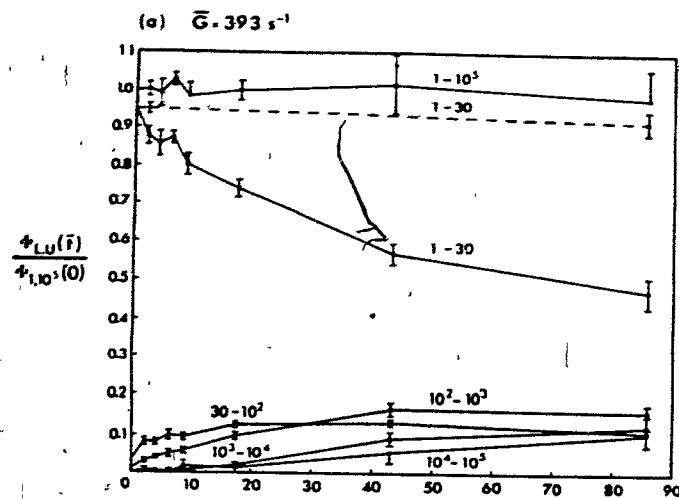


Figure 8: Volume Fraction Histograms at $\bar{G} = 1800\text{ s}^{-1}$

Three-dimensional plot of the mean, normalized class volume fraction $\bar{\Phi}(x_i)$, (\pm S.E.M, dotted line) vs particle volume at mean transit times from $\bar{t} = 0 - 86\text{ s}$ for the female donors at $\bar{G} = 1800\text{ s}^{-1}$.

Figure 9: Effect of Shear Rate on Aggregate Growth for Females

The normalized volume fraction of particles between lower, L, and upper, U, volumes, $\bar{\Phi}_{L,U}(\bar{t})/\bar{\Phi}_{1,10^5(0)}$ (\pm S.E.M.), plotted against \bar{t} for the female donors. The volume limits, L-U, from 1-30, 30-10², 10²-10³, 10³-10⁴, 10⁴-10⁵, and 1-10⁵ μm^3 are shown beside their respective plots. No particles were present in volume ranges not listed. The broken line represents the control values of single platelets (1-30 μm^3).



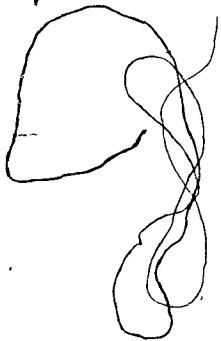
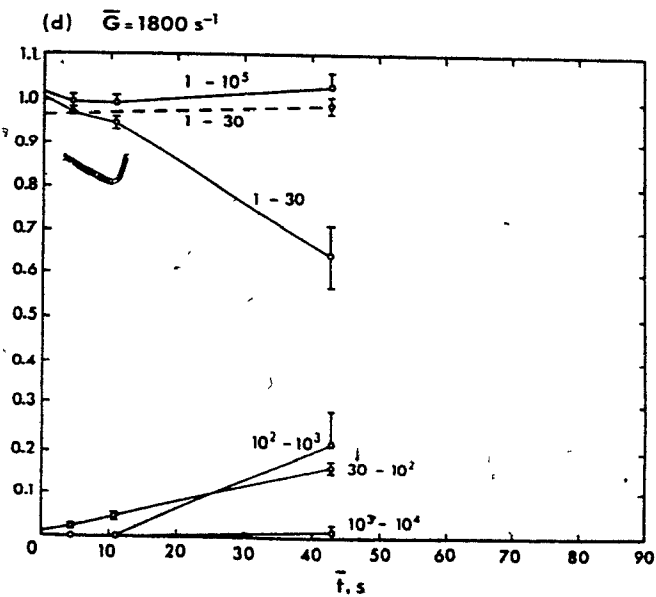
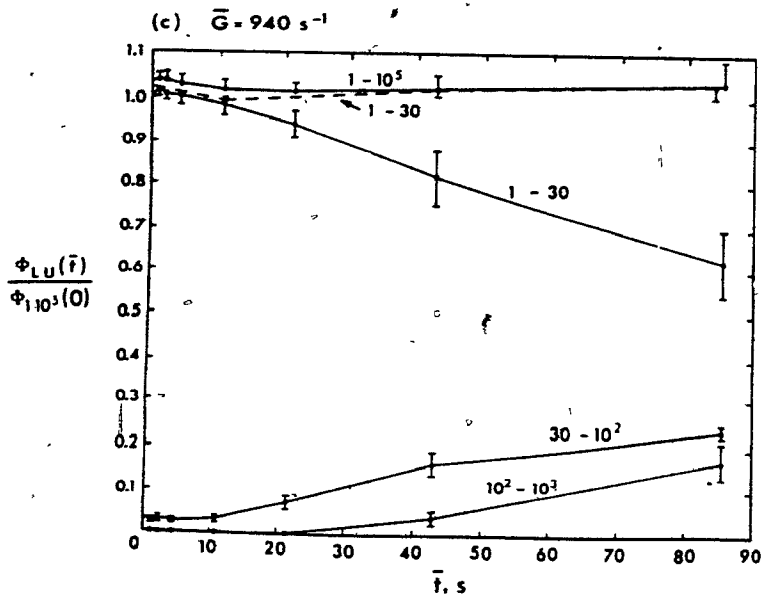
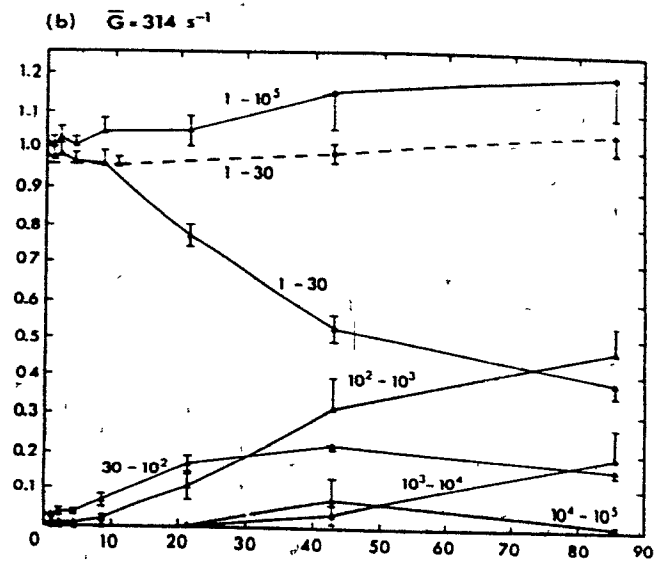
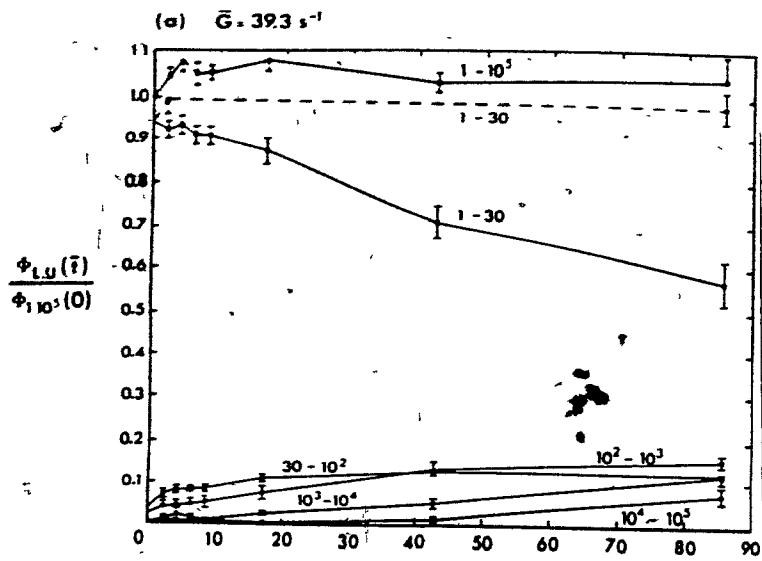


Figure 10: Effect of Shear Rate on Aggregate Growth for Males

The normalized volume fraction of particles between lower, L, and upper, U, volumes, $\Phi_{L,U}(\bar{t})/\Phi_{1,10^5}(0)$ (\pm S.E.M.), plotted against \bar{t} for the male donors. The volume limits, L-U, from 1-30, 30-10², 10²-10³, 10³-10⁴, 10⁴-10⁵, and 1-10⁵ μm^3 are shown beside their respective plots. No particles were present in volume ranges not listed. The broken line represents the control values of single platelets (1-30 μm^3).



male donors, respectively, where the volume fraction of aggregates, $\Phi_{L,U}(\bar{t})$, between lower, L, and upper, U, volume limits was normalized to the total volume fraction, $\Phi_{1,10^5}(0)$, at $\bar{t} = 0$ s. As previously noted, small aggregates were present at $\bar{t} = 0$ s. For the female donors (Fig. 9), at $\bar{G} = 39.3 \text{ s}^{-1}$, a rapid rise in the volume fraction of aggregates from $30 - 10^2 \mu\text{m}^3$ was followed by increases in the volume fraction of aggregates of successively increasing size. At higher shear rates, changes in the volume fraction of single platelets ($L = 1, U = 30$) with increasing mean transit time followed the same sigmoid curve as did changes in the single platelet and total particle number concentration described previously. The lag phase preceding aggregation was evident through delays in the onset of changes in the volume fraction of both single cells and aggregates. The lag phase increased with increasing mean tube shear rate up to $\bar{G} = 1250 \text{ s}^{-1}$ where no aggregates $> 10^4 \mu\text{m}^3$ were formed. Even though the lag phase at $\bar{G} = 1800 \text{ s}^{-1}$ was shorter and the rate of aggregation higher than at $\bar{G} = 1250 \text{ s}^{-1}$, the aggregates formed were smaller than those at $\bar{G} = 314 \text{ s}^{-1}$ at the same mean transit time. At $\bar{G} = 314 \text{ s}^{-1}$, the sequential formation of aggregates of discrete size and their subsequent incorporation into aggregates of larger size was clearly evident. The total normalized volume fraction greatly exceeded 1.0 with the appearance of aggregates greater than $10^3 \mu\text{m}^3$, but decreased again as the number of aggregates greater than $10^4 \mu\text{m}^3$ increased.

A similar pattern of aggregation at all equivalent mean tube shear rates was observed for the male donors but with consistently longer lag phases and lower rates of aggregation as seen through changes in the volume fraction of both single cells and aggregates (Fig. 10). At $\bar{G} = 314 \text{ s}^{-1}$,

however, there was a significant departure. The volume fraction of the largest aggregates measured at $\bar{t} = 43$ s ($10^4 - 10^5 \mu\text{m}^3$) was greater than that of aggregates in the next smallest group ($10^3 - 10^4 \mu\text{m}^3$). The concentration of the largest aggregates subsequently decreased at $\bar{t} = 86$ s; however, that of aggregates from $10^2 - 10^3 \mu\text{m}^3$ and $10^3 - 10^4 \mu\text{m}^3$ continued to increase, and the latter at a greater rate. This phenomenon is indicative of aggregate break-up at long transit time.

5. ADP Concentration

(a) Single Platelet Concentration

Platelet-rich plasma from single representative male and female donors of widely different hematocrit (HCT = 43.9% and 34.5%, respectively) was sheared at $\bar{G} = 39.3, 314, \text{ and } 1800 \text{ s}^{-1}$ in the presence of 0.2 and 1.0 μM ADP. The normalized single platelet concentration at three mean transit times is shown in Figure 11. At equivalent mean transit times and mean tube shear rates, the extent of aggregation was always greater at 1.0 μM ADP than at 0.2 μM ADP for both the male and the female donor. As previously found at 0.2 μM ADP, aggregation was greater for the female donor than for the male donor at all shear rates and transit times with the greatest difference at $\bar{G} = 314 \text{ s}^{-1}$. At this shear rate aggregation was minimal prior to $\bar{t} = 4.3$ s. At 1.0 μM ADP, however, the male donor exhibited a degree of aggregation greater than that of the female donor at $\bar{G} = 39.3$ and 314 s^{-1} , while both donors exhibited the greatest aggregation at $\bar{G} = 1800 \text{ s}^{-1}$ with no apparent sex difference. It is interesting that at this shear rate < 1% of single platelets remained unaggregated at $\bar{t} = 43$ s. In addition, no lag phase was apparent preceding aggregation for the male donor at 1.0 μM ADP.

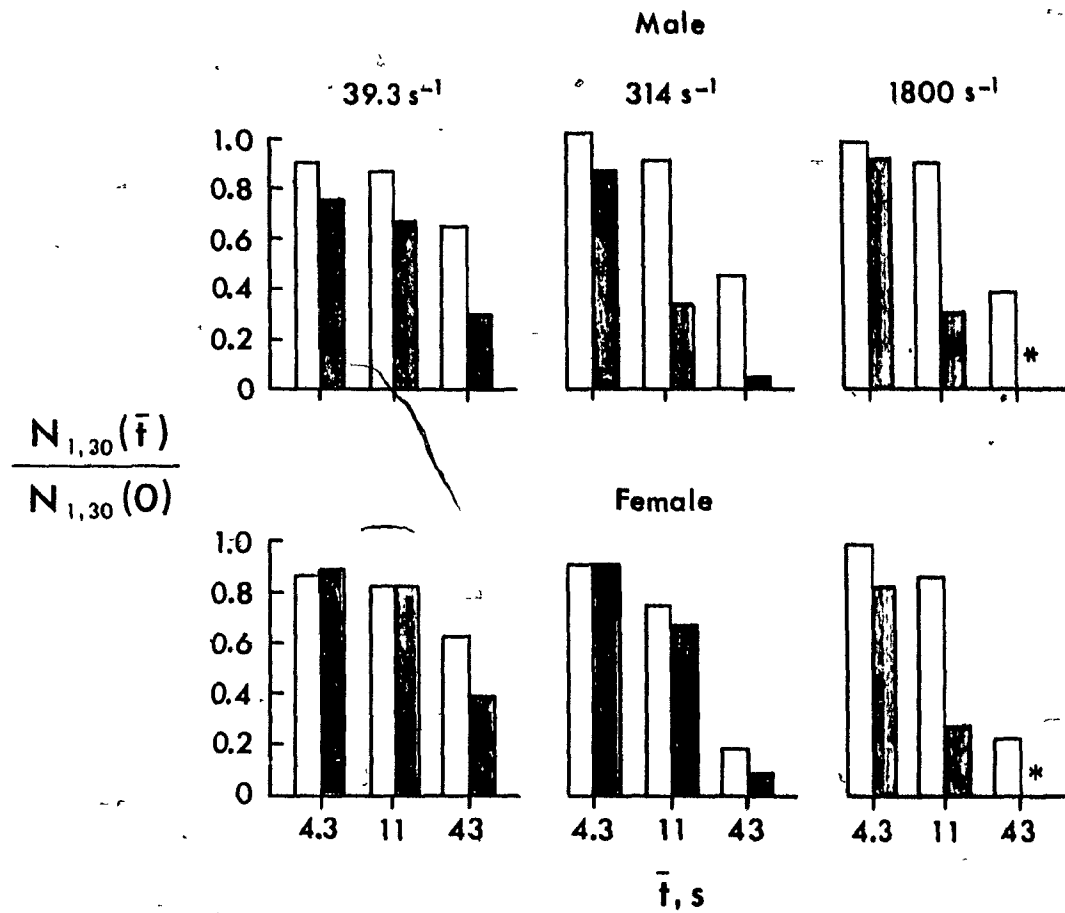


Figure 11: Effect of [ADP] on Single Platelet Concentration

The normalized single platelet concentration at $\bar{t} = 4.3, 11$ and 43 s and $\bar{G} = 39.3, 314$ and 1800 s⁻¹ for the male and female donor.

Unshaded bars denote 0.2 μM ADP and shaded bars 1.0 μM ADP.

* < 1% single platelets remaining.

(b) Collision Efficiency

Values of the collision efficiency at 0.2 μM ADP for the female donor (Table 7) were consistent with the mean values of the female donors given in Table 6, while those for the male donor showed more variation, particularly at $\bar{G} = 39.3 \text{ s}^{-1}$ where they were considerably higher. With 1.0 μM ADP there was a large increase in α_0 at all mean transit times and mean tube shear rates. A notable exception was at $\bar{G} = 39.3 \text{ s}^{-1}$ between $\bar{t} = 0$ and 4.3 s for the female donor where α_0 actually decreased. For the male donor at this shear rate and time interval, however, the collision efficiency increased dramatically from $\alpha_0 = 0.277$ to 0.765.

At all mean transit times with both 0.2 and 1.0 μM ADP, α_0 decreased with increasing mean tube shear rate. Collision efficiency varied with mean transit time, however, in a manner dependent on mean tube shear rate. At $\bar{G} = 1800 \text{ s}^{-1}$, α_0 always increased with increasing mean transit time with 0.2 μM ADP but decreased after $\bar{t} = 11$ s with 1.0 μM ADP. The concentration of TXB_2 at $\bar{t} = 43$ s was generally less than 1.0 ng ml^{-1} at all shear rates with either ADP concentration for both donors (Table 7).

(c) Rate of Aggregation

Table 7 also shows the rate of decrease of the normalized single platelet concentration over the same time interval that the two-body collision efficiency was calculated. At 0.2 μM ADP the rates of aggregation of platelets from the female donor were generally greater than those from the male donor at all mean tube shear rates and mean transit times, with maximum values for both donors at $\bar{G} = 39.3 \text{ s}^{-1}$ between $\bar{t} = 0$

TABLE 7

Effect of ADP Concentration on Collision Efficiency and Rate of Aggregation

Sex	ADP μM	* TXB ₂ ng ml ⁻¹	\bar{G} s ⁻¹	$\bar{t} = 0 - 4.3 \text{ s}$		4.3 - 11 s		11 - 43 s	
				** α_o $\times 10^3$	# rate % s ⁻¹	α_o $\times 10^3$	rate % s ⁻¹	α_o $\times 10^3$	rate % s ⁻¹
Male	0.2	1.35	39.3	277	2.2	78.7	0.6	109	0.7
		0.78	314	0.00	0.0	23.4	1.7	32.7	1.4
		0.50	1800	1.02	0.4	3.40	1.3	7.09	1.6
	1.0	2.28	39.3	765	5.7	238	1.3	317	1.2
		0.99	314	49.8	3.2	219	8.1	98.1	0.9
		0.72	1800	5.45	2.0	44.2	9.5	38.5	0.9
Female	0.2	0.52	39.3	334	3.0	83.7	0.8	84.2	0.6
		0.41	314	27.6	2.1	38.7	2.6	56.8	1.7
		0.76	1800	0.39	0.3	4.96	2.0	9.41	2.0
	1.0	0.27	39.3	246	2.6	140	1.0	237	1.4
		0.26	314	26.3	2.1	58.9	3.7	82.9	1.8
		0.65	1800	10.0	4.2	36.8	8.4	24.4	0.8

* Measured at $t = 43 \text{ s}$.

** Calculated from Eq. [21] of Chapter II.

Given as the percent decrease in the normalized single platelet concentration.

and 4.3 s. As previously found, longer transit times resulted in decreased rates of aggregation, and as the shear rate was increased the maximum rates of aggregation both decreased and occurred at progressively longer transit times.

A similar pattern was observed with 1.0 μM ADP at $\bar{G} = 39.3 \text{ s}^{-1}$ and 314 s^{-1} with the maximum rates of aggregation being generally greater than those at 0.2 μM ADP. This was particularly true for the male donor where the rates of aggregation now exceeded those for the female donor. The highest rate of aggregation also shifted to $\bar{G} = 1800 \text{ s}^{-1}$ between $\bar{t} = 4.3$ and 11 s where the single platelet concentration decreased at rates of 9.5 and 8.4 % s^{-1} for the male and female donor, respectively.

(d) Aggregate Growth

Aggregate growth at 0.2 μM ADP (Fig. 12 - 14) followed the patterns typical of Figures 6 - 8 for both donors. At all three shear rates at $\bar{t} = 43 \text{ s}$ both the number and size of aggregates of platelets from the female donor were greater than those from the male donor, while the single platelet concentration was, accordingly, much reduced. The sex difference was most pronounced at $\bar{G} = 314 \text{ s}^{-1}$. A slight degree of aggregation was present in the control of the female donor after the same mean transit time at $\bar{G} = 314 \text{ s}^{-1}$.

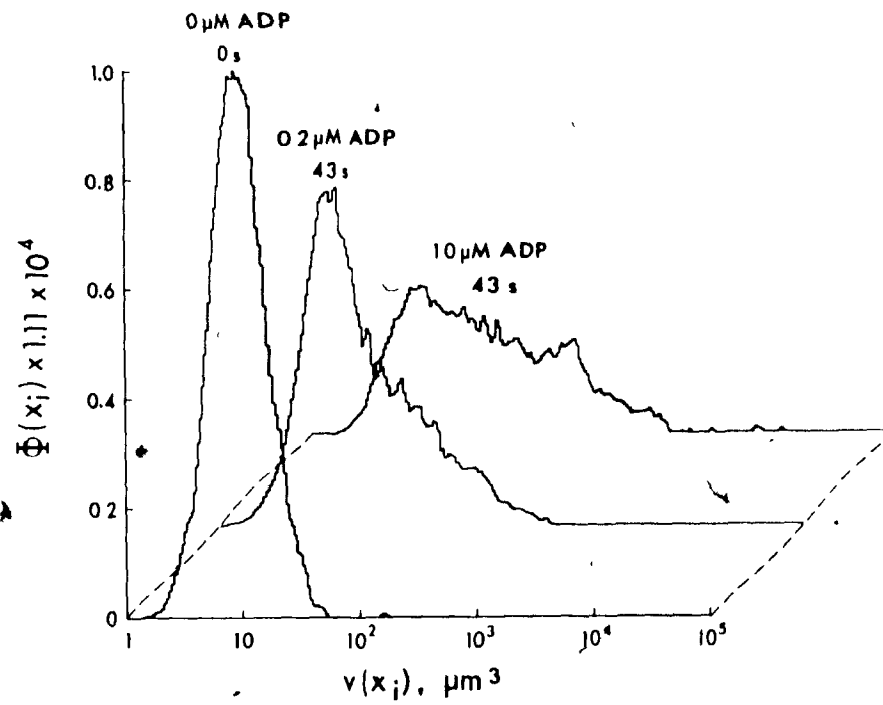
The much greater rate of aggregation at 1.0 μM ADP than at 0.2 μM ADP at the same shear rates led to the production of larger aggregates. At the higher ADP concentration, however, no sex difference was evident. Aggregates from the female donor were slightly larger than those from the

Figure 12: Aggregate Growth vs [ADP] at $\bar{G} = 39.3 \text{ s}^{-1}$.

Offset plot of the volume fraction per histogram class, $\Phi(x_i)$, vs particle volume, $v(x_i)$, for the male (a) and the female (b) donor after $\bar{t} = 43 \text{ s}$ exposure to 0.2 and 1.0 μM ADP at $\bar{G} = 39.3 \text{ s}^{-1}$. Also shown is a control at $\bar{t} = 0 \text{ s}$.

(a) Male

$\bar{G} = 39.3 \text{ s}^{-1}$



(b) Female

$\bar{G} = 39.3 \text{ s}^{-1}$

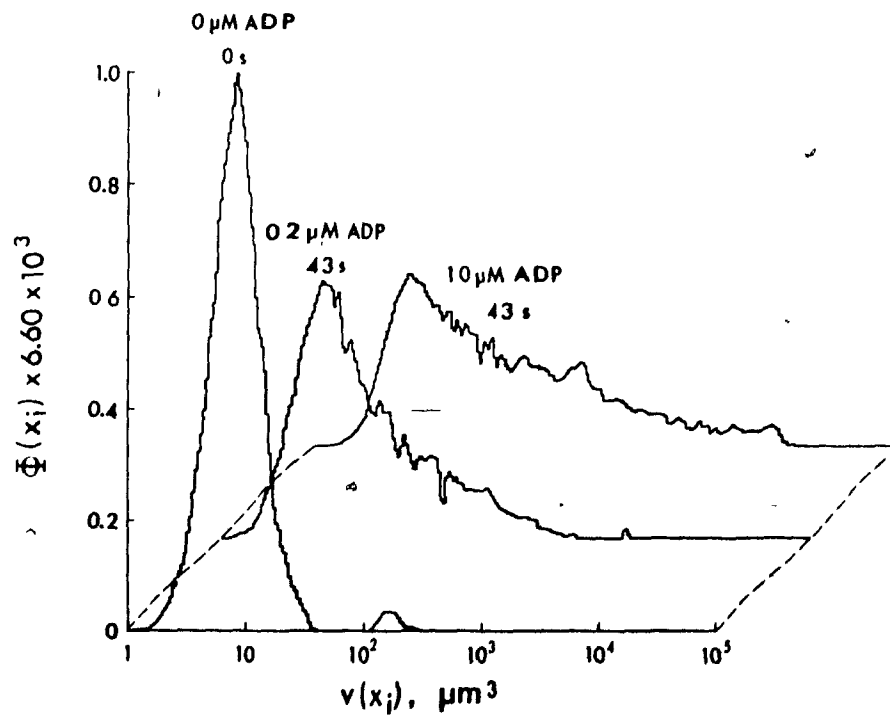


Figure 13: Aggregate Growth vs [ADP] at $\bar{G} = 314 \text{ s}^{-1}$

Offset plot of the volume fraction per histogram class, $\Phi(x_i)$, vs particle volume, $v(x_i)$, for the male (a) and the female (b) donor after $\bar{t} = 43 \text{ s}$ exposure to 0.2 and 1.0 μM ADP at $\bar{G} = 314 \text{ s}^{-1}$. Also shown is a control at $\bar{t} = 43 \text{ s}$ where modified Tyrodes was infused instead of ADP.

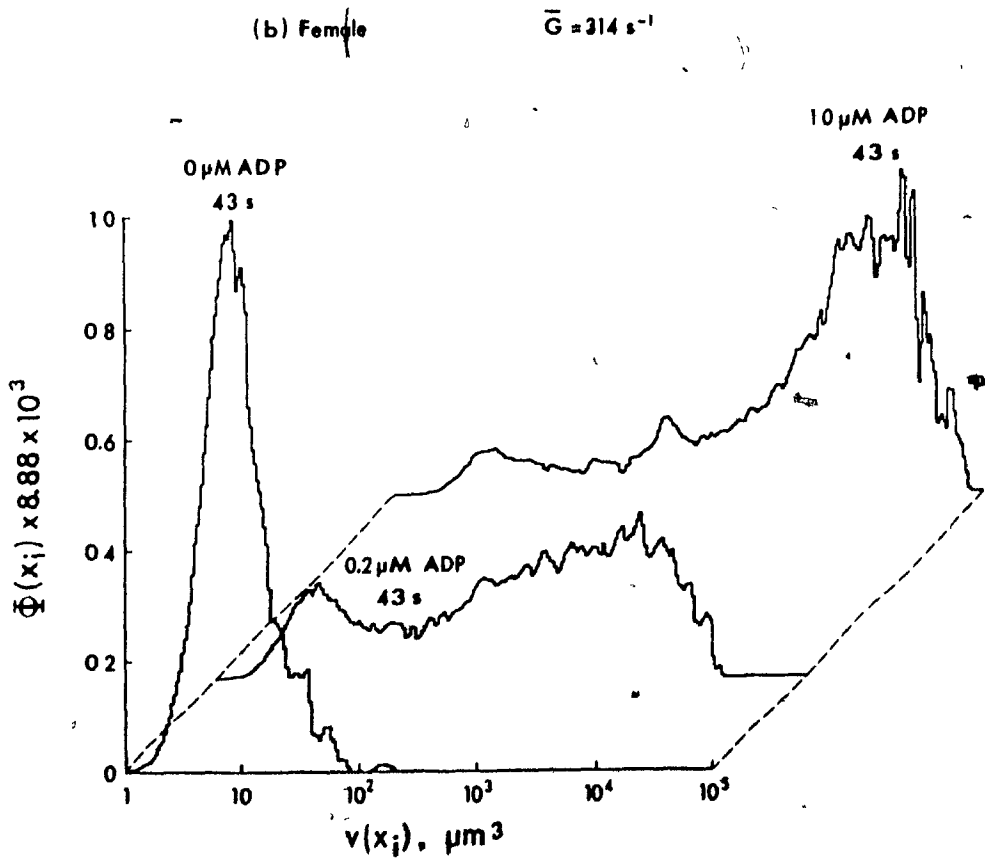
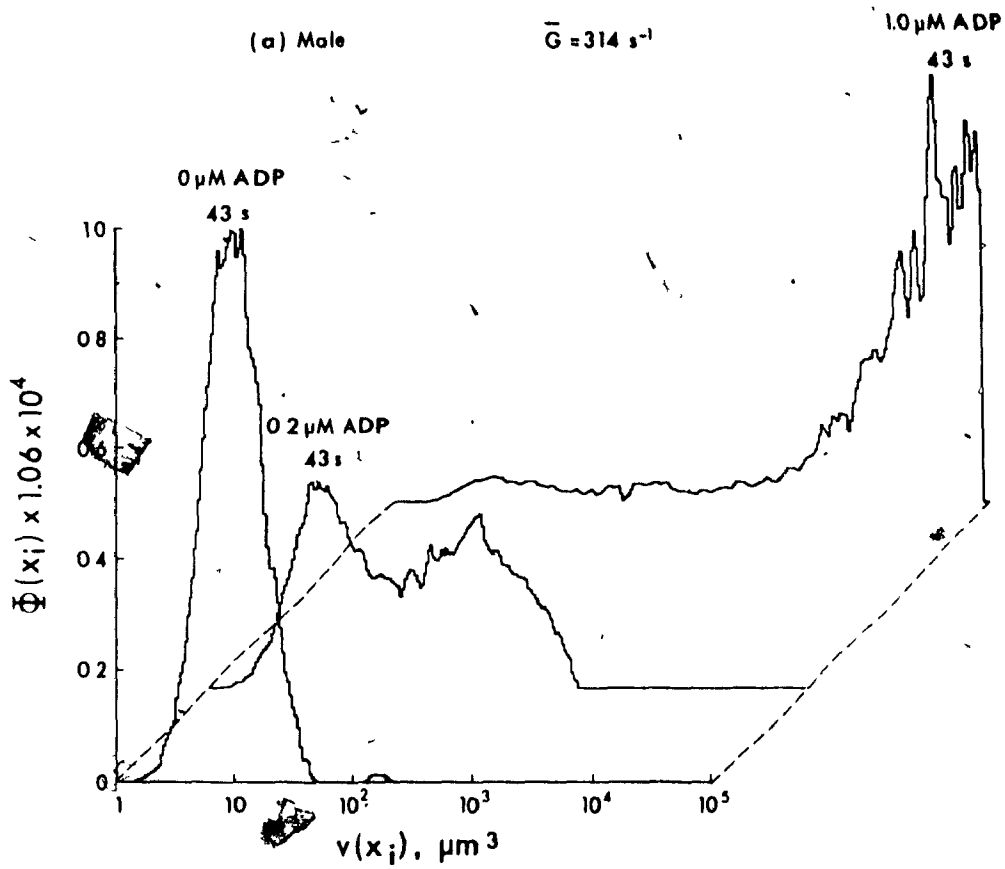
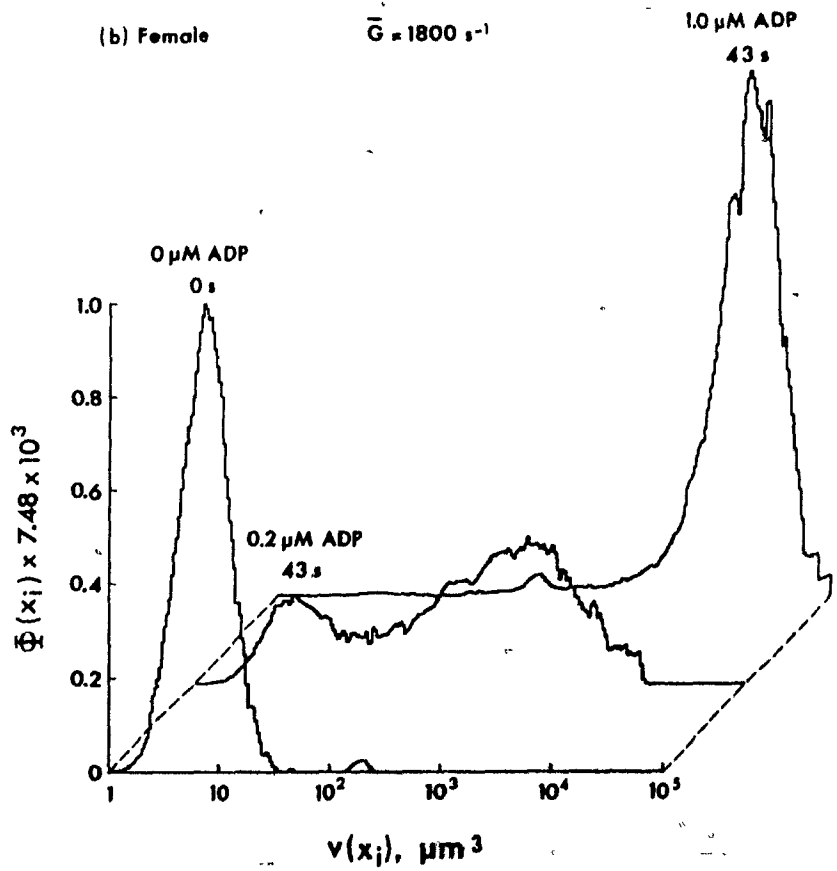
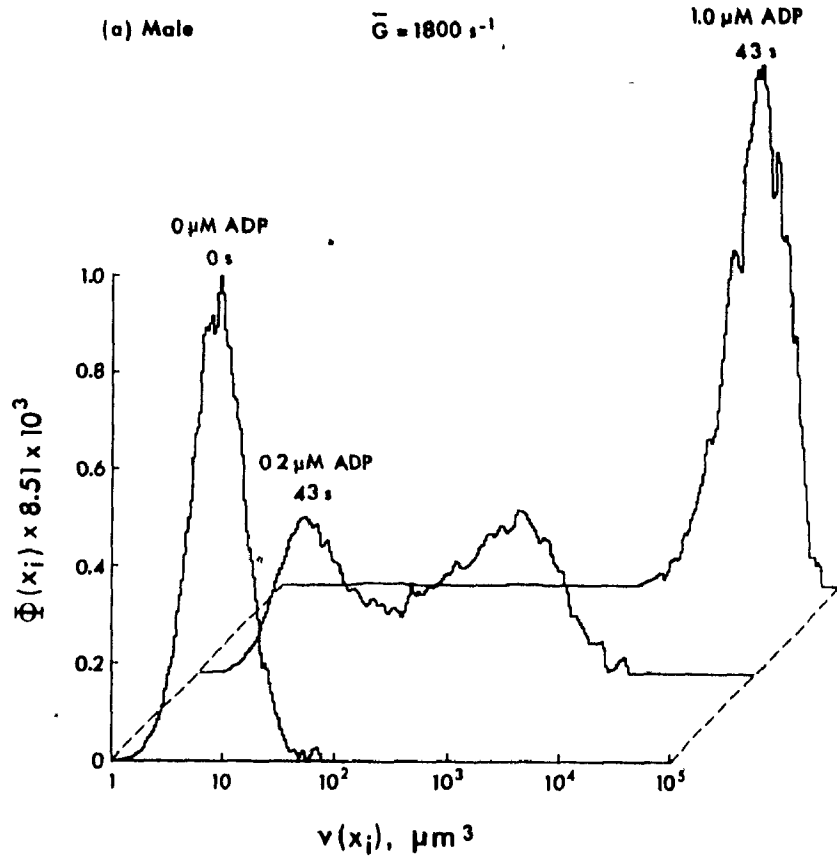


Figure 14: Aggregate Growth vs [ADP] at $\bar{G} = 1800 \text{ s}^{-1}$

Offset plot of the volume fraction per histogram class, $\Phi(x_1)$, vs particle volume, $v(x_1)$, for the male (a) and the female (b) donor after $\bar{t} = 43 \text{ s}$ exposure to 0.2 and 1.0 μM ADP at $\bar{G} = 1800 \text{ s}^{-1}$. Also shown is a control at $\bar{t} = 0 \text{ s}$.



male donor at $\bar{G} = 39.3 \text{ s}^{-1}$, while the converse was true at $\bar{G} = 314 \text{ s}^{-1}$. At the latter shear rate, a significant proportion of aggregates from the male donor exceeded the maximum volume measured ($10^5 \mu\text{m}^3$). At $\bar{G} = 1800 \text{ s}^{-1}$, the aggregates from both donors were unusually tightly grouped into a single population between 10^4 and $10^5 \mu\text{m}^3$ with no larger or smaller aggregates, and virtually no single platelets remaining. An increase in the overall volume fraction of these aggregates is seen by the magnitude of the ordinate of these log-volume distributions. The small population of particles between 130 and $260 \mu\text{m}^3$ at $\bar{t} = 0$ and 43 s are white cells which were not incorporated into aggregates.

DISCUSSION

The present work is the first account of the ADP-induced aggregation of human platelets in Poiseuille flow to span the full range of physiologically significant shear rate. Within this range, the rate of single platelet aggregation, as measured by the decrease in the concentration of single platelets, and the rate of aggregate growth were both highly dependent on mean transit time and mean tube shear rate. An increase in the lag phase preceding aggregation with increasing shear rate suggests a latency in the expression of platelet-platelet bonds of high strength. Measurement of the two-body collision efficiency also reveals the presence of more than one type of platelet-platelet bond. In addition, a strong sex difference was observed in both the rate of single platelet aggregation and size of aggregates.

1. Platelet Size

The log-normal model for the distribution of platelet size (Bahr and Zeitler, 1965; von Behrens, 1972; Paulus, 1975) was verified independently for platelet volume from male and female donors. The average mean platelet volume of $7.3 \mu\text{m}^3$, uncorrected for platelet shape, is consistent with previous uncorrected measurements of mean platelet volume obtained using electronic particle counters (Nakeff and Ingram, 1970; Paulus, 1975; Mundschenk et al., 1976; Holme and Murphy, 1980). Log-normal distributions are characteristic of particles that are generated from the multistep fragmentation (Epstein, 1947) or growth (Cramer, 1946) of another particle where the variation in size at each step is a random proportion of the size reached at the preceding step (Aitchinson and Brown, 1957). By analogy, Paulus (1975; Paulus et al., 1976) has proposed that the log-normal size distribution of platelets is a consequence of random factors controlling the combined rates of growth and demarcation of platelet territories during megakaryocyte maturation. Megakaryocyte polyploidy has also been postulated as a source of platelet heterogeneity (Pennington et al., 1976). It has also been proposed that platelet size heterogeneity is determined by aging in the circulation and that larger more dense platelets are younger and more reactive (Booyse et al., 1968; Karpatkin, 1969a,b; Corash et al., 1978; Rand et al., 1981). Whatever the source of the large variance in platelet size, the present work provides further data to confirm that platelet volume is represented by a single unimodal log-normal distribution.

The Kolmogorov-Smirnov one sample test was sensitive to small departures from log-normality and was supported by significant changes in

the shape of the log-volume distributions as measured by the statistics of skewing and kurtosis. Those distributions accepted by the K-S test as log-normal did not exhibit skewing or kurtosis. Those distributions rejected by the K-S test, however, were both significantly positively skewed and leptokurtotic, i.e., more platelets were located at the mean and extreme log-volumes than at intermediate values. Taken together, these parameters point to the presence of contaminating microaggregates that were formed during platelet preparation. Such microaggregation is unavoidable in citrated whole blood or PRP where a small degree of spontaneous aggregation can occur (Breddin et al., 1976), even after isolation under stringent conditions. Despite careful blood withdrawal and the relatively low-speed preparative centrifugation in the present work, sufficient platelet activation may have occurred (Table 4) to cause slight microaggregation. The presence of microaggregates in some of the experiments of the present work is revealed by their subsequent break-up in the controls, and at early times at $\bar{G} > 627 \text{ s}^{-1}$ in the ADP infusion runs (see Fig. 2).

2. Two-Body Collision Theory

The relationship between platelet aggregation and mean tube shear rate can be explained using the two-body collision theory that has been successful in modeling interactions between charged colloidal-size particles in shear flow (Bell and Goldsmith, 1984). In this model the hydrodynamic resistance preventing the approach of platelet surfaces and the hydrodynamic force which alternately brings platelets together and pulls them apart both increase in proportion to the rate of fluid shear. In the absence of attractive interaction forces, platelet aggregation is

impossible and all collisions result in separation. The expression of attractive forces between platelets can result in particle capture and stable doublet formation. For a given state of platelet activation, however, as the magnitude of the hydrodynamic forces increases relative to the attractive force, a critical shear rate will be reached beyond which the attractive forces are unable to preserve doublet integrity. The force resisting stable aggregate formation is commonly expressed in terms of the fluid shear stress. In the present experiments the mean tube shear stress, $\bar{\tau} = \eta \bar{G}$, ranged from 0.07 to 3.2 N m⁻², where $\eta = 1.8$ mPa s is the plasma viscosity at 22°C. As the mean tube shear rate increases, the extent of aggregation is the result of a balance between an increased frequency of collision (see Eq. [18], Chapter II) and an increased fluid shear stress. High collision rates support a high rate of aggregation in the absence of shear stresses sufficient to inhibit doublet formation. Beyond an optimum shear rate for aggregation, higher fluid shear stresses can break the platelet-platelet bond and aggregation decreases. It should be remembered that in Poiseuille flow the wall shear stress is twice the mean tube shear stress. Due to the gradient in shear rate across the tube, overall aggregation in the tube would decrease gradually with increases in mean tube shear rate beyond the optimum value, whereas in uniform shear fields aggregation would be expected to cease entirely at some critical shear rate, as has been observed in Couette flow by Yung and Frojmovic (1982).

The time available for stable bond formation between particles during collision would be expected to have a greater effect on platelet aggregation than on the aggregation of colloidal particles since the cells

express time-dependent changes in the degree of activation that are absent in inert particles. Short interaction times may limit stable doublet formation at high shear rates but, since this time is inversely proportional to the shear rate (Goldsmith and Mason, 1967), it is impossible to separate the effects of short interaction time and high shear stress in limiting stable bond formation. The two-body collision efficiency, however, takes both effects into account by measuring the fraction of total platelet-platelet collisions that result in stable doublet formation. The accuracy of the measured collision efficiency in the present experiments can be verified independently by calculation of the fraction of successful two-body collisions from the initial rate of single platelet decrease. The total number of two-body collisions per unit volume of suspension per second can be calculated from Eq. [19] of Chapter II by using the initial number concentration and volume fraction of single platelets:

$$J = \frac{4\Phi_{1,30}(0)N_{1,30}(0)\bar{G}}{\pi} \quad [1]$$

Thus, for respective rates of single platelet decrease of 2.7 and 4.2 % s⁻¹ at 0.2 μM ADP at $\bar{G} = 39.3 \text{ s}^{-1}$, 14% and 21% of all two-body collisions resulted in the formation of stable doublets for the male and female donors. The mean volume fraction of single platelets was 0.195% ± 0.023 (± S.D.) and 0.197% ± 0.023, respectively. These values are remarkably similar to the collision efficiency calculated according to Eq. [21] of Chapter II between $\bar{t} = 0$ and 4.3 s (Table 6). Although the collision efficiency was calculated well into the aggregation reaction, it is theoretically based on only two-body collisions. However, the main

result of calculating the collision efficiency at long times would be lower values due to the decrease in particle concentration with increasing aggregation. Thus, it is unlikely that the increase in collision efficiency with time is artifactual. In the following discussion, the aggregation phenomena observed in the present experiments are explained in terms of the two-body collision theory.

3. Effect of Shear Rate

ADP concentrations of 0.2 and 1.0 μM were selected to give consistently the same respective patterns of aggregation in the aggregometer as 1 and 5-10 μM ADP at 37°C, within the natural variation among donors. Thus, platelet aggregation at 22°C was $\sim 5\times$ greater than at 37°C; however, the release reaction was inhibited (Table 5). Release could only be induced in the aggregometer at 22°C. by high concentrations of thrombin. This is in agreement with Valdorf-Hansen and Zucker (1971) who showed the release of platelet serotonin induced by ADP but not thrombin to be inhibited below 27°C. In the flow experiments TXA_2 , as measured by the stable end product TXB_2 , was not significantly higher than static controls at mean tube shear rates between 39.3 and 1800 s^{-1} in either the control runs or with 0.2 and 1.0 μM ADP. Thus, it is unlikely that ADP- or shear-induced platelet release contributed to the observed aggregation. In the discussion to follow, 0.2 and 1.0 μM ADP are referred to as low and high platelet stimulation, respectively.

(a) Low Platelet Stimulation

(i) Single platelet aggregation: Neglecting for the moment the sex difference, the extent of platelet aggregation increases with

increasing mean tube shear rate up to an optimum value at $\sim 314 \text{ s}^{-1}$. Higher shear rates result in a steady decline in aggregation which increases again beyond 1250 s^{-1} . Shear stresses above 5 N m^{-2} , have been reported to induce platelet aggregation in rotational viscometers at room temperature (Brown et al., 1975; Belval et al., 1984). Platelet granule release is induced after 5 min exposure to this level of shear stress while shear stresses of 15 N m^{-2} are required to induce release within exposure times of the present experiments (Hellums and Hardwick, 1981). In the present work wall shear stress reached 6.5 N m^{-2} and, as discussed above, no release was detected. Furthermore, there was no shear-induced aggregation in the controls at the same level of shear stress. It would seem unlikely that shear-induced platelet aggregation contributed to the increase in aggregation at high shear rates in the present experiments. It is possible, however, that platelet surface activation in concert with ADP stimulation led to the enhanced affinity of existing receptors, the exposure of latent receptors or the induction of some independent mechanism of aggregation (discussed later).

It is interesting that the highest rate of aggregation was at the lowest shear rate but this was true for only the first few seconds of aggregation. The two-body collision efficiency was also highest under these conditions. Even so, at most only 28% of all collisions resulted in stable doublet formation. Although the fluid shear stress is low, the collision rate is not sufficient to sustain a high rate of aggregation. At higher shear rates there was generally a decrease in the fraction of efficient collisions but a high collision frequency accounts for the higher rates of aggregation. Theory predicts that when net attractive

forces operate between colliding particles, the collision efficiency decreases with increasing shear rate (van de Ven and Mason, 1977). This has been shown experimentally at shear rates less than 112 s^{-1} for the aggregation of model latex spheres in solutions of high ionic strength (Swift and Friedlander, 1964; Curtis and Hocking, 1970; Zeichner and Schowalter, 1977) and human platelets exposed to $1 \mu\text{M}$ ADP (Bell and Goldsmith, 1984). At the maximum shear rate in the present experiments collision efficiencies between 0.7×10^{-3} and 2.5×10^{-3} were measured. This is in good agreement with the values reported for shear-induced platelet aggregation at shear rates between 2000 and 10000 s^{-1} (Belval and Hellums, 1986). Thus, the collision efficiency decreased by approximately two orders of magnitude between shear rates of 39.3 and 1250 s^{-1} , but remained relatively constant thereafter up to shear rates of 10000 s^{-1} . The large decrease in collision efficiency at relatively low shear rates and the persistence of a nonzero collision efficiency at high shear rates suggest that more than one type of platelet-platelet bond mediates ADP-induced aggregation.

The increasing rates of aggregation with time as depicted by the sigmoid aggregation curves (Fig. 4, 9, and 10) indicate that collision efficiency increases with time, even after a delay of up to 11 s in the onset of aggregation. Indeed, not only do measurements of collision efficiency confirm this but they also indicate that the heterogeneity among platelet bonds is time-dependent (Fig. 5). At early transit times the high rate of aggregation at low shear rates is sustained by a weak bond that is easily disrupted at higher shear rates, resulting in a corresponding shear-dependent lag phase. Even at low shear rates the strength of this bond gradually diminishes with increasing transit time

and, in conjunction with a low collision rate, produces a steadily decreasing rate of aggregation. At high shear rates, the increasing rate of aggregation at times beyond the lag phase reveals the emergence of a second stronger bond. Longer times are required before each bond is sufficiently strong, or is present in sufficient numbers, to support aggregation. The two types of bonds coexist at intermediate transit times where the weak bond is disrupted at low shear rates but higher shear rates are required to disrupt the stronger bonds. The interruption in the decrease in collision efficiency with increasing mean tube shear rate between 157 and 314 s^{-1} at mean transit times between 4.3 and 8.6 s (Fig. 5) points to a transition from weak to strong bond. At very long exposure times the strong bonds are maximally expressed through either strength or numbers, and only high shear rates are sufficient to disrupt them. It is important to note that although the collision efficiency is very low at high shear rates, the high collision frequency can support a high rate of aggregation, as also found by Belval and Hellums (1986).

The effect of decreasing particle concentration in limiting aggregation through a decrease in the collision frequency is evident from the decreasing rates of aggregation at long transit times despite collision efficiencies that have remained constant or actually increased. This is best illustrated by rates of aggregation at $\bar{t} = 21$ s that are increasing at $\bar{G} = 1800$ s^{-1} but that are actually decreasing at $\bar{G} = 314$ s^{-1} . The higher initial rates of aggregation at $\bar{G} = 314$ s^{-1} depleted the single platelet concentration to a point where the rate of aggregation later in time decreased even though collision efficiency increased. At $\bar{G} = 1800$ s^{-1} the inhibition of aggregation at early transit

times preserved a particle concentration sufficient to support a high rate of aggregation once aggregation was initiated. Furthermore, the high concentration of small aggregates at $\bar{G} = 1800 \text{ s}^{-1}$ may have enhanced a high rate of single platelet aggregation by maintaining a high collision frequency between small aggregates and single platelets.

(11) Mechanisms of ADP-induced platelet aggregation: Fibrinogen is an essential cofactor for ADP-induced platelet aggregation (Simonetti et al., 1961; Cross, 1964; Born and Cross, 1964; Solum and Stormorken, 1965; McLean et al., 1965; Tollefson and Majerus, 1975). The cross-linking of bivalent fibrinogen molecules between activated glycoprotein IIb-IIIa (GPIIb-IIIa) complexes in the platelet membrane is the believed mechanism underlying aggregation. Other plasma glycoproteins such as fibronectin and von Willebrand factor (vWF) bind to GPIIb-IIIa complexes through a similar arginine-glycine-aspartic acid- (RGD) containing binding sequence to that which appears twice in the α -chain of fibrinogen (Pytela et al., 1986). However, the high concentration of fibrinogen in plasma (George et al., 1984) and the preferential binding of fibrinogen to stimulated platelets in the presence of other adhesive glycoproteins (Nurden, 1987) suggest fibrinogen is the primary plasma glycoprotein mediating platelet aggregation.

The steadily increasing lag phase preceding aggregation with increasing shear rate in the present work points to a latency in the strength of the platelet-platelet bond. An argument can be made for the requirement of latency in the expression of platelet bonds from the limitations placed on any colloid whose aggregation is mediated by polymer

cross-linking. In order for cross-linking to occur, unoccupied binding sites must be available on both surfaces. In the case of platelets, the high concentration of fibrinogen in plasma would be expected to saturate all binding sites on platelets before cross-linking could occur. In fact, cross-linking would require the simultaneous binding of opposite ends of the bivalent fibrinogen molecule to two platelets immediately after activation of GPIIb-IIIa complexes, and prior to saturation of these receptors with free fibrinogen. This scenario seems unlikely given the high concentration of fibrinogen in plasma. It is more likely that all GPIIb-IIIa complexes would be saturated with free fibrinogen long before two platelets could simultaneously bind a single fibrinogen molecule. Instead, a model of aggregation requires either a low affinity for fibrinogen binding by activated platelets, and the subsequent continuous breaking and forming of new platelet-fibrinogen bonds, or the time-dependent exposure of new bonds that permits cross-linking during the interaction time of collision. Peerschke et al. (1980) have provided evidence for both high and low affinity binding sites for ^{125}I -labelled fibrinogen on ADP stimulated platelets; however, Marguerie et al. (1980) found only a single class of receptors. In both cases binding was saturable and required the continuous presence of ADP in the absence of release. Both groups reported that binding increased with time; however, Peerschke et al. found binding to reach equilibrium after one minute while Marguerie et al. measured increased binding up to 30 minutes. In addition, fibrinogen itself appears to have a binding sequence in the carboxy terminus of the γ -chain that recognizes the GPIIb-IIIa complex, but is distinct from the RGD-containing sequence (Kloczewiak et al., 1984; Plow et al., 1984; Timmons et al., 1984; Santoro and Lawing, 1987).

Thus, the relatively slow kinetics of fibrinogen binding and the existence of heterogeneity in the affinity for fibrinogen provide a mechanism for platelet aggregation in the presence of high concentrations of the cross-linking ligand. Furthermore, the increase in the two-body collision efficiency with time and the formation of a high shear rate-resistant bond can be explained in terms of a time-dependent increase in fibrinogen binding.

Additional evidence for fibrinogen binding comes from the covalent cross-linking of fibrinogen to the GPIIb-IIIa complex (Bennett et al., 1982), and by the inhibition of binding by RGD-containing peptides (Haverstick et al., 1985; Plow et al., 1985; Gartner and Bennett, 1985) and by monoclonal antibodies that recognize the GPIIb-IIIa complex (Coller et al., 1983a; Bennett et al., 1983). These binding assays do not prove, however, that fibrinogen mediates aggregation by directly cross-linking activated platelets. It has been proposed that GPIIb-IIIa receptor clustering is a prerequisite for fibrinogen binding and platelet aggregation (Aasch et al., 1985; Newman et al., 1987). It is possible that the role of fibrinogen is to stabilize such clusters permitting them to interact in some complementary manner between activated platelets. Thus, fibrinogen cross-linking between platelets per se would not be necessary for aggregation. If the platelets were initially aggregated by a mechanism independent of fibrinogen cross-linking but which maintained close contact, cross-linking could follow as fibrinogen binding sites were expressed. Coller (1983) has proposed that platelet binding of fibrinogen alone would be sufficient to lower the electrostatic repulsion between the similarly charged platelets and permit aggregation through van der Waals

attraction. Collier also points out that platelet aggregation mediated by pseudopod-surface or pseudopod-pseudopod interactions would be enhanced by the effect of the small radius of curvature of pseudopods on lowering electrostatic repulsion. Since such aggregation is not mediated by specific fibrinogen cross-linking, it may not be resistant to high shear rates. It does, however, provide a mechanism for the relatively weak aggregation observed at short transit times in the present work.

Recent evidence also supports a stronger role for vWF in platelet aggregation than previously contended. The primary vWF receptor mediating platelet adhesion to subendothelium is GPIb (Collier et al., 1983b) and, as mentioned earlier, vWF can also bind to GPIIb-IIIa (Fujimoto and Hawiger, 1982; Fujimoto et al., 1982) but the significance of this latter binding is not clear. A role for vWF in mediating stable adhesion at high shear rates has been proposed from the observation that the adhesion defect in von Willebrand's disease (Tschopp et al., 1974), in which vWF is partially or totally missing, is more pronounced at wall shear rates greater than 2600 s^{-1} (Weiss et al., 1978). Platelet aggregation onto subendothelium has also been reported to be reduced at wall shear rates less than 1300 s^{-1} in von Willebrand's disease (Turitto et al., 1984), and a role for vWF in platelet aggregation has been postulated. Recent studies suggest that GPIIb-IIIa is involved in both platelet adhesion and aggregation onto subendothelium (Weiss et al., 1986; Sakariassen et al., 1986), and that vWF is the principal ligand involved (Weiss et al., 1988). Moreover, vWF has been found to substitute for fibrinogen in the ADP-induced aggregation of washed platelets (Timmons et al., 1986) and of platelets from patients with afibrinogenemia (de Marco et al., 1986). Work on shear-induced platelet aggregation has also shown that vWF appears

to mediate platelet aggregation in suspension at high shear rates at exposure times of 30 s and that high molecular weight forms, such as found in the α -granules of platelets, are the most effective (Moake et al., 1986; 1988). However, in the absence of significant release of vWF from the α -granules, plasma vWF can successfully mediate platelet aggregation. Both GPIb and GPIIb-IIIa appeared to be essential for the vWF-mediated aggregation, as was activation of the surface receptors by endogenous ADP released from platelets at shear stresses between 3 and 6 N m⁻². It is therefore of interest to postulate that plasma vWF binding is responsible for the high shear rate resistant bond in the present work. Although there was no release, platelet activation by ADP may have been sufficient to induce vWF binding. A role for thrombospondin (TS) in stabilizing the platelet-fibrinogen bond at high shear rates can be ruled out due to the requirement of platelet release for the expression of TS on platelet surfaces (Phillips et al., 1980), and the inability of monospecific anti-TS Fab fragments that inhibit thrombin induced platelet aggregation to inhibit primary aggregation induced by ADP (Leung, 1984).

(iii) Aggregate size: The wide spectrum of aggregate size at $\bar{G} = 39.3 \text{ s}^{-1}$ shows that aggregate growth is not limited by a shear stress of 0.07 N m⁻². Although the fluid shear stress is low, the collision rate is not sufficient to sustain a high rate of aggregation and the subsequent "snowball" effect found previously at this shear rate with 1 μM ADP (Bell and Goldsmith, 1984). In the present work this effect was evident at $\bar{G} = 314 \text{ s}^{-1}$, where large numbers of small aggregates that rapidly accumulated were subsequently incorporated into a new relatively homogeneous population of larger aggregates. Analysis of aggregate size

distributions has shown similar behavior for aggregation induced by ADP in the aggregometer (Nichols and Bosmann, 1979) or by shear rates greater than 2000 s^{-1} in rotational viscometers (Belval et al., 1984; Belval and Hellums, 1986). This form of aggregate growth is characteristic of the successive rise and fall in the number of small order multiplets of progressively increasing size predicted by Smoluchowski (1917) for model spheres and verified experimentally for platelets at $\bar{G} < 54 \text{ s}^{-1}$ (Bell and Goldsmith, 1984). The sequential formation of similarly-sized aggregates of relatively large size in the present experiments may have been encouraged by the presence of a limiting shear rate that restricts aggregate size at each mean transit time. The effect of this limit is more pronounced at $\bar{G} = 1800 \text{ s}^{-1}$ where despite a high rate of aggregation, aggregate size was much reduced compared to that at $\bar{G} = 314 \text{ s}^{-1}$. It is known that for particle aggregation in the presence of adsorbed polymer, aggregates of equal-sized particles are more readily broken up than aggregates of unequal-sized particles by shear stresses capable of disrupting polymer bonds (van de Ven, 1982). Since fibrinogen cross-linking between activated platelets is analogous to polymer bridging, this effect would favor the aggregation of single platelets and aggregates at high shear rates.

(b) High Platelet Stimulation

Comparison of the rate of single platelet aggregation for the two donors tested shows a slight shear-dependent lag phase still present. In spite of a 5-fold increase in the collision efficiency at $\bar{G} = 39.3 \text{ s}^{-1}$ for the male donor, the collision rate still could not support massive aggregation. Aggregate size was only slightly greater than at $0.2 \mu\text{M}$.

ADP. The high collision efficiency may reflect a large increase in the affinity or number of fibrinogen binding sites at the higher level of platelet stimulation. An increase in the length or numbers of platelet pseudopods may also increase the effective collision cross-section of the cells. This effect may be responsible for collision efficiencies greater than unity that have been measured for ADP-induced platelet aggregation due to Brownian motion (Frojmovic and Longmire, 1986). The opposing effects of a high collision efficiency and a size-dependent limiting shear rate are strikingly evident at high shear rates. At $\bar{G} = 314 \text{ s}^{-1}$ there was a large increase in both the rate of single platelet aggregation and aggregate size. The high rate of decrease in the single platelet concentration at $\bar{G} = 1800 \text{ s}^{-1}$ between 4.3 and 11 s of $8 - 10\% \text{ s}^{-1}$ led to the rapid depletion of virtually all single platelets; however, aggregate growth was severely limited. The aggregates were grouped into a narrow volume distribution between 10^4 and $10^5 \mu\text{m}^3$, yet at $\bar{G} = 314 \text{ s}^{-1}$ where many single platelets still remained, aggregate volume greatly exceeded $10^5 \mu\text{m}^3$. The shear stress of 3.2 N m^{-2} did not inhibit the recruitment of all platelets into aggregates but clearly inhibited aggregate growth.

It has been suggested that some platelets within a normal population typically do not aggregate (Born and Hume, 1967; Nichols and Bosman, 1979; Gear, 1982). The present work shows clearly that given a sufficient collision frequency and degree of platelet activation all platelets will aggregate. Neglecting the overlap of single platelet and microaggregate volume, the shape of the single platelet log-volume distribution remained symmetrical about the initial modal volume during aggregation indicating that all single platelets were being recruited

equally well into aggregates. Belval et al., (1984) also observed the aggregation of almost the entire single platelet population as a result of shear-induced aggregation at shear rates greater than 3000 s^{-1} .

4. Sex Difference

There is a highly significant sex difference in the aggregation of human platelets in response to $0.2 \text{ } \mu\text{M}$ ADP at room temperature over the range of mean tube shear rate $39.3 < \bar{G} < 1800 \text{ s}^{-1}$. This finding is consistent with previous work done in Poiseuille flow at $\bar{G} < 54 \text{ s}^{-1}$ with $1.0 \text{ } \mu\text{M}$ ADP (Bell and Goldsmith, 1984), and in the aggregometer at 37°C with $0.5 - 5.0 \text{ } \mu\text{M}$ ADP, collagen or epinephrine (Kelton et al., 1980; Coppe et al., 1981). In all cases the platelets from female donors aggregated more than those from male donors. Kelton et al. (1980) attributed the sex difference to the hematocrit-dependent chelation of ionized calcium, Ca^{2+} , which occurs in citrated PRP when a 1/10 (v/v) dilution of the citrate anticoagulant in whole blood is routinely employed. Since at least 96% of added citrate is excluded by the blood cells (Sakariassen et al., 1984) and female donors generally have lower hematocrits, the plasma citrate concentration would be lower, and the $[\text{Ca}^{2+}]$ correspondingly higher, for female donors than male donors. It has been shown that $[\text{Ca}^{2+}]$ in citrated PRP correlates inversely with donor hematocrit (Sakariassen et al., 1984), and in the present work an inverse relationship was found between hematocrit and aggregation. Both platelet aggregation (Gear, 1982) and adhesion to subendothelium (Sakariassen et al., 1984) have been shown to increase with $[\text{Ca}^{2+}]$ over the range of $[\text{Ca}^{2+}]$ ($30 - 60 \text{ } \mu\text{M}$) normally present in citrated PRP. Although the $[\text{Ca}^{2+}]$ in plasma was not directly measured, Kelton et al. (1980) removed the sex

difference by adjusting the volume of a fixed concentration of citrate added to whole blood according to donor hematocrit to give a constant concentration of citrate in plasma. In such a scheme, however, any other plasma factor involved in the sex difference would be diluted, also as a function of donor hematocrit, and subsequent removal of the sex difference by adjusting the volume of citrate added would be purely coincidental. In Chapter IV the $[Ca^{2+}]$ was measured using an ion selective electrode and the sex difference was shown to be due to the difference in plasma $[Ca^{2+}]$ between males and females. The sex difference was reversed when the concentration of a fixed volume of citrate was adjusted according to donor hematocrit to reverse the plasma $[Ca^{2+}]$ between the sexes.

REFERENCES

- AASCH, A.S., LEUNG, L.L.K., POLLEY, M.J., AND NACHMAN, R.L. (1985). Platelet membrane topography: colocalization of thrombospondin and fibrinogen with the glycoprotein IIb-IIIa complex Blood 66, 926-934.
- AITCHINSON, J. AND BROWN, J.A.C. (1957). The lognormal distribution with special reference to its use in economics. Cambridge Univ. Press, Cambridge, U.K.
- BAHR, G.F., AND ZEITLER, E. (1965). The determination of the dry mass in populations of isolated particles. Lab. Invest. 14, 955.
- BEGENT, N., AND BORN, G.V.R. (1970). Growth rate in vivo of platelet thrombi, produced by iontophoresis of ADP, as a function of mean blood flow velocity. Nature 227, 926-930.
- BELL, D.N., AND GOLDSMITH, H.L. (1984). Platelet aggregation in Poiseuille flow: II. Effect of shear rate. Microvasc. Res. 27, 216-330.
- BELL, D.N., TEIRLINCK, H.C., AND GOLDSMITH, H.L. (1984). Platelet aggregation in Poiseuille flow: I. A double infusion technique. Microvasc. Res. 27, 297-315.
- BELVAL, T., AND HELLUMS, J.D. (1986). The analysis of shear-induced platelet aggregation with population balance mathematics. Biophys. J. 50, 479-487.
- BELVAL, T., HELLUMS, J.D., AND SOLIS, T. (1984). The kinetics of platelet aggregation induced by shear. Microvasc. Res. 28, 279-288.
- BENNETT, J.S., HOXIE, J.A., LEITMAN, S.F., VILAIRE, G., AND CINES, D.B. (1983). Inhibition of fibrinogen binding to stimulated human platelets by a monoclonal antibody. Proc. Natl. Acad. Sci. U.S.A. 80, 2417-2421.
- BENNETT, J.S., VILAIRE, G., AND CINES, D.B. (1982). Identification of the fibrinogen receptor on human platelets by photoaffinity labeling. J. Biol. Chem. 275, 8049-8054.

- BOUYSE, F.M., HOVEKE, T.P., AND RAFELSON, M.E. (1968). Studies on human platelets. II. Protein synthetic activity of various platelet populations. Biochim. Biophys. Acta 157, 660.
- BORN, G.V.R., AND CROSS, M.J. (1964). Effects of inorganic ions and plasma proteins on the aggregation of blood platelets by adenosine diphosphate. J. Physiol. 170, 397.
- BORN, G.V.R., AND HUME, M. (1967). Effects of the numbers and sizes of platelet aggregates on the optical density of plasma. Nature 215, 1027-1029.
- BREDDIN, K., GRUN, H., KRZYWANEK, H.J., AND SCHREMMER, W.P. (1976). On the measurement of spontaneous platelet aggregation. The platelet aggregation test III. Methods and first clinical results. Thromb. Haemost. 35, 667-691.
- BROWN, C.H., LEVERETT, L.B., LEWIS, C.W., ALFREY, C.P., AND HELLUMS, J.D. (1975). Morphological, biochemical, and functional changes in human blood platelets subjected to shear stress. J. Lab. Clin. Med. 86, 462-471.
- CHANG, H.N., AND ROBERTSON, R. (1976). Platelet aggregation by laminar shear and Brownian motion. Ann. Biomed. Eng. 4, 151-183.
- CHIEN, S. (1975). Biophysical behavior of red cells in suspensions. In "The Red Cell" (D. MacN. Surgenor, ed.), pp. 1031-1133, Academic Press, New York.
- COLANTUONI, G., HELLUMS, J.D., MOAKE, J.L., AND ALFREY, C.P. (1977). The response of human platelets to shear stress at short exposure times. Trans. Am. Soc. Artif. Intern. Organs 23, 626-631.
- COLLER, B.S. (1983). Biochemical and electrostatic considerations in primary platelet aggregation. In "Surface Phenomena in Hemorheology Their Theoretical, Experimental, and Clinical Aspects" (A.L. Copley and G.V.F. Seaman eds.). Ann. N.Y. Acad. Sci. 416, 693-708.

- COLLER, B.S., PEERSCHKE, E.I., SCUDDER, L.E., AND SULLIVAN, C.A. (1983a). A murine monoclonal antibody that completely blocks the binding of fibrinogen to platelets produces a thrombasthenic-like state in normal platelets and binds to glycoproteins IIb and/or IIIa. J. Clin. Invest. **72**, 325-338.
- COLLER, B.S., PEERSCHKE, E.I., SCUDDER, L.E., AND SULLIVAN, C.A. (1983b). Studies with a murine monoclonal antibody that abolished ristocetin induced binding of von Willebrand factor to platelets: additional evidence in support of GPIb as a platelet receptor for von Willebrand factor. Blood **61**, 99-110.
- COPPE, D., WESSLINGER, S.J., RANSIL, B.J., HARRIS, W., AND SALZMAN, E. (1981). Sex differences in the platelet response to aspirin. Thromb. Res. **23**, 1-21.
- CORASH, L., SHAFER, B., AND PERLOW, M. (1978). Heterogeneity of human whole blood platelet subpopulations. II. Use of a subhuman primate model to analyze the relationship between density and platelet age. Blood **52**, 727-734.
- CRAMER, H. (1946). Mathematical methods of statistics. Princeton Mathematical Series No. 9, Princeton Univ. Press, Princeton, N.J.
- CROSS, M.J. (1964). Effect of fibrinogen on the aggregation of platelets by adenosine diphosphate. Thromb. Diath. Haemorrh. **12**, 524.
- CURTIS, A.S.G., AND HOCKING, L.M. (1970). Collision efficiency of equal spherical particles in shear flow. Trans. Faraday Soc. **66**, 1381-1390.
- DE MARCO, L., GIROLAMI, A., ZIMMERMAN, T.S., AND RUGGERI, Z. (1986). von Willebrand factor interaction with the glycoprotein IIb/IIIa complex: its role in platelet function as demonstrated in patients with congenital afibrinogenemia. J. Clin. Invest. **77**, 1272-1277.
- DEWITZ, T.S., MARTIN, R.R., SCLIS, R.T., HELLUMS, J.D., AND MCINTYRE, L.V. (1978). Microaggregate formation in whole blood exposed to shear stress. Microvasc. Res. **16**, 263-271.

- DOCUMENTA GEIGY (1962). "Scientific Tables" (K. Diem, ed.), p.164. Geigy Pharmaceuticals, Montreal, QC.
- EPSTEIN, B. (1947). The mathematical description of certain breakage mechanisms leading to the logarithmico-normal distribution. J. Franklin Institute 244, 471.
- FROJMOVIC, M.M., AND LONGMIRE, K.A. (1986). Platelet aggregation in Brownian diffusion: Evidence for long range interactions for human but not rabbit platelets. Biorheology 23, 228 (Abstract).
- FUJIMOTO, T., AND HAWIGER, J. (1982). Adenosine diphosphate induces binding of von Willebrand factor to human platelets. Nature (Lond.) 297, 154-156.
- FUJIMOTO, T., O'HARA, S., AND HAWIGER, J. (1982). Thrombin-induced exposure and prostacyclin inhibition of the receptor for Factor VIII/von Willebrand factor on human platelets. J. Clin. Invest. 69, 1212-1222.
- GARTNER, T.K., AND BENNETT, J.S. (1985). The tetrapeptide analogue of the cell attachment site of fibronectin inhibits platelet aggregation and fibrinogen binding to activated platelets. J. Biol. Chem. 260, 11891-11894.
- GEAR, A.R.L. (1982). Rapid reactions of platelets studied by a quenched flow approach: Aggregation kinetics. J. Lab. Clin. Med. 100, 866-886.
- GEORGE, J.N., NURDEN, A.T., AND PHILLIPS, D.R. (1984). Molecular defects in interactions of platelets with the vessel wall. N. Engl. J. Med. 311, 1084-1098.
- GOLDSMITH, H.L. (1972). The flow of model particles and blood cells and their relation to thrombogenesis. In "Advances in Hemostasis and Thrombosis" (T.H. Spaet, ed.), pp. 97-139, Grune and Stratton, New York.
- GOLDSMITH, H.L., AND MASON, S.G. (1967). The microrheology of dispersions. In "Rheology: Theory and Applications" (F.R. Eirich, ed.), Vol. 4, pp. 85-250. Academic Press, New York.

- GRABOWSKI, E.F., FRANTA, J.T., AND DIDISHEIM, P. (1978). Platelet aggregation in flowing blood in vitro. II. Dependence of aggregate growth rate on ADP concentration and shear rate. Microvasc. Res. 16, 183-195.
- HAVERSTICK, D.M., COWAN, J.F., YAMADA, K.M., AND SANTORO, S.A. (1985). Inhibition of platelet binding to fibronectin, fibrinogen and von Willebrand factor substrates by a synthetic tetrapeptide derived from the cell binding domain of fibronectin. Blood 66, 946-952.
- HELLUMS, J.D., AND HARDWICK, R.A. (1981). Response of platelets to shear stress - a review. In "The Rheology of Blood, Blood Vessels and Associated Tissues" (D.R. Gross and N.H.C. Hwang, eds.), pp. 160-183, Sijthoff and Noordhoff, Rockville, Maryland.
- HOLME, S. AND MURPHY, S. (1980). Coulter Counter and light transmission studies of platelets exposed to low temperature, ADP, EDTA, and storage at 22°. J. Lab. Clin. Med. 96, 480-493.
- JEN, C.J., AND MCINTIRE, L.V. (1984). Characteristics of shear-induced aggregation in whole blood. J. Lab. Clin. Med. 103, 115-124.
- KARPATKIN, S. (1969a). Heterogeneity of human platelets. I. Metabolic and kinetic evidence suggestive of young and old platelets. J. Clin. Invest. 48, 1073-1082.
- KARPATKIN, S. (1969b). Heterogeneity of human platelets. II. Functional evidence suggestive of young and old platelets. J. Clin. Invest. 48, 1083-1087.
- KELTON, J.G., POWERS, P., JULIAN, J., BOLAND, V., CARTER, C.J., GENT, M. AND HIRSH, J. (1980). Sex-related differences in platelet aggregation: influence of hematocrit. Blood 56, 38-41.
- KENNEY, J.K., AND KEEPING, E.S. (1951). "Mathematics of Statistics" (Part Two). D. Van Nostrand, Toronto, ON.
- KLOCZEWIAK, M., TIMMONS, S., LUKAS, T.J., AND HAWIGER, J. (1984). Platelet receptor recognition site on human fibrinogen. Synthesis and structure-function relationship of peptides corresponding to the carboxy-terminal segment of the γ chain. Biochem. 23, 1767-1774.

- LEUNG, L.L.K., (1984). Role of thrombospondin in platelet aggregation. J. Clin. Invest. **74**, 1764-1772.
- LILLIEFORS, H.W. (1967). On the Kolmogorov-Smirnov test for normality with mean and variance unknown. Am. Statist. Assoc. J. **62**, 399.
- MARGUERIE, G.A., EDINGTON, T.S., AND PLOW, E.F. (1980). Interaction of fibrinogen with its receptor as a part of a multistep reaction in ADP-induced platelet aggregation. J. Biol. Chem. **255**, 154-161.
- McLEAN, J.R., MAXWELL, R.E., AND HERTHER, D. (1965). Fibrinogen and adenosine diphosphate induced aggregation of platelets. Nature **202**, 605.
- MOAKE, J.L., TURNER, N.A., STATHOPOULOS, N.A., NOLASCO, L.H., HELLMUMS, J.D. (1986). Involvement of large plasma von Willebrand factor (vWF) multimers and unusually large vWF forms derived from endothelial cells in shear stress-induced platelet aggregation. J. Clin. Invest. **78**, 1456-1461.
- MOAKE, J.L., TURNER, N.A., STATHOPOULOS, N.A., NOLASCO, L., HELLMUMS, J.D. (1988). Shear-induced platelet aggregation can be mediated by vWF released from platelets, as well as by exogenous large or unusually large vWF multimers, requires adenosine diphosphate and is resistant to aspirin. J. Clin. Invest. (in press).
- MUNDSCHENK, D.D., CONNELLY, D.P., WHITE, J.G., AND BRUNNING, R.D. (1976). An improved technique for the electronic measurement of platelet size and shape. J. Lab. Clin. Med. **88**, 301-315.
- NAKEFF, A. AND INGRAM, M. (1970). Platelet count:volume relationships in four mammalian species. J. Appl. Physiol. **28**, 530-533.
- NEWMAN, P.J., McEVER, R.P., DOERS, M.P., AND KUNICKI, T.S. (1987). Synergistic action of two murine monoclonal antibodies that inhibit ADP-induced platelet aggregation without blocking fibrinogen binding. Blood **69**, 668-676.

- NICHOLS, A.R., AND BOSMANN, H.B. (1979). Platelet aggregation: newly quantified using nonempirical parameters. Thromb. Haemost. 42, 679-693.
- NURDEN, A.T. (1987). Platelet membrane glycoproteins and their clinical aspects. In "Thrombosis and Haemostasis" (M. Verstraete, J. Vermylen, R. Lijnen, and J. Arnout, eds.), pp. 93-125, Leuven Univ. Press, Leuven, Belgium.
- PAULUS, J. (1975). Platelet size in man. Blood 46, 321-336.
- PAULUS, J.M., CASALS, F.J., AND BURY, J. (1976). Cytological and clinical significance of platelet size. In "Workshop on Platelets: Platelet Function Testing" (H.J. Day, H. Holmsen and M.B. Zucker, eds.) U.S. Dept. Health, Education and Welfare, Public Health Service, NIH, Bethesda, MD. pp 322-333.
- PEERSCHKE, E.I., ZUCKER, M.B., GRANT, R.A., EGAN, J.J., AND JOHNSON, M.M. (1980). Correlation between fibrinogen binding to human platelets and platelet aggregability. Blood 55, 841-847.
- PENNINGTON, D.G., STREATFIELD, K., ROXBURGH, A.E. (1976). Megakaryocytes and the heterogeneity of circulating platelets. Br. J. Haematol. 34, 639-653.
- PHILLIPS, D.R., JENNINGS, L.K., AND PRASANNA, H.R. (1980). Ca²⁺-mediated association of glycoprotein-G (thrombin-sensitive protein, thrombospondin) with human platelets. J. Biol. Chem. 255, 11629-11632.
- PLOW, E.F., PIERSCHBACHER, M.D., RUOSLAHTI, E., MARGUERIE, G.A., AND GINSBERG, M.H. (1985). The effect of arg-gly-asp-containing peptides on fibrinogen and von Willebrand factor binding to platelets. Proc. Natl. Acad. Sci. U.S.A. 82, 8057-8061.
- PLOW, E.F., SROUJI, A.H., MEYER, D., MARGUERIE, G., AND GINSBERG, M.H. (1984). Evidence that three adhesive proteins interact with a common recognition site on activated platelets. J. Biol. Chem. 259, 5388-5391.

- PYTELA, R., PIERSCHBACHER M.D., GINSBERG, M.H., PLOW, E.F., AND RUOSLAHTI, E. (1986). Platelet membrane glycoprotein IIb/IIIa: member of a family of arg-gly-asp-specific adhesion receptors. Science **231**, 1559-1562.
- RAND, M.L., GREENBERG, J.P., PACKHAM, M.A., AND MUSTARD, J.F. (1981). Density subpopulations of rabbit platelets: Size, protein, and sialic acid content, and specific radioactive changes following labelling with ^{35}S -sulfate in vivo. Blood **57**, 741-746.
- SAKARIASSEN, K.S., OTTENHOF-ROVERS, M. AND SIXMA, J.J. (1984). Factor VIII-von Willebrand factor requires calcium for facilitation of platelet adherence. Blood **63**, 996-1003.
- SAKARIASSEN, K.S., NIEVELSTEIN, P.F.E.M., COLLER, B.S., SIXMA, J.J. (1986). The role of platelet membrane glycoproteins Ib and IIb-IIIa in platelet adherence to human artery subendothelium. Brit. J. Haemat. **63**, 681-691.
- SANTORO, S.A., AND LAWING, W.J. (1987). Competition for related but nonidentical binding sites on the glycoprotein IIb-IIIa complex by peptides derived from platelet adhesive proteins. Cell **48**, 867-873.
- SIMONETTI, C., CASILLAS, G. AND PAVLOVSKY, A. (1961). Purification du facteur VIII antihemophilique (FAH). Hemostase **1**, 57.
- SMOLUCHOWSKI, M. VON (1917). Versuch einer mathematischen Theorie der Koagulationskinetik kolloider Lösungen. Z. Physik. Chem. **92**, 129-168.
- SOKAL, R.R., AND ROHLF, F.J. (1969). "Biometry". Freeman, San Francisco, CA.
- SOLUM, N.O., AND STORMORKEN, H. (1965). Influence of fibrinogen on the aggregation of washed human blood platelets induced by adenosine diphosphate, thrombin, collagen, and adrenalin. Scand. J. Clin. Lab. Invest. **17** (Suppl. 84), 170.
- SWIFT, D.L., AND FRIEDLANDER, S.K. (1964). The coagulation of hydrosols by Brownian motion and laminar shear flow. J. Coll. Sci. **19**, 621-647.

- TIMMONS, S., AND HAWIGER, J. (1986). von Willebrand factor can substitute for plasma fibrinogen in ADP-induced platelet aggregation. Trans. Assn. Amer. Phys. **99**, 226-235.
- TIMMONS, S., KLOCZEWIAK, M., AND HAWIGER, J. (1984). ADP-dependent common receptor mechanism for binding of von Willebrand factor and fibrinogen to human platelets. Proc. Natl. Acad. Sci. U.S.A. **81**, 4935-4939.
- TOLLEFSON, D.M., AND MAJERUS, P.W. (1975). Inhibition of human platelet aggregation by monovalent anti-fibrinogen antibody fragments. J. Clin. Invest. **55**, 1259.
- TSCHOPP, T.B., WEISS, H.J., AND BAUMGARTNER, H.R. (1974). Decreased adhesion of platelets to subendothelium in von Willebrand's disease. J. Lab. Clin. Med. **83**, 296-300.
- TURITTO, V.T. (1982). Blood viscosity, mass transport and thrombogenesis. In "Progress in Thrombosis and Hemostasis", Vol. 6 (T.H. Spaet, ed.), pp. 139-177, Grune and Stratton, New York.
- TURITTO, V.T., AND BAUMGARTNER, H.R. (1982). Platelet surface interactions. In "Hemostasis and Thrombosis, Basic Principles and Clinical Practice" (R.W. Colman, J. Hirsh, V.J. Marder and E.W. Salzman, eds.), pp. 354-379, J.B. Lippincott, Philadelphia.
- TURITTO, V.T., WEISS, H.J., AND BAUMGARTNER, H.R. (1984). Platelet interaction with rabbit subendothelium in von Willebrand's disease: altered thrombus formation distinct from defective platelet adhesion. J. Clin. Invest. **74**, 1730-1741.
- VALDORF-HANSEN, J.F., AND ZUCKER, M.B. (1971). Effect of temperature and inhibitors on serotonin-¹⁴C release from human platelets. Am. J. Physiol. **220**, 105-111.
- VAN DE VEN, T.G.M. (1982). Interactions between colloidal particles in simple shear flow. Adv. Colloid Interface Sci. **17**, 105.
- VAN DE VEN, T.G.M., AND MASON, S.G. (1977). The microrheology of colloidal dispersions. VII. Orthokinetic doublet formation of spheres. Coll. Polymer Sci. **255**, 468-479.

VON BEHRENS, W.E. (1972). Platelet size. Thesis submitted for the degree of Doctor of Medicine, University of Adelaide, Adelaide, South Australia.

WEISS, H.J., HAWIGER, J., RUGGERI, Z.M., TURRITO, V.T., AND HOFFMANN, T. (1988). Evidence that von Willebrand factor, and not fibrinogen, is involved in glycoprotein IIb-IIIa mediated platelet adhesion and thrombus formation on subendothelium. J. Clin. Invest. (in press).

WEISS, H.J., TURITTO, V.T., BAUMGARTNER, H.R. (1978). Effect of shear rate on platelet interaction with subendothelium in citrated and native blood. I. Shear rate-dependent decrease of adhesion in von Willebrand's disease and the Bernard-Soulier syndrome. J. Lab. Clin. Med. **92**, 750-764.

WEISS, H.J., TURITTO, V.T., AND BAUMGARTNER, H.R. (1986). Platelet adhesion and thrombus formation on subendothelium in platelets deficient in glycoproteins IIb-IIIa, Ib, and storage granules. Blood **67**, 322-330.

WHITMORE, R.L. (1968). "Rheology of the Circulation" Pergamon Press, Oxford.

YOUNG, I.T. (1977). Proof without prejudice: Use of the Kolmogorov-Smirnov test for the analysis of histograms from flow systems and other sources. J. Histochem. Cytochem. **25**, 935-941.

YUNG, W., AND FROJMOVIC, M.M. (1982). Platelet aggregation in laminar flow. Part I. Adenosine diphosphate concentration, time and shear rate dependence. Thromb. Res. **28**, 367-378.

ZEICHNER, G.R., AND SCHOWALTER, W.R. (1977). Use of trajectory analysis to study stability of colloidal dispersions in flow fields. AI. Chem. Eng. J. **23**, 243-254.

CHAPTER IV

EXTRACELLULAR FREE Ca^{2+} ACCOUNTS FOR THE SEX DIFFERENCE
IN THE AGGREGATION OF HUMAN PLATELETS
IN CITRATED PLATELET-RICH PLASMA

ABSTRACT

The sex difference in the ADP-induced aggregation of human platelets in flowing suspensions was studied using a previously described technique for measuring the concentration and volume of single platelets and aggregates in citrated platelet-rich plasma, cPRP (Chapter II, this thesis). In Chapter III the aggregation of platelets from female donors was significantly greater than from male donors over the range of mean tube shear rate, \bar{G} , from 39.3 s^{-1} to 1800 s^{-1} and mean transit time, \bar{t} , from 0.2 to 86 s. In this chapter the sex difference was verified at $\bar{G} = 314 \text{ s}^{-1}$ and $\bar{t} = 43 \text{ s}$. The inverse correlation between the extent of single platelet aggregation and donor hematocrit, and between hematocrit and the plasma ionized calcium concentration, $[\text{Ca}^{2+}]$, as well as the positive correlation between the extent of single platelet aggregation and $[\text{Ca}^{2+}]$, indicated that the sex difference is due to hematocrit-dependent differences in the $[\text{Ca}^{2+}]$ that result when a fixed volume of the chelating agent citrate is used to anticoagulate blood. When the initial citrate concentration was adjusted independent of the variable volume dilution of citrate in plasma for each donor, the sex difference was reversed. Again, aggregation correlated with $[\text{Ca}^{2+}]$. At the physiological $[\text{Ca}^{2+}]$ in both heparinized-PRP and hirudinized-PRP, the rate of aggregation was much greater than in cPRP but no sex difference was detected. Aggregate size was also much larger than in cPRP, and in heparinized PRP virtually all single platelets had aggregated by $\bar{t} = 86 \text{ s}$. Thus, the rate of platelet aggregation in flowing suspensions has a strong Ca^{2+} -dependence in the low range of $[\text{Ca}^{2+}]$ normally present in cPRP.

INTRODUCTION

There exists substantial evidence attributing a sex difference to the behavior of human platelets. Aspirin, a well-known inhibitor of prostaglandin-mediated platelet release (Weiss and Aledort, 1967; Zucker and Peterson, 1968; Mustard et al., 1975; Roth and Majerus, 1975; Moncada and Vane, 1979), is successful in reducing post-operative deep vein thrombosis (Harris et al., 1977), and in lowering the risk of recurrent transient ischemic attacks and strokes (Canadian Cooperative Study Group, 1978) in men but not in women. Platelet aggregation in citrated platelet-rich plasma, cPRP, is greater for female donors than for male donors in response to epinephrine (Johnson et al., 1975), collagen (Coppe et al., 1981), and 0.2 - 5.0 μM ADP at 37°C (Johnson et al., 1975; Reading and Rosie, 1980; Kelton et al., 1980) or at room temperature (Bell and Goldsmith, 1984; Chapter III, this thesis).

However, the in vitro sex difference may be an artifact of anticoagulation. When whole blood is routinely anticoagulated with 1/10 volume sodium citrate the plasma citrate concentration will depend on donor hematocrit, since the added citrate is almost entirely excluded by the blood cells (Sakariassen et al., 1984). The plasma citrate concentration of a donor with a 50% hematocrit would be 20% greater than that of a donor with a 38% hematocrit, and the concentration of ionized calcium, Ca^{2+} , correspondingly lower. The $[\text{Ca}^{2+}]$ in cPRP correlates inversely with hematocrit (Sakariassen et al., 1984) as does ADP-induced aggregation (Chapter III, this thesis). Ionized calcium is an essential cofactor for platelet aggregation with the rate of aggregation increasing over the range of $[\text{Ca}^{2+}]$ from 0 to 100 μM (Gear, 1982).

Systematic variation in the plasma $[Ca^{2+}]$, in the low range normally present in cPRP, might generate significant differences in the rate of aggregation of platelets between groups of donors with sufficiently different hematocrits. A sex difference occurs because females generally have a lower hematocrit than males.

Kelton et al. (1980) removed the sex difference in cPRP by adjusting the initial volume of citrate added to whole blood to give a constant citrate concentration in plasma, independent of hematocrit. However, this does not unequivocally demonstrate that Ca^{2+} is the cause of the sex difference. Any other plasma factor responsible for the sex difference would also be subject to the same hematocrit-dependent dilution effect, and the subsequent removal of the sex difference by correcting the variable plasma dilution would be fortuitous.

In light of consistent differences found in the ADP-induced aggregation of cPRP from male and female donors in this laboratory, the role of Ca^{2+} in the sex difference was further investigated. The $[Ca^{2+}]$ was measured before and after the plasma citrate concentration of males and females was reversed without altering the hematocrit-dependent dilution effect. The $[Ca^{2+}]$ was reversed and so was the sex difference. In both cases aggregation correlated with $[Ca^{2+}]$. In contrast, no sex difference was found using either heparin or hirudin anticoagulants.

Platelet aggregation was induced using a previously described technique (Chapter II, this thesis) in which PRP and ADP are simultaneously infused into a small mixing chamber prior to flowing

through polyethylene tubing at preset mean tube shear rates. The volume distribution of particles between 1 and $10^5 \mu\text{m}^3$ was measured at various distances downstream corresponding to mean transit times through the tube. Aggregation was expressed in terms of the decrease in the single platelet concentration and of the volume fraction of single cells and aggregates. Two-body collision theory developed for colloidal-sized particles was applied to the platelet suspensions to determine the efficiency of collision between the activated cells.

MATERIALS AND METHODS

1. Platelet-Rich Plasma and Reagents

Experiments were performed as described in Chapter II. Venous blood was slowly drawn from healthy, age-matched volunteers via a 19 gauge needle and winged infusion set into 30 ml plastic syringes containing anticoagulant. All donors had refrained from aspirin ingestion for at least 10 days prior to blood withdrawal and no female donors were taking oral contraceptives. Hematocrit, HCT, was determined on undiluted venous blood at the time of blood withdrawal. After incubating the blood at 37°C for 30 min, PRP was prepared at room temperature by centrifuging the whole blood at 100g for 20 min, and platelet-poor plasma, PPP, by centrifuging the remaining blood at 2000g for a further 20 min. All platelet suspensions were maintained under a mixture of 5% CO_2 and 95% air to preserve pH 7.4. Frozen aliquots of 2.0 mM adenosine-5'-diphosphate, ADP, (Sigma, St. Louis, MO) were thawed immediately prior to use and diluted in modified Tyrodes solution (137 mM NaCl, 2.7 mM KCl, 11.9 mM NaHCO_3 , 0.36 mM $\text{NaH}_2\text{PO}_4 \cdot \text{H}_2\text{O}$) at pH 7.4. Electron microscope grade glutaraldehyde (J.B. EM Services, Pointe Claire-Dorval, QC) was diluted to

0.5% (v/v) in Isoton II (Coulter Electronics, Hialeah, FL). One per cent (v/v) silicone (Siliclad, Clay Adams, Parsippany, NJ) was used to siliconize the mixing chamber prior to experiments.

(a) Citrate

Blood from both male and female donors was drawn into 1/10 volume, 3.8% sodium citrate. In some experiments a second sample of blood was drawn into 1/10 volume of sodium citrate at an initial concentration, C_i , that was adjusted according to donor hematocrit. The initial citrate concentration of male donors was lowered and that of female donors raised to give the same final citrate concentration in plasma, C_f , as that of donors of 38 and 50% hematocrit, respectively, at $C_i = 3.8\%$, as given by:

$$C_i = C_f \times [9(1 - \text{HCT}) + 1]. \quad [1]$$

C_i ranged from 3.2 to 4.5%.

(b) Heparin

Each 30 ml syringe contained 15 μl of 10,000 units ml^{-1} sodium heparin (Organon, Toronto, ON) yielding 5 units heparin per ml of whole blood.

(c) Hirudin

Hirudin (grade IV, Sigma) was dissolved in modified Tyrodes to give 4000 units ml^{-1} and aliquots were stored at -20°C . On the day of the experiment hirudin was thawed and one ml was placed in a 30 ml syringe at an initial concentration, H_i , according to:

$$H_i = 150 \times [29(1 - \text{HCT}) + 1], \quad [2]$$

to give 150 units hirudin per ml plasma, independent of hematocrit. Since the sedimentation rate of hirudinized whole blood was observed to be much greater than that of both citrated and heparinized whole blood, PRP was prepared by omitting the 30 min incubation at 37°C and immediately centrifuging the blood at 40g for 25 min. After removing the supernatant PRP, the blood was centrifuged at 1000g for 20 min to get PPP.

2. Flow System

All experiments were done at $23 \pm 1^\circ\text{C}$. Platelet-rich plasma was adjusted with PPP to 3.30×10^5 cells μl^{-1} and infused into a small cylindrical mixing chamber (6 mm i.d., 9.5 mm o.d., 1.5 mm height) using a syringe pump. ADP was simultaneously infused into the mixing chamber via an independent syringe pump at a fixed flow ratio, PRP:ADP = 9:1. After rapid mixing, the PRP-ADP suspension exited the chamber through lengths of 0.595 mm radius, R_0 , polyethylene tubing (Clay Adams, Parsippany, NJ), for preset mean cell transit times, $\bar{t} = X_3/\bar{U}$, from 0.2 to 86 s, where X_3 is the distance down the flow tube and \bar{U} is the mean linear fluid velocity. The aggregation reaction was instantaneously and permanently arrested by collecting known volumes of the effluent into 20x the suspension volume of 0.5% (v/v) isotonic glutaraldehyde (J.B. EM Services, Pointe Claire-Dorval, QC). The total volume flow rate, Q , was preset at $104 \mu\text{l s}^{-1}$ to generate a mean tube shear rate, $\bar{G} = 2Q/\pi R_0^3$, of 314 s^{-1} .

3. Thromboxane B₂

Thromboxane B₂, TXB₂, was measured to a lower limit of 50 pg ml^{-1} in the plasma of selected experiments by radioimmunoassay, RIA, using ³H-TXB₂ (New England Nuclear, NEK700A, Lachine QC). Approximately $800 \mu\text{l}$

of unfixed effluent platelet suspension were collected into 1 ml plastic syringes and immediately filtered free of cells using 0.2 μm pore syringe filter units (Millex-GS, Millipore, Mississauga, ON). The filtered plasma was incubated for 20 min at 37°C and stored at -20°C until the RIA was performed.

4. Particle Concentration and Size

The number concentration and size of single platelets and aggregates were measured using an electronic particle counter (Coulter ZM, Coulter Electronics, Hialeah, FL) in conjunction with a logarithmic amplifier (Coulter Log Range Expander) and a 100 channel pulse height analyzer (Coulter Channelyzer C1000) to generate log-volume histograms over the volume range 1 - 10⁵ μm^3 . As described in detail in Chapter II, permanent tracings (Coulter XY4 Recorder) of each histogram were manually transposed into a microcomputer (HP 86, Hewlett Packard, Kirkland, QC) using a digitizer (HP 9111A). The distribution of background in the small volume range of the log-volume histograms was measured separately in PPP and then fitted by a decreasing exponential function using a weighted least squares regression. Using a trial and error iterative procedure, a normal curve was fitted to the distribution of single platelet log-volume over the range where the influence of background and microaggregate contamination are minimal. Background was subtracted from the measured log-volume histograms to give the same content in class 1 of the resultant histogram as that predicted by a normal distribution of single platelet log-volume. The number concentration per histogram class is $N(x_i)$, particle volume $v(x_i)$, and volume fraction $\Phi(x_i) = N(x_i)v(x_i)$, where x_i is the mark of the i^{th} class. Computer-integration of the log-volume

histograms yielded the number of particles counted, $n_{L,U}(\bar{t})$, the number concentration, $N_{L,U}(\bar{t})$, and the volume fraction, $\Phi_{L,U}(\bar{t})$, of particles between lower, L, and upper, U, volume limits at time \bar{t} .

Average log-volume histograms were generated from multiple donors at each mean transit time after the individual histograms were transformed into equivalent histograms using the average of the mean single platelet volume and standard deviation of all donors concerned. The mean, normalized volume fraction of the i^{th} class is given by $\bar{\Phi}(x_i) = [\bar{N}(x_i)v(x_i)]/[\bar{N}(x_m)v(x_m)]$, where $\bar{N}(x_i)$ is the mean normalized particle concentration per histogram class, and $\bar{N}(x_m)$ and $v(x_m)$ are the respective mean normalized number concentration and volume of the class of maximum concentration, m, at $\bar{t} = 0$ s. Details of the transformation and averaging are described in Appendix II. The ultimate effect of these procedures is to provide an estimate of the changes in particle volume in relation to the mean single platelet volume and standard deviation, as opposed to simply averaging changes in absolute volume.

5. Statistics

The mean, $\bar{\mu}$, mode, μ_{mod} , median, μ_{med} , and standard deviation, σ , of the linear volume distribution were calculated from the mean, \bar{x} , and standard deviation, s , of the log-volume distribution, assuming a normal distribution of the latter (Kenney and Keeping, 1951; Documenta Geigy, 1962). The assumption of log-normality of single platelet volume was tested using the Kolmogorov-Smirnov, K-S, one sample test (Young, 1977; Lilliefors, 1967). Skewing, g_1 , kurtosis, g_2 , of the log-volume histograms and their standard errors were determined using standard

equations for frequency distributions (Sokal and Rohlf, 1969). The significance of deviation of these sample statistics from the parametric value of zero was tested using two-tailed Student's t-tests. Two-tailed t-tests were also used to test the significance of correlation coefficients while unpaired, one-tailed t-tests were used to test the significance of differences between means.

6. Ionized Plasma Calcium

The $[Ca^{2+}]$ in plasma was measured using an ion selective electrode (ORION 93-20, Cambridge, MA) in conjunction with a single junction Ag/AgCl reference electrode (ORION 90-01). Separate standard curves were generated for each experiment over the range 10^{-5} to 10^{-2} M Ca^{2+} using highly purified $CaCl_2$ (Merck, Darmstadt, West Germany) in solutions the ionic strength of plasma (155 mM NaCl, 2.7 mM KCl, 1.0 mM $MgCl_2 \cdot 6H_2O$). On a logarithmic scale, the electrode response was linear above $80 \mu M Ca^{2+}$ and slightly curvilinear below this value. Calcium measurements in plasma were stable after 120 s equilibration at $23 \pm 1^\circ C$.

RESULTS

1. Citrate

(a) Constant C_1

Samples of citrated PRP from 10 male donors of mean age 30 ± 11 yr (\pm S.D.) and 9 female donors of mean age 32 ± 6 yr were sheared in the presence of $0.2 \mu M$ ADP at $\bar{G} = 314 s^{-1}$ for $\bar{t} = 43$ s. A good correlation was found between donor hematocrit and the normalized single platelet concentration, $N_{1,30}(\bar{t})/N_{1,30}(0)$ (Table 1). The plasma $[Ca^{2+}]$ correlated inversely with hematocrit, as did the normalized single platelet

TABLE 1

Correlation Coefficients, r, at Given Degrees of Freedom, df

Anticoagulant	df	HCT vs Singlets	HCT vs [Ca ²⁺]	[Ca ²⁺] vs Singlets
Citrate	17	0.68**	- 0.73*	- 0.76*
Heparin	20	- 0.05	0.25	0.10
Hirudin	10	- 0.13	0.46	- 0.45

* p < 0.001, ** p < 0.002

concentration with $[Ca^{2+}]$ (Fig. 1). The mean hematocrit ($p < 0.001$) and single platelet concentration ($p < 0.02$) of the male donors were also significantly higher than those of the female donors, while the mean $[Ca^{2+}]$ was significantly lower (Table 2, left; $p < 0.01$). Independent measurements of $[Ca^{2+}]$ for 33 male and 37 female donors gave a range of $[Ca^{2+}]$ from 34 to 51 μM and from 40 to 55 μM , respectively.

(b) Adjusted C_1

For the same male and female donors above, C_1 was adjusted according to Eq. [1] to give the same C_f in plasma as that of donors of 38 and 50% hematocrit, respectively, at $C_1 = 3.8\%$ (Table 2, right). After adjustment of the initial citrate concentration, the plasma $[Ca^{2+}]$ of the male donors was significantly higher than that of the female donors ($p < 0.001$), and the sex difference was reversed so that the platelets from the male donors aggregated significantly more than those from the female donors ($p < 0.002$). The $[Ca^{2+}]$ now correlated positively with HCT ($r = 0.64$, $p < 0.005$) while the single platelet concentration still correlated inversely with $[Ca^{2+}]$ ($r = -0.68$, $p < 0.002$) for all donors combined.

Figure 2 illustrates the effect of small but significant differences in the plasma $[Ca^{2+}]$ on aggregate growth. Before adjusting the plasma citrate concentration, the volume fraction of single platelets was lower and aggregate size larger at $\bar{t} = 43$ s for the female donors than the male donors. It is clear that reversing the plasma $[Ca^{2+}]$ produced volume fraction profiles similar to the profiles of the donors of the opposite sex prior to adjustment.

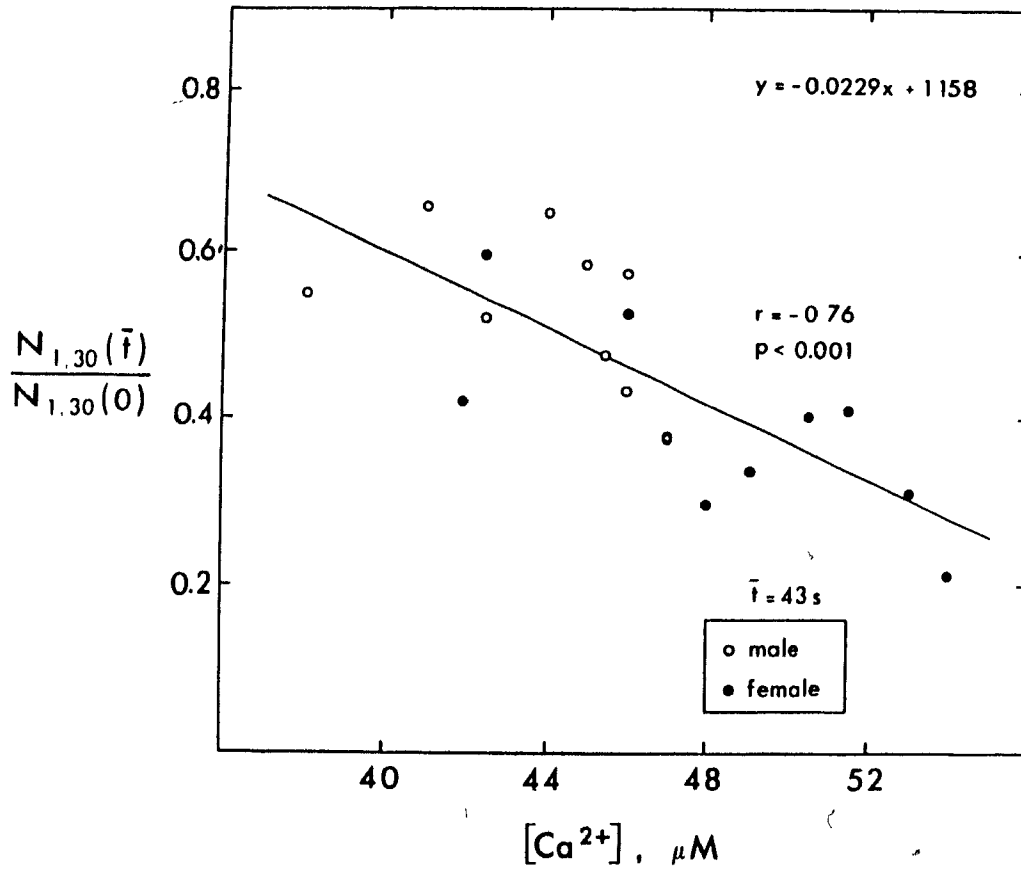


Figure 1: Aggregation vs. $[Ca^{2+}]$

Correlation of the normalized single platelet concentration, $N_{1,30}(\bar{t})/N_{1,30}(0)$, at $\bar{G} = 314 s^{-1}$ with the plasma $[Ca^{2+}]$ in cRRP.

TABLE 2

Normalized Single Platelet Concentration vs $[Ca^{2+}]$ in Citrated PRP (\pm S.D.)

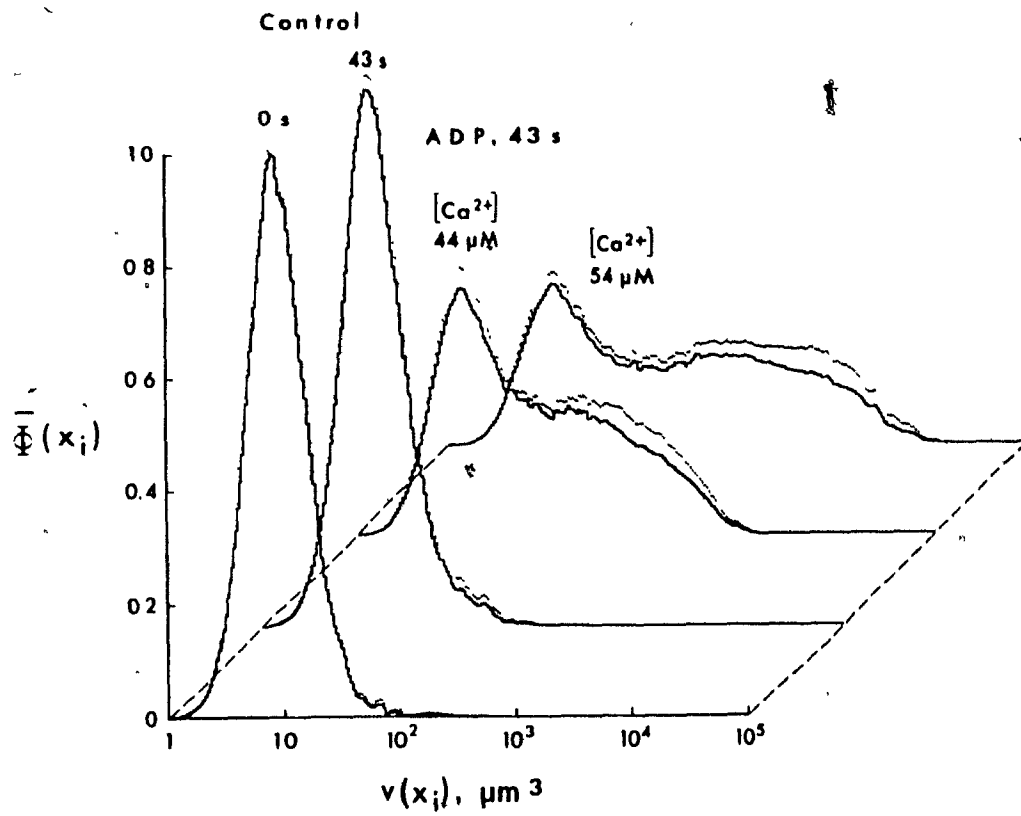
Sex	n	HCT %	NORMAL		ADJUSTED	
			$[Ca^{2+}]$ μM	$\frac{N_{1,30}(\bar{t})}{-N_{1,30}(0)}$	$[Ca^{2+}]$ μM	$\frac{N_{1,30}(\bar{t})}{N_{1,30}(0)}$
Male	10	46.2 \pm 2.3 p < 0.001	44.2 \pm 2.9 p < 0.01	0.519 \pm 0.103 p < 0.02	54.3 \pm 2.4 p < 0.001	0.347 \pm 0.080 p < 0.002
Female	9	40.4 \pm 3.6	48.5 \pm 4.3	0.389 \pm 0.118	40.0 \pm 3.2	0.513 \pm 0.125

Figure 2: Effect of $[Ca^{2+}]$ on Aggregate Growth

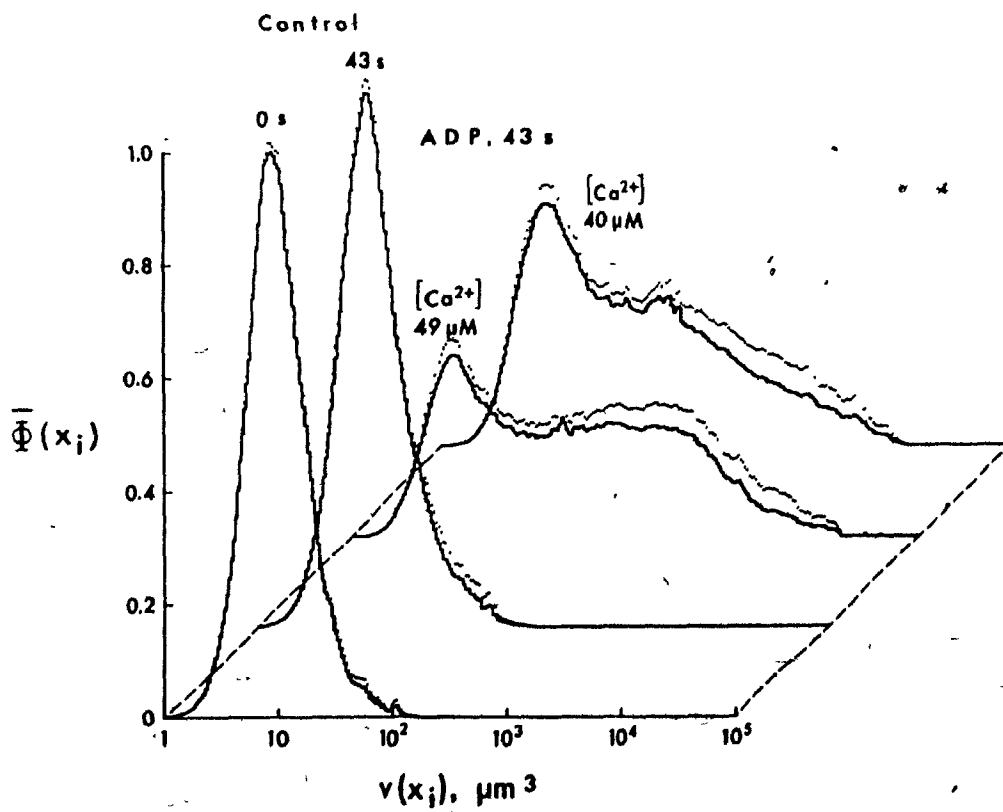
(a) The mean, normalized class volume fraction, $\bar{\Phi}(x_1)$, (\pm S.E.M.) versus particle volume, $v(x_1)$, for the male donors at $\bar{G} = 314 \text{ s}^{-1}$, $\bar{t} = 39.3 \text{ s}$ and $0.2 \text{ } \mu\text{M}$ ADP before ($[Ca^{2+}] = 44.2 \text{ } \mu\text{M}$) and after ($[Ca^{2+}] = 54.3 \text{ } \mu\text{M}$) lowering the plasma citrate concentration. Shown also is the control at $\bar{t} = 0 \text{ s}$ for the unadjusted plasma samples.

(b) Same as above for the female donors before ($[Ca^{2+}] = 48.5 \text{ } \mu\text{M}$) and after ($[Ca^{2+}] = 40.0 \text{ } \mu\text{M}$) raising the plasma citrate concentration.

(a) Male



(b) Female



2. Heparin

There was no significant sex difference in heparinized PRP, hep-PRP, although the mean hematocrit of the 10 male donors (30 ± 11 yr) was significantly higher than that of the 12 female donors (29 ± 6 yr; Table 3, $p < 0.001$). The rate and extent of aggregation in hep-PRP was much greater than that in cPRP with less than 26% of single cells remaining unaggregated after only $\bar{t} = 8.6$ s for both male and female donors. The mean $[Ca^{2+}]$ was more than an order of magnitude greater than that in cPRP, but was not significantly different between male (1.23 ± 0.08 mM) and female (1.22 ± 0.07 mM) donors. There was no relationship between hematocrit and single platelet concentration, hematocrit and $[Ca^{2+}]$, or $[Ca^{2+}]$ and the single platelet concentration (Table 1). In a larger independent study on $[Ca^{2+}]$ in hep-PRP involving 16 males and 17 females, respective mean $[Ca^{2+}]$ of 1.27 ± 0.03 and 1.27 ± 0.05 mM were obtained with a correlation coefficient between hematocrit and $[Ca^{2+}]$ of $r = 0.09$, for all donors combined.

In contrast to the time course of platelet aggregation in cPRP for the male and female donors of Chapter III there was almost no lag phase preceding aggregation in hep-PRP (Fig. 3). The rate of decrease of the single platelet concentration for the male and female donors combined increased from $6.1 \pm 0.8 \% s^{-1}$ (\pm S.E.M) during the first $\bar{t} = 2.1$ s to $11.6 \pm 0.7 \% s^{-1}$ between $\bar{t} = 2.1$ and 4.3 s. Although the rate of aggregation decreased with longer mean transit times to give the characteristic sigmoid aggregation curves found in cPRP, the collision efficiency increased to a maximum, $\alpha_0 = 0.242$, between $\bar{t} = 4.3$ and 8.6 s (Table 4).

TABLE 3

Normalized Single Platelet Concentration in Heparinized PRP (\pm S.D.)

Sex	n	HCT %	[Ca ²⁺] mM	$\frac{N_{1,30}^{(8.6)}}{N_{1,30}^{(0)}}$
Male	10	47.6 \pm 3.1 p < 0.001	1.23 \pm 0.08 n.s.	0.251 \pm 0.075 n.s.
Female	12	40.8 \pm 2.9	1.22 \pm 0.07	0.256 \pm 0.127

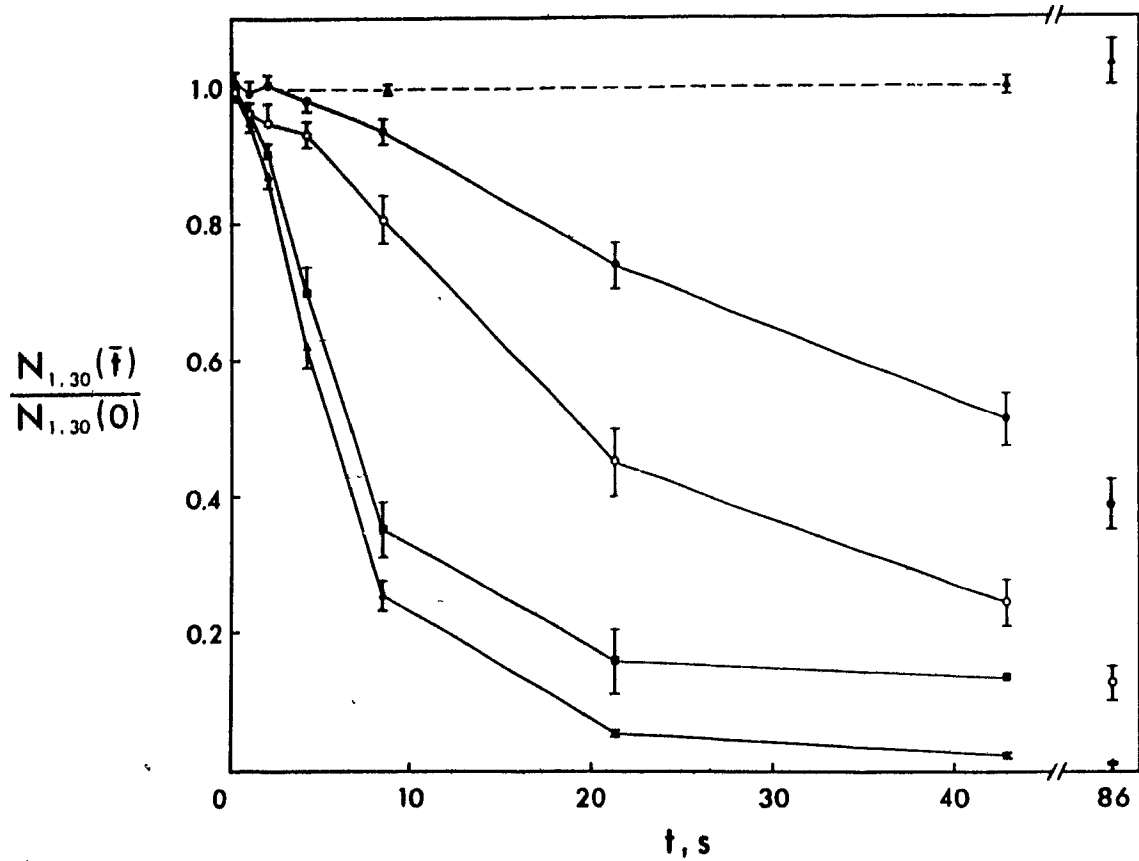


Figure 3: Effect of Anticoagulant on Platelet Aggregation

The normalized single platelet concentration, $N_{1,30}(\bar{t})/N_{1,30}(0)$, (\pm S.E.M) plotted against mean transit time at $\bar{G} = 314 \text{ s}^{-1}$ and $0.2 \mu\text{M}$ ADP: ● male donors, citrate; ○ female donors, citrate; ■ male plus female donors, hirudin; ▲ male plus female donors, heparin. In the controls modified Tyrodes was infused instead of ADP: ▲ broken line, heparin.

TABLE 4

Collision Efficiency, $\alpha_0 \times 10^3$ (\pm S.E.M.)

Anticoagulant	$\bar{t} = 0 - 4.3$ s	4.3 - 8.6 s	8.6 - 21 s
Heparin	116 \pm 10.2 (20) *	242 \pm 14.5 (22)	118 (2)
Hirudin	87.2 \pm 13.9 (12)	181 \pm 17.4 (12)	92.6 (2)

* no. of donors in parentheses

Aggregate growth in hep-PRP is shown in Figure 4. Accompanying the rapid reduction in the fraction of single cells is the growth of aggregates of progressively increasing size. By $\bar{t} = 21$ s, a significant proportion of aggregates had exceeded the largest particle volume measured ($10^5 \mu\text{m}^3$) while by $\bar{t} = 86$ s less than 1.2% of single platelets remained, and virtually all aggregates had volumes greater than $10^5 \mu\text{m}^3$. As found in cPRP the presence of a white blood cell peak (130 - 270 μm^3) at $\bar{t} = 86$ s indicates that these cells are not incorporated into platelet aggregates.

3. Hirudin

No sex difference was present in hirudinized PRP, hir-PRP, (Table 5), although the mean hematocrit of the 6 male donors (33 ± 13 yr) was significantly higher ($p < 0.02$) than that of the 6 female donors (34 ± 7 yr). The rate and extent of aggregation of hir-PRP was also much greater than that of cPRP but less than that of hep-PRP, with less than 36% of single platelets remaining unaggregated at $\bar{t} = 8.6$ s. No correlation was found between hematocrit and the single platelet concentration, hematocrit and $[\text{Ca}^{2+}]$, or $[\text{Ca}^{2+}]$ and the single platelet concentration (Table 1). The mean $[\text{Ca}^{2+}]$ in hir-PRP of the male (1.15 ± 0.04 mM) and the female (1.14 ± 0.07 mM) donors was less than that in hep-PRP but after correction for the greater dilution of plasma by the hirudin, the mean $[\text{Ca}^{2+}]$ for the male and female donors were 1.22 ± 0.04 and 1.21 ± 0.07 mM, respectively.

The sigmoid time course of platelet aggregation in hir-PRP was similar to that in hep-PRP, although the rates of aggregation were always

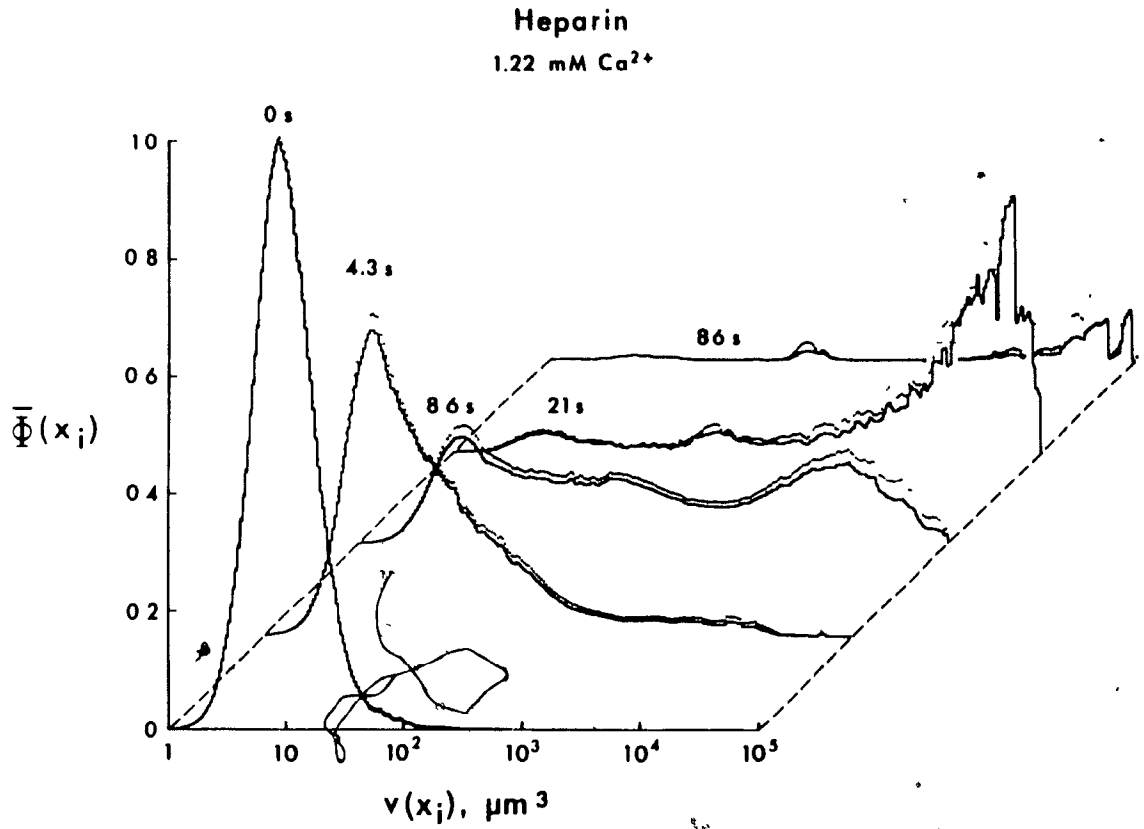


Figure 4: Aggregate Growth in Heparinized PRP

Three dimensional plot of the mean, normalized class volume fraction, $\bar{\Phi}(x_i)$, (\pm S.E.M.) versus particle volume, $v(x_i)$, for the male and female donors combined between $\bar{t} = 0$ and 86 s at $\bar{G} = 314 s^{-1}$ and 0.2 μM ADP in heparinized PRP.

TABLE 5

Normalized Single Platelet Concentration in Hirudinized PRP (\pm S.D.)

Sex	n	HCT %	[Ca ²⁺] mM	$\frac{N_{1,30}^{(8.6)}}{N_{1,30}^{(0)}}$
Male	6	46.1 \pm 2.1	1.15 \pm 0.04	0.359 \pm 0.112
		p < 0.02	n.s.	n.s.
Female	6	42.9 \pm 2.2	1.14 \pm 0.07	0.344 \pm 0.177

lower. The initial rate of aggregation ($\bar{t} < 2.1$ s) for the male and female donors combined was $4.5 \pm 0.7 \% s^{-1}$, and the maximum rate was $9.8 \pm 1.6 \% s^{-1}$ between $\bar{t} = 2.1$ and 4.3 s. The maximum collision efficiency, $\alpha_0 = .181$, was lower than that in hep-PRP, but also occurred between $\bar{t} = 4.3$ and 8.6 s. It is not clear from Figure 3 if the extent of aggregation in hir-PRP would reach that in hep-PRP; although, the extent of aggregation in cPRP from the female donors at $\bar{t} = 86$ s appears to have reached that in hir-PRP. Indeed, according to Figure 5, the volume fraction profile for cPRP from the female donors at $\bar{t} = 86$ s (Fig. 7; Chapter III, this thesis) is very similar to that for hir-PRP at $\bar{t} = 21$ s. The slightly lower rates of aggregation in hir-PRP than in hep-PRP are shown by both slightly higher single platelet volume fractions and smaller aggregate volume fractions at $\bar{t} < 8.6$ s. The difference is more pronounced at $\bar{t} = 21$ s where considerably more single platelets remained in hir-PRP. The prominent white blood cell peak at $\bar{t} = 21$ s but absent at earlier transit times in hir-PRP occurs because this histogram is the average of only two donors, one of which had a high white cell count in PRP.

The concentration of TXB_2 in the plasma of pre-shear and sheared samples exposed to $0.2 \mu M$ ADP were not significantly different for either sex or at any point between the sexes (Table 6). The concentration of TXB_2 was always well below those levels that result from the platelet release reaction.

4. Single Platelet Volume

Statistics of the platelet log-volume distributions in hep-PRP and

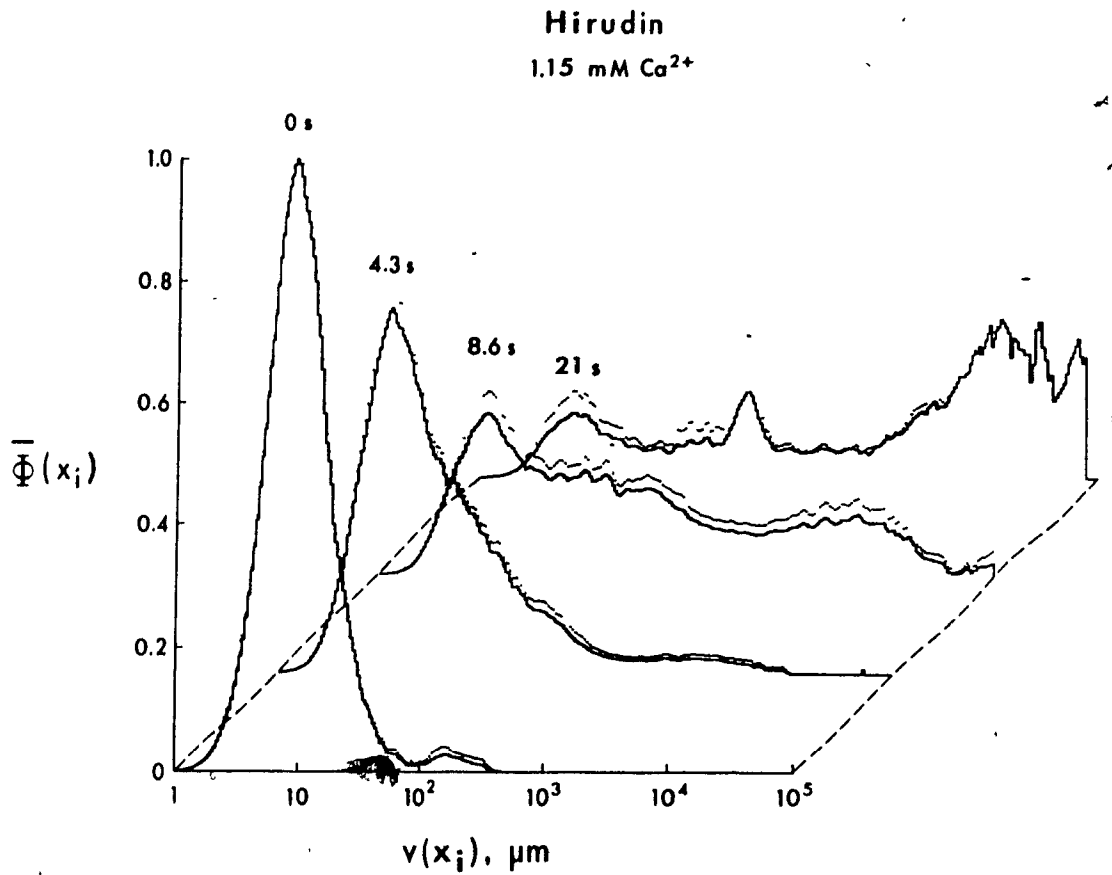


Figure 5: Aggregate Growth in Hirudinized PRP

Three dimensional plot of the mean, normalized class volume fraction, $\bar{\Phi}(x_i)$, (\pm S.E.M) versus particle volume, $v(x_i)$, for the male and female donors combined between $\bar{t} = 0$ and 21 s at $\bar{G} = 314 \text{ s}^{-1}$ and $0.2 \mu\text{M}$ ADP in hirudinized PRP.

TABLE 6

TXB₂ in Hirudinized PRP, ng ml⁻¹ (± S.D.)

Sex	PRP	PPP	PRP + 0.2 μM ADP	
			$\bar{x} = 0$ s	43 s
Male	-	0.78 (1)*	0.42 ± 0.31 (4)	0.47 ± 0.33 (4)
Female	0 (1)	0.74 (2)	0.68 ± 0.66 (3)	0.53 ± 0.63 (3)

* number of donors in parentheses

hir-PRP are provided in Table 7 for comparison with the data in cPRP in Table 2 of Chapter III of this thesis. The data for male and female donors were combined since, as with cPRP, there was no sex difference in platelet volume in either hep-PRP or hir-PRP. The mean, modal and median volumes of platelets in hep-PRP and hir-PRP were similar to those in cPRP. A substantial proportion of the distributions in hep-PRP were log-normal but almost all of those in hir-PRP were rejected by the K-S test. All distributions that were not log-normal showed significant positive skewing and leptokurtosis both of which were generally greater than that of the equivalent distributions in cPRP.

DISCUSSION

The strong inverse correlation previously found (Chapter III) between donor hematocrit and the degree of ADP-induced platelet aggregation in citrated platelet-rich plasma was verified for the present group of donors. In Chapter III a strong sex difference occurred after $\bar{t} = 43$ s exposure to $0.2 \mu\text{M}$ ADP at $G = 314 \text{ s}^{-1}$, where the normalized single platelet concentration of the female donors (0.240 ± 0.084 ; \pm S.D., $n = 6$) was significantly lower ($p < 0.001$) than that of the male donors (0.508 ± 0.095 , $n = 6$). In this chapter measurements of the single platelet concentration under the same conditions were similar to those previously found for both male and female donors but the difference was less pronounced.

It has been proposed (Kelton et al., 1980) that the source of the variable $[\text{Ca}^{2+}]$ in cPRP is a variable plasma citrate concentration caused by the HCT-dependent dilution of the citrate anticoagulant. The inverse

TABLE 7

Average Statistics of the Single Platelet Log-Volume Histograms

Statistic	Heparin		Hirudin	
	Log-Normal	Not Log-Normal	Log-Normal	Not Log-Normal
No. Donors	9	13	1	11
$\bar{\mu}$	8.0 ± 1.1	7.7 ± 1.0	7.5	7.8 ± 1.1
σ	5.0 ± 0.9	4.8 ± 0.8	4.9	5.0 ± 0.8
μ_{mod}	4.9 ± 0.6	4.7 ± 0.5	4.4	4.7 ± 0.7
μ_{med}	6.4 ± 0.8	6.5 ± 0.8	6.3	6.6 ± 0.9
g_1	0.038 ± 0.039	0.063 ± 0.091*	0.036	0.119 ± 0.063**
g_2	0.012 ± 0.091	0.231 ± 0.184**	0.060	0.205 ± 0.177**
$n_{L,U}(0)$	15514 ± 1136	14991 ± 763	15503	15424 ± 1047

Statistics of individual single platelet log-volume distributions calculated at $\bar{t} = 0$ s over the range 1 - 50 μm^3 were averaged (\pm S.D.) for the stated number of donors grouped according to anticoagulant. The distributions were further partitioned into those that were accepted as normal by the K-S one sample test and those that were rejected. Symbols are as described in the text and volumes are in μm^3 . Significantly different from zero: * $p < 0.002$, ** $p < 0.001$.

- 232 -

relationship between HCT and plasma $[Ca^{2+}]$ found in the present work and elsewhere (Sakarjassen, et al., 1984) supports this contention. Although $[Ca^{2+}]$ was not measured, Kelton et al. (1980) removed the sex difference by adjusting the volume of a fixed concentration of citrate according to HCT to give a constant dilution of plasma. However, these findings do not unequivocally demonstrate that variation in the $[Ca^{2+}]$ is the cause of the sex difference. Any other plasma factor responsible for the sex difference would also be subject to the same hematocrit-dependent dilution, and removal of the sex difference and the correlation of $[Ca^{2+}]$ with aggregation would be fortuitous. In this chapter, the citrate concentration was adjusted independent of the HCT dilution effect and the plasma $[Ca^{2+}]$ of males was thereby raised significantly above females. The sex difference was then reversed, and again aggregation correlated with $[Ca^{2+}]$.

The degree of aggregation correlated with $[Ca^{2+}]$ over the range of $[Ca^{2+}]$ normally found in cPRP, 34 - 55 μM , although the scatter of the individual measurements suggests that other factors may be involved. It would seem, however, that systematic differences in $[Ca^{2+}]$ within this narrow range are sufficient to generate a significant sex difference. The rate of ADP-induced aggregation is known to increase markedly with increasing $[Ca^{2+}]$ in the range 0 - 100 μM Ca^{2+} but to level off substantially thereafter (Gear, 1982). Indeed, in the present work a change in the plasma $[Ca^{2+}]$ of only 10 μM was found to reverse the shape of the aggregate volume fraction distributions between males and females (Fig. 2).

If citrate is responsible for the sex difference then anticoagulants that do not change the $[Ca^{2+}]$ in plasma should not produce a sex difference. Indeed, no sex difference was observed in the millimolar range of $[Ca^{2+}]$ in heparinized PRP, and aggregation did not correlate with HCT or $[Ca^{2+}]$. The rate of aggregation was so much higher than in cPRP that within one and a half minutes no single platelets remained and almost all aggregates were greater than $10^5 \mu m^3$. In fact, the rate of aggregation and size of aggregates were greater in hep-PRP at $0.2 \mu M$ ADP than in cPRP at $1.0 \mu M$ ADP (Chapter III, this thesis). It could be argued that the rate of aggregation in hep-PRP is so great that any sex difference is obliterated. The rate of aggregation in hirudinized PRP, however, was comparable to that in hep-PRP. The slight plasma dilution effect of the hirudin solution did not lower the $[Ca^{2+}]$ sufficiently to allow any detectable difference in the rate of aggregation between males and females. Again no correlations were found between aggregation and HCT, and aggregation and $[Ca^{2+}]$ in hir-PRP. The similarly high rate of aggregation in hir-PRP and hep-PRP challenges the generally-held notion that heparin directly activates platelets causing a greater rate of aggregation in hep-PRP than in cPRP. Similarity in the statistics of the distribution of single platelet volume in hep-PRP and cPRP, as well as, the lack of aggregation in the control runs in hep-PRP (Fig. 3) corroborate the contention that the platelets were not unduly activated by heparin. It would seem likely that the enhanced aggregation in hep-PRP and hir-PRP is due to the much higher $[Ca^{2+}]$.

The sigmoid decrease in the concentration of single platelets previously found in cPRP was still present in both hep-PRP and hir-PRP;

although, the lag phase preceding aggregation was much reduced and the maximum rates of aggregation much higher than in cPRP. It is interesting that the rate of aggregation was highest between 2.1 and 4.3 s in hep-PRP and hir-PRP but at the lower $[Ca^{2+}]$ in cPRP, not only was the maximum rate of aggregation lower, it occurred at later times. In Chapter III the sigmoid aggregation curves in cPRP were explained in terms of a time-dependent increase in the expression of stable platelet-platelet bonds. The mechanism believed to underly platelet aggregation is the cross-linking of bivalent fibrinogen molecules between activated glycoprotein IIb-IIIa (GP IIb-IIIa) complexes in the platelet membrane (Nurden, 1987). Ionized calcium is an essential cofactor for both fibrinogen binding (Marguerie et al., 1980) and maintenance of the GP IIb-IIIa heterodimer complex (Brass et al., 1985; Fitzgerald and Phillips, 1985). Furthermore, fibrinogen binding increases with $[Ca^{2+}]$ and requires at least one minute to reach saturation (Marguerie et al., 1980; Peerschke et al., 1980; Marguerie et al., 1982). Thus, the decrease in the lag phase at the physiological $[Ca^{2+}]$ in hep-PRP and hir-PRP (Fig. 3) may be due to a higher rate of fibrinogen binding. A difference of $\sim 10 \mu M Ca^{2+}$ between male and female donors in the low range of $[Ca^{2+}]$ in cPRP has a strong effect on both the lag phase and the maximum rate of aggregation. However, the continued increasing rate of aggregation in hep-PRP and hir-PRP reveals that the formation of stable bonds increases with time even at physiological $[Ca^{2+}]$. This is reflected by a corresponding increase in the two-body collision efficiency which reaches a maximum of 0.242 in hep-PRP between 4.3 and 8.6 s. This collision efficiency is approximately an order of magnitude greater than in cPRP over the same time interval. The collision efficiency in cPRP continues to increase with time, whereas,

in hep-PRP and hir-PRP it decreases. This may reflect a more rapid expression of stable platelet-platelet bonds at physiological $[Ca^{2+}]$, through either an increase in the number or affinity of fibrinogen binding sites. In Chapter III, the induction of aggregation at $\bar{G} = 1800 \text{ s}^{-1}$ after an $\sim 11 \text{ s}$ delay indicated the time-dependent emergence of a high shear rate resistant platelet-platelet bond. It would be of interest to examine this effect in hep-PRP and hir-PRP.

Platelet granule release does not contribute to the sex difference or the higher rates of aggregation in hep-PRP and hir-PRP. The conditions of the experiments were such that release was prevented. Temperatures less than 27°C are known to inhibit ADP-induced release (Valdorf-Hansen and Zucker, 1971; Chapter III, this thesis), and the concentration of ADP was well below the threshold required to elicit release at 37°C , although the platelets are more sensitive to ADP at room temperature. Furthermore, release that occurs at 37°C in cPRP is inhibited at the physiological $[Ca^{2+}]$ in hep-PRP and hir-PRP (Mustard et al., 1975). The shear stress was also well below the threshold required to activate the cells directly or induce release (Brown et al., 1975; Belval et al., 1984; Hellums and Hardwick, 1981). Concentrations of TXB_2 in hir-PRP were not significantly different from those in cPRP (Chapter III, this thesis) and showed no changes from pre-shear levels. No significant differences between male and female donors were found.

The sex difference in the ADP-induced aggregation of human platelets in cPRP is real but artifactual. Differences in the ionized calcium concentration that normally occur in cPRP are sufficient to affect

the degree of aggregation. Since mean hematocrits are usually significantly different between groups of male and females, and since $[Ca^{2+}]$ is controlled by the plasma citrate concentration, which in turn is determined by hematocrit, a significant sex difference exists in cPRP. In ungrouped data, sex differences are inconsequential; however, the citrate effect must be taken into account when attributing a sex link to platelet agonists, antagonists or cofactors in cPRP. This is particularly true when trying to correlate platelet aggregability with a propensity for thromboembolic disease. Evidence for an additional sex factor is given by the finding that aspirin is effective in reducing post-operative deep vein thrombosis (Harris et al., 1977) and transient cerebral ischemic attacks and strokes (Canadian Cooperative Study Group, 1978) in men but not in women. Such differences occur in vivo, however, and are independent of the hematocrit-dependent anticoagulant artifact.

It must also be remembered that due to the prevalence of citrate as an anticoagulant, many platelet studies are conducted under conditions of depressed $[Ca^{2+}]$ that consistently impede the optimum rate of aggregation. The enhanced rate of aggregation, in hep- and hir-PRP serves as a strong reminder that platelet behavior at physiological $[Ca^{2+}]$ can be substantially different. It is well established that physiological $[Ca^{2+}]$ actually inhibits the ADP-induced platelet release reaction (Mustard et al., 1975). The pivotal role of $[Ca^{2+}]$ in aggregation, adhesion and release cannot be underestimated and it must be constantly borne in mind that much of our present knowledge of platelet behavior was obtained under conditions of depressed calcium.

REFERENCES

- BELL, D.N., AND GOLDSMITH, H.L. (1984). Platelet aggregation in Poiseuille flow: II. Effect of shear rate. Microvasc. Res. **27**, 216-330.
- BELVAL, T., HELLUMS, J.D., AND SOLIS, T. (1984). The kinetics of platelet aggregation induced by shear. Microvasc. Res. **28**, 279-288.
- BRASS, L.F., SHATTIL, S.J., KUNICKI, T.J., AND BENNETT, J.S. (1985). Effect of calcium on the stability of the platelet membrane glycoprotein IIb-IIIa complex. J. Biol. Chem. **260**, 7875-7881.
- BROWN, C.H., LEVERETT, L.B., LEWIS, C.W., ALFREY, C.P., AND HELLUMS, J.D. (1975). Morphological, biochemical, and functional changes in human blood platelets subjected to shear stress. J. Lab. Clin. Med. **86**, 462-471.
- THE CANADIAN COOPERATIVE STUDY GROUP (1978). A randomized trial of aspirin and sulfapyrazone in threatened stroke. N. Eng. J. Med. **299**, 53-59.
- COPPE, D., WESSINGER, S.J., RANSIL, B.J., HARRIS, W., AND SALZMAN, E. (1981). Sex differences in the platelet response to aspirin. Thromb. Res. **23**, 1-21.
- DOCUMENTA GEIGY (1962). "Scientific Tables" (K. Diem, ed.), p.164. Geigy Pharmaceuticals, Montreal, QC.
- FITZGERALD, L.A., AND PHILLIPS, D.R. (1985). Calcium regulation of the platelet membrane glycoprotein IIb-IIIa complex. J. Biol. Chem. **260**, 11366-11374.
- GEAR, A.R.L. (1982). Rapid reactions of platelets studied by a quenched flow approach: Aggregation kinetics. J. Lab. Clin. Med. **100**, 866-886.
- HARRIS, W.H., SALZMAN, E.W., ATHANASOULIS, C.A., WALTMAN, A.C., and DESANTIS, R.W. (1977). Aspirin prophylaxis of venous thromboembolism after total hip replacement. N. Eng. J. Med. **297**, 1246-1249.

- HELLUMS, J.D., AND HARDWICK, R.A. (1981). Response of platelets to shear stress - a review. In "The Rheology of Blood, Blood Vessels and Associated Tissues" (D.R. Gross and N.H.C. Hwang, eds.), pp. 160-183, Sijthoff and Noordhoff, Rockville, Maryland.
- JOHNSON, M., RAMEY, E., RAMWELL, P.W. (1975). Sex and age differences in human platelet aggregation. Nature 253, 355-357.
- KELTON, J.G., POWERS, P., JULIAN, J., BOLAND, V., CARTER, C.J., GENT, M. ADD HIRSH, J. (1980). Sex-related differences in platelet aggregation: influence of hematocrit. Blood 56, 38-41.
- KENNEY, J.K., AND KEEPING, E.S. (1951). "Mathematics of Statistics" (Part Two). D. Van Nostrand, Toronto, ON.
- LILLIEFORS, H.W. (1967). On the Kolmogorov-Smirnov test for normality with mean and variance unknown. Am. Statist. Assoc. J. 62, 399.
- MARGUERIE, G.A., EDGINGTON, T.S., AND PLOW, E.F. (1980). Interaction of fibrinogen with its receptor as a part of a multistep reaction in ADP-induced platelet aggregation. J. Biol. Chem. 255, 154-161.
- MARGUERIE, G.A., THOMAS-MAISON, N., LARRIEU, M.-J., AND PLOW, E.F. (1982). The interaction of fibrinogen with platelets in a plasma milieu. Blood 59, 91-95.
- MONCADA, S., AND VANE, J.R. (1979). Arachidonic acid metabolites and the interactions between platelets and blood-vessel walls. N. Engl. J. Med. 300, 1142-1147.
- MUSTARD, J.F., PERRY, D.W., KINLOUGH-RATHBONE, R.L., AND PACKHAM, M.A. (1975). Factors responsible for ADP-induced release reaction of human platelets. Am. J. Physiol. 228, 1757-1765.
- NURDEN, A.T. (1987). Platelet membrane glycoproteins and their clinical aspects. In "Thrombosis and Haemostasis" (M. Verstraete, J. Vermeylen, R. Lijnen, and J. Arnout, eds.), pp. 93-125, Leuven Univ. Press, Leuven, Belgium.

- PEERSCHKE, E.I., ZUCKER, M.B., GRANT, R.A., EGAN, J.J., AND JOHNSON, M.M. (1980). Correlation between fibrinogen binding to human platelets and platelet aggregability. Blood 55, 841-847.
- READING, H.W., AND RÖSIE, R. (1980). Age and sex differences related to platelet aggregation. Biochem. Soc. Trans. 8, 180-181.
- ROTH, G.J., AND MAJERUS, P.W. (1975). The mechanism of the effect of aspirin on human platelets. J. Clin. Invest. 56, 624-632.
- SAKARIASSEN, K.S., OTTENHOF-ROVERS, M. AND SIXMA, J.J. (1984). Factor VIII-von Willebrand factor requires calcium for facilitation of platelet adherence. Blood 63, 996-1003.
- SOKAL, R.R., AND ROHLF, F.J. (1969). "Biometry". Freeman, San Francisco, CA.
- YOUNG, I.T. (1977). Proof without prejudice: Use of the Kolmogorov-Smirnov test for the analysis of histograms from flow systems and other sources. J. Histochem. Cytochem. 25, 935-941.
- VALDORF-HANSEN, J.F., AND ZUCKER, M.B. (1971). Effect of temperature and inhibitors on serotonin-¹⁴C release from human platelets. Am. J. Physiol. 220, 105-111.
- WEISS, H. J., AND ALEDORT, L.M. (1967). Impaired platelet/connective tissue reaction in man aspirin ingestion. Lancet 2, 495.
- ZUCKER, M.B., AND PETERSON, J. (1968). Inhibition of adenosine diphosphate-induced secondary platelet aggregation and other platelet functions by acetylsalicylic acid ingestion. Proc. Soc. Exp. Biol. Med. 127, 547.

CHAPTER V

WHOLE BLOOD

ABSTRACT

The effect of shear rate on ADP-induced platelet aggregation in whole blood, WB, flowing through polyethylene tubing was studied using a previously described technique for measuring the concentration and size of single platelets and aggregates in platelet-rich plasma, PRP (Chapter II, this thesis). Effluent WB was collected into 0.5% glutaraldehyde and the red cells, rbc, removed by centrifugation through Percoll. The rate of single platelet aggregation was up to 9x greater in WB than in PRP (Chapter III, this thesis) at mean tube shear rates, \bar{G} , = 39.3, 314, and 1800 s^{-1} , and at both 0.2 and 1.0 μM ADP. At 0.2 μM ADP, the rate of aggregation was greatest at $\bar{G} = 39.3 s^{-1}$ over the first 1.7 s mean transit time through the flow tube, \bar{t} , but at this shear rate the rate of aggregation decreased steadily with increasing \bar{t} . At $\bar{G} > 314 s^{-1}$ the rate of aggregation increased between $\bar{t} = 1.7$ and 8.6 s; however, aggregate size decreased with increasing \bar{G} . At 1.0 μM ADP, the initial rate of single platelet aggregation was still highest at $\bar{G} = 39.3 s^{-1}$ and large aggregates up to several millimeters in diameter and containing rbc formed within $\bar{t} = 43$ s. At $\bar{G} > 314 s^{-1}$, aggregate size was still limited at 1.0 μM ADP but the rate of single platelet aggregation was markedly increased. By $\bar{t} = 43$ s, no single platelets remained and rbc were not incorporated into aggregates. Aggregate size increased slowly and large aggregates eventually formed. White blood cells were not significantly incorporated into aggregates at any shear rate or ADP concentration. Since the present technique did not induce platelet TXA_2 formation or cause cell lysis, these experiments provide strong evidence for a purely mechanical effect of rbc in augmenting platelet aggregation in WB.

INTRODUCTION

It is commonly observed that red blood cells, rbc, are not incorporated into platelet aggregates at the high shear rates found in the arterial side of the vasculature (Begent and Born, 1970; Arfors et al., 1976). But this does not mean that rbc do not influence the process of platelet aggregation under such conditions. Ever since the discovery that the adhesion/aggregation (retention) of platelets in glass bead columns was enhanced by rbc in proportion to the hematocrit (Hellem, 1960), a mechanism has been sought to explain the role of rbc in platelet aggregation. The identification of ADP as the active agent in red cells that stimulates platelet aggregation (Gaarder et al., 1961) and the observation that it increases the platelet retention of platelet-rich plasma, PRP, in glass bead columns (Hellem et al., 1963; McPherson et al., 1974) led to the proposal that ADP liberated from damaged rbc is responsible for the enhanced platelet aggregation in whole blood, WB. This hypothesis helps to explain the shortening of the bleeding time in anemic and thrombocytopenic patients after blood transfusion that persists when platelet counts have fallen to pre-transfusion levels (Duke, 1910; Hellem et al., 1961; Livio et al., 1982). There are numerous examples in vitro of the inhibition of spontaneous platelet aggregation (Harrison and Mitchell, 1966; Fox et al., 1982; Saniabadi et al., 1984), the reduction in shear-induced platelet aggregation (Jen and McIntire, 1984) and platelet retention in glass bead columns (McPherson, et al., 1974), and in vivo of the lengthening of the bleeding time (Zawilska et al., 1982) by the addition of enzymes that degrade ADP. Red cells also promote the aggregation of platelets activated by exogenous ADP through the uptake of the platelet inhibitor, adenosine (Born and Cross, 1963; Skoza et al.,

1967), which is formed after successive dephosphorylation of adenine nucleotides by enzymes located on the external surface of rbc (Parker, 1970; DePierre and Karnosky, 1974; Bartlett, 1977). Thus, it is observed that adenosine is a more potent inhibitor of ADP-induced platelet aggregation in PRP than in WB (Gresele et al., 1986) and that dipyridamole, at concentrations which do not directly inhibit platelets but which block adenosine uptake by rbc (Harker and Kadatz, 1983), inhibits ADP-induced aggregation in WB but not in PRP (Gresele et al., 1983; Gresele et al., 1986). Dipyridamole also inhibits experimental thrombus formation in animals (Emmons et al., 1965; Didisheim, 1968; Mayer and Hammond, 1973) and reduces thromboembolic complications associated with prosthetic cardiac valves in man (Kincaid-Smith, 1969; Harker and Schlichter, 1970; Sullivan et al., 1971).

These results strongly support a role for ADP in platelet aggregation in vivo but since platelets also contain ADP (Holmsen et al., 1969) and release it (Mills et al., 1968) in response to a variety of chemical and mechanical stimuli, the source of ADP in vivo remains unclear. McPherson et al. (1974) found that the total concentration of ADP and ATP in plasma after passage of whole blood through a glass bead column of $\sim 0.2 \mu\text{M}$ at a ratio ATP:ADP of 1.6:1 was inconsistent with the 10:1 ratio in rbc (Bishop, 1961) but more consistent with that in platelets (Holmsen et al., 1969). However, the correlation between platelet retention and ADP concentration was poor. Aspirin which blocks the prostaglandin-mediated release of platelet ADP, potentiates the inhibitory action of dipyridamole in WB (Gresele et al., 1985), and prostacyclin which stimulates platelet adenylate cyclase and inhibits

platelet aggregation and release is more effective at inhibiting ADP-induced aggregation in WB than in PRP (Riess et al., 1986).

It must be remembered, however, that aggregation and adhesion normally occur in flowing blood. Shear rate is the most important physical parameter governing platelet aggregation in flowing suspensions. It determines the platelet collision frequency, the shear and normal stresses which activate single cells and break up aggregates, and the interaction time of cell-cell or cell-surface collisions. Since shear rate is proportional to fluid velocity, these factors either promote or inhibit hemostatic or thrombotic mechanisms, depending on flow rate and vessel size. Time-averaged systemic arterial wall shear rate in humans ranges from 100 - 1000 s^{-1} and may exceed 1000 s^{-1} in the capillaries, based on a parabolic velocity profile for WB (Whitmore, 1968; Chien, 1975; Turitto 1982). A higher rate of wall shear would be expected for a blunted velocity profile (Goldsmith, 1972), but it is unlikely that shear rate exceeds 2000 s^{-1} in the normal human vasculature (Turitto and Baumgartner, 1982). It has been shown in vitro that shear rates less than 2000 s^{-1} are insufficient to activate platelets directly and induce aggregation (Chang and Robertson, 1976; Gear, 1982; Yung and Frojmovic, 1982; Bell and Goldsmith, 1984; Belval et al., 1984; Belval and Hellums, 1986). However, the higher shear rates commonly found in extracorporeal flow devices and vascular prostheses can induce platelet aggregation, release and lysis depending on the magnitude of the fluid shear stress and the time of exposure to the shear field (Brown et al., 1975; Colantuoni et al., 1977; Dewitz et al., 1978; Belval et al., 1984; Jen and McIntire, 1984).

Red cells also influence the motions and distribution of platelets in flowing blood. Continual shear-induced collisions between rbc lead to a marked lateral dispersion of platelets (Goldsmith, 1971) resulting in platelet diffusion coefficients 2 - 3 orders of magnitude greater than in PRP (Turitto et al., 1972). Higher platelet collision frequencies due to the enhanced platelet diffusion could be responsible for the greater platelet aggregation in WB. Platelet aggregation could be further augmented by higher platelet concentrations at the periphery of blood vessels than in the interior, as measured by Tangelder et al. (1985) in 25 μ m diameter arterioles. Support for a physical role of rbc in enhancing platelet aggregation is provided by the ability of rbc ghosts depleted of ADP to increase platelet retention in glass bead columns (Stormorken, 1971; Zucker et al., 1972), and of washed rbc in the presence of apyrase to increase platelet adhesion to collagen-coated glass tubes in proportion to the hematocrit (Karino and Goldsmith, 1979). Hardened ADP-depleted rbc have also been shown to enhance shear-induced platelet aggregation over that in PRP, but only to a level of ~ 50% of that by native rbc (Reimers et al., 1984).

While both chemical and mechanical augmentation of platelet aggregation are likely to operate in vivo, the relative contribution of each under normal physiological and pathologically altered flow conditions remains obscure. The present work shows that much of the enhanced aggregation of activated platelets in WB at physiological shear rates can be accounted for by the purely mechanical effects of red cell motion leading to higher collision frequencies between platelets. Since most prior work on platelet aggregation in WB has been qualitative and done in

WB aggregometers or through electronic counting of single platelets, little information has been provided on the size distribution and growth rate of aggregates in WB. This issue is specifically addressed in the following work through a systematic study of the effect of shear rate on aggregate growth at shear rates generally considered physiologically significant.

MATERIALS AND METHODS

1. Whole Blood and Reagents

Experiments were performed as described in Chapter II. Venous blood was slowly drawn from healthy volunteers via a 19 gauge needle and winged infusion set into a 60 ml plastic syringe containing 1/10 volume sodium citrate. The initial concentration of citrate, C_i , was adjusted for both male and female donors as described in Chapter IV to give the same final concentration in plasma, C_f , as that of a donor of 43% hematocrit, HCT, and $C_i = 3.8\%$, according to:

$$C_i = C_f \times [9(1 - \text{HCT}) + 1]. \quad [1]$$

Hematocrit was predetermined on undiluted venous blood drawn using the same technique. All donors had refrained from aspirin ingestion for at least 10 days prior to blood withdrawal and no female donors were taking oral contraceptives. The syringe was tightly capped and the blood was left to stand at room temperature for one hour to allow equilibration to room temperature, and to simulate the handling time for normal PRP preparation (Chapter III, this thesis).

Frozen aliquots of 2 mM adenosine-5'-diphosphate, ADP, (Sigma, St. Louis, MO) in modified Tyrodes solution (137 mM NaCl, 2.7 mM KCl, 11.9 mM NaHCO_3 , 0.36 mM $\text{NaH}_2\text{PO}_4 \cdot \text{H}_2\text{O}$) were thawed immediately prior to use. Electron microscope grade glutaraldehyde (J.B. EM Services, Pointe Claire-Dorval, QC) was diluted to 0.5% (v/v) in Isoton II (Coulter Electronics, Hialeah, FL). One per cent (v/v) silicone (Siliclad, Clay Adams, Parsippany, NJ) was used to siliconize the mixing chamber prior to experiments.

2. Flow System

All experiments were done at $23 \pm 1^\circ\text{C}$. Whole blood was infused into a small cylindrical mixing chamber (6 mm i.d., 9.5 mm o.d., 1.5 mm height) using a syringe pump. ADP was simultaneously infused into the mixing chamber via an independent syringe pump at a fixed flow ratio, WB:ADP = 9:1. After rapid mixing, the WB-ADP suspension exited the chamber through lengths of 0.595 or 0.38 mm radius, R_0 , polyethylene tubing, corresponding to preset mean cell transit times, $\bar{t} = X_3/\bar{U}$, from < 1.0 to 43 s where, X_3 is the distance down the flow tube and \bar{U} is the mean linear fluid velocity. The aggregation reaction was instantaneously and permanently arrested by collecting known volumes of the effluent into $20\times$ the suspension volume of 0.5% isotonic glutaraldehyde. Total volumetric flow rates, Q , were preset from 13 to $155 \mu\text{l s}^{-1}$ to generate mean tube shear rates, $\bar{G} = 2Q/\pi R_0^3$, between 39.3 and 1800 s^{-1} assuming Poiseuille flow¹.

3. ADP Concentration

Stock ADP was prepared at an initial concentration, ADP_i , to give a constant final concentration in plasma, ADP_f , independent of both donor

¹ Blunting of the velocity distribution will result in higher wall shear rates than in Poiseuille flow at the same Q . For HCT $> 20\%$, and cell-to-tube diameter ratios of ~ 0.06 , the degree of blunting in ghost cell suspensions increased with increasing HCT and cell-to-tube diameter ratio, and decreased with increasing Q (Goldsmith and Marlow, 1979). Extrapolating from this data, significant blunting is not expected at the present flow rates, even at $Q = 13 \mu\text{l s}^{-1}$, due to the low cell-to-tube diameter ratio (0.007) and the high mean velocity (> 9.8 tube diameters s^{-1}). The contribution of rouleaux formation to blunting is not likely to be significant in the present range of shear rate.

hematocrit and the 10x dilution of ADP in whole blood in the mixing chamber. Final ADP concentrations of 0.2 and 1.0 μM were used to calculate ADP_1 , according to:

$$\text{ADP}_1 = \text{ADP}_f \times [8.1(1 - \text{HCT}) + 1.9] \quad [2]$$

4. Thromboxane B₂

Thromboxane B₂, TXB₂, was measured to a lower limit of 50 pg ml^{-1} in the plasma of selected experiments by radioimmunoassay, RIA, using ³H-TXB₂ (New England Nuclear, NEK700A, Lachine QC). Unfixed effluent WB was collected into 1.5 ml polypropylene microfuge tubes and immediately centrifuged at $\sim 10,000g$ for 30 s. Approximately 0.75 ml of supernatant plasma were quickly filtered free of any cells inadvertently introduced during plasma extraction using 0.2 μm pore syringe filter units (Millex-GS, Millipore, Mississauga, ON). The filtered plasma was incubated for 20 min at 37°C and then stored at -20°C until the RIA was performed.

5. Separation of Single Platelets and Aggregates from Red Cells

Approximately 5 ml of effluent WB fixed in glutaraldehyde were carefully layered onto 40 ml of isotonic Percoll solution (1.097 g ml^{-1} , Pharmacia, Dorval, QC) in a 50 ml polycarbonate tube and centrifuged in a horizontal swingout rotor at 4000g for 20 min. The rbc formed a tight pellet at the bottom of the tube while single platelets and aggregates formed a thin layer at the glutaraldehyde-Percoll interface. The latter were carefully removed using a wide-mouthed polyethylene Pasteur pipette and resuspended in ~ 8.0 ml Percoll.

6. Particle Concentration and Size

The number concentration and size of single platelets and aggregates were measured using an electronic particle counter (Coulter ZM) in conjunction with a logarithmic amplifier (Coulter Log Range Expander) and a 100 channel pulse height analyzer (Coulter Channelizer C1000) to generate log-volume histograms over the volume range $1 - 10^5 \mu\text{m}^3$. As described in detail in Chapter II, permanent tracings (Coulter XY4 Recorder) of each histogram were manually transposed into a microcomputer (HP 86, Hewlett Packard, Kirkland, QC) using a digitizer (HP 9111A). The distribution of background in the small volume range of the log-volume histograms was measured separately in platelet-poor plasma, PPP, and then fitted by a decreasing exponential function using a weighted least squares regression. Using a trial and error iterative procedure, a normal curve was fitted to the distribution of single platelet log-volume over the range where the influence of background and microaggregate contamination are minimal. Background was subtracted from the measured log-volume histograms to give the same content in class 1 of the resultant histogram as that predicted by a normal distribution of single platelet log-volume. The number concentration per histogram class is $N(x_1)$, particle volume $v(x_1)$, and volume fraction $\Phi(x_1) = N(x_1)v(x_1)$, where x_1 is the mark of the i^{th} class. Computer-integration of the log-volume histograms yielded the number of particles counted, $n_{L,U}(\bar{t})$, the number concentration, $N_{L,U}(\bar{t})$, and the volume fraction, $\Phi_{L,U}(\bar{t})$, of particles between lower, L, and upper, U, volume limits at time \bar{t} .

Average log-volume histograms were generated from multiple donors at each mean transit time after the individual histograms were transformed

into equivalent histograms using the average of the mean single platelet volume and standard deviation of all donors concerned. The mean, normalized volume fraction of the i^{th} class is given by $\bar{\Phi}(x_i) = [\bar{N}(x_i)v(x_i)]/[\bar{N}(x_m)v(x_m)]$, where $\bar{N}(x_i)$ is the mean normalized particle concentration, and $\bar{N}(x_m)$ and $v(x_m)$ are the respective mean normalized particle concentration and volume of the class of maximum concentration, m , at $\bar{t} = 0$ s. Details of the transformation and averaging are described in Appendix II. The ultimate effect of these procedures is to provide an estimate of the changes in particle volume in relation to the mean single platelet volume and standard deviation, as opposed to simply averaging changes in absolute volume.

7. Statistics

The mean, $\bar{\mu}$, mode, μ_{mod} , median, μ_{med} , and standard deviation, σ , of the linear volume distribution were calculated from the mean and standard deviation of the log-volume distribution, assuming a normal distribution of the latter (Kenney and Keeping, 1951; Documenta Geigy, 1962). The ~~assumption~~ of log-normality of single platelet volume was tested using the Kolmogorov-Smirnov, K-S, one sample test (Young, 1977; Lilliefors, 1967). Skewing, g_1 , and kurtosis, g_2 , of the log-volume histograms and their standard errors were determined using standard equations for frequency distributions (Sokal and Rohlf, 1969). The significance of deviation of these sample statistics from the parametric value of zero was tested using two-tailed, Student's t-tests. Unpaired, one-tailed t-tests were used to test the significance of differences between means.

EXPERIMENTAL ERROR

1. Platelet Extraction Efficiency

Counting platelets and aggregates in a suspension containing rbc by using upper and lower size discriminators on the particle counting equipment was not possible with the present instrument configuration. Due to the far greater number of rbc in the volume range of the aggregates under consideration in the present study, a method of first removing the rbc from the WB suspension was required.

The density of hardened rbc was independently determined in this laboratory to be 1.155 g ml^{-1} , and that of hardened platelets 1.04 g ml^{-1} . The density of the Percoll suspension was constant at 1.097 g ml^{-1} , and provided a good separation of platelets and rbc. When a platelet suspension was carefully layered over the Percoll and then centrifuged, a thin turbid layer of platelets was present at the interface between the yellowish, translucent fixed plasma and the Percoll. The interface was easily identified by the difference in refractive index of the plasma and the Percoll. The extraction of platelets and aggregates adjacent to the interface was facilitated by the reduction in the suspension turbidity as particles were removed from this region. At the bottom of the tube, the rbc formed a tight pellet with a sharp interface which was separated from the plasma/Percoll interface by a clear region of Percoll indistinguishable from the original Percoll suspension.

The efficiency of the extraction of single platelets and aggregates from the glutaraldehyde-fixed whole blood suspensions was evaluated by layering suspensions of PRP, platelet aggregates and WB onto

Percoll and comparing the particle counts (Table 1). Unless stated otherwise all PRP was collected into citrate anticoagulant as described in Chapter III. When a 3.0 ml sample of glutaraldehyde-fixed PRP was layered onto 40 ml of Percoll and then centrifuged at 4000g, all the platelets were recovered in the top 7.0 ml, with greater than 83% of the cells located in the thin layer at the plasma/Percoll interface. In order to recover all the cells, it was necessary to withdraw at least 6.0 ml total volume from this region alone. As will be seen in the subsequent particle log-volume histograms, large numbers of white blood cells, wbc, were also extracted with the platelets due to the similarity in the densities of these two cell types. The number of wbc, however, was not large enough to interfere with the identification and quantitation of aggregates of similar volume. No platelets, wbc or rbc were found between the interface and the rbc pellet at the bottom of the centrifuge tube. In addition, because most of the plasma remained at the top of the tube and was not extracted with the platelets at the interface, the background in the log-volume distributions produced by the fixed plasma proteins was much reduced compared to that in fixed, neat PRP.

A suspension of single platelets and aggregates was prepared by mixing PRP and ADP in an aggregometer cuvette until the aggregates were visible to the naked eye, at which point they were fixed in glutaraldehyde. Again, after centrifuging this suspension through Percoll, all particles were recovered in the top 7.0 ml, more than 88% of which were at the interface.

Although no measure of the single platelet concentration in WB was

TABLE 1

Extraction of Single Platelets and Aggregates from PRP and WB

Suspension	Particle Concentration, μl^{-1}			
	Initial [*]	Top 1.0 ml	Interface 6.0 ml	Total 7.0 ml
PRP	173,144	29,305	143,535	172,840
aggregates	40,189	4,550	34,887	39,437
WB	-	13,748	297,435	311,183
WB, 2x ^{**}	-		18,249 ^{***}	18,249
WB + aggregates	-	7,159	314,672	321,831
WB + aggregates 2x ^{**}	-		4,352 ^{***}	4,352

* without centrifugation through Percoll

** rbc pellet resuspended in bottom 4.0 ml Percoll;
recentrifuged through 40 ml neat Percoll

*** no interface when rbc pellet resuspended in Percoll;
top 4.5 ml extracted

available prior to centrifugation through Percoll, more than 96% of the platelets recovered in the top 7.0 ml were at the interface. The fixed rbc were washed free of excess glutaraldehyde on transit through the Percoll and did not agglutinate after being compressed into a pellet at the bottom of the tube, but readily dispersed with mild agitation. When the rbc pellet was resuspended in the bottom 4.0 ml of Percoll and this suspension relayered onto another tube of Percoll, an extra 5% of platelets were recovered from the rbc residue. Of the aggregates that were added to WB, 98% were recovered at the interface during the first extraction and only 1% of additional particles were recovered from the rbc pellet.

Thus, an excellent separation of fixed platelets and aggregates from fixed rbc was achieved using the present technique and density of Percoll. The rbc did not entrap significant numbers of single platelets or aggregates as they migrated through the Percoll, with at most 5% of platelets and 1% of aggregates co-sedimenting with the rbc. In the present experiments 8.0 ml of suspension was extracted from the plasma/Percoll interface to ensure the recovery of all particles from this region.

2. Wall Adhesion

Visual inspection of the polyethylene flow tubes after each experiment failed to reveal the presence of adherent aggregates with either PRP or WB. In contrast, many large aggregates visible to the naked eye were recovered in the effluent of PRP and of WB after the rbc were removed. The adhesion of large aggregates to the tube wall after being

formed entirely within suspension at the wall shear rates in the present experiments is unlikely due to the known inward radial migration of both deformable and rigid particles (Goldsmith and Mason, 1967; Gauthier et al., 1972), and to the large gradient of shear across large aggregates acting to prevent adhesion (Hyman, 1972).

The following experiment was carried out to determine the extent, if any, of platelet wall-adhesion in the present work. Whole blood was collected into glutaraldehyde-free Isoton II after $\bar{t} = 43$ s exposure to $0.2 \mu\text{M}$ ADP at $\bar{G} = 39.3$ and 1800 s^{-1} in the flow tube. As will be shown below, extensive aggregation was present under these conditions. The effluent WB suspension was kept on a rotator for 2 hr in order to facilitate aggregate break-up and then fixed in 0.5% glutaraldehyde. Particle concentrations were compared to those of an unsheared control, $\bar{t} = 0$ s. At $\bar{G} = 39.3 \text{ s}^{-1}$, where the extent of aggregation was the greatest, 97% of platelets in the control were recovered after aggregate dispersal, and at $\bar{G} = 1800 \text{ s}^{-1}$, 78% of platelets were recovered. Since almost the same number of single platelets could be recovered before aggregation and after aggregate break-up, it would seem that significant wall adhesion did not occur in the present experiments.

RESULTS

Five male (33 ± 15 yr) and six female (32 ± 6 yr) donors were used in a series of 13 experiments involving 0.2 and $1.0 \mu\text{M}$ ADP at $\bar{G} = 39.3$, 314 , and 1800 s^{-1} . The mean hematocrit of the male donors ($45.1\% \pm 1.7$; \pm S.D, $n = 7$) was significantly higher ($p < 0.005$) than that of the female donors ($42.4\% \pm 1.3$, $n = 6$) but, after the initial citrate concentration

was adjusted, there was no significant difference in $[Ca^{2+}]$ in WB between the male ($45.7 \pm 6.7 \mu M$) and female ($48.3 \pm 4.7 \mu M$) donors, and no correlation between $[Ca^{2+}]$ and donor hematocrit ($r = -0.02$). Thus, the efforts to correct the hematocrit-dependent dilution of citrate (Chapter IV, this thesis) and keep the plasma $[Ca^{2+}]$ the same for both sexes were successful. As such, the data for both sexes at the same mean tube shear rate and ADP concentration were pooled.

1. Single Platelet Volume

Table 2 shows average values of the statistics of the individual single platelet log-volume histograms after background was subtracted as described in Chapter II. The mean single platelet volume ($\bar{\mu} = 7.5 \pm 0.8 \mu m^3$) was not significantly different from that obtained in PRP ($\bar{\mu} = 7.3 \pm 0.9 \mu m^3$) in Chapter III. All other statistics of the log-volume distributions from WB and PRP were virtually identical as well. Distributions from 9 out of the 11 donors tested were also log-normal according to the K-S one sample test. On average, however, the log-normal distributions of platelets in WB tended to be more positively skewed ($g_1 > 0$, $p < 0.05$) than those in PRP, pointing to the presence of some microaggregates in the suspensions prior to shearing. The high fraction of log-normal distributions in both WB and PRP, and the similarity of the statistics characterizing the distributions from these suspensions, indicate that the shape of the single platelet log-volume distributions of those cells extracted from WB is identical with that of cells in PRP without extraction. Thus, the entire single platelet population was recovered from WB by the present technique, and a unique subset of platelets was not preferentially recovered due to differences in cell density.

TABLE 2

Average Statistics of the Single Platelet Log-Volume Histograms

Statistic	
No. Donors	11
No. Log-Normal	9
$\bar{\mu}$	7.5 \pm 0.8
σ	4.6 \pm 0.7
μ_{mod}	4.6 \pm 0.4
μ_{med}	6.4 \pm 0.6
g_1	* 0.045 \pm 0.039
g_2	-0.024 \pm 0.117
$n_{L,U}(0)$	15700 \pm 1060

Statistics of individual single platelet log-volume distributions in WB calculated at $\bar{t} = 0$ s over the range 1 - 50 μm^3 were averaged (\pm S.D.) for the stated number of donors. Also given is the number of distributions that were accepted as log-normal by the K-S one sample test. Symbols are as described in the text and volumes are in μm^3 .

Significantly different from zero: * $p < 0.05$.

2. Single Platelet Concentration

(a) ADP

At all three mean tube shear rates, the rate and extent of aggregation in WB were always greater than those in PRP at both ADP concentrations. For the purpose of comparison, the combined average values of aggregation in PRP from the male and female donors of Chapter III are also shown. Figure 1 shows the single platelet concentration at time \bar{t} , $N_{1,30}(\bar{t})$, normalized to that at $\bar{t} = 0$ s as a function of mean transit time at $\bar{G} = 39.3 \text{ s}^{-1}$. As discussed in Chapter II of this thesis, the volume range from 1 to $30 \mu\text{m}^3$ was selected to be single platelets despite some overlap of microaggregate volume. The initial single platelet concentration per unit volume of WB in the flow tube was $170,550 \pm 36,210$ (\pm S.D., $n = 11$) and that per unit volume of PRP for the pooled donors from Chapter III was $279,000 \pm 29,100$ ($n = 144$). At $0.2 \mu\text{M}$ ADP, the rate of aggregation was highest over the first $\bar{t} = 1.7$ s where $26\% \pm 2.5$ (\pm S.E.M., $n = 5$) of the initial single platelets aggregated per second. This rate of aggregation is more than $7\times$ greater than in PRP. In both platelet suspensions no lag phase preceded aggregation, and the rate of aggregation decreased steadily with increasing mean transit time. At $\bar{t} = 43$ s, however, only $13\% \pm 1.4$ ($n = 5$) of platelets remained unaggregated in WB as compared to $64\% \pm 2.7$ ($n = 18$) in PRP. At $1.0 \mu\text{M}$ ADP, the initial rate of aggregation in WB of $37\% \text{ s}^{-1} \pm 2.8$ ($n = 5$) was $9\times$ greater than the mean value for the single male donor and female donor from Chapter III. Although the initial rate of aggregation in WB also decreased steadily with increasing mean transit time, it remained sufficiently high to leave only $6.8\% \pm 0.7$ of the single platelets unaggregated at $\bar{t} = 43$ s.

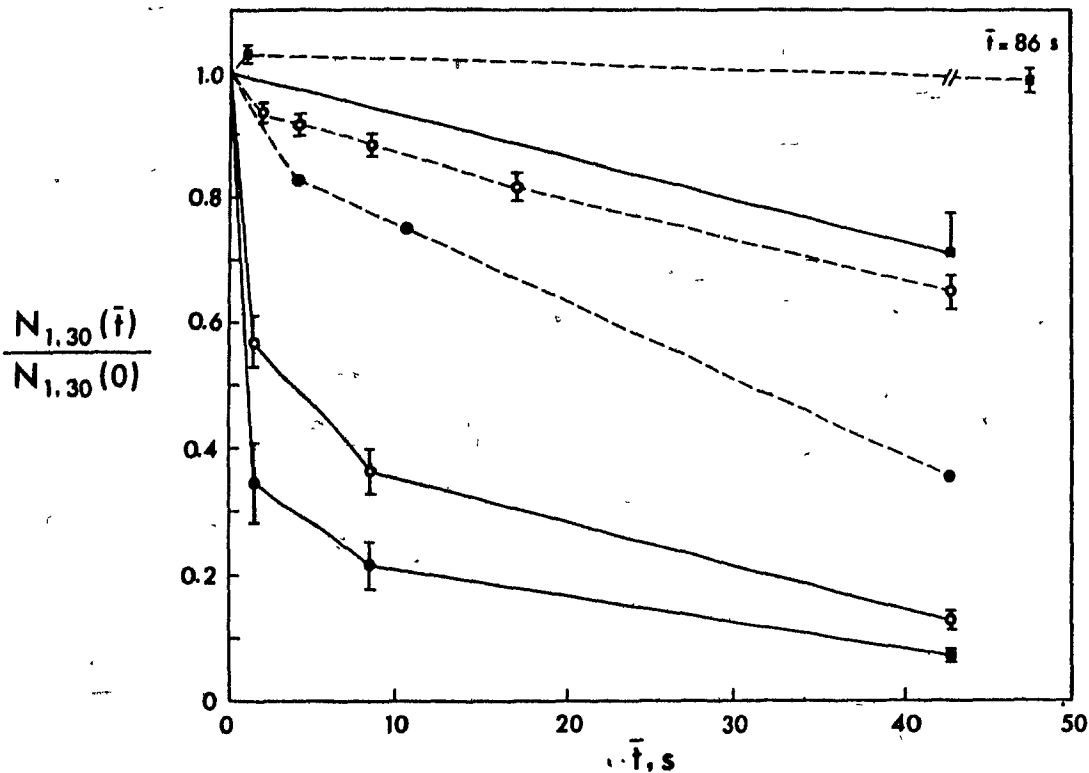


Figure 1: Single Platelet Concentration vs. \bar{t} at $\bar{G} = 39.3 \text{ s}^{-1}$

The normalized single platelet concentration, $N_{1,30}(\bar{t})/N_{1,30}(0)$, (\pm S.E.M) at $\bar{G} = 39.3 \text{ s}^{-1}$ as a function of mean transit time. Solid line WB; broken line, PRP; \circ 0.2 μM ADP; \bullet 1.0 μM ADP; \blacksquare modified Tyrodes.

As found at $\bar{G} = 39.3 \text{ s}^{-1}$, the aggregation of platelets in WB at $\bar{G} = 314 \text{ s}^{-1}$ (Fig. 2) was always greater than that in PRP at both 0.2 and 1.0 μM ADP. Although the initial rates of aggregation at both ADP concentrations at $\bar{G} = 314 \text{ s}^{-1}$ were less than the respective values at $\bar{G} = 39.3 \text{ s}^{-1}$, they decreased to a lesser extent with increasing mean transit time so that the extent of aggregation at $\bar{t} = 43 \text{ s}$ was greater at $\bar{G} = 314 \text{ s}^{-1}$ than at $\bar{G} = 39.3 \text{ s}^{-1}$. At 0.2 μM ADP, a low initial rate of aggregation increased between $\bar{t} = 1.7$ and 8.6 s before decreasing. This pattern of aggregation produced the characteristic sigmoid aggregation curve found in PRP. At 1.0 μM ADP, the initial rate of aggregation of $11\% \text{ s}^{-1} \pm 1.7$ ($n = 5$) at $\bar{G} = 314 \text{ s}^{-1}$ was higher than that at 0.2 μM ADP but less than that at either ADP concentration at $\bar{G} = 39.3 \text{ s}^{-1}$. The rate of aggregation at 1.0 μM ADP at $\bar{G} = 314 \text{ s}^{-1}$, however, remained almost constant until $\bar{t} = 8.6 \text{ s}$ at which point $84\% \pm 1.8$ ($n = 5$) of the single cells had aggregated. The rate of aggregation slowed considerably thereafter, but by $\bar{t} = 43 \text{ s}$, $99\% \pm 0.2$ ($n = 5$) of the cells had aggregated.

The pattern of aggregation at $\bar{G} = 1800 \text{ s}^{-1}$ in WB was almost identical with that at $\bar{G} = 314 \text{ s}^{-1}$ at the same respective ADP concentrations (Fig. 3). At 0.2 μM ADP, the rate and extent of aggregation was so similar at the two shear rates that the aggregation curves were virtually superimposable. At 1.0 μM ADP, the initial rate of aggregation was higher than that at $\bar{G} = 314 \text{ s}^{-1}$ but still less than that at $\bar{G} = 39.3 \text{ s}^{-1}$. Again, as at $\bar{G} = 314 \text{ s}^{-1}$, the rate of aggregation barely decreased between $\bar{t} = 1.7$ and 8.6 s so that by the latter mean transit time $95\% \pm 0.8$ ($n = 5$) of the single platelets had aggregated. Due to

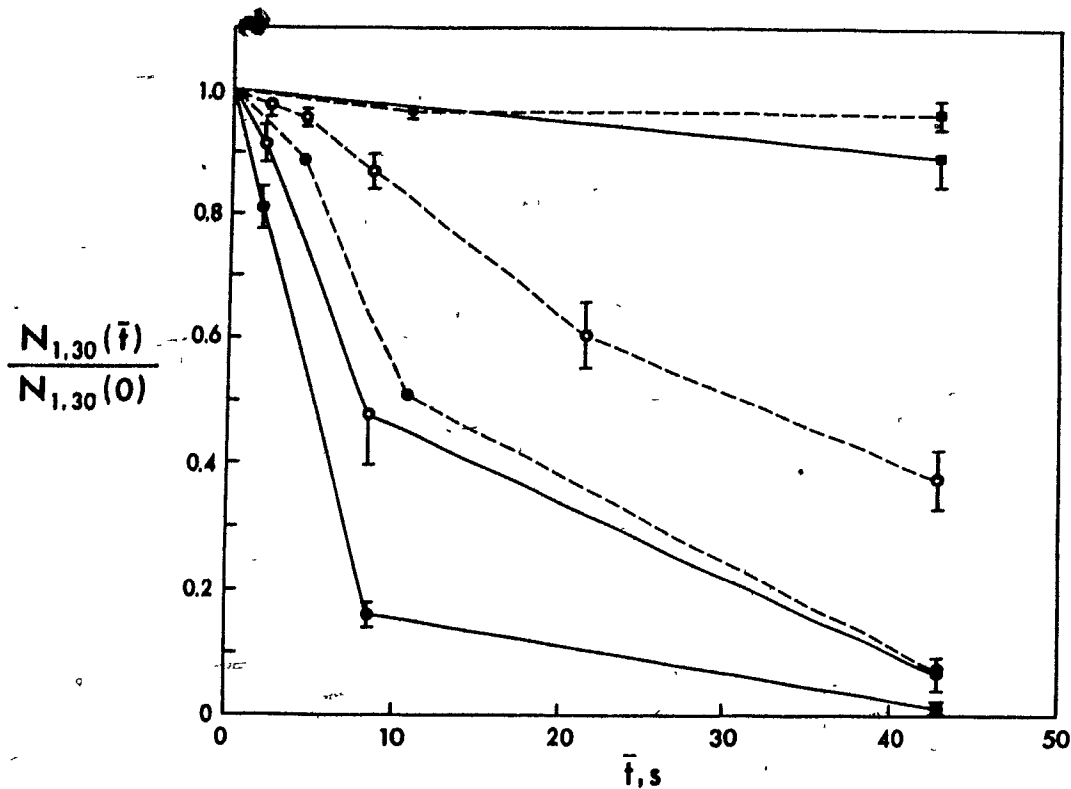


Figure 2: Single Platelet Concentration vs. \bar{t} at $\bar{G} = 314 \text{ s}^{-1}$

The normalized single platelet concentration, $N_{1,30}(\bar{t})/N_{1,30}(0)$, (\pm S.E.M) at $\bar{G} = 314 \text{ s}^{-1}$ as a function of mean transit time. Solid line WB; broken line, PRP; ○ 0.2 μM ADP; ● 1.0 μM ADP; ■ modified Tyrodes.

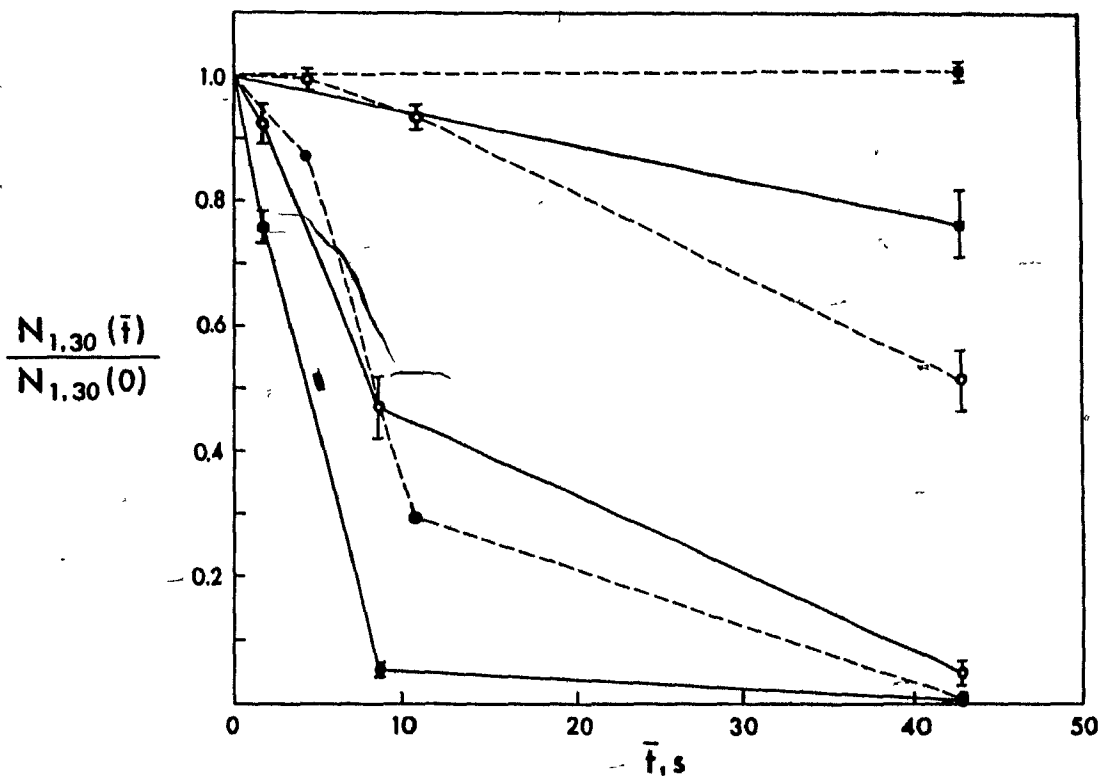


Figure 3: Single Platelet Concentration vs. \bar{t} at $\bar{G} = 1800 \text{ s}^{-1}$

The normalized single platelet concentration, $N_{1,30}(\bar{t})/N_{1,30}(0)$, (\pm S.E.M) at $\bar{G} = 1800 \text{ s}^{-1}$ as a function of mean transit time. Solid line WB; broken line, PRP; \circ 0.2 μM ADP; \bullet 1.0 μM ADP; \blacksquare modified Tyrodes.

the enormous depletion of single platelets, the rate of aggregation beyond $\bar{t} = 8.6$ s decreased considerably, yet by $\bar{t} = 43$ s virtually no (0.5% \pm 0.2, n = 5) single platelets remained. This tremendous extent of aggregation was also achieved for the male donor and female donor in PRP at 1.0 μ M ADP in Chapter III. Here, the initial rate of aggregation was much slower than in WB at either 0.2 or 1.0 μ M ADP. Only after $\bar{t} = 1.7$ s did the rate of aggregation increase to approximately the same value as at 1.0 μ M ADP in WB between $\bar{t} = 1.7$ and 8.6 s. Although the rate of aggregation in PRP also decreased after $\bar{t} = 8.6$ s, it remained higher than at 1.0 μ M ADP in WB beyond this mean transit time, presumably due to the larger number of unaggregated platelets remaining.

(b) Controls

Compared to similar shear rates in PRP, the extent of aggregation at $\bar{t} = 43$ s was generally greater in the controls in WB in which modified Tyrodes was infused instead of ADP. The aggregation in the controls was greatest at $\bar{G} = 39.3$ and 1800 s^{-1} , but was not significantly different from that in PRP at $\bar{G} = 314$ s^{-1} . The enhanced aggregation in the controls was not due to the release of platelet granule contents since the level of TXB₂ in either the control runs or the ADP runs at $\bar{t} = 43$ s was not significantly higher than at $\bar{t} = 0$ s at any of the three mean tube shear rates (Table 3). In addition, the mean plasma lactate dehydrogenase concentration, LDH, in WB for two donors was the same at all three shear rates as in the static controls. Since the concentration of LDH was in the normal range for plasma (Dittmer, 1961), the flow system did not induce significant hemolysis.

TABLE 3

TXB₂, ng ml⁻¹ (± S.D.) and LDH, U l⁻¹

	\bar{t} , s	n*	\bar{G} s ⁻¹			
			0	39.3	314	1800
TXB ₂ CONTROL	0	10	0.14 ± 0.19	-	-	-
	43	7	-	0.56 ± 1.08	0.25 ± 0.42	1.30 ± 1.93
	ADP	43	9	-	0.61 ± 0.78	0.29 ± 0.56
LDH CONTROL	0	2	102	113	95	94 (1)
	43	2	-	108	99	101 (1)
	300	2	101			

* number of donors except where indicated in parentheses

3. Aggregate Size and Growth Rate

The pattern and extent of aggregate growth at both ADP concentrations and at all three mean tube shear rates is illustrated by the continuous volume fraction histograms in the upper half of Figures 4, 8 and 9. Here, the mean normalized class volume fraction, $\bar{\Phi}(x_i)$, is plotted against particle volume, $v(x_i)$, over the range from 1 to $10^5 \mu\text{m}^3$.

(a) $\bar{G} = 39.3 \text{ s}^{-1}$

Prior to exposure to $0.2 \mu\text{M}$ ADP and $\bar{G} = 39.3 \text{ s}^{-1}$ (Fig. 4a; $\bar{t} = 0 \text{ s}$), the single platelet volume fraction followed an apparent log-normal distribution with relatively few aggregates present. The reduction in the volume fraction of single platelets at $\bar{t} = 1.7 \text{ s}$ was accompanied by the growth of aggregates of a wide range of volume but always less than $10^4 \mu\text{m}^3$. The continued formation of aggregates of many sizes led to the broad aggregate volume fraction distribution at $\bar{t} = 43 \text{ s}$. The large peaks of modal volume ~ 200 and $380 \mu\text{m}^3$ correspond to wbc. The standard error of these peaks is large since the extraction procedure was designed to recover platelets not wbc. Consequently the number of wbc inadvertently coextracted varied more strongly from donor to donor and extraction to extraction. It is evident by the persistent wbc peak at $\bar{t} = 43 \text{ s}$ that these cells were not incorporated into aggregates.

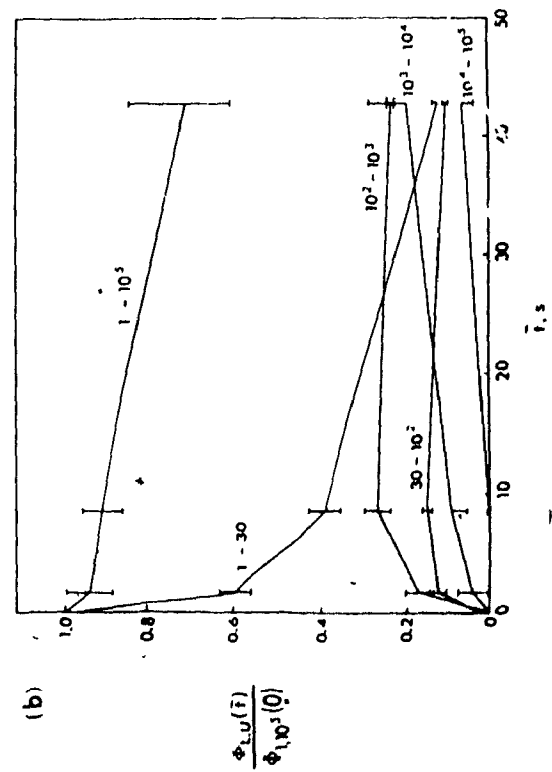
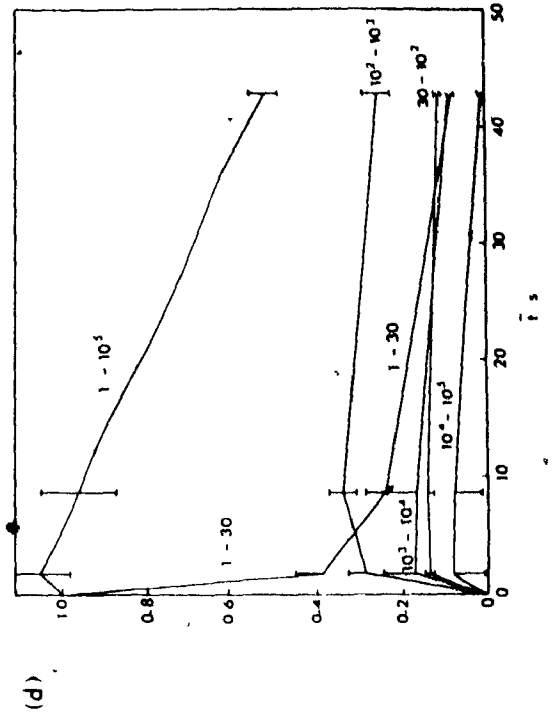
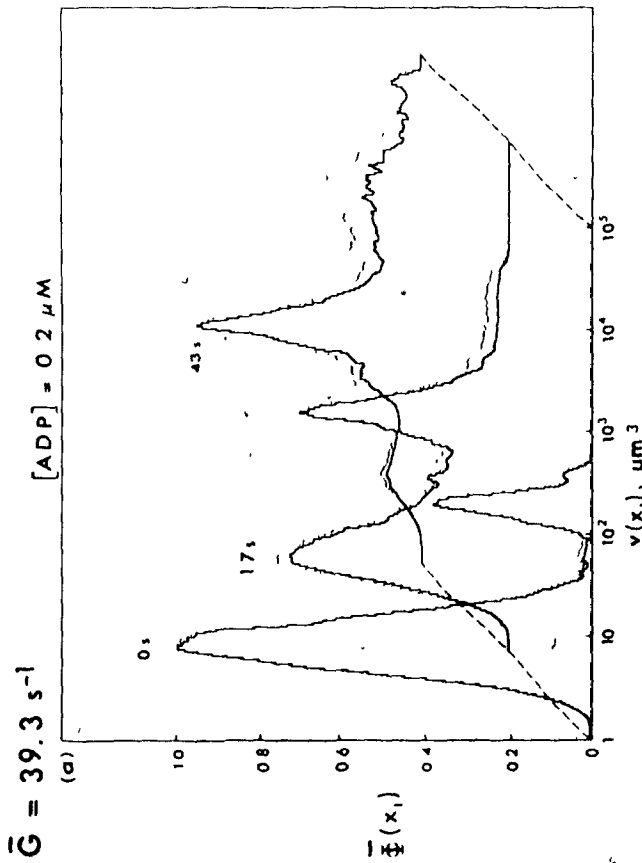
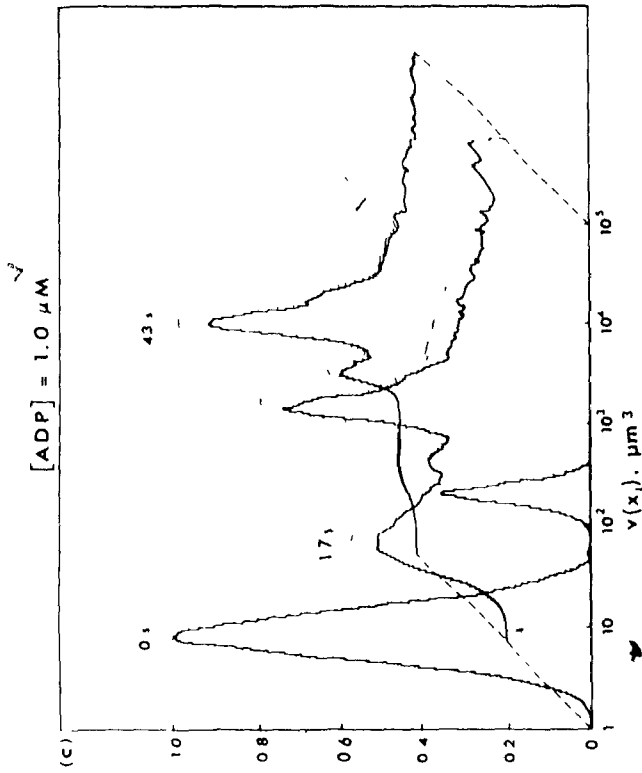
The rate of growth of aggregates of progressively increasing size is also shown in the respective lower halves of Figures 4, 8 and 9. In these figures, the volume fraction of particles at time \bar{t} , $\Phi_{L,U}(\bar{t})$, between lower, L, and upper, U, volume limits was normalized to the total volume fraction at time $\bar{t} = 0 \text{ s}$, $\Phi_{1,10^5}(0)$ and plotted against mean

Figure 4: Aggregate Growth at $\bar{G} = 39.3 \text{ s}^{-1}$

Upper: Three dimensional plots of the mean, normalized class volume fraction, $\bar{\Phi}(x_1)$, (\pm S.E.M., dotted line) versus particle volume, $v(x_1)$, at mean transit times, $\bar{t} = 0, 1.7,$ and 43 s .

Lower: The normalized volume fraction of particles between lower, L, and upper, U, volumes, $\Phi_{L,U}(\bar{t})/\Phi_{1,10^5}(0)$ (\pm S.E.M), plotted against \bar{t} . The volume limits, L-U, from $1-30, 30-10^2, 10^2-10^3, 10^3-10^4, 10^4-10^5$ are shown beside their respective plots.

a,b) $0.2 \mu\text{M ADP}$; c,d) $1.0 \mu\text{M ADP}$



transit time. At any given mean transit time, the combined volume fraction of aggregates and single cells equals the total particle volume fraction. The rate of growth of aggregates between $L = 10^2$ and $U = 10^3 \mu\text{m}^3$ was more clearly revealed by deleting the particle counts corresponding to wbc. All particles in this volume interval at $\bar{t} = 0$ s were subtracted from those in the same interval at all other mean transit times. The decrease in the normalized volume fraction of single cells (Fig. 4b; $L = 1$, $U = 30 \mu\text{m}^3$) closely paralleled that of the normalized single platelet concentration (Fig. 1). The rapid growth of aggregates of many sizes concurrently is also evident. This is in contrast to the sequential rise in the volume fraction of aggregates of successively increasing size found at higher shear rates in WB and in PRP. The total particle volume fraction at first remained relatively constant and only began to decrease with the formation of large aggregates of volume greater than $10^5 \mu\text{m}^3$, the maximum volume measured in the present experiments.

It should be noted that at both ADP concentrations and all three mean tube shear rates, aggregates were plainly visible to the naked eye after the rbc were removed, and that the increase in the extent of aggregation with increasing mean transit time could be followed during platelet extraction. The aggregates were almost always white in color and similar in shape to those obtained in PRP. The largest aggregates were also more like flakes than spheres which was easily demonstrated by swirling the suspension after extraction. The major axis of these aggregates often exceeded 1 mm.

The higher rate of single platelet decrease at 1.0 μM ADP than at 0.2 μM ADP at $\bar{G} = 39.3 \text{ s}^{-1}$ (Fig. 1) was accompanied by a larger range of aggregate size that extended beyond $10^5 \mu\text{m}^3$ at $\bar{t} = 1.7 \text{ s}$ (Fig. 4c). The steady decrease in the volume fraction of single platelets, and of aggregates between 30 and $10^5 \mu\text{m}^3$ beyond $\bar{t} = 8.6 \text{ s}$ (Fig 4d), accompanied the continued growth of aggregates to volumes greater than the maximum volume measured. This was reflected in a concomitant decrease in the total particle volume fraction. By $\bar{t} = 43 \text{ s}$, almost all the aggregates exceeded $10^5 \mu\text{m}^3$, although some single platelets still remained.

The peak present at $\sim 64 \mu\text{m}^3$ at both $\bar{t} = 1.7$ and 43 s corresponded to contaminating rbc in these preparations. The equivalent sphere volume of the rbc is smaller than their real volume because, as discussed in Chapter II, the amplitude of volume signals generated in the Coulter Counter depends on particle shape. The fixed rbc are rigid discs of shape factor ~ 1.2 but the Coulter scale is calibrated with spheres of shape factor 1.5. By correcting for the difference in shape factor, a modal rbc volume of $80 \mu\text{m}^3$ is obtained. This is close to the normal mean rbc volume ($88 \mu\text{m}^3$) considering the assumptions made regarding cell shape. The presence of rbc is not surprising since only at 1.0 μM ADP at $\bar{G} = 39.3 \text{ s}^{-1}$, were the aggregates visibly red in color after extraction from WB. The aggregates were still flake-like but also much larger, often with a major axis of several millimeters, than those described above that contained exclusively platelets. Some of these aggregates were completely red while others had a red central core with the remainder of the particle from pink to white. It is possible that some rbc incorporated at the periphery of the aggregates were dislodged during the constant agitation

of the suspensions that was maintained between extraction and measurement to prevent sedimentation and possible clumping at the bottom of the tube. These free rbc would give rise to the peaks seen on the log-volume histograms.

Light micrographs taken under epi-illumination differential interference contrast, D.I.C., microscopy (Fig. 5a) show numerous rbc interspersed among the tightly packed platelets, as well as some free rbc. At a lower magnification under transmitted light, the red colour of these aggregates is clearly evident (Fig. 5b). A transmission electron micrograph, T.E.M., of a section through an aggregate (Fig. 6) verified that rbc were trapped within the interior of platelet aggregates and not simply attached to their surface as an artifact of fixation. In contrast the aggregates at $\bar{t} < 43$ s at $\bar{G} = 314$ s⁻¹ (Fig. 7a) and at $\bar{G} = 1800$ s⁻¹ (Fig. 7b) were not red in colour and few rbc were observed trapped within the aggregates.

(b) $\bar{G} = 314$

The volume fraction histogram at $\bar{G} = 314$ s⁻¹ (Fig. 8a) shows that after $\bar{t} = 43$ s exposure to 0.2 μ M ADP, the aggregates were grouped into a single large population of volume less than 6.0×10^4 μ m³. Furthermore, at this mean tube shear rate, the formation of large aggregates was preceded by the formation of smaller aggregates (Fig. 8b). An early rise in the volume fraction of aggregates between 30 and 10^2 μ m³ was succeeded by that of aggregates between 10^2 and 10^3 μ m³. By $\bar{t} = 8.6$ s, a significant number of aggregates between 10^3 and 10^4 μ m³ had appeared. At this mean transit time there were very few aggregates between 10^4 and

Figure 5: Light Micrographs of Platelet Aggregates Containing Rbc

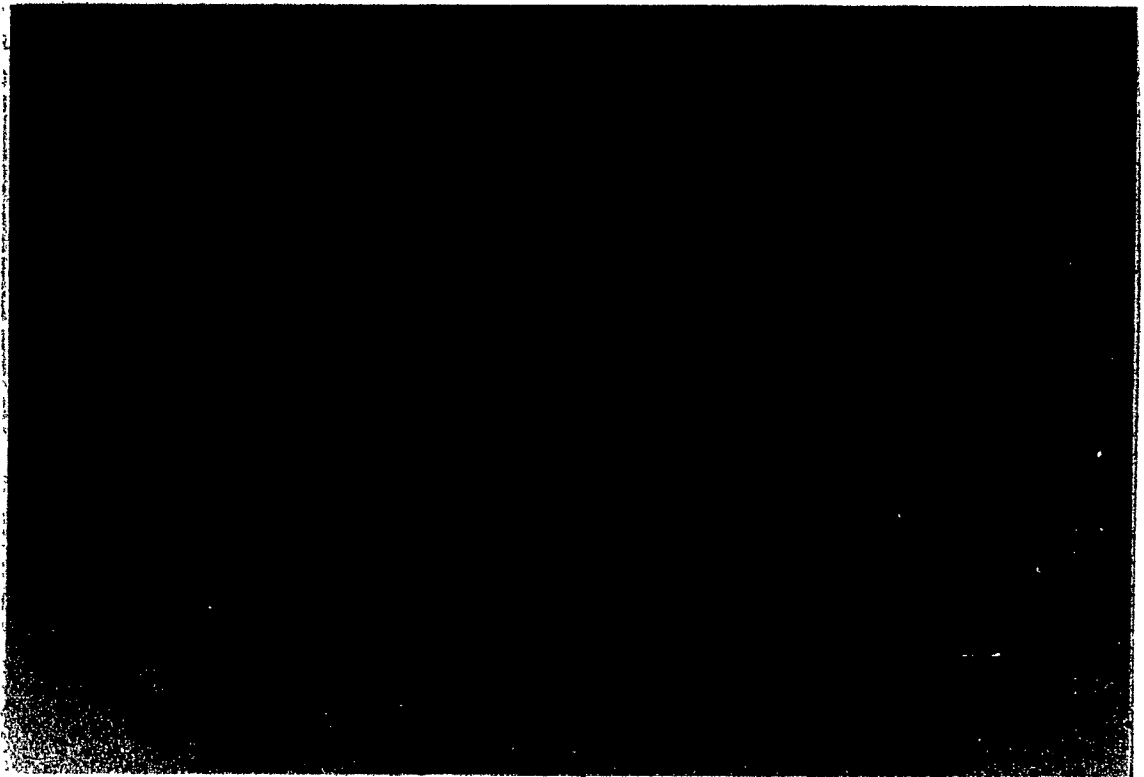
a) Epi-illumination D.I.C. micrograph of platelet aggregate formed after $\bar{t} = 43$ s exposure to $1.0 \mu\text{M}$ ADP at $\bar{G} = 39.3 \text{ s}^{-1}$. The smooth surface and distinctive shape of the larger rbc are evident at numerous locations in the aggregate (500 \times magnification).

b) Transmitted light D.I.C. micrograph of aggregate showing red color due to rbc (79 \times magnification).

(a)



(b)



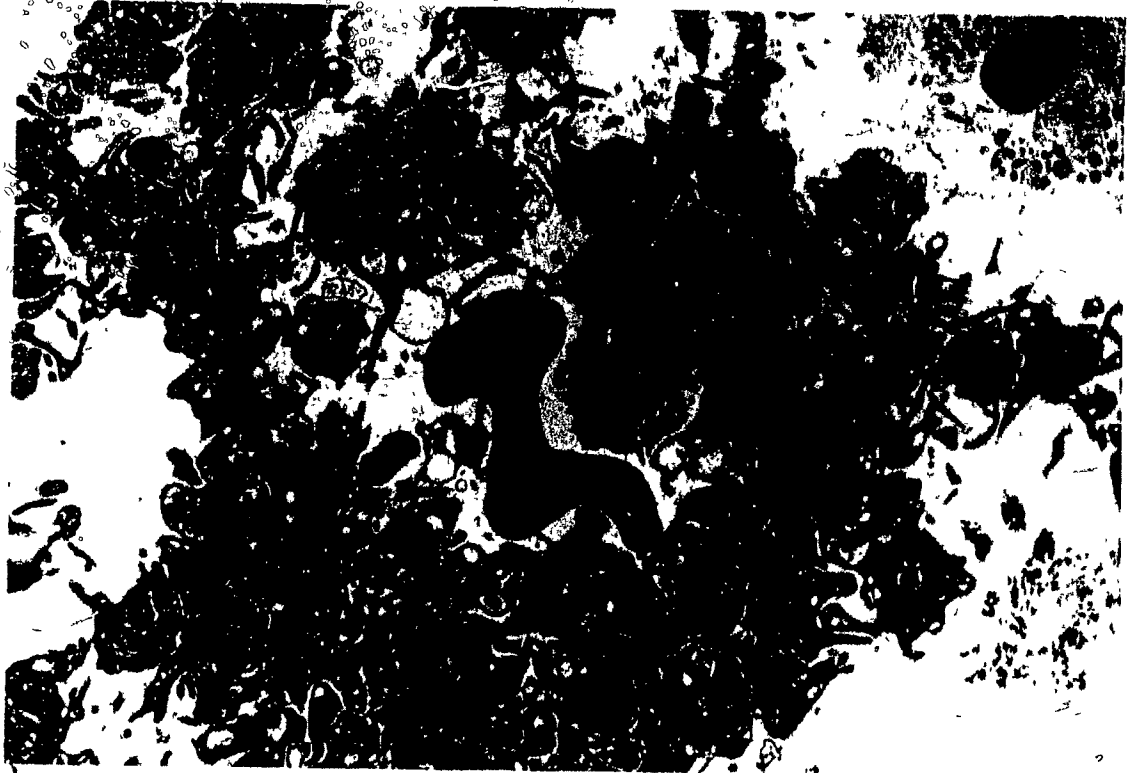


Figure 6: T.E.M. of Section Through Platelet Aggregate Containing Rbc

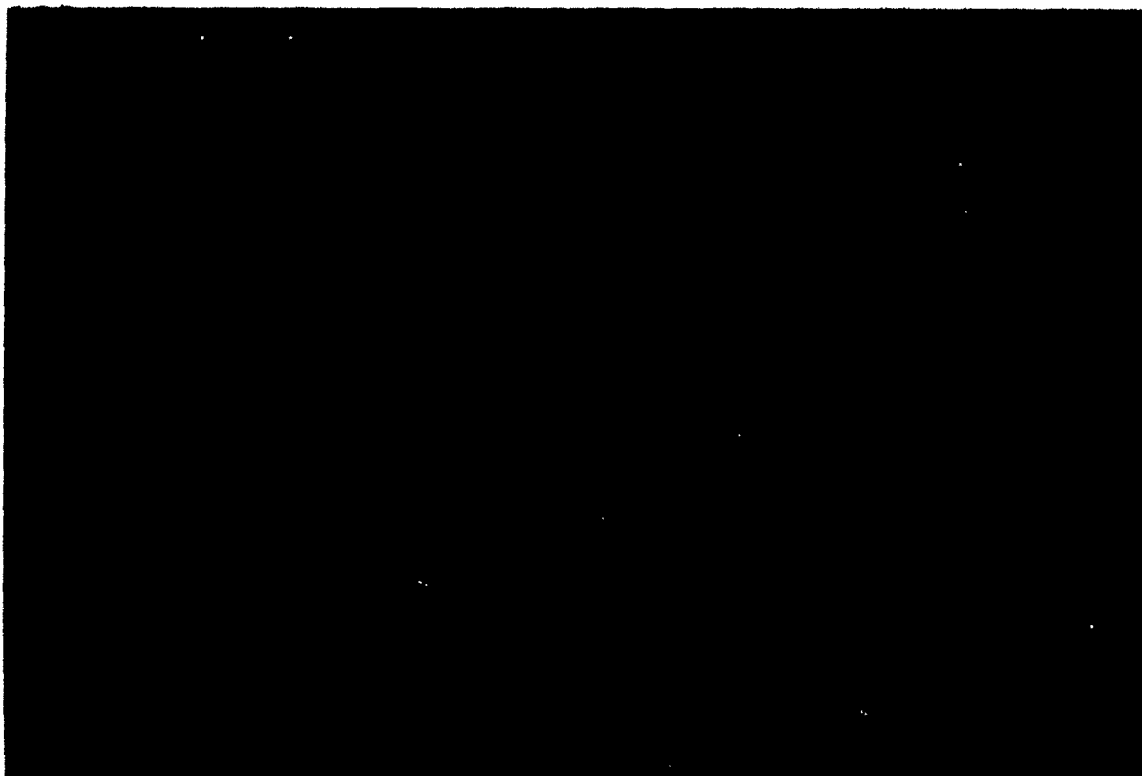
A single rbc is shown deformed to conform to the confines of the aggregate. Since all cells and aggregates were quickly fixed in glutaraldehyde the rbc could not have been deformed during any of the preparatory steps for the T.E.M. (~6000× magnification).

Figure 7: Light Micrographs of Platelet Aggregates Without Rbc

a) Epi-illumination D.I.C. micrograph of platelet aggregate formed after $\bar{t} = 43$ s exposure to $1.0 \mu\text{M}$ ADP at $\bar{G} = 314 \text{ s}^{-1}$. In contrast to Fig. 5a, no rbc can be discerned on or within the aggregate (500 \times magnification).

b) Transmitted light DIC micrograph of platelet aggregate formed after $\bar{t} = 43$ s exposure to $1.0 \mu\text{M}$ ADP at $\bar{G} = 1800 \text{ s}^{-1}$. In contrast to Fig. 5b, the aggregate is not red in color (200 \times magnification).

(a)



(b)

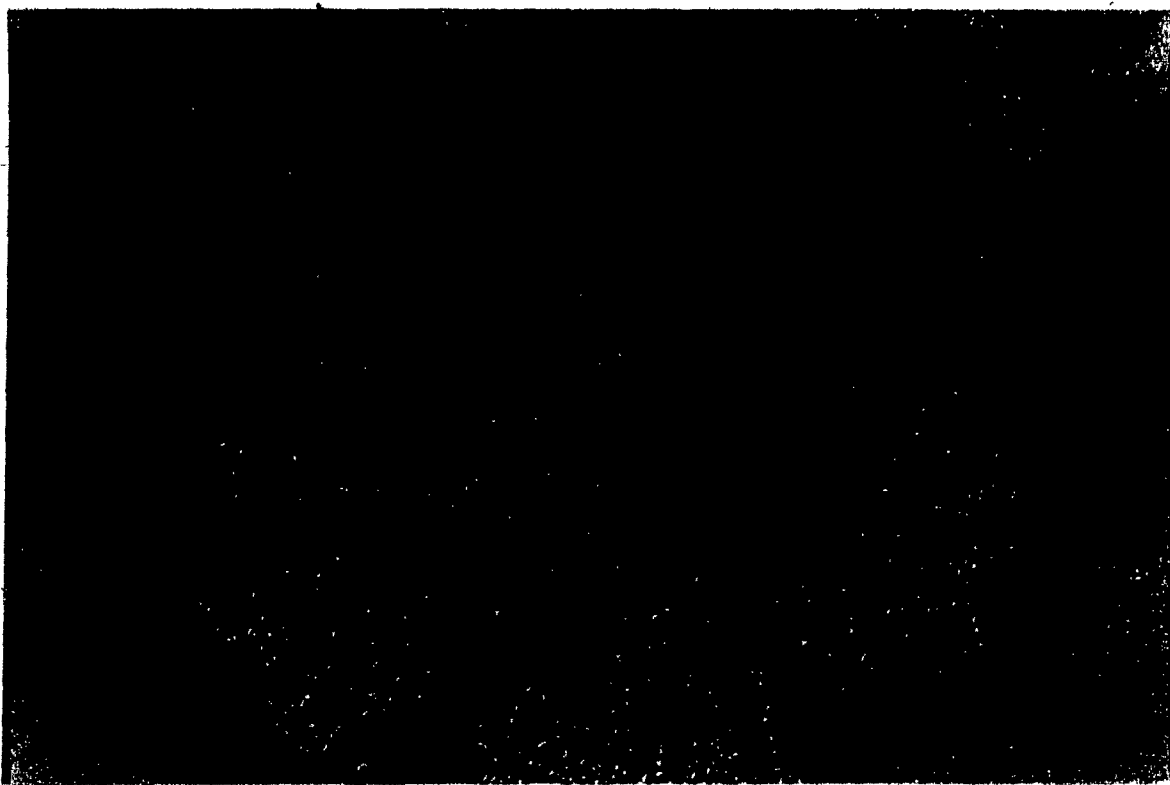
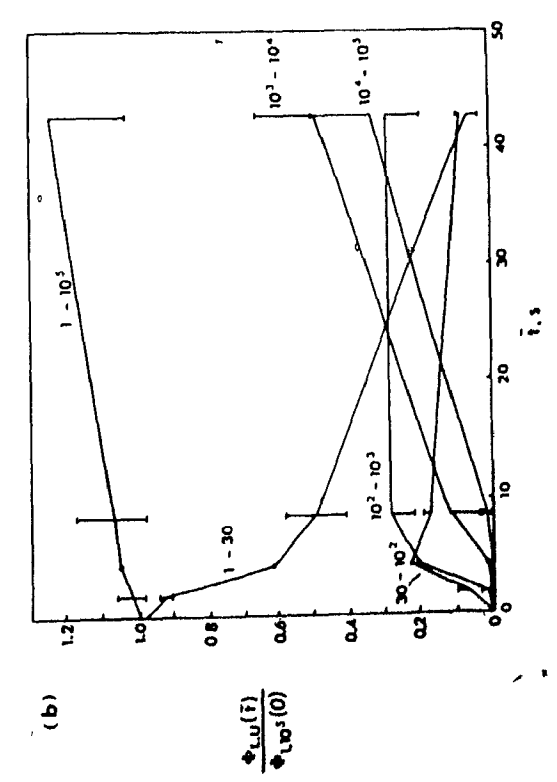
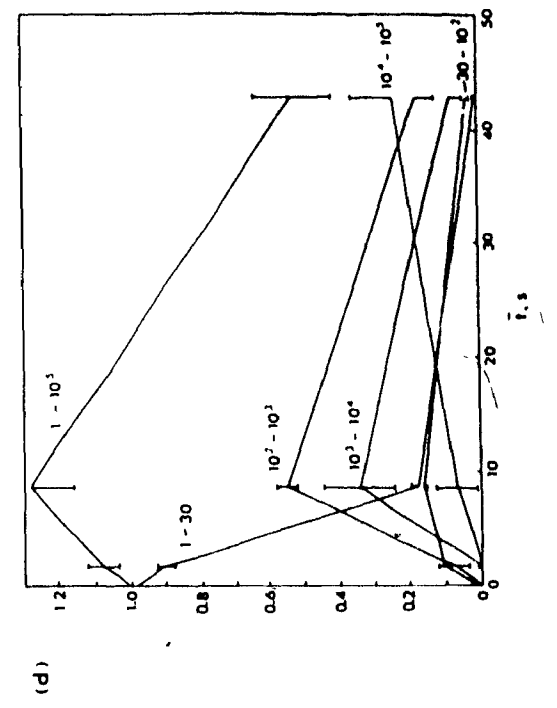
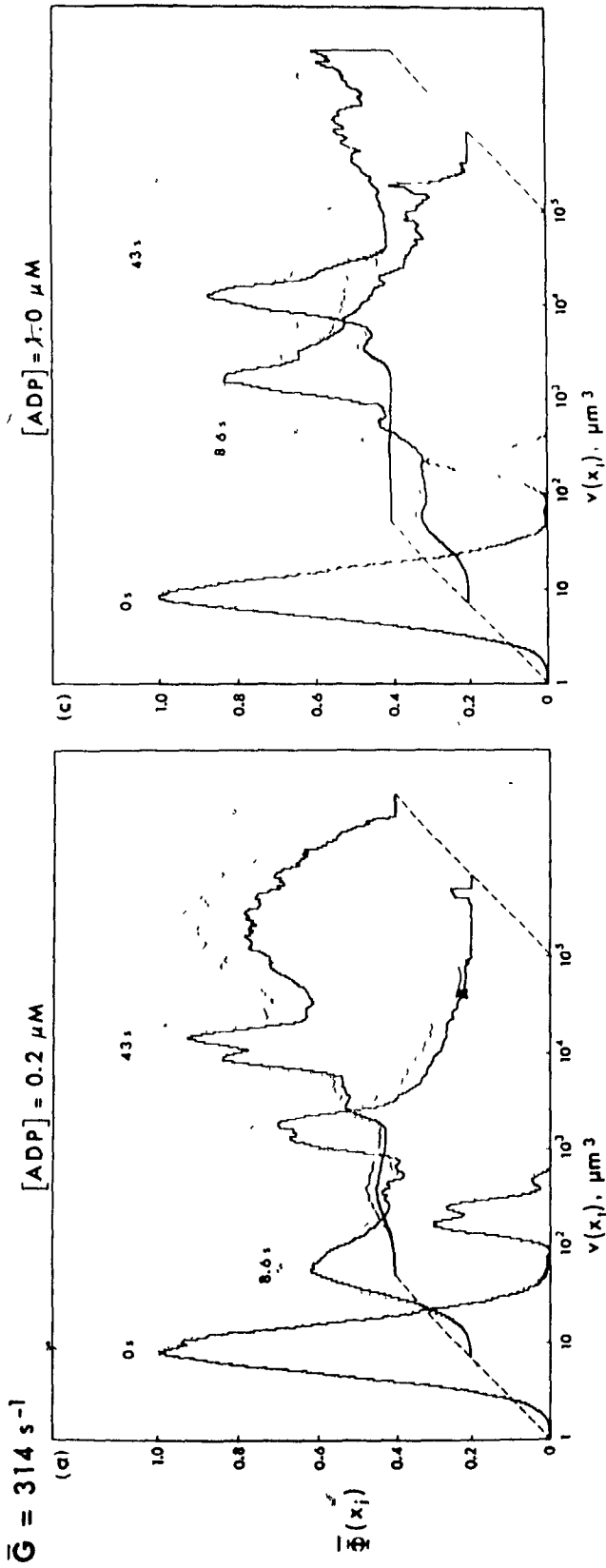


Figure 8: Aggregate Growth at $\bar{G} = 314 \text{ s}^{-1}$

Upper: Three dimensional plots of the mean, normalized class volume fraction, $\bar{\Phi}(x_1)$, (\pm S.E.M., dotted line) versus particle volume, $v(x_1)$, at mean transit times, $\bar{t} = 0, 8.6, \text{ and } 43 \text{ s}$.

Lower: The normalized volume fraction of particles between lower, L, and upper, U, volumes; $\Phi_{L,U}(\bar{t})/\Phi_{1,10^5}(0)$ (\pm S.E.M), plotted against \bar{t} . The volume limits, L-U, from $1-30, 30-10^2, 10^2-10^3, 10^3-10^4, 10^4-10^5$ are shown beside their respective plots.

a,b) $0.2 \mu\text{M ADP}$; c,d) $1.0 \mu\text{M ADP}$



$10^5 \mu\text{m}^3$ but by $\bar{t} = 43$ s, the large population of aggregates shown in Figure 8a resulted from a sharp increase in the rate of formation of aggregates of volume from 10^3 to $10^5 \mu\text{m}^3$. The single platelet volume fraction followed a sigmoid decline with the rate of decrease steepest accompanying the formation of small aggregates between 30 and $10^3 \mu\text{m}^3$.

At $1.0 \mu\text{M}$ ADP (Fig. 8c), the higher rate of aggregation was accompanied by an increase in aggregate size. The constant decline in the volume fraction of single platelets between $\bar{t} = 1.7$ and 8.6 s was paralleled by a sharp rise in the volume fraction of aggregates of volume from 10^2 to $10^4 \mu\text{m}^3$ (Fig. 8d), although aggregates as large as $5 \times 10^5 \mu\text{m}^3$ were also prevalent. The volume fraction of aggregates of volume greater than $10^4 \mu\text{m}^3$ steadily increased between $\bar{t} = 8.6$ and 43 s, while that of smaller aggregates declined sharply. By $\bar{t} = 43$ s, almost all of the single platelets had aggregated, yet many of the aggregates were still less than $10^5 \mu\text{m}^3$. It is apparent here that, as in PRP (Chapter III, this thesis), the total volume fraction rose above its initial level when large numbers of aggregates between 10^3 and $10^4 \mu\text{m}^3$ accumulated. Again, as aggregate volume eventually exceeded $10^5 \mu\text{m}^3$, the total volume fraction decreased.

(c) $\bar{G} = 1800 \text{ s}^{-1}$

The time-dependent increase in the volume fraction of aggregates of successively increasing size was even more pronounced at $\bar{G} = 1800 \text{ s}^{-1}$ at $0.2 \mu\text{M}$ ADP (Fig. 9b), where the aggregates occupied a narrow range of volume (Fig. 9a). A slight delay of $\bar{t} = 1.7$ s preceding the decrease in the volume fraction of single platelets was accompanied by a similar delay

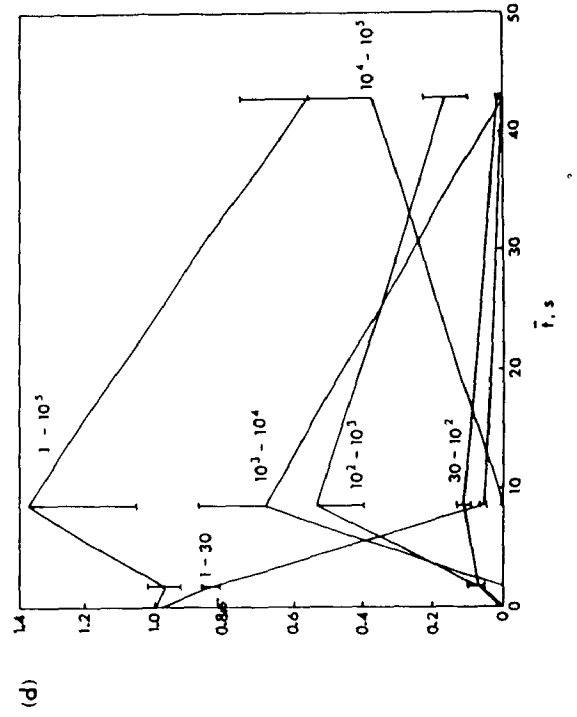
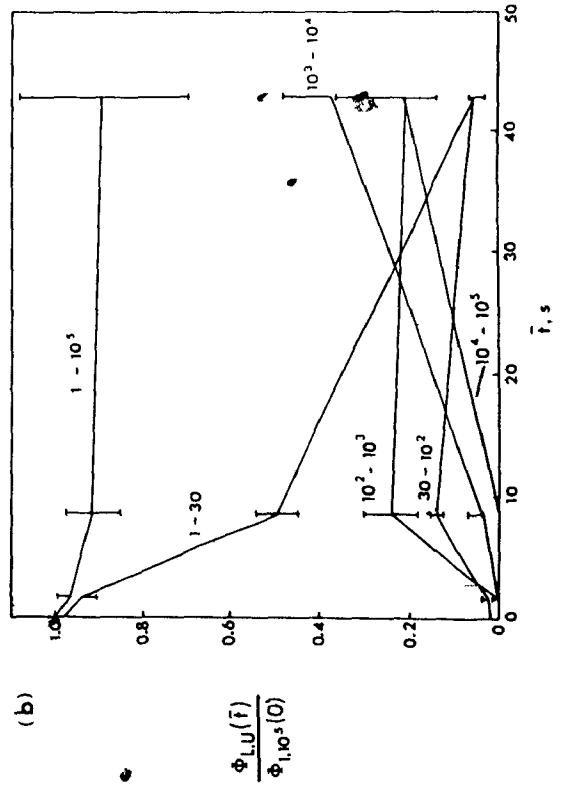
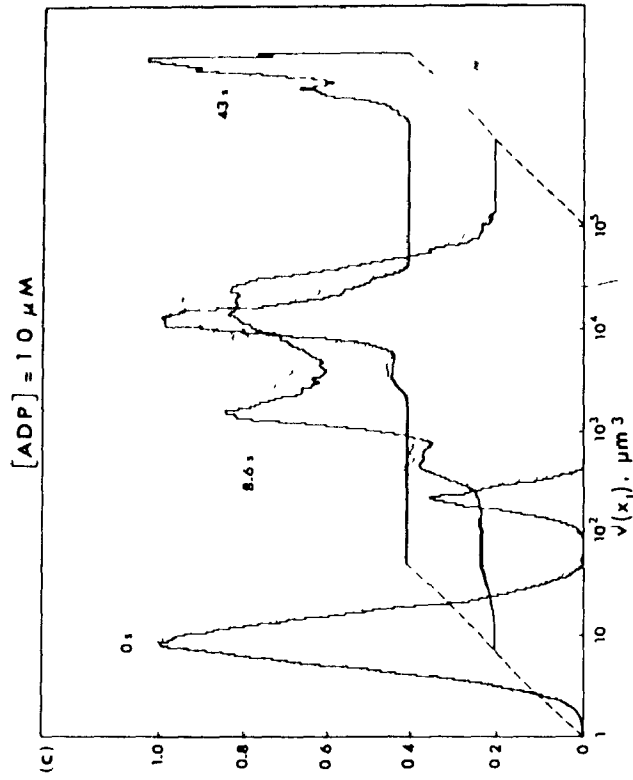
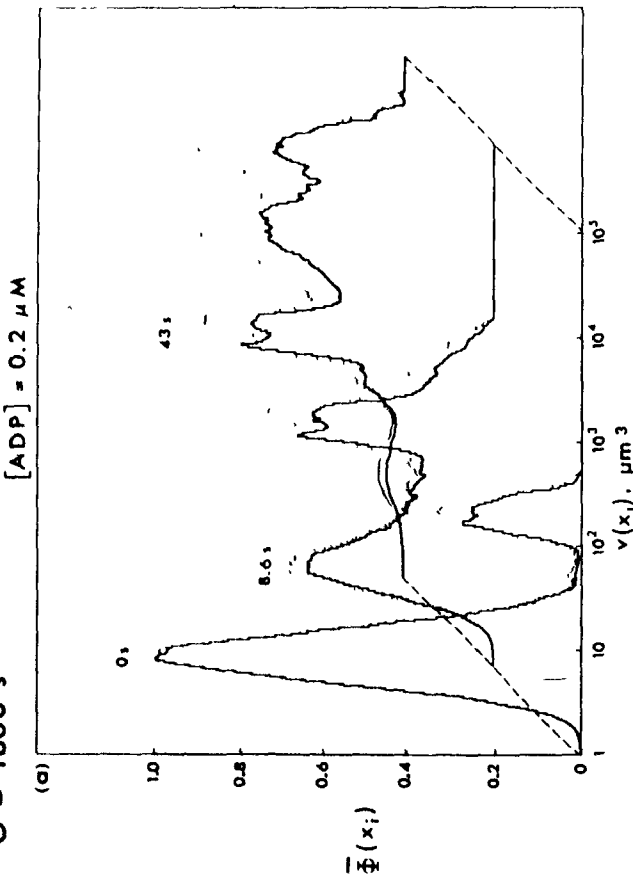
Figure 9: Aggregate Growth at $\bar{G} = 1800 \text{ s}^{-1}$

Upper: Three dimensional plots of the mean, normalized class volume fraction, $\bar{\Phi}(x_i)$, (\pm S.E.M., dotted line) versus particle volume, $v(x_i)$, at mean transit times, $\bar{t} = 0, 8.6, \text{ and } 43 \text{ s}$.

Lower: The normalized volume fraction of particles between lower, L, and upper, U, volumes $\Phi_{L,U}(\bar{t})/\Phi_{1,10^5}(0)$ (\pm S.E.M), plotted against \bar{t} . The volume limits, L-U, from $1-30, 30-10^2, 10^2-10^3, 10^3-10^4, 10^4-10^5$ are shown beside their respective plots.

a,b) $0.2 \mu\text{M ADP}$; c,d) $1.0 \mu\text{M ADP}$

$\bar{C} = 1800 \text{ s}^{-1}$



in the growth of aggregates. Once aggregation was initiated, the volume fraction of aggregates between 30 and $10^2 \mu\text{m}^3$ peaked at $\bar{t} = 8.6$ s and declined thereafter. The volume fraction of aggregates between 10^2 and $10^3 \mu\text{m}^3$ also peaked at $\bar{t} = 8.6$ s but remained at relatively the same value. By $\bar{t} = 8.6$ s, aggregates between 10^3 and $10^4 \mu\text{m}^3$ had started to form. Although the single platelet concentration at $\bar{t} = 8.6$ s at $0.2 \mu\text{M}$ ADP was similar to that at $\bar{G} = 314 \text{ s}^{-1}$, the maximum aggregate size was much reduced ($< 2.1 \times 10^3 \mu\text{m}^3$) compared to that at the two lower shear rates. Aggregates between 10^4 and $10^5 \mu\text{m}^3$ did not appear until $\bar{t} = 43$ s where, together with a distinct population between 10^3 and $10^4 \mu\text{m}^3$, they formed a bimodal aggregate population.

At $1.0 \mu\text{M}$ ADP, the single platelets aggregated so fast that within $\bar{t} = 8.6$ s they were almost exclusively incorporated into one large aggregate population between 10^2 and $10^4 \mu\text{m}^3$ (Fig. 9c,d). Once formed this population appeared to increase in volume as a unit in discrete steps. Further aggregation resulted entirely from the self assembly of these similarly-sized aggregates into larger aggregates also of narrow size range. The total volume fraction decreased suddenly at $\bar{t} = 43$ s as this group of aggregates associated into a single population of volume greater than $5 \times 10^4 \mu\text{m}^3$. Below this volume, only wbc remained. Again, the steepest decline in the single platelet volume fraction was associated with formation of relatively small aggregates between $\bar{t} = 1.7$ and 8.6 s, at the end of which the total volume fraction showed a characteristic increase.

DISCUSSION

The present work shows that platelet aggregation is much greater in WB than in PRP. At $\bar{G} = 39.3 \text{ s}^{-1}$ and at $1.0 \mu\text{M}$ ADP, rbc were incorporated into aggregates but this did not occur at higher shear rates or at lower ADP concentrations. Wbc were largely excluded from aggregates at all shear rates and both levels of platelet stimulation. High shear rates were successful in recruiting all platelets into aggregates but aggregate growth exhibited a progressive time-dependent inhibition with increasing mean tube shear rate. As will be discussed below, the augmentation of platelet aggregation can be interpreted in terms of the physical effect of rbc on the frequency and efficiency of collisions between activated platelets, and between platelets and aggregates.

1. Wall Adhesion

Measurements of the total volume fraction of suspended particles independently support the contention that significant wall adhesion did not occur in the present experiments. For any given suspension the total particle volume fraction should remain constant during aggregation, independent of the distribution of platelets within aggregates and independent of aggregate size. As was observed in Chapters II and III of this thesis, the total particle volume fraction did not decrease until aggregates of volume greater than $10^5 \mu\text{m}^3$ were formed. The total volume fraction decreased at this point because such large aggregates were beyond the range of particle volume measured in the present experiments. If wall adhesion was occurring concomitantly with aggregation then a steady decrease in the total volume fraction with increasing mean transit time

would have been observed from the onset of aggregation. In fact, as discussed in Chapter II, the total volume fraction actually increased as the concentration of aggregates from 10^3 to $10^5 \mu\text{m}^3$ increased before decreasing again as these aggregates were incorporated into larger aggregates whose volume exceeded $10^5 \mu\text{m}^3$. This transient rise in the total volume fraction was due to the artifactual over-estimation of the volume of particles of diameter that is more than 20% of the aperture diameter of the electronic particle counter (Smythe, 1961; 1964). Since aggregates of volume greater than $100 \mu\text{m}^3$ were measured on a $100 \mu\text{m}$ diameter aperture, particles of equivalent sphere diameter greater than $20 \mu\text{m}$, or of volume greater than $4.2 \times 10^3 \mu\text{m}^3$, would be over-estimated. In addition, a void volume of plasma trapped between platelets comprising aggregates (Born and Hume, 1967; Belval and Hellums, 1986) increases with increasing aggregate size. Since electronic particle counters measure the envelope volume of particles, the volume of aggregates would be over-estimated.

It is unlikely that platelet thrombi growing from nidi on the tube wall were shed intermittently into the mainstream as observed in vivo. In patent blood vessels single platelets first adhere to a site of intimal injury and a mural thrombus grows into the vessel lumen as new platelets are recruited (Begent and Born, 1970; Arfors et al., 1976). In the absence of complete vessel occlusion, the thrombus eventually embolizes or sheds fragments once an unstable size is reached. The same process is often repeated continuously at a given site of vessel injury. If such a process were occurring in the tube in the present experiments there would have been large fluctuations in both the number and size of aggregates at

a given mean transit time instead of the observed continuous increase in the concentration of aggregates of progressively increasing size.

2. Platelet size

The mean platelet volume after platelet extraction from WB through Percoll was the same as that in PRP prepared under standardized conditions (Chapter III, this thesis). A mean value of $7.5 \mu\text{m}^3$, uncorrected for particle shape, was obtained that is consistent with previous estimates of uncorrected mean platelet volume obtained using electronic particle counters (Nakeff and Ingram, 1970; Paulus, 1975; Mundschenk et al., 1976; Holme and Murphy, 1980). The descriptive statistics of the distribution of platelet volume were virtually identical for the two methods of harvesting platelets. In both cases platelet volume closely follows a single log-normal model as previously reported for the distribution of platelet diameter, mass, and volume (von Behrens, 1972; Bahr and Zeitler, 1965; Paulus, 1975). Due to the high density of the Percoll suspending phase, not only does the present technique not extract a subset of platelets based on density, it demonstrates that only one continuous population of platelets exists with respect to size and density, and that this same population is normally retrieved in PRP.

Numerous reports of platelet size and density heterogeneity have indicated that a subset of large dense, more reactive platelets exists (Booyse et al., 1968; Karpatkin, 1969a,b; Corash et al., 1977). It is further contended that the large variance in platelet size is determined by platelet aging in the circulation and that the larger platelets are younger (Karpatkin, 1969b; Corash et al., 1978; Rand et al., 1981). The

increased reactivity of large platelets may primarily reflect their higher content of dense bodies and α -granules (Thompson et al., 1983; Corash, et al., 1984). It has also been suggested that platelet heterogeneity is determined by the factors controlling platelet production in the bone marrow (Paulus, 1975; Pennington et al., 1976). The log-normal size distribution has been modeled mathematically in terms of random factors controlling the rates of megakaryocyte membrane demarcation and platelet fragmentation (Paulus, 1975).

The converse of the hypothesis of a subset of more reactive platelets would suggest that some platelets within a normal population typically do not aggregate (Born and Hume, 1967; Nichols and Bosmann, 1979; Gear, 1982). The present work shows clearly that given a sufficient collision frequency and degree of platelet activation all platelets will aggregate. Neglecting the influence of microaggregates, the shape of the single platelet log-volume distribution remained symmetrical about the initial modal volume during aggregation indicating that all single platelets were being recruited equally-well into aggregates, as also observed by Belval et al. (1984) for shear-induced aggregation. The same extent and pattern of single platelet aggregation was also demonstrated at room temperature in citrated PRP at $1 \mu\text{M}$ ADP at $\bar{G} = 1800 \text{ s}^{-1}$ (Chapter III, this thesis) and in heparinized PRP at $0.2 \mu\text{M}$ ADP at $\bar{G} = 314 \text{ s}^{-1}$ (Chapter IV, this thesis). That this is so with ADP at room temperature where serotonin release from platelets is inhibited in citrated plasma (Valdorf-Hansen and Zucker, 1971) and often absent in heparinized plasma even at 37°C (Mustard et al. 1975; Skoza et al., 1967) suggests that more potent platelet agonists such as thrombin and collagen would also cause

all platelets in suspension to aggregate. Whatever the source of size heterogeneity, the present data confirm that platelet volume follows a single unimodal log-normal distribution, and that all platelets appear to aggregate with equal ability in the absence of release.

3. Shear-Induced and Spontaneous Platelet Aggregation

The higher degree of platelet aggregation in the controls in WB than in PRP indicates that some prior platelet activation may have been present in WB. At a plasma viscosity of $\eta = 1.8 \text{ mPa s}$ at 22°C and at exposure times of 43 s, the maximum mean tube shear stress, $\bar{\tau} = \eta\bar{G}$, of 3.2 N m^{-2} in the present experiments is below the threshold for shear-induced platelet aggregation and release in PRP (Brown et al., 1975; Belval et al., 1984) and WB (Dewitz et al., 1978; Jen and McIntire, 1984). Furthermore, no shear-induced platelet aggregation or release was present in PRP at the same shear rates and exposure times using the same flow system and method of measuring the concentration of single platelets and aggregates (Chapter III, this thesis). Since aggregation in the controls was greatest at $\bar{G} = 39.3 \text{ s}^{-1}$, where $\bar{\tau} = 0.07 \text{ N m}^{-2}$, it is highly unlikely that shear-induced platelet activation contributed significantly to platelet activation in the controls or the ADP-infusion runs.

It has been proposed that the transient accumulation of ADP as a result of rbc damage or lysis is responsible for both spontaneous aggregation in vitro (Hellem, 1960; Gaarder et al., 1961) and normal hemostasis in vivo (Born and Wehmeier, 1979). The extension of this mode of platelet activation to thrombosis has given impetus to this hypothesis. However, in the present experiments the maximum mean tube shear stress is

well below the threshold for shear-induced hemolysis at equivalent exposure times (Nevaril et al., 1968; Leverett et al., 1972). Hemolysis due to the interaction of rbc with surfaces (Bernstein et al., 1967) is only important at exposure times on the order of several minutes (Leverett et al., 1972; Hellums and Hardwick, 1981). Measurement of plasma TXB₂ and LDH concentrations confirm that ADP from platelet release or lysis, as well as hemolysis, did not contribute to the induction of aggregation in the present experiments.

The possibility of sublytic adenine nucleotide leakage from damaged rbc at low shear stresses is still a subject of debate. Spontaneous aggregation in stirred WB (Burgess-Wilson et al., 1984) or rotating plastic vials (Saniabadi et al., 1985) shows a positive correlation with hematocrit in the absence of detectable hemolysis, and can be reduced by the addition of enzymes that degrade ADP (Fox et al., 1982; Saniabadi et al., 1984). Other groups have failed to detect significant spontaneous aggregation in stirred WB (Riess et al., 1986; Abbate et al., 1986) and have reported instead diminished ADP-induced aggregation in WB compared to PRP. The discrepancy in reports of spontaneous aggregation may reflect differences in the method of extracting and handling blood. Spontaneous aggregation in PRP has been shown to be greater in samples stored at room temperature than at 37°C and to reach a maximum 2 - 3 hr after blood withdrawal, but is inhibited if the plasma pH is prevented from rising (Breddin et al., 1976). Moreover, there was no difference if the platelets were stored in WB or PRP before testing.

Due to the 10:1 ratio of ATP:ADP in rbc (Bishop, 1961), and the higher rate of dephosphorylation of ATP than ADP in plasma (Holmsen, 1982), the slow leakage of adenine nucleotides from rbc could transiently generate enough ADP to activate platelets. However, due to the short half life of both nucleotides (Holmsen, 1982), it is not likely that after the one hour incubation at room temperature sufficient ADP remains to activate platelets. The accumulation of ADP may actually promote a period of refractoriness to stimulation by exogenous ADP, as observed by Abbate et al. (1986). At shear stresses sufficient to generate significant hemolysis and release large amounts of adenine nucleotides, the ratio of ATP:ADP:AMP after 5 min. exposure was 1:2:20 with an ADP concentration of 0.6 μM (Reimers et al., 1984). At 30 s exposure to flow through collagen-coated glass tubes at a wall shear rate of 320 s^{-1} , Adams and Feuerstein (1981) did not measure any significant release of ATP and ADP from washed rbc. The possibility that slight shear-induced leakage of adenine nucleotides from platelets could generate sufficient ADP to induce aggregation during the 43 s of flow is also unlikely given the quantities released and half lives of ATP and ADP in plasma.

4. ADP-Induced Platelet Aggregation

(a) Physical Effect of Red Cells on Platelet Aggregation

The results of the present experiments clearly show that the rate of single platelet aggregation is much greater in WB than in PRP at the same mean tube shear rate and ADP concentration. The effect of shear rate on platelet aggregation in PRP and in WB can be interpreted in terms of the number of collisions between activated platelets and the fraction of collisions yielding stable aggregates. The kinetics of single platelet

aggregation in flowing suspensions has been previously described for dilute suspensions such as PRP in terms of classical two-body collision theory (Bell and Goldsmith, 1984; Chapter III, this thesis). The two-body collision frequency between spherical particles in Poiseuille flow is given by (Smoluchowski, 1917; Manley and Mason, 1952):

$$J = \frac{32}{3} G b^3 N, \quad [3]$$

where N is the number concentration of spheres of radius b . Application of Eq. [3] to collisions between unactivated or activated platelets [$N = N_{1,30}(0)$] requires that the cells be treated as the equivalent spherical particle. During the initial stages of single platelet aggregation, the number of collisions resulting in stable doublet formation is $J_c = \alpha_o J$, where α_o is the fraction of collisions yielding stable doublet formation, or the collision efficiency. Thus, the two-body collision frequency increases in proportion to the mean tube shear rate and the cube of the particle radius, but would be expected to decrease significantly in the later stages of aggregation when the single platelet concentration is much reduced. The frequency of collisions between particles of all sizes also decreases as the total particle concentration diminishes. The collision efficiency has been previously shown to decrease with increasing shear rate for both model particles (Curtis and Hocking, 1970; Zeichner and Schowalter, 1977; van de Ven and Mason, 1977), and for human platelets stimulated by shear rates greater than 5000 s^{-1} (Belval and Hellums, 1986) and by ADP at mean tube shear rates less than 2000 s^{-1} (Bell and Goldsmith, 1984; Chapter III, this thesis). However, the high collision frequencies accompanying high shear rates can often support a rate of aggregation that increases with increasing shear rate despite the decrease in collision efficiency. In Chapter III it was

shown that the average collision efficiencies for the male and female donors measured over the first 4.3 s of flow at $\bar{G} = 39.3, 314$ and 1800 s^{-1} were 0.204, 0.013, and 0.001, respectively, and that the greatest extent of aggregation at $\bar{t} = 43 \text{ s}$ occurred at $\bar{G} = 314 \text{ s}^{-1}$. The collision efficiency between platelets, unlike that of inert spheres, is also dependent on the time of exposure to the activating agent. Although collision efficiency showed a shear-dependent variation with time, in general at $\bar{G} > 39.3 \text{ s}^{-1}$, it increased between $\bar{t} = 8.6$ and 21 s. (Chapter III, this thesis).

In concentrated suspensions, rbc have been shown to increase the diffusivity of platelets in plasma by at least two orders of magnitude (Turitto et al., 1972) due to an increase in the lateral dispersion of platelets caused by the erratic motions of the rbc (Goldsmith, 1971; Goldsmith and Marlow, 1979). This could translate into a higher platelet-platelet collision frequency and, hence, a higher rate of aggregation for activated cells, but calculation of the collision frequency between platelets in WB is not possible using Eq. [3]. However, if one assumes that at the same ADP concentration, mean transit time and mean tube shear rate, the collision efficiency is the same in WB and PRP, then the collision frequency in WB can be estimated from comparison of the initial rates of single platelet aggregation. This approach assumes that multiple collisions between rbc, platelets and aggregates do not significantly alter the collision efficiency, particularly with regard to the velocity of approach and time of interaction during collision (Takamura et al., 1981), and to the stresses acting on the interacting cells. These assumptions do not seem to be too restrictive in light of

the avidity with which platelets cohere.

Considering that in the flow tube the initial single platelet concentration per unit volume of WB was ~ 60% of that of PRP, calculations using the initial rates of single platelet aggregation reveal that collision frequencies in WB are from 7 to 15 times greater than in PRP at $\bar{G} = 314$ and 39.3 s^{-1} , respectively, for both ADP concentrations. This corresponds to the level of augmented platelet diffusion in WB (Turitto et al., 1972) and indicates that enhanced collision frequencies in WB are sufficient to account for the higher rates of aggregation compared to PRP. Turitto and Baumgartner (1975) have used classical mass transport theory to show that the greater adhesion of platelets to subendothelium in WB than in PRP is due to the enhanced diffusion of platelets in the former. Higher collision frequencies could also be generated in tubular vessels if at the periphery, where the shear rate is highest, the platelet concentration is two-fold greater than at the center of the vessel, as observed by Tangelder et al. (1985). It is interesting to note that in the present experiments the platelet concentrations per microliter of plasma were approximately equal in WB and PRP.

Comparison of the rate and extent of ADP-induced aggregation with that in the controls supports the contention that platelet or rbc-derived ADP did not contribute to aggregation in either case. Since the infusion of $0.2 \mu\text{M}$ ADP induced much greater aggregation than did modified Tyrodes, and $1.0 \mu\text{M}$ ADP increased aggregation even further, the effects of ADP released from platelets and/or rbc in the submicromolar range would have produced more marked effects than observed. Instead, it is believed that

slight platelet activation is the same in WB and PRP and typical of normal blood extraction and handling where $\sim 30\%$ of platelets exhibit some degree of shape change (Frojmovic and Milton, 1982). Since shape change is generally considered a prerequisite for ADP-induced aggregation (Milton and Frojmovic, 1984), the high collision frequencies in WB enhance the formation of small weakly-bound aggregates at low shear rates that are easily disrupted at higher shear rates. The reappearance of aggregation in the controls at $\bar{G} = 1800 \text{ s}^{-1}$ may, however, represent a slight degree of platelet activation since the wall shear stress, $\sim 6 \text{ N m}^{-2}$, is near the threshold for shear-induced platelet activation. Reimers et al. (1984) reported that glutaraldehyde-fixed rbc depleted of ADP could augment shear-induced platelet aggregation over that in PRP after 5 min exposure to 5 N m^{-2} but only to $\sim 50\%$ of that by native rbc. Although the lateral dispersion of platelets, and hence the collision frequency, would be expected to be higher in suspensions of rigid rbc than of deformable rbc, this work is supportive of a mechanical effect of rbc on ADP-induced platelet aggregation.

(b) Low Shear Rates

At low levels of platelet activation ($0.2 \mu\text{M ADP}$), the primary determinants of the rate of single platelet aggregation are the collision frequency and the fluid shear stress inhibiting stable aggregate formation. At low shear rates, $\bar{G} = 39.3 \text{ s}^{-1}$, the rate of aggregation in both PRP and WB decreased steadily with time. In PRP this was due to the inability of the low collision frequency to sustain a high rate of aggregation (Bell and Goldsmith, 1984; Chapter III, this thesis) despite initial collision efficiencies of $\alpha_0 = 0.204$. Even at high levels of

platelet activation where the mean $\alpha_0 = 0.505$, the low collision frequency was unsuccessful in sustaining a high rate of aggregation. The higher collision frequencies in WB produced higher initial rates of single platelet aggregation but in this case the rapid formation of large aggregates led to an enormous depletion of particles and a steady decrease in the rate of aggregation with time. Mean tube shear stresses of 0.07 N m^{-2} did not appear to interfere with aggregate growth. At higher levels of platelet activation in WB ($1.0 \mu\text{M ADP}$), the rate of single platelet aggregation increased but followed the same pattern. The combination of a high collision frequency, low shear stress and the incorporation of red cells into platelet aggregates led to the formation of aggregates much greater than $10^5 \mu\text{m}^3$ within 1.7 s.

(c) High Shear Rates

The rates of single platelet aggregation in WB at low ADP concentrations support the finding in PRP of a two phase process of aggregation at higher shear rates. The sigmoid single platelet aggregation curves in PRP at $\bar{G} > 314 \text{ s}^{-1}$ were previously explained in terms of time-dependent bond heterogeneity with an initial weak bond gradually reinforced by a stronger bond (Chapter III, this thesis). This explains the absence of sigmoid aggregation curves at $\bar{G} = 39.3 \text{ s}^{-1}$ where the shear stress is not sufficient to break the weak bond. At higher shear rates the latency of the expression of the stronger bond was revealed through the progressively increasing lag phase with increasing mean tube shear rate. Despite high collision rates, the initial rate of aggregation decreased with increasing mean tube shear rate due to the decrease in collision efficiency.

The sigmoid aggregation curves found in PRP at $\bar{G} > 314 \text{ s}^{-1}$ are still present in WB but are much less pronounced. The higher collision frequency in WB partially compensates for low collision efficiencies at early exposure times. The similar rates of aggregation at $\bar{G} = 314$ and 1800 s^{-1} indicate that the collision frequency in WB is high enough not to limit the rate of single platelet aggregation despite the decrease in collision efficiency at the higher shear rate. This effect is missing in PRP, even at high levels of activation where, in the absence of collisions induced by the motion of rbc, the platelet collision frequency is more sensitive to single platelet and aggregate concentration and is not sufficient to override the effect of low collision efficiencies. The constant rate of aggregation up to $\bar{t} = 8.6 \text{ s}$ at $1.0 \text{ }\mu\text{M}$ ADP may reflect the presence of a higher concentration of aggregates of smaller size than at $\bar{G} = 39.3 \text{ s}^{-1}$. Although the rates of single platelet aggregation were rapid at the higher shear rates, aggregate size was severely limited from the outset. At $\bar{G} = 39.3 \text{ s}^{-1}$ small aggregates were rapidly incorporated into larger aggregates; however, a time-dependent inhibition of aggregate growth was apparent at $\bar{G} = 314 \text{ s}^{-1}$ ($\bar{\tau} = 0.6 \text{ N m}^{-2}$), and extremely marked at $\bar{G} = 1800 \text{ s}^{-1}$ ($\bar{\tau} = 3.2 \text{ N m}^{-2}$). At low levels of platelet stimulation the size range of aggregates decreased with increasing mean tube shear rate at exposure times less than 8.6 s. Even at high levels of platelet stimulation the high collision frequency at $\bar{G} = 1800 \text{ s}^{-1}$ allowed a very high rate of single platelet aggregation but aggregate size was not significantly greater than that at low levels of platelet activation until longer exposure times. The eventual growth of aggregates later in time at high shear rates coincides with the increase in collision efficiency discussed above, and likely reflects the expression of a more

shear-resistant bond.

5. Summary

The data of the present experiments indicate that red cells at normal hematocrits can increase the frequency of collisions between platelets by an order of magnitude at physiological shear rates. The enhanced collision frequencies lead to a high rate of single platelet aggregation but the shear-dependent kinetics of aggregate growth ultimately determines the extent of single platelet aggregation. Shear stresses of $\sim 0.07 \text{ N m}^{-2}$ do not inhibit aggregate growth; however, the rapid formation of large aggregates decreases the number of collisions between single cells and aggregates and limits the rate of aggregation. Higher shear stresses ($\tau > 0.6 \text{ N m}^{-2}$) limit aggregate size at short exposure times and, by maintaining relatively high particle concentrations, sustain a higher rate of single platelet aggregation. At longer exposure times, the expression of stronger bonds allows aggregates to grow to larger sizes. The incorporation of rbc into aggregates at shear rates found in the venous side of the vasculature (Turitto, 1982) suggests a more active role for rbc in promoting the growth of red thrombi in the veins than simply through the passive entrapment of rbc into a growing platelet-fibrin mesh. Although the involvement of wbc in platelet aggregation cannot be excluded in the present work, these cells were not significantly incorporated into platelet aggregates.

REFERENCES

- ABBATE, R., FAVILLA, S., BODDI, M., COSTANZO, G., AND PRISCO, D. (1986). Factors influencing platelet aggregation in whole blood. Am. J. Clin. Path. **86**, 91-96.
- ADAMS, G.A., AND FEUERSTEIN, I.A. (1981). Platelet adhesion and release: Interfacial concentration of released materials. Am. J. Physiol. **240**, H99-H108.
- ARFORS, K.-E., COCKBURN, J.S., AND GROSS, J.F. (1976). Measurement of growth rate of laser-induced intravascular platelet aggregation and the influence of blood flow velocity. Microvasc. Res. **11**, 79-87.
- BAHR, G.F., AND ZEITLER, E. (1965). The determination of the dry mass in populations of isolated particles. Lab. Invest. **14**, 955-977.
- BARTLETT, G.R. (1977). Metabolism by man of intravenously administered adenine. Transfusion **17**, 367-373.
- BEGENT, N., AND BORN, G.V.R. (1970). Growth rate in vivo of platelet thrombi, produced by iontophoresis of ADP, as a function of mean blood flow velocity. Nature **227**, 926-930.
- BELL, D.N., AND GOLDSMITH, H.L. (1984). Platelet aggregation in Poiseuille flow: II. Effect of shear rate. Microvasc. Res. **27**, 316-330.
- BELVAL, T., AND HELLUMS, J.D. (1986). The analysis of shear-induced platelet aggregation with population balance mathematics. Biophys. J. **50**, 479-487.
- BELVAL, T., HELLUMS, J.D., AND SOLIS, T. (1984). The kinetics of platelet aggregation induced by shear. Microvasc. Res. **28**, 279-288.
- BERNSTEIN, E.F., BLACKSHEAR, P.L., AND KELLER, K.H. (1967). Factors influencing erythrocyte destruction in artificial organs. Am. J. Surg. **114**, 126-138.

- BISHOP, C. (1961). Changes in nucleotides of stored or incubated human blood. Transfusion 1, 349-354.
- BOUYSE, F.M., HOVEKE, T.P., AND RAFELSON, M.E. (1968). Studies on human platelets. II. Protein synthetic activity of various platelet populations. Biochim. Biophys. Acta 157, 660-663.
- BORN, G.V.R., AND CROSS, M. (1963). The aggregation of blood platelets. J. Physiol. (London) 168, 178-195.
- BORN, G.V.R., AND HUME, M. (1967). Effects of the numbers and sizes of platelet aggregates on the optical density of plasma. Nature 215, 1027-1029.
- BORN, G.V.R., AND WEHMEIER, A. (1979). Inhibition of platelet thrombus formation by chlorpromazine acting to diminish haemolysis. Nature 282, 212-213.
- BREDDIN, K., GRUN, H., KRZYWANEK, H.J., AND SCHREMMER, W.P. (1976). On the measurement of spontaneous platelet aggregation. The platelet aggregation test III. Methods and first clinical results. Thromb. Haemost. 35, 667-691.
- BROWN, C.H., LEVERETT, L.B., LEWIS, C.W., ALFREY, C.P., AND HELLUMS, J.D. (1975). Morphological, biochemical, and functional changes in human blood platelets subjected to shear stress. J. Lab. Clin. Med. 86, 462-471.
- BURGESS-WILSON, M.E., GREEN, S., HEPTINSTALL, S., AND MITCHELL, J.R.A. (1984). Spontaneous platelet aggregation in whole blood: dependence on age and haematocrit. Lancet 2, 1213.
- CHANG, H.N., AND ROBERTSON, R. (1976). Platelet aggregation by laminar shear and Brownian motion. Ann. Biomed. Eng. 4, 151-183.
- CHIEN, S. (1975). Biophysical behavior of red cells in suspensions. In "The Red Cell" (D. MacN. Surgenor, ed.), pp. 1031-1133, Academic Press, New York.
- COLANTUONI, G., HELLUMS, J.D., MOAKE, J.L., AND ALFREY, C.P. (1977). The response of human platelets to shear stress at short exposure times. Trans. Am. Soc. Artif. Intern. Organs 23, 626-631.

- CORASH, L., COSTA, J.L., SHAFER, B., DONLON, J.A., AND MURPHY, D. (1984). Heterogeneity of human whole blood platelet subpopulations. III. Density-dependent differences in subcellular constituents. Blood 64, 185-193.
- CORASH, L., SHAFER, B., AND PERLOW, M. (1978). Heterogeneity of human whole blood platelet subpopulations. II. Use of a subhuman primate model to analyze the relationship between density and platelet age. Blood 52, 727-734.
- CORASH, L., TAN, H., AND GRALNICK, H.R. (1977). Heterogeneity of human whole blood platelet subpopulations. I. Relationship between buoyant density, cell volume, and ultrastructure. Blood 49, 71-87.
- CURTIS, A.S.G., AND HOCKING, L.M. (1970). Collision efficiency of equal spherical particles in shear flow. Trans. Faraday Soc. 66, 1381-1390.
- DE PIERRE, J.W., AND KARNOSKY, M. (1974). Evidence for an ecto-adenosine monophosphate, adenosine triphosphate and p-nitrophenyl phosphatase. J. Biol. Chem. 249, 7111-7120.
- DEWITZ, T.S., MARTIN, R.R., SOLIS, R.T., HELLUMS, J.D., AND MCINTYRE, L.V. (1978). Microaggregate formation in whole blood exposed to shear stress. Microvasc. Res. 16, 263-271.
- DIDISHEIM, P. (1968). Inhibition by dipyridamole of arterial thrombosis in rats. Thromb. Diath. Haemorrh. 20, 256-266.
- DITTMER, D.S. (ed.) (1961). "Blood and Other Body Fluids", p. 102 Federation of American Society for Experimental Biology, Washington, D.C.
- DUKE, W.W. (1910). The relation of blood platelets to hemorrhagic disease: description of method for determining the bleeding time and report of three cases of hemorrhagic disease relieved by transfusion. J. Am. Med. Assoc. 55, 1185-1192.
- DOCUMENTA GEIGY (1962). "Scientific Tables" (K. Diem, ed.), p.164. Geigy Pharmaceuticals, Montreal, QC.

- EMMONS, P.R., HARRISON, M.G.J., HONOUR, A.J., AND MITCHELL, J.R.A. (1965). Effect of a pyrimidopyrimidine derivative on thrombus formation in the rabbit. Nature, **208**, 255-257.
- FOX, S., BURGESS-WILSON, M.E., HEPTINSTALL, S., AND MITCHELL, J.R. (1982). Platelet aggregation in whole blood determined using the Ultra-Flo 100 platelet counter. Thromb. Haemost. **48**, 327-329.
- FROJMOVIC, M.M., AND MILTON, J.G. (1982). Human platelet size, shape, and related functions in health and disease. Physiol. Rev. **62**, 185-261.
- GAUTHIER, F.P., GOLDSMITH, H.L., AND MASON, S.G. (1972). Flow of suspensions through tubes. X. Liquid drops as models of erythrocytes. Biorheology **9**, 205-244.
- GAARDER, A., JONSEN, J., LALAND, S., HELLEM, A., AND OWREN, P.A. (1961). Adenosine diphosphate in red cells as a factor in the adhesiveness of human blood platelets. Nature **192**, 531-532.
- GEAR, A.R.L. (1982). Rapid reactions of platelets studied by a quenched-flow approach: Aggregation kinetics. J. Lab. Clin. Med. **100**, 866-886.
- GOLDSMITH, H.L. (1971). Red cell motions and wall interactions in tube flow. Fed. Proc. **30**, 1578-1588.
- GOLDSMITH, H.L. (1972). The flow of model particles and blood cells and their relation to thrombogenesis. In "Advances in Hemostasis and Thrombosis" (T.H. Spaet, ed.), pp. 97-139, Grune and Stratton, New York.
- GOLDSMITH, H.L. AND MARLOW, J.C. (1979). Flow behavior of erythrocytes. II. Particle motions in sheared suspensions of ghost cells. J. Colloid Interface Sci. **71**, 383-407.
- GOLDSMITH, H.L., AND MASON, S.G. (1967). The microrheology of dispersions. In "Rheology: Theory and Applications" (F.R. Eirich, ed.), Vol. 4, pp. 85-250. Academic Press, New York.
- GRESELE, P., ARNOUT, J., DECKMYN, H., AND VERMYLEN, J. (1985). Combining antiplatelet agents: potentiation between aspirin and dipyridamole. Lancet **1**, 937-938.

- GRESELE, P., ARNOUT, J., DECKMYN, H., AND VERMYLEN, J. (1986). Mechanism of the antiplatelet action of dipyridamole in whole blood: modulation of adenosine concentration and activity. Thromb. Haemost. 55, 12-18.
- GRESELE, P., ZOJA, C., DECKMYN, H., ARNOUT, J., VERMYLEN, J., AND VERSTRAETE, M. (1983). Dipyridamole inhibits platelet aggregation in whole blood. Thromb. Haemost. 50, 852-856.
- HARKER, L.A., AND KADATZ, R.A. (1983). Mechanism of action of dipyridamole. Thromb. Res. Suppl. 4, 39-46.
- HARKER, L.A., AND SCHLICHTER, S.J. (1970). Studies of platelet and fibrinogen kinetics in patients with prosthetic heart valves. N. Eng. J. Med. 283, 1302-1305.
- HARRISON, M.J., AND MITCHELL, J.R. (1966). The influence of red blood-cells on platelet adhesiveness. Lancet 2, 1163-1164.
- HELLEM, A.J. (1960). The adhesiveness of human blood platelets in vitro. Scand. J. Clin. Lab. Invest. 12, (Suppl. 51), 1-117.
- HELLEM, A.J., BORCHGRENVINK, F., AND AMES, S.B. (1961). The role of red cells in hemostasis: the relation between haematocrit, bleeding time and platelet adhesiveness. Br. J. Haematol. 7, 42-50.
- HELLEM, A.J., ODEGAARD, A.E., AND SKALHEGG, B.A. (1963). Investigation of adenosine diphosphate (ADP) induced platelet adhesiveness in vitro. Part I. The ADP-platelet reaction in various experimental conditions. Thromb. Diath. Haemorrh. 10, 61-70.
- HELLUMS, J.D., AND HARDWICK, R.A. (1981). Response of platelets to shear stress - a review. In "The Rheology of Blood, Blood Vessels and Associated Tissues" (D.R. Gross and N.H.C. Hwang, eds.) pp. 160-183, Sijthoff and Noordhoff, Rockville, MD.
- HOLME, S., AND MURPHY, S. (1980). Coulter Counter and light transmission studies of platelets exposed to low temperature, ADP, EDTA, and storage at 22°. J. Lab. Clin. Med. 96, 480-493.

- HOLMSEN, H. (1982). Platelet secretion. In "Hemostasis and Thrombosis, Basic Principles and Clinical Practice" (R.W. Colman, J. Hirsh, V.J. Marder and E.W. Salzman, eds.), pp. 390-403, J.B. Lippincott, Philadelphia.
- HOLMSEN, H., DAY, H.J., AND STORM, E. (1969). Adenine nucleotide metabolism of blood platelets. VI. Subcellular localization of nucleotide pools with different functions in the platelet release reaction. Biochem. Biophys. Acta 186, 254-266.
- HYMAN, W.A. (1972). Shear flow over a protrusion from a plane wall. J. Biomech. 5, 45.
- JEN, C.J., AND MCINTIRE, L.V. (1984). Characteristics of shear-induced aggregation in whole blood. J. Lab. Clin. Med. 103, 115-124.
- KARINO, T., AND GOLDSMITH, H.L. (1979). Adhesion of human platelets to collagen on the walls distal to a tubular expansion. Microvasc. Res. 17, 238-262.
- KARPATKIN, S. (1969a). Heterogeneity of human platelets. I. Metabolic and kinetic evidence suggestive of young and old platelets. J. Clin. Invest. 48, 1073-1082.
- KARPATKIN, S. (1969b). Heterogeneity of human platelets. II. Functional evidence suggestive of young and old platelets. J. Clin. Invest. 48, 1083-1087.
- KENNEY, J.K., AND KEEPING, E.S. (1951). "Mathematics of Statistics" (Part Two). D. Van Nostrand, Toronto, ON.
- KINCAID-SMITH, P. (1969). Modification of the vascular lesions of rejection in cadaveric renal allografts by dipyridamole and anticoagulants. Lancet 2, 920-922.
- LEVERETT, L.B., HELLUMS, J.D., ALFREY, C.P., AND LYNCH, E.C. (1972). Red blood cell damage by shear stress. Biophys. J. 12, 257-273.
- LILLIEFORS, H.W. (1967). On the Kolmogorov-Smirnov test for normality with mean and variance unknown. Am. Statist. Assoc. J. 62, 399.

- LIVIO, M., GOTTI, E., MARCHESI, D., MECCA, G., REMUSSI, G., AND DE GAETANO, G. (1982). Uraemic bleeding: role of anaemia and beneficial effect of red cell transfusion. Lancet II, 1013-1015.
- MANLEY, R. ST.J., AND MASON, S.G. (1952). Particle motions in sheared suspensions. II. Collisions of uniform spheres. J. Coll. Sci. 7, 354-369.
- MAYER, J.E., AND HAMMOND, G.L. (1973). Dipyridamole and aspirin tested against an experimental model of thrombosis. Ann. Surg. 178, 108-112.
- MCPHERSON, V.J., ZUCKER, M.B., FRIEDBERG, N.M., AND RIFKIN, P.L. (1974). Platelet retention in glass bead columns: further evidence for the importance of ADP. Blood 44, 411-425.
- MILLS, D.C.B., ROBB, I.A., AND ROBERTS, G.C.K. (1968). The release of nucleotides, 5-hydroxytryptamine and enzymes from human blood platelets during aggregation. J. Physiol. 195, 715-729.
- MILTON, J.G., AND FROJMOVIC, M.M. (1984). Adrenaline and ADP-induced platelet aggregation require shape change: importance of pseudopods J. Lab. Clin. Med. 104, 805-815.
- MUNDSCHENK, D.D., CONNELLY, D.P., WHITE, J.G., AND BRUNNING, R.D. (1976). An improved technique for the electronic measurement of platelet size and shape. J. Lab. Clin. Med. 88, 301-315.
- MUSTARD, J.F., PERRY, D.W., KINLOUGH-RATHBONE, R.L., AND PACKHAM, M.A. (1975). Factors responsible for ADP-induced release reaction of human platelets. Am. J. Physiol. 228, 1757-1765.
- NAKEFF, A., AND INGRAM, M. (1970). Platelet count:volume relationships in four mammalian species. J. Appl. Physiol. 28, 530-533.
- NEVARIL, C.G., LYNCH, E.C., ALFREY, C.P., AND HELLUMS, J.D. (1968). Erythrocyte damage and destruction induced by shearing stress. J. Lab. Clin. Med. 71, 784-790.
- NICHOLS, A.R., AND BOSMANN, H.B. (1979). Platelet aggregation: newly quantified using nonempirical parameters. Thromb. Haemost. 42, 679-693.

- PARKER, J.C. (1970). Metabolism of external adenine nucleotides by human red blood cells. Am. J. Physiol. 218, 1568-1574.
- PAULUS, J. (1975). Platelet size in man. Blood 46, 321-336.
- PENNINGTON, D.G., STREATFIELD, K., ROXBURGH, A.E. (1976). Megakaryocytes and the heterogeneity of circulating platelets. Br. J. Haematol. 34, 639-653.
- RAND, M.L., GREENBERG, J.P., PACKHAM, M.A., AND MUSTARD, J.F. (1981). Density subpopulations of rabbit platelets: Size, protein, and sialic acid content, and specific radioactive changes following labelling with ³⁵S-sulfate in vivo. Blood 57, 741-746.
- REIMERS, R.C., SUTERA, S.P., AND JOIST, J.H. (1984). Potentiation by red blood cells of shear-induced platelet aggregation: relative importance of chemical and physical mechanisms. Blood 64, 1200-1206.
- RIESS, H., BRAUN, G., BREHN, G., AND HILLER, E. (1986). Critical evaluation of platelet aggregation in whole human blood. Am. J. Clin. Path. 85, 50-56.
- SANIABADI, A.R., LOWE, G.D.O., BARBENEL, J.C., AND FORBES, C.D. (1984). A comparison of spontaneous platelet aggregation in whole blood with platelet rich plasma: additional evidence for the role of ADP. Thromb. Haemost. 51, 115-118.
- SANIABADI, A.R., LOWE, G.D.O., BARBENEL, J.C., AND FORBES, C.D. (1985). Further studies on the role of red blood cells in spontaneous platelet aggregation. Thromb. Res. 38, 225-232.
- SKOZA, L., ZUCKER, M.B., JERUSHALMY, Z., AND GRANT, R. (1967). Kinetic studies of aggregation induced by adenosine diphosphate and its inhibition by chelating agents, guanido compounds, and adenosine. Thromb. Diath. Haemorrh. 18, 713-725.
- SMOLUCHOWSKI, M. VON (1917). Versuch einer mathematischen Theorie der Koagulationskinetik kolloider Lösungen. Z. Physik. Chem. 92, 129-168.

- SMYTHE, W.R. (1964). Flow around spheroids in a circular tube. Phys. Fluids 7, 633-638.
- SOKAL, R.R., AND ROHLF, F.J. (1969). "Biometry". Freeman, San Francisco, CA.
- STORMORKEN, H. (1971). Platelets, thrombosis and hemolysis. Fed. Proc. 30, 1551-1555.
- SULLIVAN, J.M., HARKEN, D.W., AND GORLIN, R. (1971). Pharmacologic control of thromboembolic complications of cardiac-valve replacement. N. Eng. J. Med. 284, 1391-1394.
- TAKAMURA, K, GOLDSMITH, H.L., AND MASON, S.G. (1981). The microrheology of colloidal dispersions. XII. Trajectories of orthokinetic pair collisions of doublets of spheres in a simple electrolyte. J. Colloid Interface Sci. 82, 175-189.
- TANGELDER, G.J., TEIRLINCK, H.C., SLAAF, D.W., AND RENEMAN, R.S. (1985). Distribution of blood platelets in flowing arterioles. An. J. Physiol. 248, H318-H323.
- TANGELDER, G.F., SLAAF, D.W., TEIRLINCK, H.C., ALEWIJNGE, R., AND RENEMAN R.S. (1982). Localisation with a thin optical section of fluorescent blood platelets flowing in a microvessel. Microvasc. Res. 23, 214-230.
- THOMPSON, C.B., JAKUBOWSKI, J.A., QUINN, P.G., DEYKIN, D., AND VALERI, R.C. (1983). Platelet size as a determinant of platelet function. J. Lab. Clin. Med. 101, 205-213.
- TURITTO, V.T. (1982). Blood viscosity, mass transport and thrombogenesis. In "Progress in Thrombosis and Hemostasis", Vol. 6 (T.H. Spaet, ed.), pp. 139-177, Grune and Stratton, New York.
- TURITTO, V.T., AND BAUMGARTNER, H.R. (1975). Platelet interaction with subendothelium in a perfusion system: physical role of red blood cells. Microvasc. Res. 9, 335-344.
- TURITTO, V.T., AND BAUMGARTNER, H.R. (1982). Platelet surface interactions. In "Hemostasis and Thrombosis, Basic Principles and Clinical Practice" (R.W. Colman, J. Hirsh, V.J. Marder and E.W. Salzman, eds.), pp. 354-379, J.B. Lippincott, Philadelphia.

- TURITTO, V.T., BENIS, A.M., AND LEONARD, E.F. (1972). Platelet diffusion in flowing blood. Ind. Eng. Chem. Fundam. 11, 216-223.
- WHITMORE, R.L. (1968). "Rheology of the Circulation" Pergamon Press, Oxford.
- VALDORF-HANSEN, J.F., AND ZUCKER, M.B. (1971). Effect of temperature and inhibitors on serotonin-¹⁴C release from human platelets. Am. J. Physiol. 220, 105-111.
- VAN DE VEN, T.G.M., AND MASON, S.G. (1977). The microrheology of colloidal dispersions. VII. Orthokinetic doublet formation of spheres. Coll. Polymer Sci. 255, 468-479.
- VON BEHRENS, W.E. (1972). Platelet size. Thesis submitted for the degree of Doctor of Medicine, University of Adelaide, Adelaide, South Australia.
- YOUNG, I.T. (1977). Proof without prejudice: Use of the Kolmogorov-Smirnov test for the analysis of histograms from flow systems and other sources. J. Histochem. Cytochem. 25, 935-941.
- YOUNG, D.F., CHOLUIN, N.R., ROTH, A.C. (1975). Pressure drop across artificially induced stenoses in the femoral arteries of dogs. Circ. Res. 36, 735-743.
- YUNG, W., AND FROJMOVIC, M.M. (1982). Platelet aggregation in laminar flow. Part I. Adenosine diphosphate concentration, time and shear rate dependence. Thromb. Res. 28, 367-378.
- ZAWILSKA, K.M., BORN, G.V.R., AND BEGENT, N.A. (1982). Effect of ADP-utilizing enzymes on the arterial bleeding time in rats and rabbits. Br. J. Haematol. 50, 317-325.
- ZEICHNER, G.R., AND SCHOWALTER, W.R. (1977). Use of trajectory analysis to study stability of colloidal dispersions in flow fields. Al. Chem. Eng. J. 23, 243-254.
- ZUCKER, M.B., RIFKIN, P.L., FRIEDBERG, N.M., AND COLLER, B.S. (1972). Mechanisms of platelet function as revealed by the retention of platelets in glass bead columns. Ann. N.Y. Acad. Sci. 201, 138-144.

CHAPTER VI

GENERAL CONCLUSIONS

CLAIMS TO ORIGINAL RESEARCH

SUGGESTIONS FOR FURTHER WORK

GENERAL CONCLUSIONS

This thesis has examined the effect of shear rate on the ADP-induced aggregation of human platelets in suspensions flowing through tubes. Analysis of the complete particle volume distribution from $1 - 10^5 \mu\text{m}^3$ allowed the simultaneous measurement of the rate of change in the concentration of single platelets and aggregates. The kinetics of aggregation were explained in terms of the product of the frequency and efficiency of collisions between activated cells. The collision frequency is dependent on the shear rate and particle concentration while the collision efficiency is governed by the magnitude of the fluid shear stress in relation to the level of platelet activation and the time after stimulation. This work provides the first rheological evidence for heterogeneity in the bonds mediating stable aggregation at physiological shear rates. It is also quite apparent that the conditions which lead to the greatest aggregation of single platelets do not necessarily produce the largest aggregates. In the following discussion low, moderate and high shear rates refer to $\bar{G} = 39.3, 314, \text{ and } 1800 \text{ s}^{-1}$, respectively, and low and high levels of platelet stimulation refer to $0.2 \text{ and } 1.0 \mu\text{M ADP}$, respectively.

It was found that at the low concentration of ionized calcium, $[\text{Ca}^{2+}]$, in citrated PRP, the formation of stable aggregates was highly dependent on mean transit time and mean tube shear rate. At low shear rates and low levels of platelet stimulation, the rapid formation of a relatively weak bond led to high initial rates of aggregation and the formation of aggregates having a broad distribution of size. The strength of this bond gradually diminished with time, and the rate of aggregation

decreased steadily due to the inability of the low collision frequency to sustain a high rate of aggregation. The weak strength of the early bond was revealed by a progressively increasing delay in the onset of aggregation with increasing shear rate. The collision efficiency at early exposure times decreased with increasing shear rate in accordance with established theory for colloidal-sized particles. At longer transit times, however, the rate of aggregation at higher shear rates increased due to an increase in the efficiency of collision. This may reflect the gradual expression of a more shear-resistant platelet-platelet bond, perhaps through an increase in the number or affinity of fibrinogen binding sites. The maximum extent of aggregation was reached at $\bar{G} = 314 \text{ s}^{-1}$ as a result of the combination of a sufficiently high collision frequency and collision efficiency. The magnitude of the collision efficiency at high shear rates, however, was much less than at early exposure times at low shear rates and, consequently, a high collision frequency was required to support a high rate of aggregation. The induction of aggregation at $\bar{G} = 1800 \text{ s}^{-1}$ after an $\sim 11 \text{ s}$ delay illustrates the emergence of the stronger platelet-platelet bond. Due to the extremely low collision efficiency only a high collision frequency was able to support a high rate of aggregation. At this level of platelet stimulation aggregate growth rate decreased with increasing shear rate.

At high levels of platelet stimulation, the rates of aggregation were generally much higher than at low levels of stimulation, as reflected in the much higher collision efficiencies. As observed at low levels of platelet stimulation, the rate of aggregation at low shear rates exhibited a steady decrease with time due to a steady decrease in collision

efficiency. Aggregate size was only marginally greater than at the lower level of platelet stimulation. The maximum rate of single platelet aggregation, however, occurred at the highest shear rate, $\bar{G} = 1800 \text{ s}^{-1}$. The effect of even a small increase in collision efficiency is readily apparent in the presence of a high collision frequency. Even though all platelets were observed to aggregate, aggregate size was severely limited at the mean tube shear stress of 3.2 N m^{-2} with all aggregates between 10^4 and $10^5 \mu\text{m}^3$ after 43 s of flow. At high shear rates, a slight lag phase preceding aggregation remained and the collision efficiency increased with time indicating that the time-dependent expression of stronger platelet-platelet bonds persists at high levels of platelet stimulation.

The high rate of aggregation in whole blood was attributed to an enormous increase in the platelet-platelet collision frequency caused by the erratic motions of the red cells. As a consequence, the rates of aggregation in whole blood are much less affected by decreases in collision efficiency and particle concentration. Thus, despite the decrease in the collision efficiency with time at low shear rates in PRP, a high rate of aggregation was maintained at this shear rate in whole blood. At high shear rates the initial lag preceding aggregation in PRP was almost absent in whole blood and aggregation proceeded at a high initial rate. At high levels of platelet stimulation, the extent of single platelet aggregation increased with increasing shear rate. At $\bar{G} = 1800 \text{ s}^{-1}$ fewer than 5% of the initial single platelets remained after only 8.6 s. Moreover, the much higher collision frequency could sustain a high rate of aggregation despite the enormous depletion in the single platelet concentration. This effect also promoted collisions between

aggregates, and consequently their growth to much larger sizes than at the same shear rate and ADP concentration in PRP. The work in whole blood demonstrates the ability of a high collision frequency to produce a high rate of aggregation in the presence of a small collision efficiency. The increased platelet-platelet collision frequency caused by red cells at all shear rates and the incorporation of red cells into aggregates at low shear rates suggest a stronger role than generally considered for red cells in promoting platelet aggregation in regions of the vasculature where shear rates are low.

A steadily increasing rate of aggregation and a time-dependent increase in the collision efficiency was also observed in heparinized-PRP and hirudinized-PRP. The much higher rate of aggregation at physiological $[Ca^{2+}]$, may have reflected a higher initial rate of fibrinogen binding. However, the steadily increasing collision efficiency suggests the continued expression of binding sites at high $[Ca^{2+}]$. Aggregate size was also much greater than in citrated PRP, and this suggests a role for ionized calcium in both the initial fibrinogen binding and stability of large aggregates. A persistent sex difference in citrated PRP was shown to be due to an artifact of platelet preparation. Because of the consistently lower hematocrits for female donors, the dilution of citrate in plasma is greater, and the $[Ca^{2+}]$ correspondingly higher, than in the plasma of male donors. Platelet aggregation was shown to be very sensitive to small changes in $[Ca^{2+}]$ in the low range of $[Ca^{2+}]$ normally present in citrated PRP.

Single platelet volume in citrated, heparinized, and hirudinized

plasma, and in citrated whole blood followed a single unimodal log-normal distribution. Under conditions of high platelet stimulation or high $[Ca^{2+}]$ in PRP, or the high collision frequencies in whole blood at low platelet stimulation and low $[Ca^{2+}]$, all platelets were observed to aggregate equally well and no platelets remained unaggregated after 43 s of flow. Finally, the results in citrated whole blood show that white blood cells are not significantly incorporated into platelet aggregates.

CLAIMS TO ORIGINAL RESEARCH

These are summarized as follows:

1. A mixing chamber and flow system were designed to allow the rapid exposure of all platelets in suspension to an aggregating agent prior to flowing through fixed lengths of polyethylene tubing corresponding to preset mean transit times, \bar{t} , from 0.2 to 86 s. The flow rate and agonist concentration were adjusted independently to cover the range of mean tube shear rate, \bar{G} , from 39.3 to 1800 s^{-1} at both 0.2 and 1.0 μM ADP.

2. A particle counting and sizing technique were developed that allowed the measurement of the continuous distribution of single platelet and aggregate volume over the range 1 - 10⁵ μm^3 in the fixed effluent suspensions. Statistical analysis of the particle volume histograms allowed the characterization of the distribution of single platelet volume in terms of the log-normal model, and the detection of contaminating microaggregates.

3. A large group of blood donors was tested over a large range of mean tube shear rate at several mean transit times. As a consequence, average log-volume histograms were generated for multiple donors at each mean transit time by first transforming the individual histograms into standard normal deviates of their respective mean single platelet volume and standard deviation. As such, the shape of the individual histograms was preserved during the averaging procedure.

4. In citrated PRP at $0.2 \mu\text{M}$ at room temperature, the rate of aggregation was dependent on mean transit time and mean tube shear rate. A progressively increasing lag phase with increasing mean tube shear rate preceded aggregation. The maximum extent of aggregation was reached at $\bar{G} = 314 \text{ s}^{-1}$ but aggregate size decreased from $\bar{G} = 39.3$ to 1800 s^{-1} . The increasing rates of aggregation and collision efficiency with time at high shear rates were explained in terms of a heterogeneity in platelet-platelet bonds.

5. At $1.0 \mu\text{M}$ ADP the lag phase was still present. The rate of aggregation increased with increasing mean tube shear rate up to $\bar{G} = 1800 \text{ s}^{-1}$ but aggregate size was severely limited.

6. A strong sex difference was found in citrated PRP over the range of \bar{G} from 39.3 to 1800 s^{-1} and \bar{t} from 0.2 to 86 s . This was shown to be an artifact introduced by the citrate anticoagulant. The sex difference was reversed by accounting for the differences in donor hematocrit that generate small but significant differences in plasma $[\text{Ca}^{2+}]$.

7. No sex difference was found in the physiological range of $[\text{Ca}^{2+}]$ in heparinized or hirudinized plasma. In both cases the rate of aggregation and size of aggregates were much greater than in citrated plasma.

8. A method of extracting single platelets and aggregates from glutaraldehyde-fixed whole blood was developed in which the red cells were removed by centrifugation through Percoll.

9. The rate and extent of aggregation was much higher in whole blood than in PRP due to much higher platelet and aggregate collision frequencies caused by the motion of the red cells. At $1.0 \mu\text{M}$ ADP and at $\bar{G} = 39.3 \text{ s}^{-1}$, red cells were incorporated into aggregates. At higher shear rates red cells were excluded from aggregates. White blood cells were not incorporated into aggregates.

10. Under the appropriate conditions in citrated, heparinized and hirudinized PRP, as well as in citrated whole blood all platelets were observed to aggregate and no population of nonaggregating platelets was detected.

SUGGESTIONS FOR FURTHER WORK

1. By using washed platelet suspensions the effects of fibrinogen concentration and of purified von Willebrand factor at high and low $[Ca^{2+}]$ can be investigated in terms of the time- and shear rate-dependency in the expression of stable bonds between platelets in flowing suspensions.

2. The effects of shear rate on platelet aggregation in heparinized and hirudinized PRP can be tested to determine if the same shear-dependent delay precedes aggregation at high $[Ca^{2+}]$ and to see if aggregate size is also limited under these conditions at high shear rates. Platelet aggregation in heparinized and hirudinized whole blood can also be examined to measure the effects of high $[Ca^{2+}]$ and high collision frequencies at low and high shear stresses.

3. The effects of red cells in augmenting the collision frequency between platelets can be further examined by adjusting the hematocrit over a large range. Specific platelet release inhibitors as well as enzyme systems that degrade ADP can be used to establish if the greater platelet aggregation in the controls in whole blood is due to a mechanical effect or due to leakage of ADP from platelets and/or red cells.

APPENDIX I

APERTURE-IMPEDANCE PARTICLE COUNTERS

NOMENCLATURE

a, b	semi-axis of revolution, semi-equatorial axis of ellipsoid of revolution
d	equatorial diameter of right cylinder
i	aperture current
l, L	cylinder, aperture length
m	spheroid axis ratio, a/b
q_1	cross-sectional area normal to aperture axis of the face of right cylinder
q_2	cross-sectional area of aperture
R, R_0	radial distance, aperture radius
Re	tube Reynolds number
ΔU	voltage increment
V; ΔV	aperture volume; particle volume
x	axial distance

GREEK

$\delta; \delta'$	fractional particle volume, $\Delta V/V$; $\delta/(\delta-1)$
γ_e, γ'_e	shape factor for ellipsoid of revolution with a-axis aligned with aperture axis, with b-axis aligned

γ_s

shape factor for sphere

$\bar{\gamma}$

average shape factor

ρ, ρ_1, ρ_2

effective suspension, particle, electrolyte
resistivity

Proper size and concentration measurement of particles in suspension using an aperture-impedance particle counter requires knowledge of both the underlying theory and the limitations of the instrument. In light of these considerations a specialized technique was developed to derive a continuous size distribution of single platelets and aggregates from measurements of a single suspension. The following is a description of the sizing and counting principle leading to the design of the present technique.

THEORY

1. Principle and General Description

The aperture-impedance counter is essentially an electrical transducer for detecting and sizing particles suspended in an electrolytic medium. This transducer consists of a cylindrical aperture separating two electrode chambers filled with electrolyte (Fig. 1). The aperture is commonly fabricated from ruby or glass with a diameter, $2R_0$, between $3 \mu\text{m}$ and 1 mm , and a nominal length, L , $= 2R_0$.

When a constant current d.c. voltage is applied between the electrodes, the aperture and a small hemispherical volume at either end of it provide the major electrical resistance. A known volume of electrolyte containing the particles to be measured is drawn through the aperture from the outer electrode chamber. As a particle passes through the aperture it displaces electrolyte, producing a change in electrical resistance observed as a voltage pulse. Voltage pulses measured across the two electrodes are then amplified and fed to a threshold circuit with an adjustable level. Pulses reaching or exceeding this level are counted.

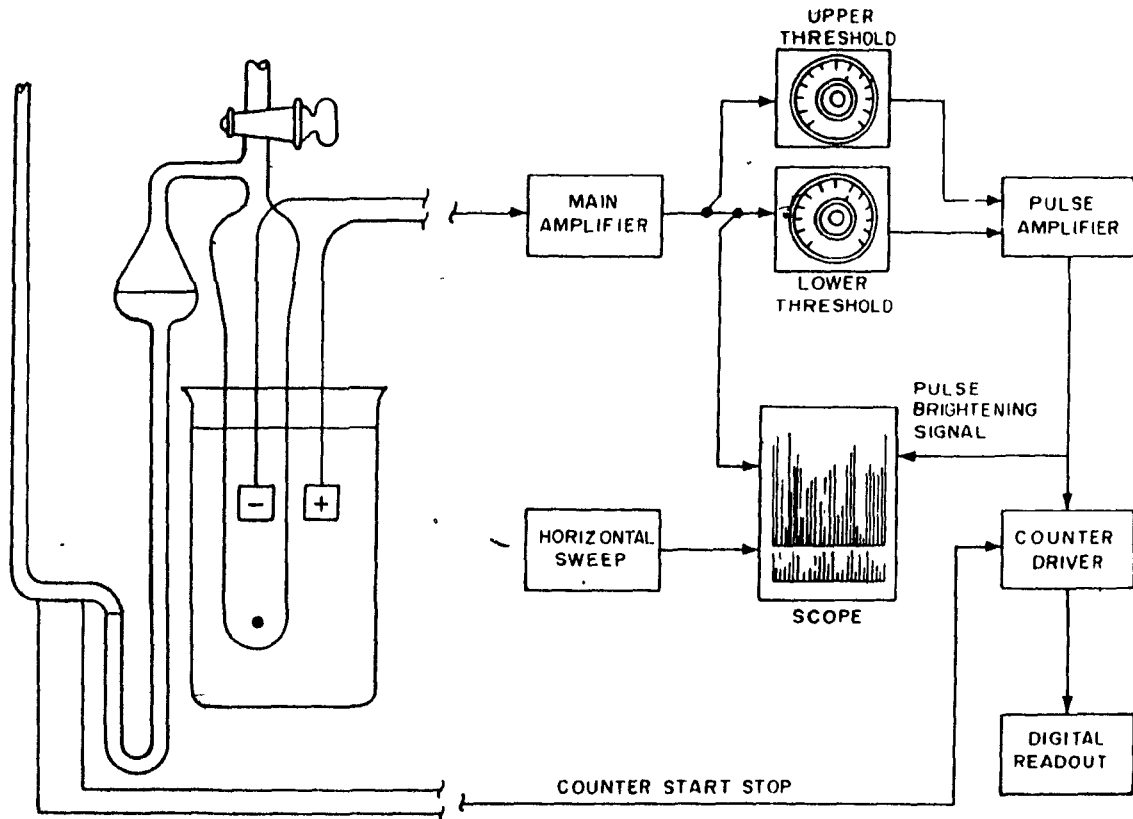


Figure 1: Aperture-Impedance Particle Counter

Schematic of a conventional counter showing the mercury manometer, as well as the glass aperture and electrodes immersed in electrolyte. Preset independent lower and upper voltage thresholds select a particle size window (from Jones, 1982).

Particle volume vs frequency distributions can be generated with the aid of multichannel pulse-height analyzers. Here, the voltage pulses are collated into a spectrum of pulse-heights in which the channel number (voltage increment) is proportional to the volume of the particle sensed.

2. Pulse Height vs Particle Volume

Originally, the theory of the relationship between pulse height and particle volume relied on the following assumptions:

(a) The passage of individual particles occurs at random and the particles are evenly distributed across the aperture cross-section.

(b) The electrically effective volume of the particle in the aperture is that of a right cylinder of length $< L$ and of the same resistivity as the particle and aligned with the aperture axis (Fig. 2).

(c) The aperture forms a cylindrical resistor in which current density is uniform.

The voltage pulse height produced by a particle in the aperture, ΔU , was given by (Kubitschek, 1958):

$$\frac{\Delta U}{i} = \frac{\rho_2 \Delta V}{q_2^2} \left(\frac{1}{1 - \rho_2 / \rho_1} - q_1 / q_2 \right)^{-1} \quad [1]$$

where i = constant aperture current

ΔV = particle volume

ρ_1 = effective particle resistivity

ρ_2 = electrolyte resistivity

q_1 = cross-sectional area normal to aperture axis of the face of the equivalent right cylinder of a particle

q_2 = cross-sectional area of aperture.

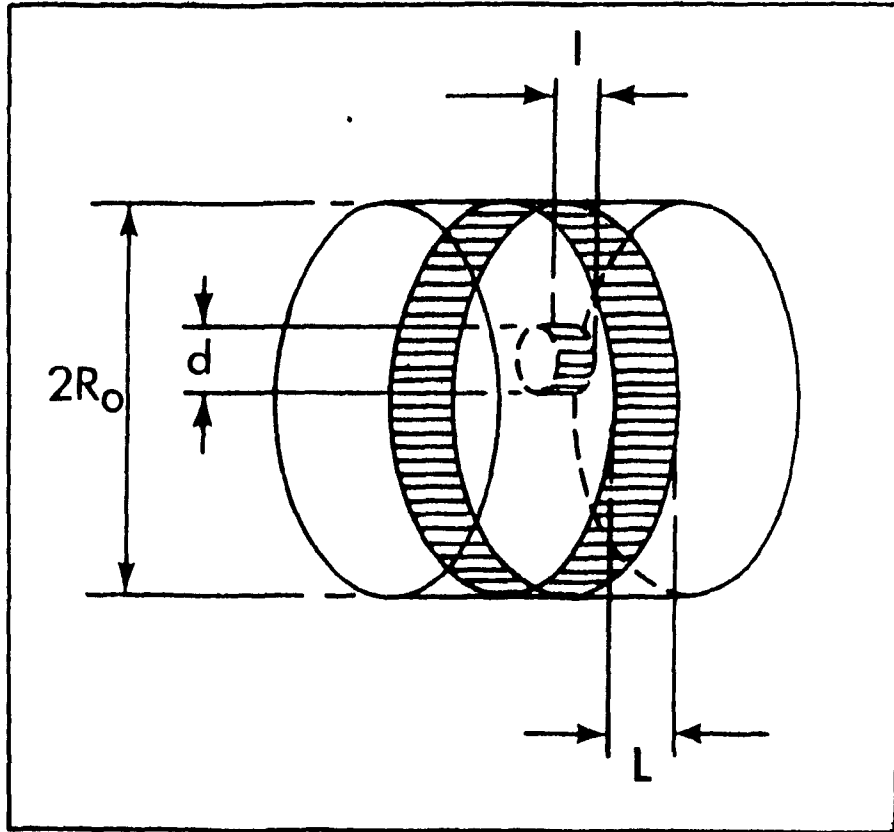


Figure 2: Particle within Aperture

Mathematical model of a particle as a right cylinder suspended within the aperture at moment of sensing (from Jones, 1982).

If $q_1 \ll q_2$ and $\rho_1 \gg \rho_2$, then the response becomes independent of q_1 and ρ_1 and Eq. [1] reduces to:

$$\frac{\Delta U}{i} = \frac{\rho_2 \Delta V}{q_2^2} \quad [2]$$

However, for given electrical conditions and aperture size, the relationship between voltage pulse height and particle volume cannot be explained simply by the volume of electrolyte displaced in the aperture by the particle. Particle shape and the orientation of nonspherical particles with respect to the lines of current determine the extent to which particles disrupt the electrical field within the aperture. Rigid latex spheres, with diameters accurately measured by optical or scanning electron microscopy, generate pulses that are about 50% higher than the amplitude predicted by their geometric volume (Gregg and Steidley, 1965). Hardened red blood cells (rbc) also give volume measurements considerably different from those determined by centrifugation and measurement of the packed cell volume for a known concentration of the same cells. Fluid shear stresses in the flow field can also cause the deformation of nonrigid particles and the rotation of nonspherical particles, leading to variations in particle shape and orientation, respectively.

(a) Shape Factor and Conductivity

Distortion of the electrical field in the aperture by a particle causes the lines of current to follow the essential surface of the particle rather than each crevice and wrinkle, thus sensing the "envelope volume" (Berg, 1958). When the electrical field does not conform to the particle shape an "electrical shadow" is formed which makes the particle

appear to displace a volume larger than its actual volume (Fig. 3). The shape factor for a sphere is 1.5 (Grover et al., 1969a; Grover et al., 1969b; Hurley, 1970) which is the ratio of the pulse height produced by a sphere to the minimum pulse height produced by a particle of the same volume.

Equations relating voltage pulse height to particle volume which account for particle shape and resistivity have been derived for both spherical and ellipsoidal conducting particles. For spheres, the following equation is used (Maxwell, 1883):

$$\rho = \frac{2\rho_1 + \rho_2 + \delta(\rho_1 - \rho_2)}{2\rho_1 + \rho_2 - 2\delta(\rho_1 - \rho_2)} \rho_2, \quad [3]$$

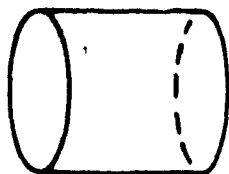
where $\delta = \Delta V/V$, $V =$ aperture volume, and $\rho =$ effective resistivity of the suspension. Assuming $\delta \ll 1$, Eq. [3] reduces to:

$$\Delta V = \frac{-\Delta U q_2^2}{\rho_2 \gamma_s}, \quad [4]$$

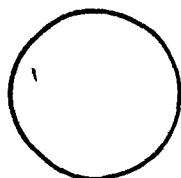
where the shape factor for spheres,

$$\gamma_s = \frac{3((\rho_2/\rho_1)-1)}{(\rho_2/\rho_1)+2}. \quad [5]$$

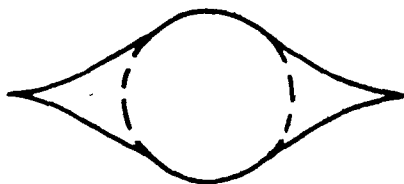
For nonconducting spheres the magnitude of $\gamma_s = 3/2$. It is assumed that the electrical field within the aperture is uniform and the particle diameter is $\ll 2R_0$. High particle-to-aperture diameter ratios result in overestimates of particle volume which depend on particle shape (Fig. 4a; Smythe, 1961). However, for particles moving near the aperture axis, this error does not exceed 1% if the ratio is below 0.2.



A MATHEMATICAL ASSUMPTION



B SPHERICAL EQUIVALENT



C MEASURED SHAPE

Figure 3: Electronically Sensed Particle Volume

All particles were initially treated mathematically as right cylinders, A. Shown is the overestimation, C, of the measured volume of the equivalent sphere, B (from Jones, 1982).

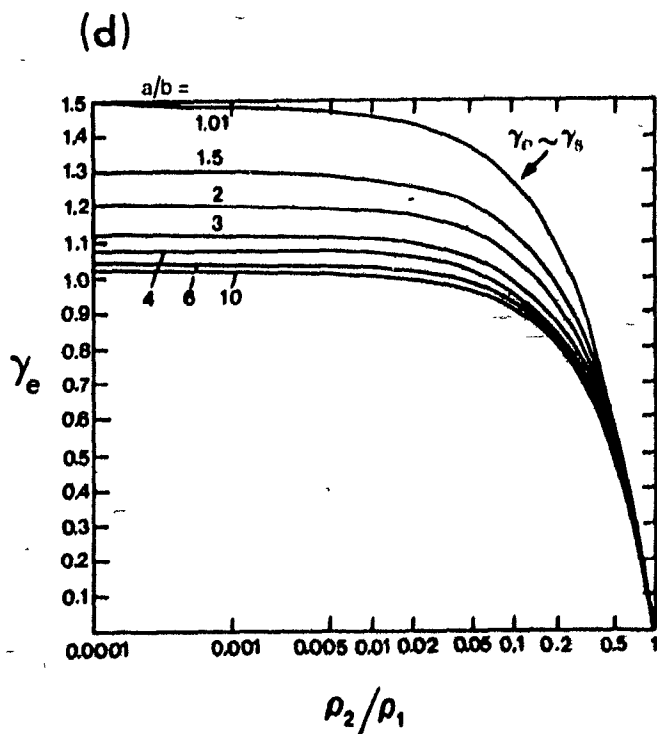
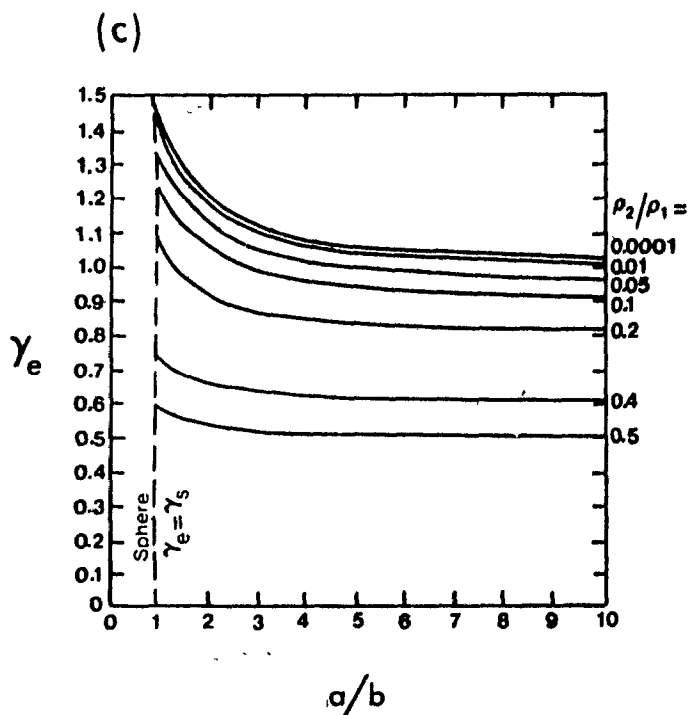
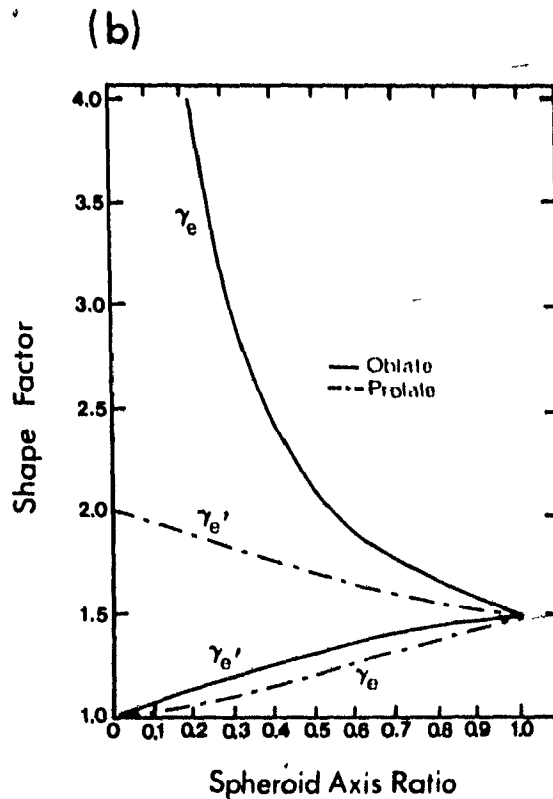
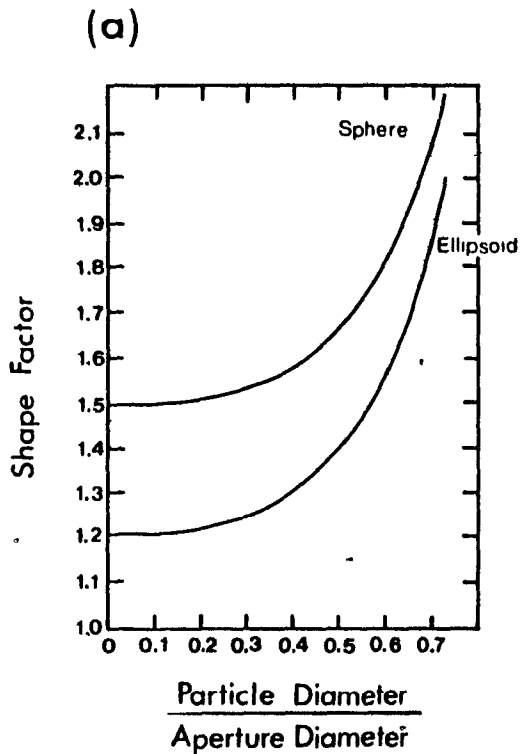
Figure 4: Particle Shape Factor

(a) Shape factor as a function of the particle diameter to aperture diameter ratio for spheres and ellipsoids of revolution (from Smythe, 1961).

(b) Shape factor for oblate (solid line) and prolate (dashed line) spheroids in relation to the spheroid axis ratio, a/b for oblate and b/a for prolate, and the orientation of the spheroid axis with respect to the aperture axis. γ_e : a-axis parallel to aperture axis. γ_e' : either b-axis parallel to aperture axis (from Grover et al., 1969a).

(c) Shape factor for oblate spheroids as a function of axis ratio for several particle resistivities (from Kachel, 1979).

(d) Shape factor for oblate spheroids as a function of particle resistivity for several axis ratios (from Kachel, 1979).



Equation [3] has been extended to ellipsoids of revolution of principal axes a and b , where a is the semi-axis of revolution and b the semi-equatorial axis (Velick and Gorin, 1940; Grover et al., 1969a):

$$\rho = \frac{\rho_1 + (\gamma_e - 1)\rho_2 + (\gamma_e - 1)(\rho_1 - \rho_2)\delta}{\rho_1 + (\gamma_e - 1)\rho_2 - (\rho_1 - \rho_2)\delta} \rho_2, \quad [6]$$

where γ_e is the shape factor for ellipsoids of revolution.

When $\rho_1 \gg \gamma_e \rho_2$, Eq. [6] reduces to:

$$\frac{\Delta\rho}{\rho_2} = \gamma_e \delta', \quad [7]$$

where $\Delta\rho = \rho - \rho_2$, and $\delta' = \delta/(\delta - 1)$.

Equation [7] can also be expressed in the form of Eq. [4] assuming $\delta \ll 1$:

$$\Delta Y = \frac{-\Delta U q_2^2}{\rho_2^2 \gamma_e}. \quad [8]$$

When the a -axis is aligned parallel to the aperture axis the shape factor for oblate ellipsoids of revolution ($m = a/b < 1$) is given by:

$$\frac{1}{\gamma_e} = \frac{m \cos^{-1} m}{(1 - m^2)^{3/2}} - \frac{m^2}{1 - m^2} \quad [9]$$

while for prolate ellipsoids of revolution ($m = a/b > 1$),

$$\frac{1}{\gamma_e} = \frac{m^2}{m^2 - 1} - \frac{m \cosh^{-1} m}{(m^2 - 1)^{3/2}}. \quad [10]$$

If the b-axis is aligned parallel to the aperture axis, γ_e is replaced by $\gamma_e' = 2\gamma_e/(2\gamma_e - 1)$.

Equations [4] and [8] are identical except for the shape factors γ_e and γ_s . Figure 4b shows the calculated shape factor for fixed orientations of both oblate and prolate ellipsoids of revolution as the axis ratio approaches 1. The orientation of the spheroid also has a strong effect on the shape factor. For nonconducting prolate spheroids aligned with the aperture axis, Figure 4c shows that at high particle axis ratios, $\gamma_e \sim 1.0$. It is evident that the ideal particle is a slender, tapered body aligned with the aperture axis. Here, $\gamma_e = 1.0$. With $a/b = 1$, $\gamma_e = \gamma_s$.

The effect of particle conductivity is shown in Figure 4d. For most axis ratios γ_e and γ_e' are constant as long as $\rho_2/\rho_1 < 0.01$. Thus, the particle resistivity is only important if it is less than 100x the resistivity of the electrolyte. The resistivity of most particles is many orders of magnitude greater than that of the electrolyte. In fact, it is difficult to find particles which do not behave as perfect insulators (Jones, 1982). Even for metal particles, a high field strength is required before ionic conduction through the particle occurs. This is hypothesized as being due to oxide surface films and ionic inertia of the Helmholtz electrical double layer and associated solvent molecules at the surface of such particles. Electrical charges on the particles have otherwise no effect (Berg, 1958; Grover *et. al.*, 1969a). Biological particles behave as nonconducting particles (Kachel, 1979).

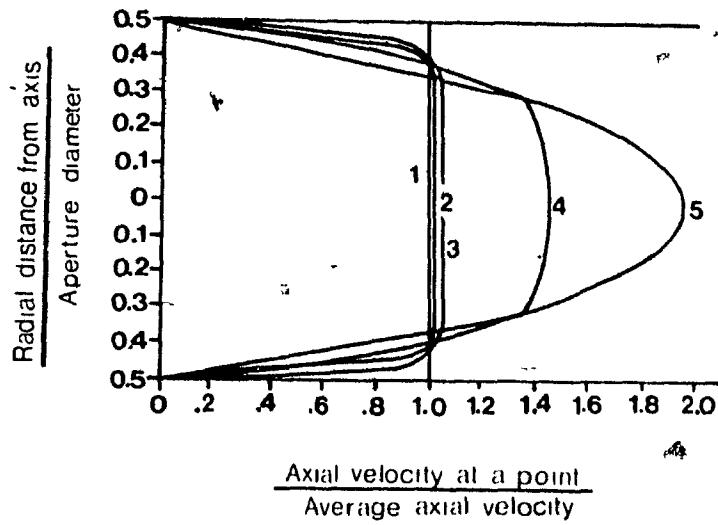
(b) Particle Orientation and Hydrodynamic Field

Assuming a uniform electrical potential through the aperture, the effect of the electrical field on particle rotation and deformation is negligible (Grover et al., 1969a). For suspensions of biological cells, such deformation should be less than 1% for cells below 10 μm diameter. Although the electrical field is not uniform, the major factor determining particle orientation and/or deformation is the hydrodynamic field within the aperture.

At distances $> 2R_0$ from the aperture entrance, the fluid is essentially at rest. Hence, the fluid accelerates from rest to its average velocity at the aperture entrance in the space of $2R_0$. Because of this acceleration nonspherical particles tend to align with the aperture axis and nonrigid particles may deform.

The tube Reynolds numbers in the aperture, Re , are below 1,000 for pressures and aperture diameters commonly used (Grover et al., 1969a). This indicates that the flow is laminar; however, the distance for parabolic (Poiseuille) flow to fully develop is usually $> L$. Assuming the axial velocity is uniform across the entrance of the aperture and zero at a radial distance from the tube axis, $R = R_0$, the radial velocity profile through the length of the aperture can be constructed (Fig. 5a). Due to the finite viscosity of the fluid electrolyte, the thickness of the viscous boundary layer originating at the aperture wall increases downstream until, for sufficiently long tubes, it becomes equal to R_0 , at which point there is fully-developed Poiseuille flow. As the velocity of the fluid in the boundary layer decreases, the central core accelerates to

(a)



(b)

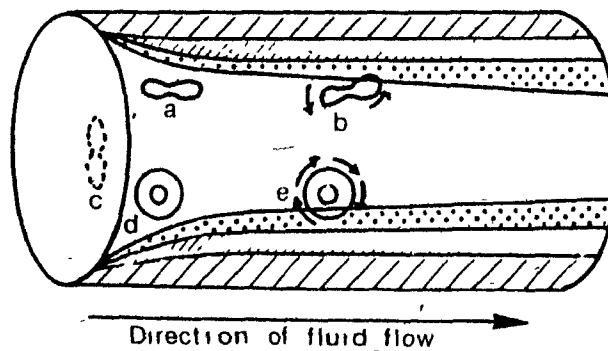


Figure 5: Fluid Velocity Profile in Aperture

(a) Velocity profile as a function of axial distance, x , and tube Reynolds number, Re . Numbers represent dimensionless axial distance, $x/(2R_0 Re)$.

(b) Cells travelling through the central core of the aperture do not rotate but those contacting the encroaching boundary layer rotate continuously.

preserve the mass balance. For the apertures and flow rates usually employed, the exit flow is not fully developed, falling somewhere between profiles 3 and 4 of Figure 5a (Grover et al., 1969a). Therefore, a central core of uniform velocity exists in which particles experience no shear and hence do not rotate. It is in the viscous boundary layer that the shear rate is sufficient to rotate particles through more than 90° (Grover et al., 1969a).

The previous treatment of particle shape factor considered only finite fixed orientations with respect to the electrical field. Rotation of nonspherical particles passing through the aperture, however, will lead to continuously changing shape factors. The native, undeformed rbc approximates an oblate spheroid and in its minimum and maximum orientations has a calculated shape factor of 1.174 and 3.365, respectively (Velick and Gorin, 1940). Theoretical analysis of nondeformable rbc at the moment they enter the aperture shows the shape factor to vary cyclically with particle orientation (Breitmeyer et al., 1971). The orientation of rigid rbc entering the aperture is not random but, due to the orienting effect of fluid acceleration, most cells enter with their major axes aligned with the aperture axis (Goldsmith and Mason, 1967; Thom et al., 1969; Grover et al., 1972). In transit through the central core there is general agreement that cell rotation is negligible. Cells within the boundary layer, however, will rotate and, depending on their initial orientation, the shape factor may continuously change throughout much of their transit (Fig. 5b). Thus, in the outer region of the aperture, identical particles can produce voltage pulses of widely varying height because of differences in their orientation at the moment

they are sensed.

The residence time of particles within the aperture is also radially dependent. In the central core region particle transit time through the aperture is constant but increases sharply at $R > 0.8R_0$. Thus, the duration of pulses in the outer region of the aperture is also longer.

3. Electrical Field

The previous analysis of the relationship between pulse height and particle shape and orientation has assumed a uniform electrical field across and through the aperture. Actually, the field becomes uniform only at $L/2R_0 > 1$ (Fig. 6; Grover et al., 1969a). Since $L/2R_0 < 1$ for most apertures, no homogeneous electrical field exists and the field strength at any point in the aperture depends on both the axial and radial coordinates of the particle.

The potential drop between exit and entrance planes of the aperture is $< 60\%$ of the total potential drop between electrodes for $L/2R_0 > 1.5$ and, due to symmetry, the 50% equipotential area is in the middle of the aperture. The remaining potential difference extends into the electrolyte in a hemispherical manner diminishing to 2% of the total at $6R_0$. In the region of $R < 0.6R_0$, the field strength steadily increases from the entrance of the aperture to the middle, and reaches a radially uniform value when $L/2R_0 > 1$. Hence, particles travelling through the central core region experience fields of successively increasing and decreasing strength, and produce bell- or trapezoidal-shaped voltage pulses that, in long apertures, are of equal height for particles of equivalent shape and

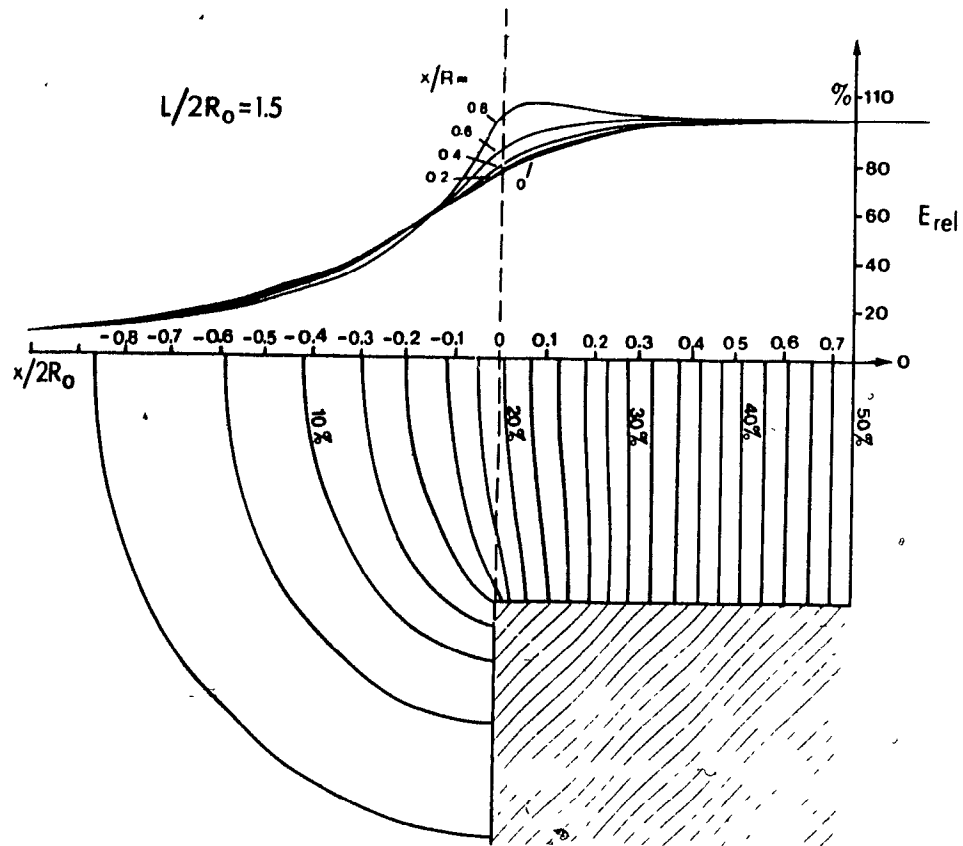


Figure 6: Electrical Field within Aperture

Electrical field is symmetrical with respect to the middle of the aperture and only becomes uniform in both axial and radial directions at $x > 2R_0$. The sensing zone of the aperture extends in a hemispherical manner into the bulk electrolyte at both aperture entrance and exit.

orientation.

However, if the assumption of an equal distribution of particles across the aperture is correct, 35% of the particles will enter the aperture at $R > 0.8R_0$. In this region, high current densities near the aperture wall and distortion of the field by edge effects at the aperture entrance and exit produce altered voltage pulses (Fig. 7). Since voltage pulse height is proportional to current density, particle paths near the aperture wall produce large, 'M'-shaped voltage pulses that tend to give volumes greater than determined on the basis of particle shape and orientation alone. Hence, in short apertures such particles produce a pronounced positive skew in volume distributions.

For the special case of rbc, the size distribution of native cells is strongly bimodal in contrast to the much less skewed distribution of fixed cells. It has been proposed that the nature of the hydrodynamic field preceding entry into the aperture may cause a greater fraction of the deformable cells to select trajectories through regions of high current density, as opposed to trajectories selected simply on the basis of a uniform distribution of particles across the entrance of the aperture (Shank et al., 1969; Akeson and Mel, 1986).

Currently, there is no mathematical analysis to calculate the volume-pulse-height relationship for nonhomogeneous electrical fields. However, several methods have been developed for improving the shape of particle size distributions by removing the artifacts in pulse size and

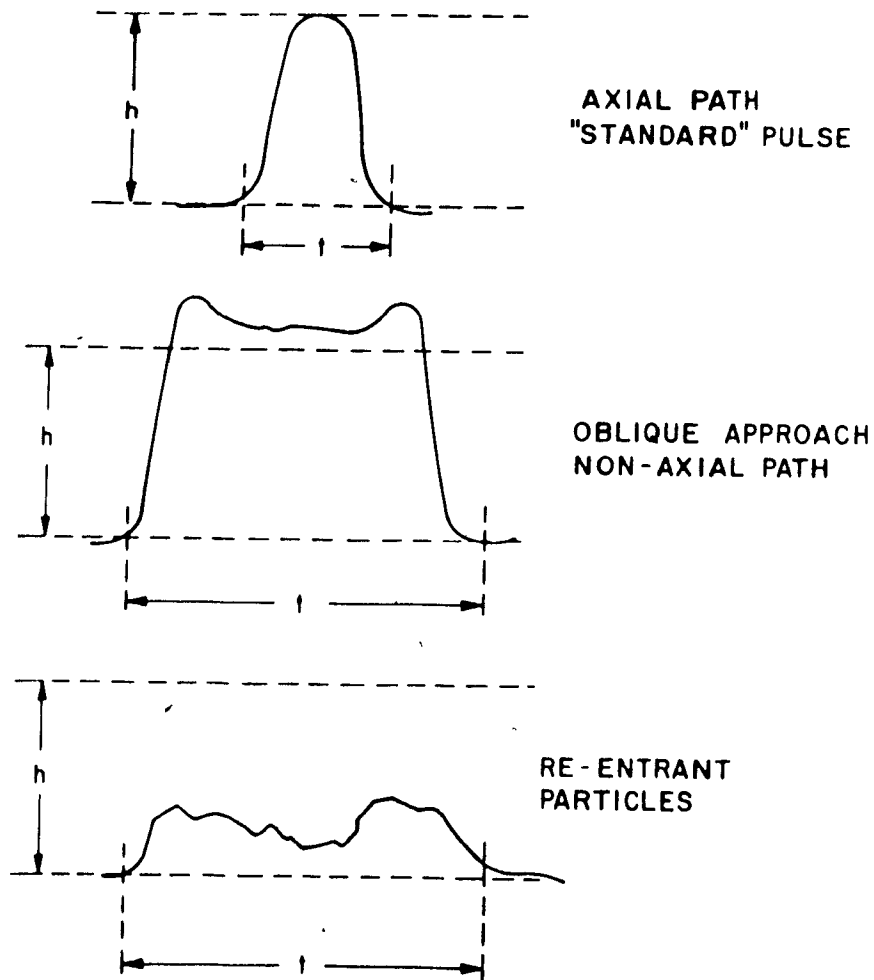


Figure 7: Voltage Pulse Shape

Particles sensed while travelling through the core region produce symmetrical "bell"-shaped voltage pulses as the field strength successively increases and decreases. Particles near the aperture wall where the field strength is stronger at the entrance and exit produce large "M"-shaped pulses.

shape induced by the hydrodynamic and electrical fields. Since both effects are most prominent at $R > 0.8R_0$, they are often reduced concomitantly. Pulses of longer duration produced by slower moving particles in the outer region of the aperture can be electronically filtered (Fig. 8). The shape factor then becomes less variable since particles in this region of the aperture also exhibit large rotations. Aberrant pulses produced by particles that reenter the sensing zone because of a region of fluid recirculation immediately downstream of the aperture exit are also removed. Other electronic editing devices rely on the suppression of the first peak of fast-rising 'M'-shaped pulses by slow rise-time amplifiers or the rejection of pulses with more than one peak, and the selection of uniform ratios of pulse height-to-width or, time from pulse initiation-to-peak.

It is possible to reduce the positive skew of volume distributions through the use of longer apertures. A delayed sensing circuit can also be added in which pulses are evaluated only in the region where the electrical field has become more uniformly distributed. Longer apertures, however, increase particle coincidence and generate greater electronic noise.

The skew can also be removed by focusing a narrow stream of particles into the core of the aperture (Spielman and Goren, 1968; Kachel, 1979). This technique is very efficient at removing the electrical field and viscous boundary layer artifacts without the use of complicated electronic circuitry. By moving the focus of the stream of particles, the change in pulse shape, and corresponding volume, for particles measured in

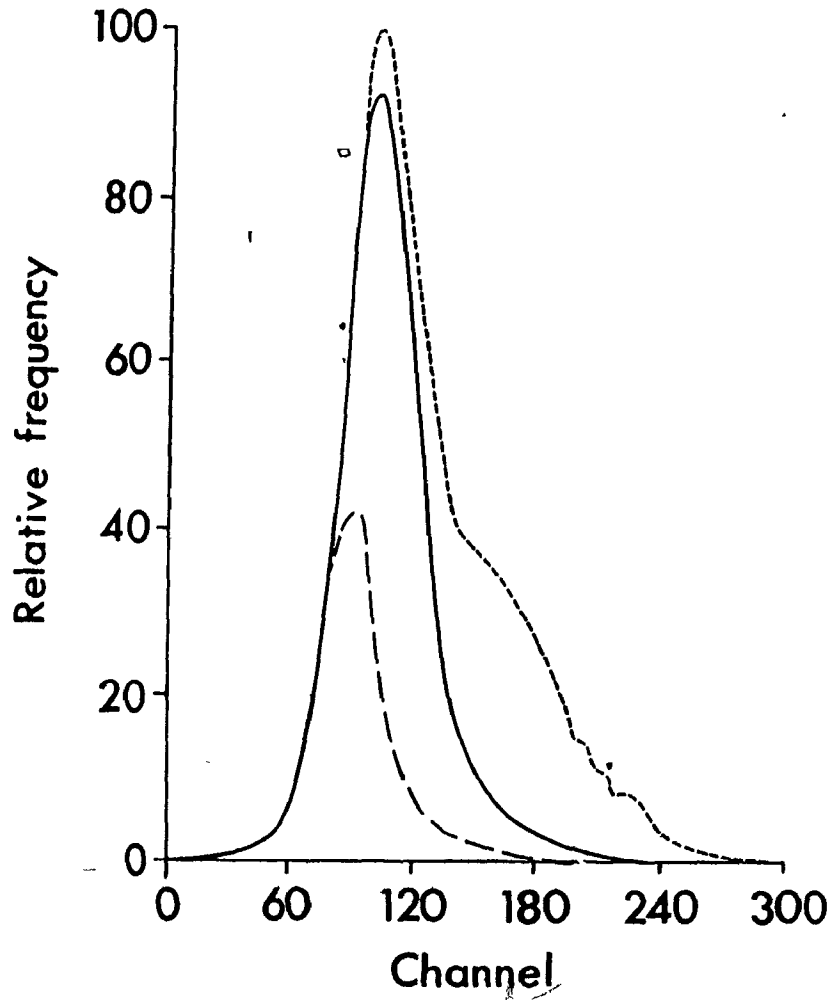


Figure 8: Electronic Filtration of Voltage Pulses

Reduction in the positive skew and in particle counts of native rbc by rejection of pulses of long duration.

the outer layer of the aperture was readily demonstrated. Since both electrical and hydrodynamic artifacts are significantly reduced in such systems, the shape factor for native rbc is very close to 1.0 (Kachel, 1970; Waterman et al., 1975), indicating that most of the cells measured are deformed into elongated, spindle shapes.

Using either standard or deep-bore apertures without electronic editing or hydrodynamic focusing, an average shape factor, $\bar{\gamma}$, accounting for all particle orientations and positions in the aperture can be calculated by independently determining the true mean or modal particle volume. Hence,

$$\bar{\gamma} = \frac{\text{measured volume}}{\text{true volume}} \quad [11]$$

Due to their ease of deformation, the average shape factor for native rbc is 1.18 (Grover et al., 1972). In the core the cells stretch because of fluid acceleration and approach the ideal spindle shape with $\bar{\gamma} = 1.0$. High current densities and the rotation and bending of rbc within the fluid boundary layer contribute to a higher mean $\bar{\gamma} = 1.18$.

4. Summary

The major influences altering the linear relationship between particle volume and voltage pulse height are particle shape and the hydrodynamic and electrical fields in and around the aperture. A correction factor can be determined which accounts for particle shape while the hydrodynamic and electrical effects are mainly important at $R > 0.8R_0$. The alignment with the axis and negligible rotation of nonspherical particles in the central core region, as well as the uniform

radial velocity and the homogeneous electrical field in this region for $L/2R_0 > 1$, produce voltage pulses of relatively uniform shape and height for equivalent particles. Approximately 65% of all particles are measured under these conditions. The major sizing artifact affecting the remaining particles is induced by entrance and wall effects where periodically varying shape factors and trajectories through regions of high current density lead to overestimates of particle volume. Such particles contribute to a broadening of volume distributions in the direction of larger volume.

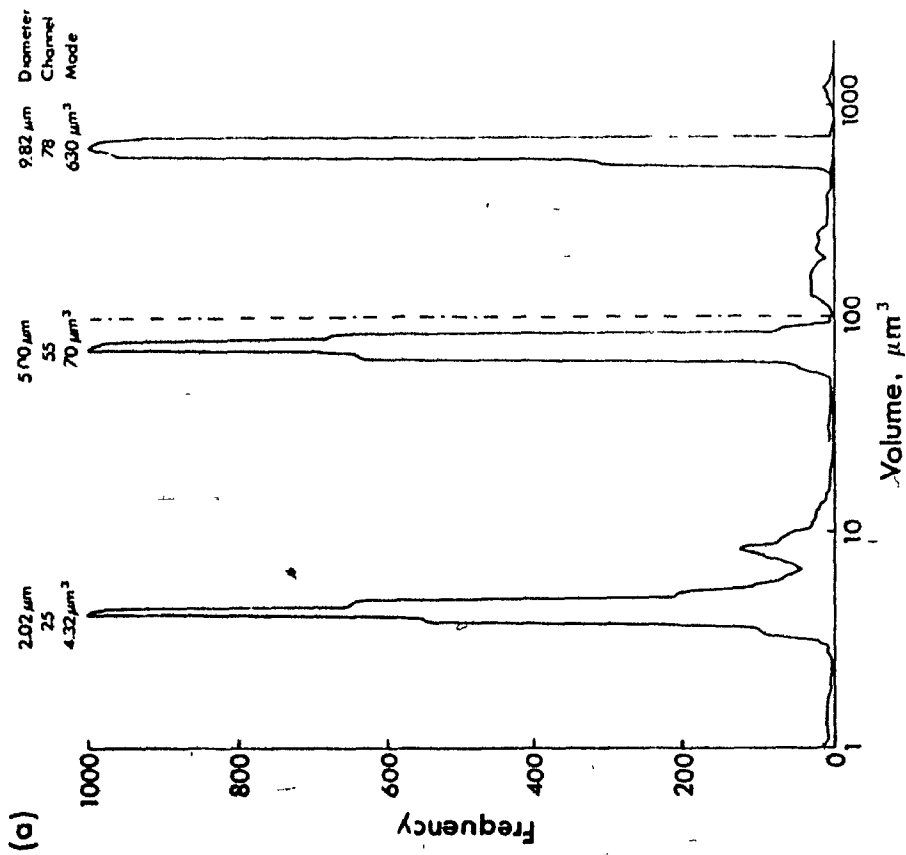
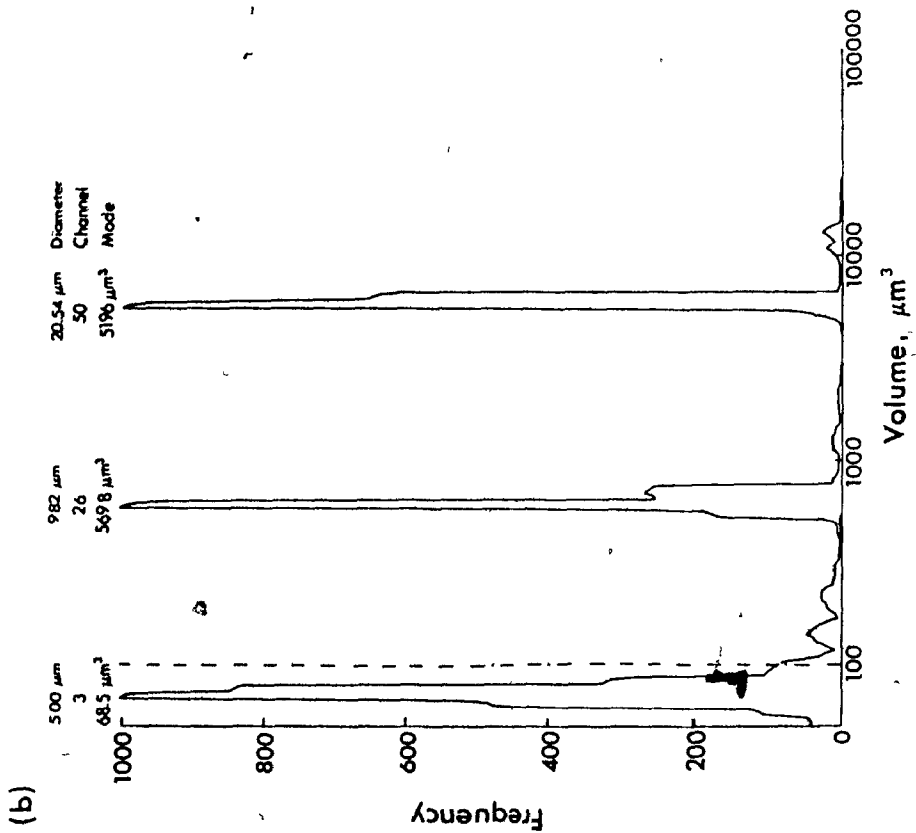
PRACTICE

The present technique is designed to measure the size and concentration of glutaraldehyde-fixed single platelets and aggregates in suspension. A dual aperture counting and sizing procedure was necessary to minimize errors introduced by variable shape factors, and to compensate for the substantial decrease in particle concentration with increasing aggregate size. The dynamic working range of each aperture was increased by logarithmically amplifying voltage pulses originating from the Coulter ZM pre-amplifier. As explained in the METHODS section of Chapter II of this thesis, the scale was calibrated with a range of polystyrene latex spheres and the amplifier was found to respond logarithmically over the size range used on each aperture (Fig. 9a,b). A logarithmic expansion was also chosen because numerous studies have established a log-normal distribution of platelet size, whether determined by diameter, mass, or volume (von Behrens, 1972; Bahr and Zeitler, 1965; Paulus, 1975). Single platelets and all other particles from $1-10^2 \mu\text{m}^3$ were measured using a $50 \mu\text{m}$ diameter \times $60 \mu\text{m}$ length aperture, and particles from $10^2-10^5 \mu\text{m}^3$ were

Figure 9: Coulter ZM Calibration

(a) $50 \times 60 \mu\text{m}$ (length/diameter) aperture: measured volume range $1-10^2 \mu\text{m}^3$. Dashed line denotes maximum volume measured in present experiments. Polystyrene spheres of small c.v. have a narrow distribution on a logarithmic scale. Given are the measured modal volume, modal channel number of the pulse-height analyzer and the mean sphere diameter stated by the manufacturer. Doublets of the $2.02 \mu\text{m}$ diameter spheres are almost completely separated from the single particles.

(b) $100 \times 120 \mu\text{m}$ aperture: measured volume range $10^2-10^5 \mu\text{m}^3$. The $5.00 \mu\text{m}$ diameter spheres are used to match the scale of the $50 \times 60 \mu\text{m}$ aperture to that of the $100 \times 120 \mu\text{m}$ aperture. Dashed line denotes minimum volume measured in present experiments.



measured using a 100 μm diameter \times 120 μm length aperture.

1. Aperture Length

Deep-bore apertures were employed to enhance the development of a homogeneous electrical field in the middle of the aperture. At $L/2R_0 = 1.2$, the resolution of particle size was considerably improved by greatly reducing the positive skew (Fig. 10). Although hydrodynamic focusing might better reduce the positive skew, the present technique was more convenient for processing the large number of samples to be counted in each experiment. The Coulter C1000 pulse-height analyzer is equipped with an electronic editor which rejects voltage pulses that do not adequately match the pulse shape of an internally generated standard. The editor is intended for relatively monodisperse systems, however, and cannot be used with a logarithmic amplifier due to the large variation in voltage pulse size and shape generated by particles of widely varying size and shape.

Since the volume of deep-bore apertures is larger than that of standard apertures of the same diameter, low particle concentrations were required to minimize particle coincidence within the sensing zone of the aperture. Low particle concentrations were also required to prevent the concentration-dependent shift in volume distributions caused by the slow response time of the the log amplifier. As explained in the METHODS section of Chapter II of this thesis, sample dilution was adjusted to count an equivalent number of particles in each sample after 100 s of counting.

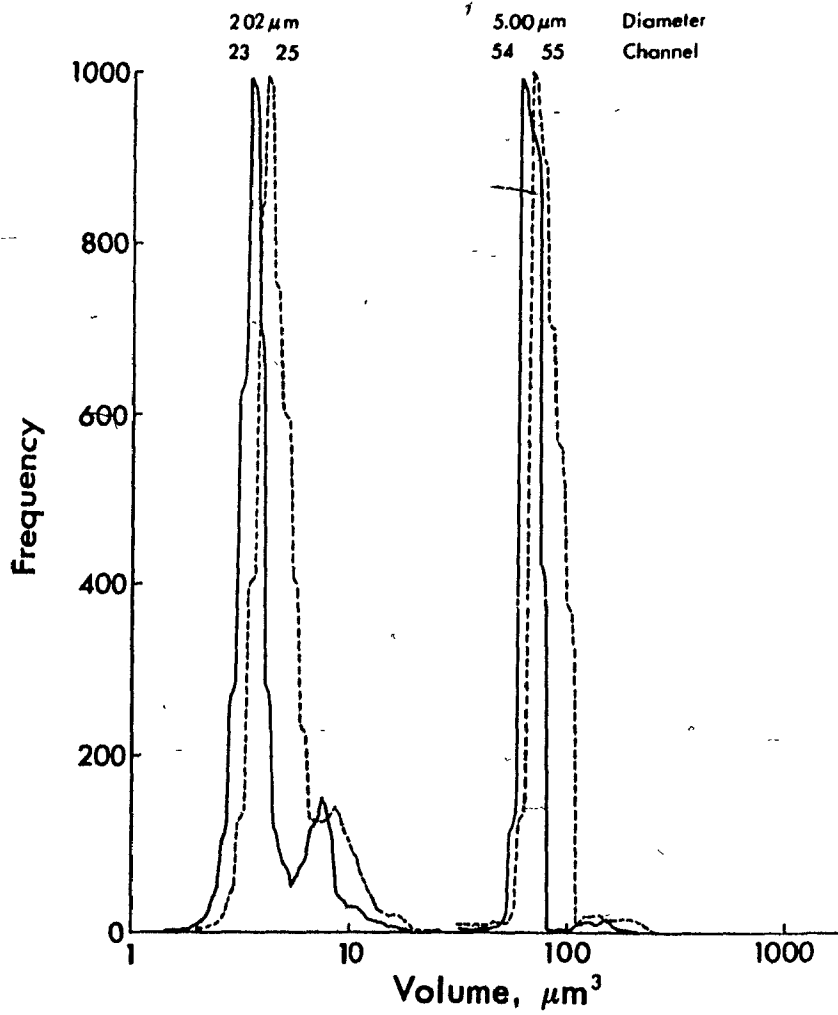


Figure 10: Deep-Bore Apertures

Standard 50 x 50 μm aperture (broken line) showing the large positive skew and shift of the volume distribution of the 2.02 and 5.00 μm spheres, and the concomitant loss of resolution of multiplets compared to that for the 50 x 60 μm aperture (solid line).

2. Background Counts

For a given particle, aperture and electrical conditions, voltage pulse height is proportional to aperture current. Thus, high currents produce high voltage signals and high signal-to-noise ratios. High currents, however, produce excessive heating of the electrolyte in the aperture (Berg, 1958; Kachel, 1979). An aperture current and amplification were empirically determined which minimized background electronic noise yet provided sufficient separation of the single platelet volume distribution from the baseline.

At an electrolyte resistivity of 62.4 ohm-cm for 0.9% NaCl (Samyn and McGee, 1965), background counts in the electrolyte alone never exceeded 0.5% and 0.05% of the total counts on the 50 × 60 and 100 × 120 μm apertures, respectively. A higher background was produced by platelet-poor plasma fixed in 0.5% glutaraldehyde when measured on the 50 × 60 μm aperture and was proportional to the volume of the fixed plasma added to the electrolyte for counting. The details of the subtraction of this background from the single platelet volume distributions is given in the METHODS section of Chapter II.

3. Shape Factor

Good agreement was found with the log-normal model for the distribution of single platelet volumes. Both native and fixed platelets behave as rigid discs and, therefore, do not exhibit the deformation-dependent bimodal volume distribution typical of native red blood cells, but their volumes have a greater natural variance. In shear flow unactivated, single platelets behave as oblate ellipsoids of

revolution with a mean axis ratio of 0.36 (Projmovic et al., 1976), and hence $\gamma_e \sim 1.2$ (Fig. 4b; Grover et al., 1969a). Since the major axis of most discoid platelets will be aligned with the aperture axis in the central core region of deep-bore apertures where the electrical field has become radially homogeneous and cell rotation is negligible, an approximate absolute, mean volume of the unactivated cells can be determined by applying this γ_e uniformly to all single platelets measured in the aperture. Furthermore, since the radius of the largest equivalent spherical particle measured on the $50 \times 60 \mu\text{m}$ aperture is only $0.12R_0$, γ_e is independent of particle size. An additional correction factor of 1.5 must be applied since the scale was calibrated with spheres. Thus, the final shape factor for single, unactivated platelets measured on a scale calibrated with spherical particles is $\gamma_s/\gamma_e = 1.25$. The mean volume of activated cells can also be measured as the equivalent spherical particle in suspensions in which the concentration of multiplets is low.

Since a unique shape factor is required for each aggregate shape and orientation in the $100 \times 120 \mu\text{m}$ aperture, aggregation is expressed as the relative fraction of single cells and aggregates of a given equivalent sphere volume. However, the radius of the largest equivalent sphere measured on the $100 \times 120 \mu\text{m}$ apertures was $28.8 \mu\text{m}$ ($10^5 \mu\text{m}^3$), corresponding to $0.58R_0$. Consequently, on this aperture, the shape factor for particles of $> 10 \mu\text{m}$ radius will increase with increasing particle size. Although the absolute size measurement of particles of this diameter is not exact, all platelet suspensions were measured under the same conditions.

REFERENCES

- AKESON, S.P., AND MEL, H.C. (1986). Deformability and other rheological interactions of red blood cells in electronic sizing. Biorheology 23, 1-5.
- BAHR, G.F., AND ZEITLER, E. (1965). The determination of the dry mass in populations of isolated particles. Lab. Invest. 14, 955.
- BERG, R.H. (1958). Electronic size analysis of subsieve particles by flowing through a small liquid resistor. Symp. Part. Size Meas., Publ. No. 234, pp. 1-5, Am. Soc. Testing Materials.
- BREITMEYER, M.O., LIGHTFOOT, E.N., AND DENNIS, W.H. (1971). Model of red blood cell rotation in flow toward a cell sizing orifice. Biophys. J. 11, 146-157.
- FROJMOVIC, M.M., NEWTON, M., AND GOLDSMITH, H.L. (1975). The microrheology of mammalian platelets: Studies of rheo-optical transients and flow in tubes. Microvasc. Res. 11, 203-215.
- GOLDSMITH, H.L. AND MASON, S.G. (1967). The microrheology of dispersions. In "Rheology" (F.R. Eirich, ed). Vol. 4 pp. 85-250, Academic Press, New York, N.Y.
- GREG, E.C., AND STEIDLEY, K.D. (1965). Electrical counting and sizing of mammalian cells in suspension. Biophys. J. 5, 393-405.
- GROVER, N.B., NAAMAN, J., BEN-SASSON, S., AND DOLJANSKI, F. (1969a). Electrical sizing of particles in suspensions. I, Theory. Biophys. J. 9, 1398-1414.
- GROVER, N.B., NAAMAN, J., BEN-SASSON, S., DOLJANSKI, F., AND NADAV, E. (1969b). Electrical sizing of particles in suspensions. II. Experiments with rigid spheres. Biophys. J. 9, 1415-1425.
- GROVER, N.B., NAAMAN, J., BEN-SASSON, S., AND DOLJANSKI, F. (1972). Electrical sizing of particles in suspensions. III. Rigid spheres and red blood cells. Biophys. J. 12, 1099-1117.
- HURLEY, R.J. (1970). Sizing particles with a Coulter counter. Biophys. J. 10, 74.

- JONES, A.R. (1982). Counting and sizing of blood cells using aperture-impedance systems. In "Advances in Hematological Methods: The Blood Count" (O.W. van Assendelft and J.M. England, eds.), pp. 49-72, CRC Press, Boca Raton, FL.
- KACHEL, V., METZGER, H., AND RUHENSTROTH-BAUER, G. (1970). The influence of the particle path on the volume distribution curves according to the Coulter method. Z. Ges. Exp. Med. **153**, 331-347.
- KACHEL, V. (1979). Electrical resistance pulse sizing (Coulter sizing). In "Flow Cytometry and Sorting" (M.R. Melamed, P.F. Mullaney, and M.L. Mendelsohn, eds.), pp. 61-104, Wiley, New York, N.Y.
- KUBITSCHKEK, H.E. (1958). Electronic counting and sizing of bacteria. Nature (London) **182**, 234-235.
- MAXWELL, J.C. (1883). "Lehrbuch der Electricitat und des Magnetismus" Springer Verlag, Berlin.
- PAULUS, J. (1975). Platelet size in man. Blood **46**, 321-336.
- SAMYN, J.C., AND MCGEE, J.P. (1965). Count loss with the Coulter counter. J. Pharm. Sci. **54**, 1794-1799.
- SHANK, B.B., ADAMS, R.B., STEIDLEY, K.D., AND MURPHY, J.R. (1969). A physical explanation of the bimodal distribution obtained by electronic sizing of erythrocytes. J. Lab. Clin. Med. **74**, 630-641.
- SMYTHE, W.R. (1961). Flow around spheroids in a circular tube. Phys. Fluids **7**, 633-638.
- SPIELMAN, L. AND GOREN, S.L. (1968). Improving resolution in Coulter counting by hydrodynamic focusing. J. Coll. Int. Sci. **26**, 175-182.
- THOM, R., HAMPE, A., AND SAUERBREY, G. (1969). Die elektronische Volumenbestimmung von Blutkörperchen und ihre Fehlerquellen. Z. Ges. Exp. Med. **151**, 331-349.
- VELICK, S., AND GOREN, M. (1940). The electrical conductivity of suspensions of ellipsoids and its relation to the study of avian erythrocytes. J. Gen. Physiol. **23**, 753-771.

VON BEHRENS, W.E. (1972). Platelet size. Thesis submitted for the degree of Doctor of Medicine, University of Adelaide, Adelaide, South Australia.

WATERMAN, C.S., ATKINSON, E.E, WILKINS, B., FISCHER, C.L., AND KIMZEY, S.L. (1975). Improved measurement of erythrocyte volume distribution by aperture-counter signal analysis. Clin. Chem. 21, 1201-1211.

APPENDIX II

AVERAGE LOG-VOLUME HISTOGRAMS

AVERAGE LOG-VOLUME HISTOGRAMS

As described in Chapter II of this thesis, a platelet counting and sizing technique was developed that generated continuous 250 class log-volume histograms over the range of particle volume from $1 - 10^5 \mu\text{m}^3$. In order to follow the time-dependent changes in particle volume during the aggregation of platelets from all the donors at each mean tube shear rate, it is necessary to average the histograms. However, due to the natural variation in mean platelet volume and standard deviation, a straight forward scheme of averaging each histogram class would broaden the average log-volume histogram and reduce the resolution of changes in single cell and aggregate volume (Fig. 1). This effect can be minimized by first expressing the particle log-volume for each donor at all mean transit times in terms of the mean single platelet log-volume and standard deviation of the same donor at $t = 0$ s. At this mean transit time the influence of microaggregate contamination on the mean and standard deviation is minimal. The transformed log-volume histograms are then standardized to the average of the mean single platelet volume and standard deviation of all donors concerned. After correcting for changes in class width introduced during transformation, the contents of the individual classes can then be averaged. The ultimate effect of this procedure is to provide an estimate of the changes in particle volume in relation to mean single platelet volume and standard deviation, as opposed to simply averaging changes in absolute volume.

1. Standard Normal Deviates

Prior to averaging all the histograms at the same mean transit time at each mean tube shear rate, the histograms from each individual

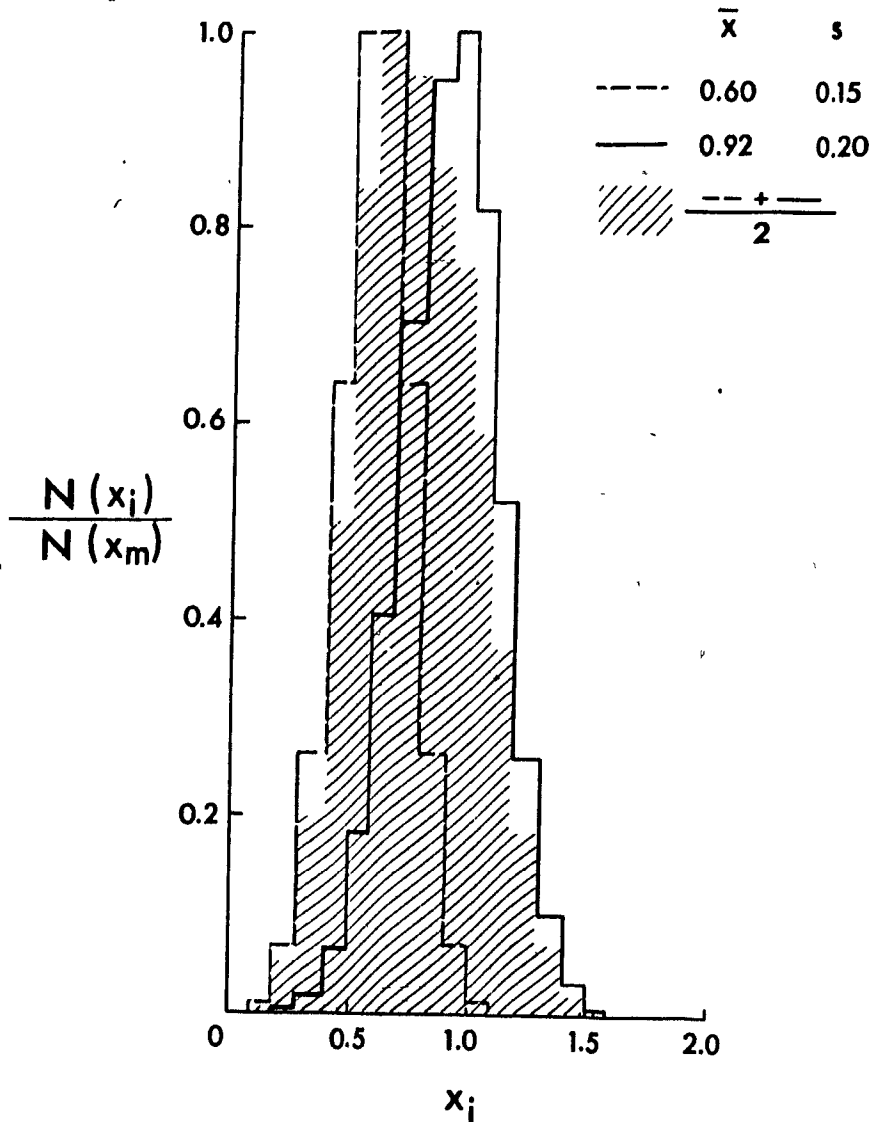


Figure 1: Broadening of Single Platelet Log-Volume Histogram by Averaging

Histograms of two normal distributions of x_i with separate mean, \bar{x} , and standard deviation, s . The contents of each of the i classes, $N(x_i)$, were normalized to the respective class, m , of maximum content, $N(x_m)$. The normalized average of the two histograms (cross-hatched) is much broader than either of the original histograms.

donor were treated independent of those from the other donors at the same shear rate. In accordance with the nomenclature of Chapter II, the normalized content of the i^{th} class of the histogram of the j^{th} donor at mean transit time, \bar{t} , is given by:

$$N'(j, \bar{t}, x_i) = \frac{N(j, \bar{t}, x_i)}{N(j, 0, x_m)} \quad [1]$$

where $N(j, \bar{t}, x_i)$ is the corresponding absolute content, x_i the mark of this class, and m , the class of maximum content at $\bar{t} = 0$ s. For each donor the mark of the $i = 250$ classes of the histogram at each mean transit time was transformed to a standard normal deviate of the mean, $\bar{x}(j)$, and standard deviation, $s(j)$, at $\bar{t} = 0$ s, and then expressed in terms of the average

mean, $\bar{x}_{av} = \frac{1}{h} \sum_{j=1}^h \bar{x}(j)$, and standard deviation, $s_{av} = \frac{1}{h} \sum_{j=1}^h s(j)$, of all h

donors, according to:

$$x'_i = \frac{[x_i - \bar{x}(j)]s_{av}}{s(j)} + \bar{x}_{av} \quad [2]$$

where x'_i is the transformed mark of the i^{th} class.

2. Standard Log-Volume Histograms

Due to variation in the histogram range and class width after transformation, $\Delta x(j) = \frac{s_{av}}{s(j)} \Delta x$, prior to averaging each histogram was mapped back onto the standard 250 class histogram of equal class width, $\Delta x = 0.02$, over the range $1 - 10^5 \mu\text{m}^3$.

(a) $\Delta x(j) = \Delta x$

In the case where the classes of the transformed histogram are of

width equal to those of the standard histogram, a straight forward 1:1 mapping is used:

$$N'(j, \bar{t}, x_i) = N'(j, \bar{t}, x'_i). \quad 1 < i < 250. \quad [3]$$

(b) $\Delta x(j) < \Delta x$

Since the class widths of the transformed and standard histograms are not equal, the respective class numbers will not coincide at the same point on the abscissa. Consequently, the classes of the transformed histograms are mapped onto those of the standard histogram at equivalent log-volume. The class numbers at this point on the abscissa are determined by the multiples of class widths at this log-volume.

The contents of multiple classes of the transformed histogram that fell within the limits of a single class, i , of the standard histogram were averaged (Fig. 2a):

$$N'(j, \bar{t}, x_i) = \frac{1}{q-p} \sum_{o=p}^q N'(j, \bar{t}, x'_o), \quad (p < o < q) \quad [4]$$

where p and q are the respective lower and upper classes of the transformed histogram within the bounds of class i as given by:

$$(i - 1)\Delta x < x'_o < i\Delta x. \quad [5]$$

Vacant classes in the standard histogram between $1 \mu\text{m}^3$ and the first occupied class of the transformed histogram were assigned values based on a log-normal volume distribution according to:

Figure 2: Mapping of Transformed Histograms onto Standard Histograms

Transformed histograms were mapped onto the standard histogram of equal class width, $\Delta x = 0.02$. The changes in class width after transformation have been exaggerated to illustrate the mapping procedure. In actuality, due to the narrow range of the standard deviation, of platelet log-volume among donors, class widths varied by at most 17% after transformation. The vertical dashed lines designate the class limits of the standard histogram.

(a) $\Delta x(j) < \Delta x$: Vacant classes at the ends of the narrower transformed histogram were assigned values (solid dots) as described in the text. The contents of multiple classes of the transformed histogram that fell within the limits of a single class of the standard histogram as shown by similar shading were averaged.

(b) $\Delta x(j) > \Delta x$: Arrows show the assignment of classes of the transformed histogram into the corresponding class of the standard histogram according to the location of the transformed class mark, x'_0 , between the lower and upper class limits of the standard histogram as given by Eq. [5]. The content of vacant classes formed between occupied classes were assigned a value that was the average of the lower and upper adjacent classes.

$$N'(j, \bar{t}, x_1) = e^{-0.5(x_1 - \bar{x}_{av})^2 / s_{av}^2}, \quad [6]$$

and the contents of classes of histograms that fell short of $10^5 \mu\text{m}^3$ were assigned a value of zero:

$$N'(j, \bar{t}, x_1) = 0. \quad x'_{250} < x_1 < 5 \quad [7]$$

(c) $\Delta x(j) > \Delta x$

Transformed histograms that extended below $1 \mu\text{m}^3$ [$x'_0 < 0$] or beyond $10^5 \mu\text{m}^3$ [$x'_0 > 5$] were truncated at these respective limits while vacant classes in the standard histograms were assigned contents that were the average of the lower and upper adjacent occupied classes (Fig. 2b):

$$N'(j, \bar{t}, x_1) = \frac{1}{2} [N'(j, \bar{t}, x_{1-1}) + N'(j, \bar{t}, x_{1+1})] \quad [8]$$

3. Average Standard Histograms

Once transformed into standard format, the log-volume histograms at the same mean tube shear rate were averaged over all donors at each mean transit time. The average, normalized content of each of the 250 classes at mean transit time, \bar{t} , is given by:

$$\bar{N}(\bar{t}, x_1) = \frac{1}{h} \sum_{j=1}^h N'(j, \bar{t}, x_1) \quad [9]$$

and the class content standard deviation by:

$$N_s(\bar{t}, x_1) = \sqrt{\frac{\sum_{j=1}^h [N'(j, \bar{t}, x_1) - \bar{N}(\bar{t}, x_1)]^2}{h - 1}} \quad [10]$$

At each mean transit time, the average normalized volume fraction per histogram class is given by:

$$\bar{\Phi}(x_1) = \frac{\bar{N}(\bar{t}, x_1) v(\bar{t}, x_1)}{\bar{N}(0, x_m) v(0, x_m)}, \quad [11]$$

where $\bar{N}(0, x_m)$ and $v(0, x_m)$ are the respective average, normalized content and particle volume of the histogram class of maximum content, m , at $\bar{t} = 0$ s.

In the experiments of this thesis, the average values of the mean log-volume and standard deviation for all donors were 0.79 and 0.25, respectively. The standard deviation ranged between 0.22 and 0.30, leading to respective transformed class widths that were 14% larger and 17% smaller than the standard class width. Consequently, few classes had to be estimated or deleted in order to average the transformed histograms, and any error introduced by these procedures would be slight.